University of Nottingham
UK | CHINA | MALAYSIA

Scalable and Continuous Production of Dehydrated Protein Microparticles as an Alternative to Lyophilisation

Thomas Booth

Thesis submitted to the University of Nottingham
for the degree of Doctor of Philosophy

March 2022

Abstract

The work described within this thesis had the primary aim to investigate a protein dehydration technique named Critical Concentration Precipitation (CCP) and to assess the potential of this technique for industrial use an alternative to lyophilisation.

The physical mechanism underlying this technique was studied using a dual micropipette method capable of generating individual aqueous droplets within a solvent reservoir. It was demonstrated that protein concentration within the droplet can be calculated at any time point within the experiment and that through further experimentation the particle size and process time could be modelled as a function of initial droplet size and concentration.

Bulk CCP microparticle samples were later prepared, rehydrated and analysed spectroscopically to assess any degradation to the protein molecules caused by the CCP process. Analysis of protein structure and aggregation showed that the CCP process and subsequent reconstitution did not induce significant structural changes or increase aggregation of the protein. Scale up of the process was then demonstrated using laboratory-scale representations of industrial processes.

To further assess the applicability of the CCP process for use as an alternative to lyophilisation, a year-long stability study was conducted. Bovine serum albumin (BSA) and human serum albumin (HSA) formulations were dehydrated and stored at 5°C, 25°C and 40°C for up to one year with characterisation carried out at defined timepoints throughout the study. Spectroscopic analysis of the samples throughout the year demonstrated that all protein formulations tested, across all temperatures, experienced no significant disruptions to their tertiary structure. Aggregation measurements showed that the CCP formulations experienced greater overall increases in aggregation than their lyophilised counterparts. However, it was also

shown that the lyophilised samples experienced a greater increase in larger, non-soluble aggregates.

Continuous fluidic devices were tested to demonstrate the feasibility of continuous CCP manufacture, with the T-reactor method showing control of aqueous droplet size through manipulation of flow rates. However, this size control did not translate to the resultant microparticles with all samples measuring similar size profiles. This was shown to be due to a homogenisation effect from the stirred reservoir used to suspend the droplets. Replacing the stirred reservoir with an unstirred design resulted in the production of highly uniform microparticles of a different size, implying that the new process did not have the same homogenising effect.

For CCP technology to be accepted as an industrial technique it must be capable of solidifying more proteins than just albumins. Through two screening studies it was shown that a potentially wide range of solvents can be used as the drying solvent and that multiple proteins could be dehydrated and rehydrated without causing degradation to the protein structure. Interestingly, the use of methyl acetate as the drying solvent resulted in large flakes of protein material that started to solidify as soon as the aqueous phase was added to the reservoir, before droplet dispersion via vortex mixing. Furthermore, it was shown that any salts present within the aqueous protein solution were also dehydrated to form crystalline structures, implying that other molecules may also be dehydrated using this technique.

The final work discussed in this thesis is preliminary data showing the potential for CCP microparticle formulations to be used in high concentration, non-aqueous suspensions for injectables and as a dissolution aid and transport scaffold for low solubility drugs. These proof-of-concept studies showed that high concentration protein suspensions in benzyl benzoate measured lower viscosity than an equivalent concentration aqueous solution and that the low solubility drug, indomethacin appeared to have been incorporated into a BSA microparticle formulation with an encapsulation efficiency of 33%.

Acknowledgements

I would like to thank my supervisors Prof Jonathan Aylott and Prof Phil Williams for their guidance, support, and encouragement throughout my PhD. I would particularly mention the support and understanding provided to me during the COVID-19 lockdowns.

I would also like to thank the collaborating academics, Prof Paul Dalby and Prof Nicolas Szita, at the UCL Biochemical Engineering Department. Also included in this are all the CDT staff at UCL for their help and assistance when required.

I would like to thank my industrial partners Marie Claire Limb and Eleonora Cerasoli at Albumedix Ltd. for their support and guidance when running the stability study. Many thanks also for sample analysis and the provision of proprietary albumins.

I would like to acknowledge the EPSRC-funded Future Targeted Healthcare Manufacturing Hub and the EPSRC CDT in Innovative Manufacturing in Emergent Macromolecular Therapies, as well both the University of Nottingham and UCL for the financing of this project.

I would also acknowledge the nmRC at the University of Nottingham for training and access to electron microscopy technologies.

At the University of Nottingham, I would particularly like to thank Adam Dundas, Veeren Chauhan, Charlotte Henshaw and Reem Abohujel for their help and support throughout. The technical team, Colin Rowe, Paul Cooling, Esmé Ireson, Tammy Lydamore and Douglas Crackett for their amazing behind the scenes work as well as their knowledge and problem-solving support. I also extend my warmest thanks to all my colleagues within the AMHT, and the Boots Building as a whole.

Finally, I send my eternal love and gratitude to my wife and children for helping to keep me sane and forcing me to go out on occasion.

Contents

List of Figures

the organic phase via the central channel to create a focused central stream where nanoprecipitation can take place. The width of the central stream (W_f) can be varied by altering the flow rates of the three streams.

Fig. 1.7: Optical micrographs of the two flow-focusing geometries and a representation of the flow characteristics generated using the hydrodynamic flow focusing technique. a) Flow-focusing geometry with a smaller central inlet channel and two larger side channels entering at an acute angle. b) Flow-focusing geometry with a 4-way cross formation, all inlet channels have an equal diameter and the two side channels enter at right angles. c) A representation of the flow characteristics observed when using the 4-way cross geometry. The IPA+Lipid flow is tightly focused into a central stream with no evidence of widening.

Fig. 1.8: A schematic of a staggered herringbone mixer chamber showing the asymmetric herringbone ridges.

Fig. 2.1: Schematic of the silanization process showing hexamethyldisilazane binding to the hydrophilic surface of the glass to form a hydrophobic surface.

Fig. 2.2: Experimental setup for the single particle technique.

Fig. 2.3: Schematic of the micropipette system used for single particle studies. The left-hand micropipette contains aqueous BSA solution and an aqueous droplet is formed through the application of pressure. The right-hand micropipette is then used to remove the droplet from the aqueous solution source through the application of a weak vacuum. The water within the droplet then dissolves into the surrounding medium and dehydration of the droplet takes place.

Fig. 2.4: Illustration of the 5 steps to producing CCP BSA microparticles. 1. 50 µL of aqueous BSA solution is added to 1 mL of dried pentanol. 2. The fluid mixture is vortex mixed for 30 s to disperse the aqueous solution throughout the pentanol as droplets and keep them suspended whilst the dehydration process completes. 3. The sample is centrifuged at 10,000 rpm for 30 s to pelletise the microparticles. 4.

The supernatant is removed to leave only residual solvent. 5: The sample is stored under vacuum over night to remove residual solvent, leaving a dried microparticle powder.

Fig. 2.5: Experimental setup for the single flow continuous production method. Aqueous protein solution was pumped through a single piece of FEP tubing directly into the stirred solvent reservoir.

Fig. 2.6: Experimental setup for the microfluidic flow focusing merthod. Aqueous protein solution (dispersed phase, dark blue) flowed into the central inlet channel, and drying solvent (continuous phase, light blue) flowed into the two outer inlet channels. Droplets of dispersed phase were formed at the intersection which then travelled to the stirred reservoir where dehydration could occur.

Fig. 2.7: Experimental setup for the dual flow continuous production method. Aqueous protein solution (dispersed phase, bottom pump) and pentanol (continuous phase, top pump) were flowed into the T-connector where aqueous droplets were formed and travelled into the stirred solvent reservoir via the outlet tubing.

Fig. 2.8: Diagrams showing the two reservoir designs used with the continuous flow production techniques. (Left) The stirred vessel reservoir which uses the stirring action to suspend the aqueous droplets with the CCP process completes. (Right) The unstirred reservoir which allows the aqueous droplets to fall through a column of solvent with the CCP process completes.

Fig. 2.9: Image processing using Fiji to identify and size particles in a brightfield microscope image. (Top Left): Raw image before any processing. (Top Right): Image after application of a thresholding process. (Bottom Left): A Find Edges process is applied to show particle outlines. (Bottom Right) Output from Hough Circle Transform, all coloured circles were found by the algorithm and are automatically measured.

fluorescence of tryptophan residues. Rehydrated lyophilised BSA powder was used as positive control whilst GdnHCl-denatured BSA was used as the negative control (marked with a dotted line).

Fig. 3.13: DLS results from (Top) Rehydrated glassified samples produced using the overhead stirrer technique. (Middle) Positive control of rehydrated lyophilised BSA powder. (Bottom) Negative control of BSA solution purposefully denatured using GdnHCl.

Fig. 4.1: Chart showing peak emission wavelength of rehydrated lyophilised BSA and BSA microparticles prepared via CCP samples stored at 5**°**C at each time point with the excitation wavelength set at 295 nm. Samples were recorded in triplicate and error bars = 1 S.D. of the mean.

Fig. 4.2: Chart showing peak emission wavelength of rehydrated lyophilised BSA and BSA microparticles prepared via CCP samples stored at 25**°**C at each time point with the excitation wavelength set at 295 nm. Samples were recorded in triplicate and error bars = 1 S.D. of the mean.

Fig. 4.3: Chart showing peak emission wavelength of rehydrated lyophilised BSA and BSA microparticles prepared via CCP samples stored at 40**°**C at each time point with the excitation wavelength set at 295 nm. Samples were recorded in triplicate and error bars = 1 S.D. of the mean.

Fig. 4.4: Chart showing peak emission wavelength of rehydrated lyophilised HSA and HSA microparticles prepared via CCP samples stored at 5**°**C at each time point with the excitation wavelength set at 295 nm. Samples were recorded in triplicate and error bars = 1 S.D. of the mean.

Fig. 4.5: Chart showing peak emission wavelength of rehydrated lyophilised HSA and HSA microparticles prepared via CCP samples stored at 25**°**C at each time point with the excitation wavelength set at 295 nm. Samples were recorded in triplicate and error bars = 1 S.D. of the mean.

Fig. 5.2: Image showing a droplet of aqueous phase formed using the single-flow technique after it has detached from the tubing end with no stirring applied to the solvent reservoir.

Fig. 5.3: Image of the Dolomite Microfluidics 3D Flow Focusing microfluidic chip. The chip contains two flow focusing junctions and can be reversed to allow access to either junction. The inlets and outlets of the chip were connected to PTFE tubing allowing the introduction of the two fluid phases. For aqueous droplet generation, the continuous phase (solvent) is connected to the top and bottom inlet (labelled 1 and 3), whilst the dispersed phase (aqueous) is connected to the middle inlet (labelled 2). The fluids intersect at the flow focusing junction and, if conditions are correct, droplets are formed by constriction of the dispersed phase and droplets of dispersed being forced through the junction by the local pressure build up.

Fig. 5.4: (Top) Flow focusing operating in the dripping regime. (Bottom) Flow focusing operating in the jetting regime.

Fig. 5.5: Two light microscopy images recorded using a high-speed camera of droplet production achieved via microfluidic flow focusing. Qc = 100 μL/min, Qd = 5 μL/min to give a flow rate ratio of 20:1 (Top) image recorded at 20k fps. (Bottom) image recorded at 50k fps

Fig. 5.6: Images of droplets produced using the dual-flow technique showing a clear size difference with varying conditions. Left: solvent phase: 100 μL/min, aqueous phase: 25 μL/min. Right: solvent phase:100 μL/min, aqueous phase: 100 μL/min.

Fig. 5.7: Light microscopy images of droplets produced using the dual-flow continuous production technique. Images were obtained of droplets within the outlet tubing. (Left) Continuous phase: 100 μL/min, Dispersed phase: 5 μL/min. (Right) Continuous phase: 300 μL/min, Dispersed phase: 50 μL/min.

Fig. 6.2: Digital images of the two follow-up tests with 2-methyl-1-propanol. (Left) 50 µL of BSA solution added to 1 mL solvent and mixed for 1 minute. (Right) 247.5 µL BSA solution added to 1 mL solvent and mixed for 2 minutes.

Fig. 6.3: Digital images of sample produced during the protein screening study 5 minutes after vortex mixing. showing particulate precipitate was produced with all proteins and all solvents.

Fig. 6.4: Representative images of CCP BSA microparticles produced using pentanol and decanol. (Top) Light microscope images. (Bottom) SEM image.

Fig. 6.5: Microscopy images of samples produced using 2-methyl-1-propanol as drying solvent with 247.5 µL of aqueous BSA added. (Top) light microscope images. (Bottom): SEM image.

Fig. 6.6: SEM images obtained to x200 magnification. (Top Left) Microparticles produced using heptanol as drying solvent and 37.5 µL aq. BSA solution. (Top Right) Microparticles produced using 4-methyl-2-pentanol as drying solvent and 33.8 µL aq. BSA solution. (Bottom Left) Microparticles produced using octanol as drying solvent and 19.7 µL aq. BSA solution. (Bottom Right) Microparticles produced using 2-ethyl-1-hexanol as drying solvent and 11.2 µL aq. BSA solution.

Fig. 6.7: (Left): SEM image taken of material produced when using methyl acetate as drying solvent. (Right): SEM image of a single microparticle produced using ethyl acetate is the drying solvent.

Fig. 6.8: Microscopy images of samples produced using benzyl alcohol as drying solvent with 60.0 µL of aqueous BSA added. (Left): Brightfield image obtained at 4x magnification. (Right): SEM image obtained at 200x magnification.

Fig. 6.9: SEM images of CCP material produced from multiple proteins in multiple solvents. (Top Left) HSA in 2M1P (Top Middle) HSA in methyl acetate (Top Right)

HSA in 4M2P (Bottom Left) Lysozyme in 2M1P (Bottom Middle) Lysozyme in pentanol (Bottom Right) Lysozyme in 4M2P

Fig. 6.10: SEM images of material produced from CCP of insulin in various solvents. (Top Left) 2M1P (Top Right) Pentanol (Bottom Left) Methyl acetate (Bottom Right) 4M2P.

Fig. 6.11: SEM imaging of the result of CCP using various proteins dissolved in phosphate buffer and various solvents. (Top) Catalase in 2M1P, pentanol and 4M2P. (Middle) Peroxidase in 2M1P, pentanol and methyl acetate. (Bottom) Glucose Oxidase in 2M1P, pentanol and 4M2P

Fig. 6.12: Distribution of particle sizes (measured as particle diameter in μm) observed in samples produced using six different solvents. Particles were split into three different size ranges: 0-5 μm, 5-10 μm and > 10 μm.

Fig. 6.13: Distribution of particle sizes (measured as particle diameter in μm) observed in protein samples produced using three different solvents. Proteins used were HSA, lysozyme and insulin. Solvents were 2M1P, pentanol and 4M2P. Particles were split into three different size ranges: 0-5 μm, 5-10 μm and > 10 μm.

Fig. 6.14: (Left) Averaged and normalised fluorescence intensity spectra showing the peak emission wavelengths of BSA microparticle samples prepared with several organic solvents and reconstituted in de-ionised water. Control samples were BSA solution from lyophilised powder and denatured BSA. (Right) Mean peak emission wavelength of samples produced with each solvent. Error bars = 1 SD.

Fig. 6.15: Smoothed and normalised fluorescence spectra of rehydrated proteins. HSA, lysozyme, peroxidase, glucose oxidase and catalase were excited at 280 nm to measure the innate fluorescence of Tryptophan residues, whilst insulin was excited at 276 nm to measure the innate fluorescence of Tyrosine. Rehydrated lyophilised proteins powders were also measured as positive control samples (marked with a dotted line).

List of Tables

List of Abbreviations

CCP	Critical Concentration Precipitation
BSA	Bovine serum albumin
mRNA	Messenger RNA
DLS	Dynamic light scattering
LD	Laser diffraction
PBS	Phosphate buffered saline
GdnHCl	Guanidine hydrochloride
SEM	Scanning electron microscope
FT-IR	Fourier Transform infrared spectroscopy
ATR	Attenuated Total Reflectance
PDI	Polydispersity Index
RI	Refractive Index
A.I.	Aggregation Index
SEC	Size Exclusion Chromatography
HRP	Horseradish peroxidase
GO	Glucose oxidase
IND	Indomethacin
BB	Benzyl benzoate
IPM	Isopropyl myristate

Chapter 1

Main Thesis Introduction

1.1 Thesis Introduction

Proteins are large biological molecules found in all living organisms and can be considered as a biological toolkit, used to carry out a vast array of biological functions required for life. Comprised of long chains of amino acid residues folded upon themselves due to intra-molecular forces, protein structures are as diverse as the functions which they carry out and are vital to all known forms of biological life.

Proteins were first recognised as a distinct class of molecule in 1789 by Antoine Fourcry and were distinguished from other biological molecules by their propensity to coagulate or flocculate when exposed to heat or acidic conditions [1]. However, the understanding that proteins were a biological polymer did not surface until 1902 through the work of Franz Hofmeister and Hermann Fischer, and the importance of the role of proteins and enzymes as biological tools was not realised until 1926 through the work of James Sumner [2], [3]. In the near century since this work, the understanding of the role played by proteins and their molecular structure has increased greatly and we now have the tools and techniques needed to elucidate the complex protein structure and make predictions about their biological function. The large-scale study of proteins and their function is known as proteomics and deals with the entire set of proteins produced by an organism, focusing on protein composition, structure, and biological function [4], [5].

Over the past few decades, the use of pharmaceutical products derived from biological sources, known as biotherapeutics or biopharmaceuticals, has been growing in popularity and is now a major focus for pharmaceutical research. Biotherapeutic products cover a range of different therapeutic agents including therapeutic enzymes, peptide hormones, cytokines, monoclonal antibodies, and

vaccines [6], [7]. Protein and peptide-based biotherapeutics are well established in modern healthcare systems and are in use for a variety of applications including the treatment of cancers, autoimmune diseases, genetic disorders, mental disorders, hypertension, and certain cardiovascular and metabolic diseases [8], [9]. The development and manufacture of therapeutic proteins is a highly complex process compared to that of small-molecule drugs, often requiring in excess of 5000 critical process steps [9]. Most engineered proteins are produced in mammalian cells and so recent technological advances in large-scale fermentation and purification processes have helped to drive the manufacture of therapeutic proteins [7], [8].

However, in aqueous solution many proteins are inherently unstable [10]. Environmental changes in both the physical (such as agitation or shear) and chemical (such as pH or ionic strength) state can lead to degradative processes such as misfolding, aggregation and denaturation [6], [11]. These degradative processes can be attributed, either directly or indirectly, to the presence of water, and as such protein stability in the absence of water is often greatly improved [12]. As such, dehydration techniques such as lyophilisation (also known as freeze drying), or spray drying are often employed to produce dry powder protein formulations for storage and transport, however, these techniques themselves can cause degradation of the protein structure and often require the inclusion of protective additives. More recently, in 2014, a technique described as Microglassification™ was shown to produce dehydrated protein microparticle formulations at room temperature without the need for protective additives [13]. Throughout this thesis, Microglassification™ has been renamed as Critical Concentration Precipitation (CCP) to provide a more descriptive title to the process.

Microfluidic devices, which appeared commercially in the mid-90s, offer a platform for the design and production of polymer microparticles using very small volumes of material which can be easily and cost-effectively scaled up to establish high-throughput, bulk production processes [14], [15]. Over the past decade, the use of

microfluidic devices to formulate biotherapeutic microparticles has become widespread, with the production of drug-carrying polymers and biologicals now considered routine [16]–[23]. Recent works by Yamada *et al*. and Mbanjwa *et al*. have demonstrated that microfluidics is also a suitable platform for the production of dehydrated protein microparticles utilising a precipitation-based approach similar to that used by CCP [24]–[27]. However, these works were not focused on the use of proteins as therapeutics and protein microparticles were immobilised by use of a cross-linking reaction rendering the proteins biologically inactive.

The use of microfluidics to produce protein-based therapeutic microparticles could provide a number of benefits over current techniques. In addition to the inherent scalability of the technology, microfluidic devices allow for the production of particles with a high degree of sphericity and uniformity and have been demonstrated to provide precise control over particle size by manipulation of parameters such as flow rates, channel diameters and solution concentrations. As such, a microfluidic-based platform to produce dehydrated therapeutic protein microparticles offers the exciting possibility of manufacturing well-defined spherical microparticles (and potentially nanoparticles) for long-term storage and transport. Such a technology may also offer applications such as protein encapsulation and inhalable dry powder formulations. A further advantage of such a technology would be the manufacture of high dosage formulations in the form of concentrated microspheres with the ability to be delivered via subcutaneous injection using a biocompatible, non-aqueous suspension medium. High concentration formulations are advantageous for many therapeutic applications to facilitate the delivery of high dosage drugs. However, aqueous formulations of high dosage protein therapeutics are not always possible due to stability issues and increased solution viscosity [28]. The principle of utilising a non-aqueous suspending medium to formulate high concentration formulations has already been demonstrated with the use of vegetable oils to manufacture monoclonal antibody suspensions [29].

1.2 Aims of Thesis

The work presented here aims to further explore the CCP process with a view towards industrial applicability as an alternative protein dehydration technique. The scale up potential of the technology is explored and discussed along with an investigation into the possibility of using microfluidic technologies to facilitate continuous production of CCP microparticles. Reconstituted protein solutions from CCP microparticles were also analysed and compared with lyophilised formulations to assess whether the technique causes undue damage to the protein structure. Beyond this introductory chapter and a materials and methods chapter, the thesis is split into four research chapters, each exploring a different aspect of this work, with a final concluding chapter that discusses some of the potential future applications:

Chapter 3: CCP Technology and Scale Up

This chapter explores the mechanics underpinning the CCP process and how the technology compares to lyophilisation. Secondly, the chapter explores scale-up of the production technique using laboratory-scale representations of how this could be achieved in an industry setting.

Chapter 4: CCP Microparticle Stability

This chapter describes a stability study comparing CCP and lyophilised Bovine Serum Albumin (BSA) and Human Serum Albumin (HSA) formulations. Samples were stored at multiple temperatures for up to one year and a suite of analytical tests were applied at time points throughout the year to study the molecular structure and level of aggregation experienced by the protein samples.

Chapter 5: Continuous Manufacture of CCP Microparticles

This chapter explores techniques for the continuous production of CCP microparticles. Multiple techniques were explored utilising fluidic instrumentation on multiple scales to generate aqueous protein droplets.

Techniques were investigated for their ability to produce size-tuneable and highly uniform CCP microparticles.

Chapter 6: Solvent and Protein Screening

This chapter focuses on the screening of multiple solvents and proteins for use in the CCP process. The resultant microparticles were analysed for size and uniformity before reconstitution and comparison with reconstituted, lyophilised protein.

Chapter 7: Preliminary Works and Final Conclusions

This chapter explores further applications of CCP formulations, including some initial proof-of-concept experiments, beyond the initial aim of providing an alternative protein dehydration method.

1.3 Proteins and Stability

1.3.1 Protein Structure

Proteins are a diverse group of large biological macromolecules which carry out an expansive list of functions within living organisms. At the cellular level, proteins are responsible for virtually every function required for life including the catalysation of metabolic reactions, DNA replication, response to stimuli, cellular structure, and the transport of small molecules. Proteins are comprised of chains of amino acids, small organic molecules consisting of a central carbon atom linked to an amino group, a carboxyl group, a hydrogen atom, and a variable side chain. This variation in the side chain gives rise to a set of twenty amino acids found in the human genome, each with a different side chain and thus, different chemistries (Fig. 1.1).

Some amino acids can be synthesised within an organism through various metabolic pathways with substrates obtained via the organism's diet. However, not all organisms have the ability to synthesise all amino acids, and so these must be obtained directly through diet by the breakdown of proteins [30]. Humans are able to synthesise 11 of the 20 amino acids with the other 9 required to be obtained

through diet [30]. As the building blocks of proteins, amino acids are critical in protein biosynthesis which occurs inside cells and can be divided into two stages: transcription and translation. During the transcription phase, sections of DNA known as genes are "read" by enzymes known as RNA polymerases within the nucleus of the cell [31]. These enzymes read the nucleotides making up the gene and synthesise a single-stranded copy named messenger RNA (mRNA) [31]. The mRNA is then passed from the nucleus of the cell into the cytoplasm where translation occurs. In the translation phase, the mRNA molecules are read by ribosomes which use the nucleotide sequence of the mRNA to determine a sequence of amino acids, binding them together with covalent peptide bonds to form a polypeptide chain [31]. When peptide bonds are formed a water molecule is expelled as the amino group and carboxyl group bond. These amino acids held within a peptide chain are known as amino acid residues.

Polypeptides can be formed with varying chain lengths, shorter chains of less than about 30 amino acid residues are often not regarded as proteins and instead known as peptides. Despite being categorised separately from proteins, peptides can still be found in every cell in an organism and perform a wide range of functions often acting as hormones, which are used to carry information throughout the body. The smallest known functional polypeptide is Glutathione, made up of only three amino acid residues, whereas the longest human protein is Titin, comprised of 34,350 amino acid residues [32].

As a polypeptide is formed, the amino acid residues interact with each other depending upon their individual side chain chemistries. The largest group of amino acids have nonpolar side chains whilst a smaller group have polar sidechains, these can be positively or negatively charged, or uncharged. Charged side chains form ionic bonds with oppositely charged side chains, polar side chains can form hydrogen bonds and hydrophobic side chains can interact via Van der Waals interactions. These side chain interactions cause the polypeptide to bend and fold

upon itself to form a complex three-dimensional macromolecular structure. Larger proteins can consist of multiple polypeptide chains which interact and fold together to form even more complex structures. Fig. 1.2 shows the steps of protein formation from a chain of amino acids to a folded protein structure.

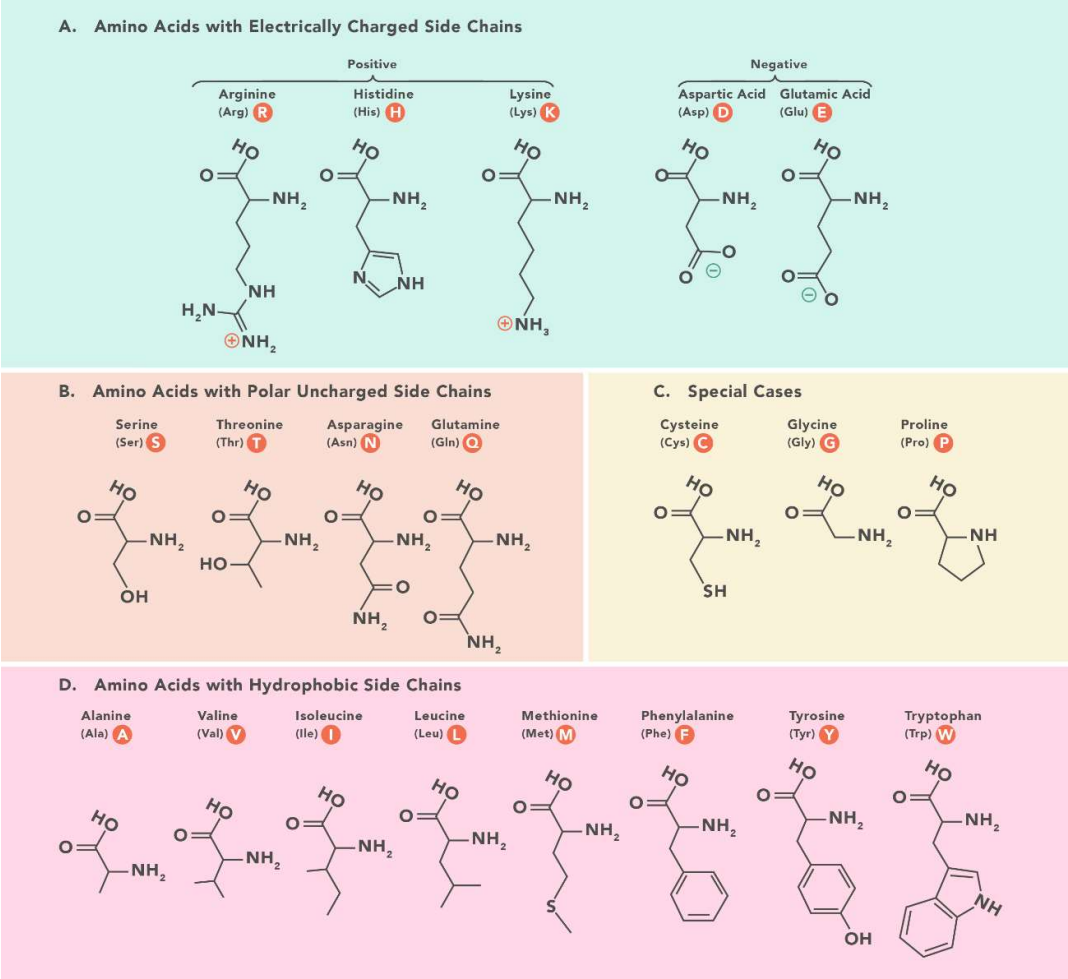

Fig: 1.1: This chart shows the chemical structures of the 20 amino acids that make up proteins. The amino acids have been grouped according to their chemistries [33].

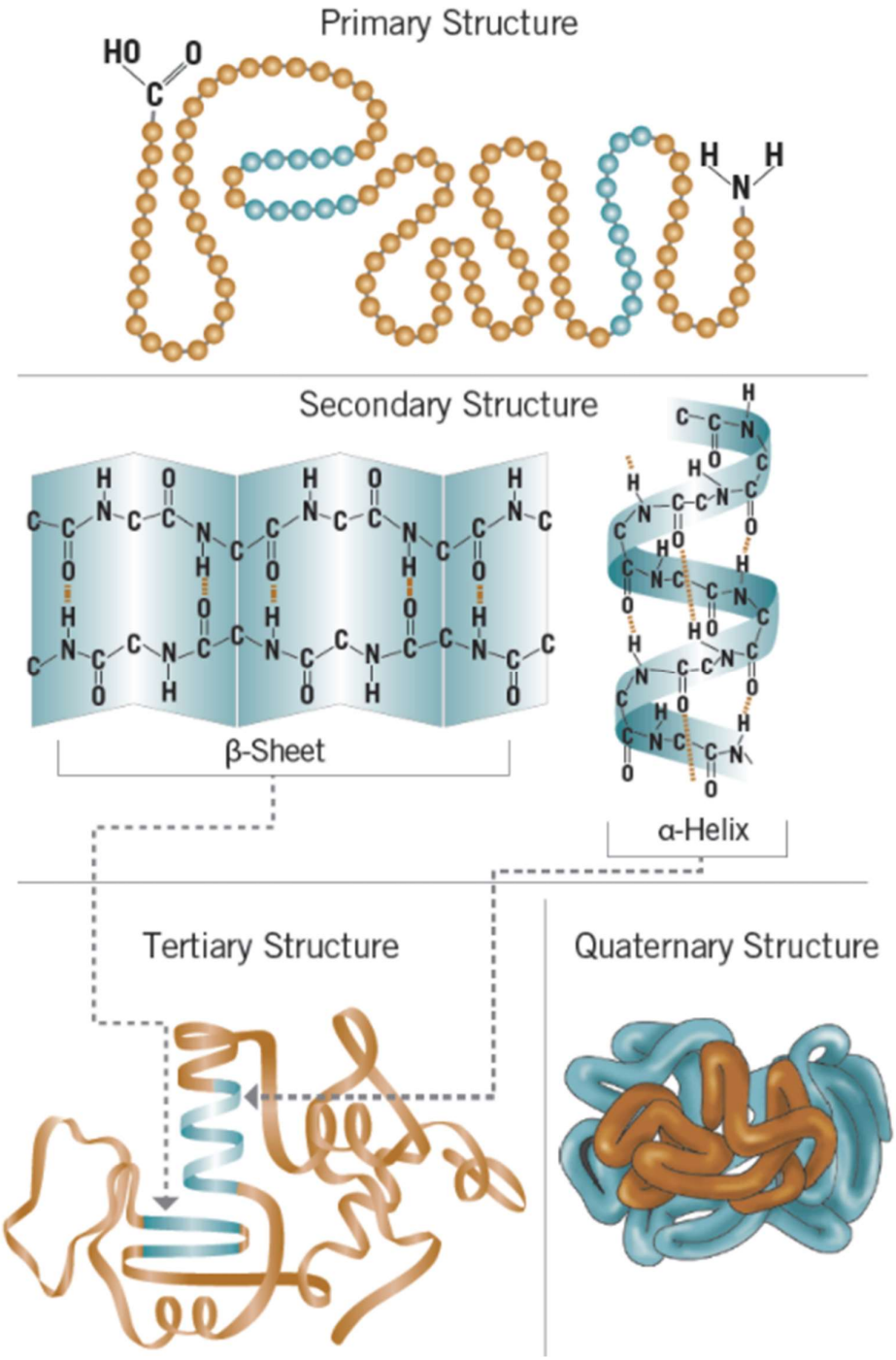

Fig. 1.2: The structural components and naming conventions of proteins. (Top) Representation of protein primary structure as a chain of amino acid residues. (Middle) Protein secondary structures: common localised structures found within many proteins. (Bottom Left) Tertiary structure: the final 3-dimensional structure formed once a protein has folded upon itself due to molecular interactions, two secondary structures are shown in blue. (Bottom Right) Quaternary structure: Some proteins then bond with other proteins to form a large quaternary structure made of multiple polypeptide chains [34].

Proteins and peptides perform many different functions within the cells of an organism. They can function as antibodies, binding to foreign bodies to help protect the organism, or enzymes binding to substrates within the cell to catalyse and regulate a wide variety of chemical reactions. Proteins can also act as chemical messengers or transport and storage vehicles as well as providing structural support to cells. In general, these functions require the protein to chemically bind with a substrate molecule and proteins display very high specificity towards their target substrate. This specificity was first explained by Emil Fischer in 1894 who suggested the lock-and-key model in which both the protein and substrate possess a specific complimentary geometric structure allowing the two molecules to bind together [35]. This model was later replaced with the induced-fit model, suggested by Daniel Koshland in 1958. This model proposes that after the protein and substrate bind together via the lock-and-key model, both molecules may then undergo structural change. If the correct target substrate has attached to the protein, then the induced structural change will allow the protein to perform it's intended function [36].

As the overall structure of a protein is dependent upon the sequence of the amino acid residues of the polypeptide chain, the sequence is defined as the primary structure of the protein. When reporting the primary structure of a protein, the conventional notation utilises a string of single letters to represent each amino acid and the amino acid residues are listed sequentially from amino-terminus to the carboxyl-terminus. Primary protein structure can be directly sequenced using mass spectrometry, although this results in an unordered sequence as the protein must be fragmentated prior to analysis. Edman degradation is a further analytical technique which allows for the determination of an ordered polypeptide chain and identification of the terminus of the chain. Unfortunately, this technique only allows for analysis of chains up to approximately 30 amino acid residues, but this can be overcome by cleaving the chain into smaller fragments [37]. Nowadays, partial or fragmentated sequencing of a protein primary structure is often sufficient for

identification due to the introduction of high-throughput sequencing technologies and large databases of protein sequence, structure and function, such as those held by the National Center for Biotechnology Information, US [38]. The ability to predict the overall structure of a protein from the amino acid sequence has long remained elusive, yet these resources have now also allowed for the use of artificial intelligence and deep learning to predict protein structure and function with ever-improving results [39]–[42].

The interactions between amino acid residues which result in the folding of the polypeptide chain are also responsible for the formation of highly regular localised structures within the protein structure which often form spontaneously as an intermediate step in the folding of the overall structure. These local segments are known as secondary structures and three common secondary structures are defined, helices, strands and turns, with each structure having several variations. Fig 1.2 shows the two most common secondary structures, α-helix and β-sheet conformations. The term 'random coil' is also often used whilst discussing secondary structure and, whilst not a true secondary structure, is used to reference an unstructured region of the protein. Determination of the secondary structures present within a protein is used to aid in the prediction of the overall protein structure as roughly 50% of the structure of all proteins is made up of secondary structures [43]. When combined with knowledge of the amino acid sequence and the use of databases and online tools, such as the Dictionary of Secondary Structure of Proteins (DSSP), it is possible to infer much about the protein structure and function from the secondary structure composition [43], [44]. Secondary structure is usually determined via X-ray crystallography, nuclear magnetic resonance or spectroscopically via circular dichroism or infrared spectroscopy. However, these techniques are costly, time-consuming and, in the case of infrared spectroscopy, have shown issues surrounding repeatability [45]. In attempts to improve the determination of secondary structures within proteins in recent years, artificial

intelligence and machine learning have been employed to improve the throughput and repeatability [46]–[51]. Whilst this work is still being pursued by researchers across the world, big increases in the predicting power of protein structure are being realised, such as in the work carried out using the Google AI offshoot DeepMind which has been heralded as a "game changer" [52].

Finally, the overall three-dimensional structure of a protein is known as the tertiary structure which consists of a single polypeptide chain folded upon itself and containing one or more secondary structures. Some proteins then also form more complex structures consisting of multiple tertiary structures folding together into a quaternary structure consisting of multiple polypeptide chains bound together to act as a single molecule. Furthermore, many proteins then bind with other proteins in events known as protein interactions, to create so-called molecular machines. These interactions, similar to other protein interactions, are highly specific and are driven by electrostatic forces, hydrogen bonding and the hydrophobic effect [53]. These protein complexes are vital to virtually all cellular processes including DNA replication, transcription, translation, splicing, secretion, cell cycle control, signal transduction and intermediary metabolism, to name but a few [54]. Tertiary and quaternary structure is most commonly determined using X-ray crystallography as well as cryogenic electron microscopy and nuclear magnetic resonance spectroscopy.

1.3.2 Protein-based Therapeutics

Recent decades have seen significant advances in the field of biologics and in recombinant DNA technology, driving a change in pharmaceutical research from small molecule therapeutics towards biological macromolecular formulations. Whilst technically any protein-based therapeutic can be classified as a therapeutic protein, the term is generally used to describe genetically engineered, or recombinant, versions of naturally occurring human proteins. Due to the biological nature and functionality of proteins they offer a highly versatile platform for therapeutics with

high target specificity and low toxicity, making them excellent candidates for new drug products [55]. Protein and peptide-based therapeutics make up a large proportion of today's biologics market with applications in the therapeutic, vaccine and diagnostic sectors [56], [57]. Protein therapeutics can be broadly split into five categories, depending upon the pharmacological effect of the product: replacing a protein that is deficient or abnormal, augmenting an existing pathway, providing a novel function or activity, interfering with a molecule or organism, and delivering other compounds or proteins [58].

Whilst protein-based therapeutics offer a number of advantages and opportunities over small molecule therapeutics, there are several challenges and limitations that remain with the technology. The low aqueous solubility of many proteins impacts upon administration and user compliance, requiring regular self-administration or regular hospital visitations. Protein therapeutics are almost exclusively administrated via subcutaneous injection and, as such, liquid formulations are the most convenient format for the end user [59]. However, technical issues regarding the stability of aqueous protein formulations persist. In aqueous solutions, many proteins are only marginally stable and environmental changes in either the physical (such as agitation or shear) or chemical (such as pH or ionic strength) state can lead to degradative processes. Protein instability is primarily caused by the formation and breaking of molecular interactions, primarily ionic bonds, hydrogen bonds and Van der Waals interactions, both within the protein molecular structure and with the external environment [60]. The result of these chemical interactions affects the physical structure of the protein, which can result in aggregation, precipitation, surface adsorption and denaturation [6], [11], [61], [62]. Chemical processes such as deamidation, oxidation and disulphide exchange are common protein interactions capable of inducing structural change, leading to physical instability [62].

Due to protein instability, the long-term storage and transportation of aqueous protein formulations can pose serious risk of product degradation and as such, excipients such as cryoprotectants, stabilisers and surfactants are often required to stabilise the formulation [63]. Stabilising additives can take many forms, such as ionic compounds, detergents and osmolytes. The large number of potential compounds causes difficulty when making predictions, and method optimisation often requires not only selection of the best additives but also the optimal pH, concentrations, and buffer type [64], [65]. As such, screening tests can often be lengthy and expensive. Another widely used approach to combatting protein instability is the production of dry formulations by dehydration of an aqueous solution [12].

1.3.3 Protein Dehydration Techniques

Techniques such as lyophilisation and spray drying are commonly used to dehydrate protein in aqueous solution to produce solid formulations [6], [10], [66]–[70]. However, these processes themselves can cause structural degradation and biological inactivation and, as such, protective excipients are often still required [63]. The work discussed in this thesis focuses on an alternative dehydration technique known as CCP. CCP is a precipitation-based technique which has been demonstrated to result in the dehydration of proteins in solution to form a microparticle powder, at room temperature and without the need for additives or excipients. The three techniques discussed here are now described in greater detail.

Lyophilisation

Lyophilisation has long been an industry standard technique for the production of solid protein formulations with hundreds of approved therapeutic protein products now available and the annual growth in these products increasing year on year [59]. Lyophilisation is a batch-driven technique in which a wet sample is first frozen below the triple point of water where sublimation of water vapour can be induced by reducing the pressure within the freeze-drying chamber. Once the majority of water

has been removed by sublimation the temperature is slowly increased to remove 'bound water' trapped within the structure, resulting in dry powder formulations with more than 99% of water removed from the sample and increased stability and shelf-life over aqueous products [71]. However, the initial freezing step causes ice crystals to form which can damage protein structure. To combat this issue cryo-protective additives can be included, such as trehalose or sucrose, and the cooling rate can be reduced to produce larger ice crystals which results in less protein damage [71], [72]. Although lyophilisation has been in use for many years and is well understood, the process is not without issues. Lyophilisation of proteins is an energy intensive, batch driven technique that can take several days and often requires the inclusion of additives to the formulation to protect the protein from the freeze-thaw cycle [73]. Furthermore, lyophilisation is not a one-size-fits-all technique with each new protein requiring extensive method development and testing prior to pharmaceutical approval [74].

Spray-drying

Spray-drying is a process in which a solution is atomised through a spray nozzle to form size-controlled droplets which are then dried rapidly with hot gas to form a dry powder. Whilst not as commonly used as lyophilisation for the production of solid protein formulations, a number of protein-based therapeutics produced using spray-drying techniques have been approved over the past 15 years [59]. The first commercially approved spray-dried protein therapeutic was produced by Pfizer in 2006 and known as Exubera®, an inhaled insulin powder which was later withdrawn from the market citing "commercial reasons" [75]. Despite the withdrawal of this product, at least three further spray-dried therapeutic protein formulations have been approved in the US with a wide array of further products under clinical development [76].

The technique of spray-drying utilises a spray nozzle to disperse a solution containing the material to be dehydrated into a controlled droplet size. A number of

variations on the nozzle design are commonly used, dependent upon the process requirements and droplets in the size range 10 to 500 μm diameter are often reported [77]. The droplets exit from the spray nozzle into a drying chamber, where the pre-heated gas (usually oxygen or nitrogen) heats and dries the droplets, leaving behind a fine powder. The heated gas can either flow in the same direction as the atomised droplets, known as a co-current system, or against the droplets, known as counter-current. The co-current system is the most commonly used technique allowing more efficient operation, whilst the counter-current technique allows the droplets to spend more time in the drying chamber but often requires additional steps to achieve the desired particle properties. The most common and basic form of spray-dryers operate as described above and the resultant particles are collected at the end of the drying chamber. However, this often produces not only a fine powder of dehydrated particle, but also a large amount of non-uniform debris which affects the flow properties of the powder [77]. To combat this effect, a newer generation of spray-dryers makes use of a two-step drying process. The first step is the same as described above and the particles are then transferred to the second stage which utilises a static bed at the bottom of the chamber. This provides a humid environment which causes the smaller particles and debris to aggregate into larger particle, producing a more uniform particle size overall [77].

Spray-drying is a technique of great interest as it produces particles with a much higher degree of uniformity than lyophilisation, has been demonstrated to allow for the encapsulation of one material inside another and has scale-up potential for continuous production [78]. However, in the case of protein-based therapeutics it has the disadvantage of utilising heat to remove water from the formulation, as such care must be taken to ensure the heat does not degrade the protein.

Critical Concentration Precipitation

CCP is a relatively new technique for the dehydration of proteins, being first described by Aniket *et al*. in 2014 (then named Microglassification™) [13]. This

technique produces dehydrated, amorphous, protein microparticles at room temperature without the need for protective additives. CCP is a precipitation-based process in which aqueous protein microdroplets are generated within a reservoir of solvent, which must be non-miscible with water yet able to dissolve water, the water from the microdroplets then diffuses from the aqueous protein droplets into the surrounding solvent, inducing precipitation and leaving behind dehydrated, solid protein microparticles. The process has been shown to produce solid protein formulations with good stability, on a par with lyophilised protein formulations, and upon rehydration, have been shown to retain structural integrity and biological activity [13], [79]. The process of CCP can be split into two distinct stages: 1. The formation of aqueous protein microdroplets. 2. Diffusion of water from the droplets to a drying solvent and precipitation of protein microparticles. During the first stage, an aqueous protein solution is dispersed into discrete droplets within the solvent reservoir using high energy mixing, such as vortex mixing [80]–[88]. During the second stage of the process, the water within the aqueous protein droplets diffuses into the drying solvent, increasing the protein concentration as the droplet reduces in size. Once the protein concentration within the droplet reaches a critical level the protein precipitates out of the solution into a solid amorphous sphere with water content well below mono-layer coverage [13]. The use of long-chain alcohols, such as pentanol and octanol, as the drying solvent have been shown to produce formulations that retain the greatest level of biological activity, whilst other solvents such as triacetin, butyl lactate and methyl acetate showed markedly lower activity [79]. Once the process is complete, the particles can be collected by centrifugation, filtration or evaporation and stored as a dry powder. The protein can then be readily rehydrated at a later date where it reverts to its native state whilst retaining biological activity [79].

1.4 Microparticles, Microfluidics and Continuous Production

1.4.1 Microparticles and Analysis

A microparticle is defined by the IUPAC as a "particle with dimensions between 1 x 10^{-7} and 1 x 10^{-4} m" (i.e. 0.1 to 100 μm) and are encountered regularly in everyday life in materials such as pollen, sand, dust and flour [89]. Particles with dimensions below these limits are regarded as nanoparticles and, whilst sharing many properties and uses, will not be discussed here. However, the definitions surrounding microparticles and nanoparticles can be confusing with different fields using different definitions [90]. Materials in a microparticle form have a much larger surface area than an equivalent amount at the macroscale and this can greatly affect the properties of the material, such as aluminium microparticles becoming explosive in air due to the rapid exothermic reaction produced when pure aluminium is oxidised [91]. Microparticles have found use in a variety of different fields from plastics and ceramics manufacture to cosmetics and personal care products [92]. Microspheres are even used to produce electronic paper and retroreflective coatings for road signs [93]. However, the field in which the use of microparticles has had the greatest impact is that of pharmaceutical technologies, particularly in the form of drug delivery systems.

In recent decades it has become apparent that organic microparticles are released from many cell types within an organism and that they are often actively involved in physiology and pathophysiology [94]. These microparticles are generated by a budding of the cell membrane of their host cell and are primarily formed from lipids arranged to form a liposome interspaced with membrane proteins, the exact composition of a biological microparticle is determined by its host cell [95]. The pathological effect of these microparticles is still poorly understood but their presence has been shown to occur in blood samples from both healthy and ill populations [95]. Despite this, their role in various disease states is a focus of research due to changes in microparticle count, origin and composition when an

organism suffers an illness, as well as evidence that some currently used therapies may operate through the act of blocking microparticle formation [94]. Further studies into the role of microparticles could lead to novel therapies and diagnostic tests.

Synthetic microparticles formed from biocompatible, biodegradable polymers have also found use in pharmaceutical research as drug delivery agents. Microscale drug delivery systems are routinely used as transport mechanisms to deliver biotherapeutics to a target location and can provide several advantages over traditional drug delivery systems: increased control over their physical characteristics, the ability to deliver a wide variety of therapeutic agents and to release them in a controlled manner at a target location, and increased stability and solubility of encapsulated drug [96]. Microscale delivery systems are commonly synthesised from either biocompatible polymers or liposomes and can transport a therapeutic agent either encapsulated within the particle or distributed throughout the particle. Fig. 1.3 shows a representation of the structural difference between three microparticle formulations commonly used in pharmaceutical research. More recently, therapeutics made entirely from natural biomolecules such as proteins and polysaccharides have been developed, either to act as a therapeutic themselves or as a drug delivery system [96]–[98]. Biotherapeutic medicines created entirely from biomolecules are viewed as a valuable alternative to synthetic polymers due to their inherently low toxicity and biodegradability, and because they remove the need for expensive polymers and excipients.

Analysis of Microparticles

The analysis and characterisation of microparticles usually relates to measurements of particle size and uniformity. However, there are many other important characteristics which may be relevant for the intended purpose of the particles. Microparticle friability, flowability and bulk density are all important physical characteristics of a microparticle formulation, whilst characteristics such as residual

solvent content, drug loading capacity and dissolution rate are important properties in the field of biopharmaceuticals [99].

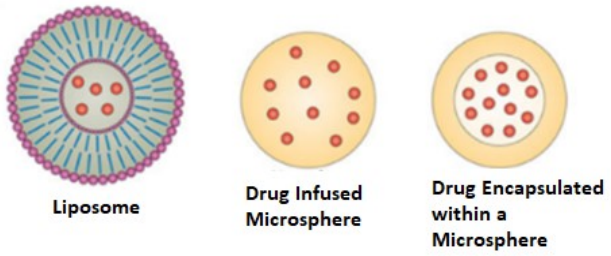

Fig 1.3: A representation of the structural difference between microparticle designs commonly used in pharmaceutical research. Left to right, this image shows a drug-loaded liposome microparticle, a polymer microparticle with drug infused throughout the particle matrix and a polymer microparticle with encapsulated drug molecules. Adapted from [100]

Particle size is perhaps the most obvious characteristic to measure when analysing a microparticle formulation but reporting an average particle size does not provide a full picture of the particle population size without also reporting details on the particle size distribution. As the majority of microparticle applications require the manufacture of a repeatable product, this necessitates the ability to produce microparticles with size and uniformity measurements within defined limits.

The traditional method of particle sizing, which is still in common use today, is sieve analysis [101]. Particle sizing via sieve analysis is carried out using a sieve stack, several sieves with increasing aperture size stacked upon one another. The particles are added to the top sieve and then entire stack is then shaken until particles are no longer passing through the sieve apertures. As a result, the particles are distributed throughout the sieve stack according to their size and the sieves can be weighed to calculate the relative mass of each size distribution. Due to the shaking action applied to the sieves, the majority of particles will pass through the smallest possible sieve aperture for their dimensions and as such, this technique tends to provide a measurement of the smallest dimension of the particles. Sieving is generally used for particles with dimensions larger than about 20 μm.

Over the past few decades multiple particle sizing systems have been developed to compliment or replace sieve-sizing. Many of these systems are electronic, bench-top instruments based on complex physical mechanics but are mostly automated to aid in usability [102]. Due to the level of complexity and automation of process designed into these instruments, care must be taken that they are not treated as a "black box" where samples are placed into the instrument and the result is simply read out. Without understanding of the processes involved in these measurements it can be easy to misreport the results [103]. The processes by which these instruments measure particle size can be split broadly into two categories: 1. Indirect measurements using light scattering. 2. Direct measurements using image analysis.

Light Scattering Techniques

Particle size measurements using light scattering are generally split into two separate methodologies: dynamic light scattering (DLS) and laser diffraction (LD). DLS utilises a monochromatic light source which passes through a polariser and into a liquid sample. Whilst passing through the sample, photons collide with the particles of interest and scatter in all directions, a process known as Rayleigh scattering, a detector placed at a specific angle from the incident light path then picks up scattered photons and the intensity over time is measured. The wavelength of light used for this process must be greater than 20-times larger than the dimension of the particles to be measured to ensure there is no angular dependence to the scattering and a single detector can be used [103]. As particles within a liquid sample undergo constant movement due to Brownian motion, the scattering pattern will also change leading to constructive and destructive interference. The correlation between time points is plotted and the decay of correlation can be used to make direct inferences about the motion of the particles. Larger particles move slower due to Brownian motion, allowing for the hydrodynamic diameter of particles to be calculated using the Stokes-Einstein equation, relating the particles size to particle

diffusion rate, temperature and viscosity. DLS is a common analytical technique for the measurement of particle size but is generally more suited to nanoparticle measurements as the sizing range is approximately between 0.8 nm to 10 μm, with increasing imprecise measurements above 1 μm [101]. As a complex and sensitive methodology, DLS measurements are easily disrupted, and user experience is often required to spot these issues. As this technique relies upon the particles experiencing Brownian motion anything which disrupts this, such as contaminants or large particles moving under gravity (ie. dust particles), will affect the measured result. Sample concentration is also important as if there are not enough collisions or multiple scatterings the accurate determination of particle size becomes increasingly difficult.

The other common light scattering technique, LD, is based on the phenomenon that the intensity distribution of light scattered by particles correlates with particle size. Larger particles scatter light at smaller angles than smaller particles. Using multiple detectors at known angles from the incident light source, LD instruments can measure the intensity distribution from scattered light and calculate particle size distribution based on the scattered light pattern [101]. Larger particles produce well resolved intensity distribution which become more diffuse with lower intensity as particle size decreases. As such, the measurement of highly polydisperse samples becomes difficult due to overlapping signals. LD is usually employed to measure particles in the size range 10 nm to 4000 μm [101].

Image Analysis Techniques

Image analysis, as the name implies, is based upon taking microscopic images of a particle population and measuring the size directly. This process can be carried out manually or through the use of automated instruments. Manual processing of image analysis requires the operator to prepare a sample on a microscope slide and to capture digital images of the particles. In order to acquire a statistically significant number of particle images it is usually required to capture multiple images from

different areas of the sample. Once captured images have been recovered, they can be analysed using image processing algorithms. This technique is widely used when measuring small numbers of samples, but due to the time-consuming nature of the technique is not suitable for large numbers of samples or high-throughput work. To counter this drawback, automated image analysis systems have been developed known as dynamic image analysis.

In dynamic image analysis, a flow cell is used to pass a large amount of sample through a microscope focal plane and high-speed images are taken and measured in real time. As the focal plane of a microscope is limited in depth, especially at high magnification, the flow cell used to transport the sample past the microscope optics must also have a tightly controlled and limited depth to ensure the particles remain in focus. This means that particles within the sample must be compatible with the flow cell or risk clogging of the system. One example of a dynamic image analysis instrument is micro-flow imaging which utilises microfluidic channels to allow precise control of the sample flow. This allows for the capture of high-resolution images with up to 85% sampling efficiency [104].

1.4.2 Microparticle Production

Traditional Methods

The traditional approaches to the preparation of polymer-based microparticles can be categorised into three types based upon the general principles of the particle formation technique. Emulsion, precipitation and direct compositing methods have been widely used for several decades now and all are well understood [105]. Emulsion-based methods require the dissolution of the particle precursors in a water-immiscible organic solvent which is then added to a larger volume of aqueous solvent to produce an emulsion. Organic phases are then removed by evaporation, causing the particle precursors to precipitate out of solution and leaving particles dispersed in the aqueous phase [106]. For pharmaceutical uses, polymers such as polylactide (PCL), polylactide-co-glycolide (PLGA) and poly-ε-caprolactone (PCL)

are often cited as choice materials due to their biodegradability and low toxicity [107].

In contrast to the emulsion-based methods, which require two or more immiscible phases, nanoprecipitation utilises two miscible phases: an organic phase and an aqueous phase. A hydrophobic polymer is dissolved in a water miscible organic solvent, usually ethanol, acetone or tetrahydrofuran, to create the organic phase. The organic phase is then added to a large volume of aqueous phase, usually a water-surfactant solution. Upon mixing, the organic-aqueous mixture becomes a non-solvent for the polymer causing phase separation to occur and resulting in the formation of particles of the hydrophobic polymer. The use of a surfactant in the aqueous phase is often an important addition as it can adsorb onto the polymer aggregates during formation and effectively limit the size of the particles. However, the use of block copolymers, such as poly(ethylene glycol-bl-poly(lactic acid-coglycolic acid)) (PEG-PLGA) effectively negates the need for surfactant due to the inherent amphiphilicity of their structure [108]. Nanoprecipitation is often used to produce drug-loaded nanoparticles and has been shown to be a simple and reproducible method for formulating both nanocapsules (drug encapsulated within a polymer shell) and nanospheres (drug dispersed throughout the particle matrix). To load drugs into the nanoparticle formulation the drug is dissolved into the organic phase along with the polymer prior to the precipitation process. For hydrophobic drugs, this process has long been considered an efficient and reproducible process which results in a high encapsulation efficiency [107]. However, hydrophilic drugs have proven more difficult due to phase migration and dissolution into the aqueous phase resulting in low encapsulation efficiency [109].

Direct compositing methods, such as spray drying and in-situ formation, provide a variety of different techniques which can avoid the drawbacks of other methods, such as manufacturing costs and complexities, but introduce their own difficulties, such as toxicity of solvents [106]. Despite the broad use of these technologies, they

present problems with a lack of particle size uniformity and control of the physical characteristics of the generated particles.

Microfluidic Methods

Microfluidic devices are now routinely used for the production of microparticles and nanoparticles and offer a number of advantages over traditional, macro-sized techniques. Microfluidic systems, by their very nature, utilise minimal quantities of reagents and can achieve faster reaction times when compared with their macro-scale equivalents [110]. Microfluidic systems can also be designed to incorporate many different components, such as pumps, valves, mixers and heaters allowing them to replicate almost any macro-sized experimental setup [15]. As such, these 'lab-on-a-chip' devices can help to both overcome the limitations of macro-sized experimentation and increase manufacturing throughput. Microfluidic approaches to polymeric microparticle and nanoparticle preparation have been shown to produce particles with a high degree of size tunability and uniformity [111], [112]. This is particularly advantageous for the highly regulated pharmaceutical market as a highly uniform product is a good indicator of a fully-controlled process and the fact that the size of a drug-loaded particle is a primary determinant of the drug release kinetics [113]. The use of microfluidic systems in the creation of polymeric particles is generally based upon either emulsion-based or precipitation-based techniques [105].

Single emulsion techniques within microfluidic devices usually involves the injection of discrete droplets of one liquid phase into a second liquid phase using specially designed junction geometries. The two liquids must be immiscible with one another to form an emulsion droplet upon mixing, usually water and a non-water miscible organic solvent are used. The polymer and therapeutic agent can be dissolved into either phase depending upon their hydrophilicity. The three common geometries used are: T-junction, co-flowing and flow-focusing. Fig. 1.4 shows a representation of these three junction geometries. The production of droplets using a T-junction

geometry (Fig 1.4: A) comprises of a continuous phase (the carrier liquid) flowing through the larger capillary and a dispersed phase (the liquid to be dispersed into droplets) flowing through the smaller capillary, perpendicular to the continuous phase [114]. The method of droplet formation in this process is known as perpendicular rupture and is driven by the drag force that the continuous phase exerts on the dispersed phase. Parameters such as flow rates, viscosities and interfacial tension have all been shown to affect droplet formation [115].

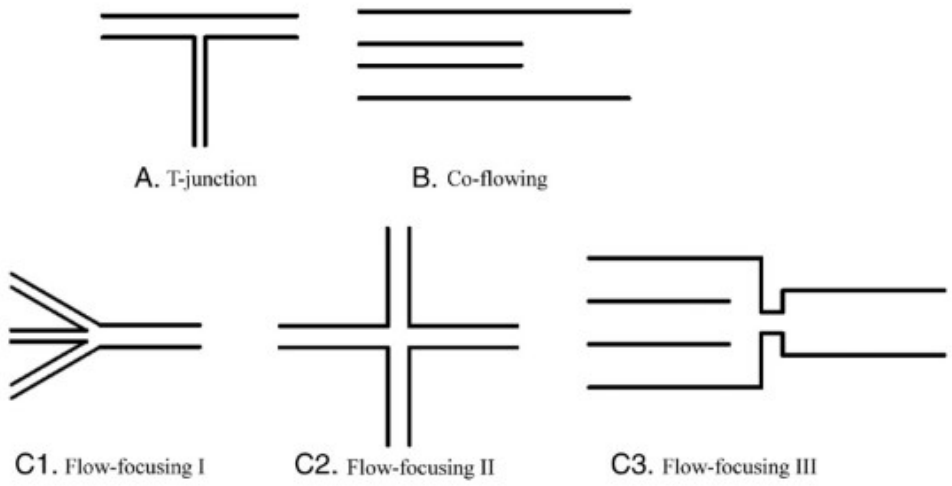

Fig. 1.4: Representation of three common junction geometries. A) T-junction geometry; B) co-flowing geometry; C) three different flow-focusing geometries. Adapted from Zhao, 2013 [23].

In a co-flowing geometry (Fig 1.4: B), the continuous phase is flowing through a larger capillary whilst the immiscible dispersed phase is introduced into the middle of the flow via a smaller capillary or needle. Droplets form due to breakup of the dispersed phase as it enters the continuous phase and can occur either close to the capillary or at the end of an extended jet of liquid. This behaviour is governed primarily by the flow rates of the two liquid phases and the interfacial tension [116].

Flow-focusing geometries have been designed in a variety of configurations (Fig. 1.4: C shows three common configurations), however, the mechanisms of droplet formation are essentially the same [23]. In a flow-focusing system, the dispersed phase flows through a central channel whilst the continuous phase is introduced

through side channels. At the junction of the channels, the dispersed phase is constricted, causing instability and break-up of the flow and producing a controlled droplet formation [81]. Droplets generated in this fashion have been shown to be highly periodic and reproducible, with generation frequencies up to and exceeding 10^4 s^{-1} [117]. Flow rates, viscosities and interfacial tension have all been demonstrated to affect droplet formation [81].

Double and multiple emulsions can be described as "droplets inside droplets" or "emulsions of emulsions" and consist of one or more droplet phases inside a larger droplet, or outer phase, which is then dispersed inside a continuous phase. Double emulsions can either be composed of water-in-oil-in-water (W/O/W) or oil-in-water-in-oil (O/W/O) [118]. In pharmaceutical applications, W/O/W emulsions have long been studied due to the ability of the internal aqueous phase to store water soluble drugs for controlled release and targetable delivery [119], [120]. The preparation of controlled, mono-disperse, double and multiple emulsion droplets has proven challenging using traditional methods, but the introduction of microfluidics has enabled their formation with highly controlled size, structure and composition [23]. In a microfluidics system, double and multiple emulsions are generally formed using either traditional two-step methods or, more recently, complex single-step methods. Two-step methods employ two junction geometries connected together in either a serial or three-dimensional construct, allowing the inner emulsions to be formed at the first geometry and then passing through to the second geometry to form the outer emulsion. Control of characteristics such as droplet size, thickness of the inner layer and number of inner droplets can all be tuned by adjusting the junction geometries and flow rates [121]. Fine control of droplet formation has been further improved by the addition of active components, such as moving walls, within the microfluidic setup [122], [123]. Despite the tunability afforded by these devices there are still limitations to the control of the internal structure of the emulsions

which need addressing [124]. However, the advent of single step methods addressed many of these limitations.

As the name implies, single-step methods utilise only a single step to generate double or multiple emulsions, as opposed to the two junction geometries employed in two-step methods. A number of complex microfluidic devices have been developed to enable one-step production and have been shown to produce highly controlled and tuneable double and multiple emulsions, thus resolving the problems associated with two-step methods [125]. Four such devices are shown in Fig. 1.5. Utada *et el.* fabricated a microcapillary device to generate double emulsions with highly controlled size and internal structure [124] (Fig. 1.5: A). Duncanson *et al.* created a device for producing gas-filled microparticles with tuneable size and structure, allowing for the formation of double emulsions with distinct internal droplets [126] (Fig. 1.5: B). Kim *et al*. introduced a device to produce nanoscale double emulsions with an ultra-thin wall as a middle layer, these structures were very stable and showed great potential for drug encapsulation [127] (Fig. 1.5: C). Finally, Kim and Weitz produced device capable of generating triple emulsion droplets of water-in-oil-in-water-in-oil (W_1-O_2-W_3-O_4) [125] (Fig. 1.5: D).

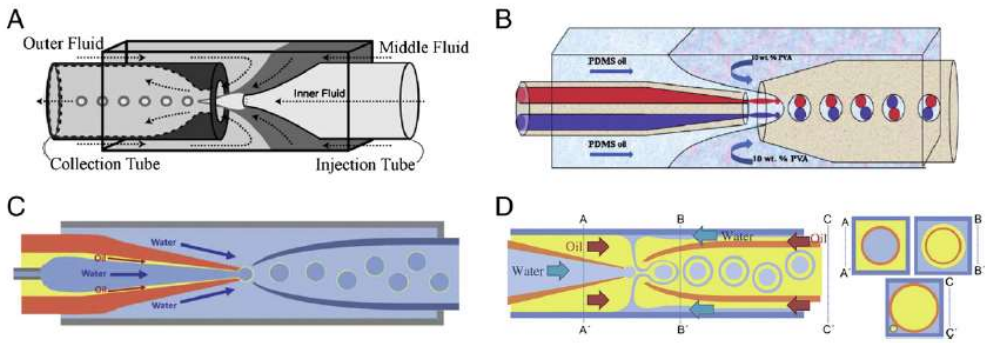

Fig. 1.5: Schematic representation of four microfluidic devices for the preparation of double and multiple emulsions using single-step methods. A: A device to generate double emulsions with highly controlled size and internal structure; B: A device for producing gas-filled microparticles with tuneable size and structure; C: A device to produce nanoscale double emulsions with an ultra-thin wall as a middle layer; D: A device capable of generating triple emulsion droplets of water-in-oil-in-water-in-oil. Adapted from [23].

Precipitation-based techniques

Microfluidic-based nanoprecipitation methods are relatively modern, being pioneered in the late 2000s following work by Karnik and Kolishetti [128], [129]. Microfluidic-based precipitation has many advantages over its macro-scale counterpart as it provides more reproducible, rapid, and easily scalable results and provides a high level of control over the size of the particles produced [108]. The flow properties of the microfluidic channels are of particular relevance in this respect as the flow dynamics produce a laminar flow regime and any mass transfer is dominated by diffusive mixing. In addition, microfluidic systems generally operate under extremely stable conditions, resulting in highly reproducible conditions [130]. Traditional nanoprecipitation methods can suffer from poor uniformity and reproducibility of the resultant particles due to variables such as differences in the flow properties of the phase mixing and the rate at which the organic phase is added to the aqueous phase [108]. These properties can be difficult to control in batch-scale production but under a microfluidic regime, they can be finely tuned and easy to control.

The standard procedure for carrying out microfluidic nanoprecipitation involves the use of a flow-focusing geometry, as described earlier, in which the aqueous phase is introduced via the two side channels and the organic phase via the central channel to produce a stable hydrodynamic focusing flow with a central stream of organic phase surrounded by aqueous phase (Fig. 1.6). The width of the central stream (W_f) can be controlled by altering the flow rates of the streams, which will directly influence the mixing time of the nanoprecipitation process. As mixing time is the primary parameter responsible for the size of the resultant particles, this provides a direct means to control the characteristics of the formulation [130].

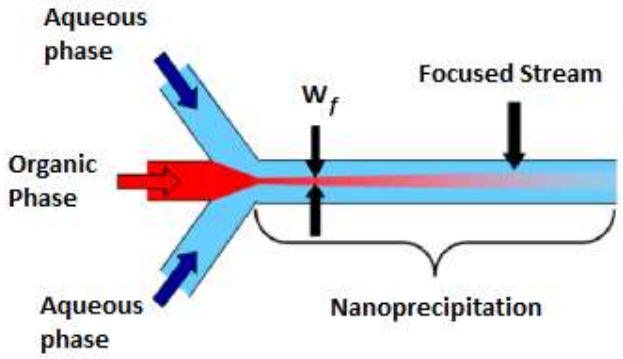

Fig. 1.6: Schematic representation of a nanoprecipitation device using a flow focusing geometry. The aqueous phase is introduced via the two side channels and the organic phase via the central channel to create a focused central stream where nanoprecipitation can take place. The width of the central stream (W_f) can be varied by altering the flow rates of the three streams. Adapted from [130]

Liposome-based delivery systems

Liposomes, also known as lipid vesicles, are spherical biological structures constructed from one or more lipid bilayers. Liposomes self-assemble in an aqueous solution due to the hydrophilic head and hydrophobic tail of the lipid building blocks. They can act as a biological carrier molecule capable of encapsulation of material such as DNA and proteins, and due to their biological nature are intrinsically non-toxic and biodegradable. The use of liposomes as a drug carrier system was first described by Gregoriadis and Ryman in 1971 and has been well documented since [131]. Today there are a broad range of liposome-based therapeutic products available for patients [132]. Since their inception in 1971, liposome-based delivery systems have been used to enable the delivery of aqueous soluble drugs, due to the water filled internal cavity. However, more recently studies have shown that drugs with low aqueous solubility can be solubilised into the lipid bilayer of the molecule [98], [132], [133]. The ability of liposomes to solubilise these materials is particularly exciting as more than 40% of new drugs developed in the pharmaceutical industry are poorly soluble in water [134]. It is important to note that the addition of cholesterol, which has a stabilising effect on liposome

formulations, inhibits the drug loading in the lipid bilayer as it resides in the same space, effectively reducing the 'porosity' of the bilayer [135].

Traditionally, liposomes have been produced using a number of common techniques including extrusion through porous membranes, freeze-drying, double emulsions (W/O/W), and budding, to name a few [136]–[139]. Despite their widespread use, these techniques are known to produce highly heterogeneous samples with poor control and reproducibility with respect to size and lamellarity [140]. In the past decade, microfluidic systems have been developed for the controlled formulation of liposomes and, more recently, techniques have become available for the single-step formation of drug-loaded liposomes [98], [132], [133].

In a review of microfluidic methods for the formation of liposomes van Swaay and deMello described eight distinct techniques [141]: electroformation and hydration, extrusion, flow-focusing, pulsed jetting, double emulsion templates, ice droplet hydration, transient membrane ejection and droplet emulsion transfer [18]–[20], [140], [142]–[145]. Each of these techniques presents unique advantages and disadvantages but for the field of drug delivery only the flow-focusing technique has been shown to produce drug encapsulated liposomes in a continuous flow system with a high degree of encapsulation efficiency [83].

The hydrodynamic flow-focusing approach was first described in 2004 [140]. Using this technique, the research group was able to reproducibly formulate liposomes with a mean diameter of 50 – 150 nm and relative standard deviations of <10% for smaller vesicles and <20% for larger vesicles. This is notable for drug delivery as particles at the lower end of this range experience reduced opsonisation in the bloodstream [146]. This technique relies upon microfluidic flow-focusing geometries, similar to those used in emulsion-based techniques, for the formation of polymer particles. Fig. 1.7 shows optical micrographs of the two flow-focusing geometries used along with a schematic representation of the flow characteristics generated. In both methods, lipids were first dissolved in propan-2-ol (isopropyl

alcohol, IPA) and introduced via the centre channel and PBS solution was introduced via the two side channels. With optimised flow rates, this method produces a focused stream of lipid solution in a central channel surrounded by the aqueous phase (PBS). Due to the low Reynolds numbers associated with microfluidic devices, laminar flow conditions are experienced and the mixing of the two miscible phases is governed by molecular diffusion at the liquid-liquid interface, diluting the alcohol concentration below the solubility limit of the lipids and initiating liposome self-assembly [83]. The size of the liposomes produced by this method can be finely tuned by changing the ratio between the flow rates of the aqueous buffer and organic phase, the concentration of lipid molecules in the organic phase, or by adapting the channel geometry.

In the past few years, another exciting microfluidic technology has been reported which utilises a chaotic advection mixing profile to formulate drug encapsulated liposomes with sizes varying between 50 – 450 nm and a high level of encapsulation efficiency [98], [132], [133]. This technique is based upon the nanoprecipitation model and makes use of a commercially available, 'lab-on-a-chip' device known as a staggered herringbone mixer. A staggered herringbone mixer is characterised by asymmetric ridges, known as 'herringbones', etched into the floor of a channel (Fig. 1.8). It has been demonstrated that this design will create a chaotic flow even with the low Reynolds numbers encountered within microfluidic channels [147]. This is achieved by disrupting the laminar flow conditions and inducing a rotational flow, which acts to wrap the fluids around each other [148].

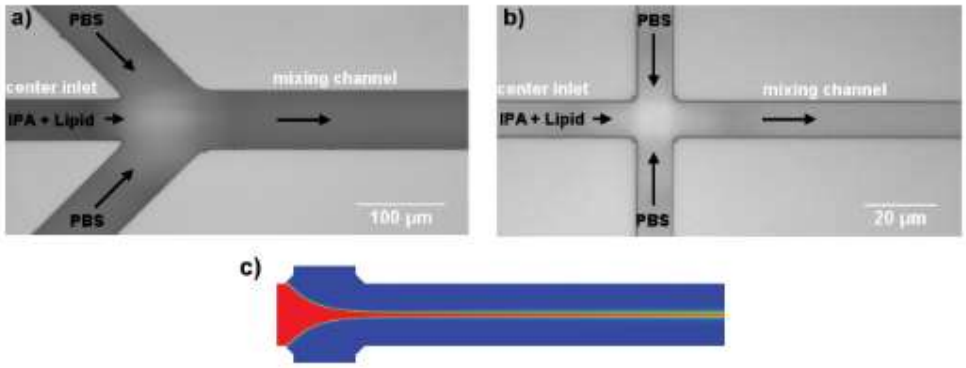

Fig. 1.7: Optical micrographs of the two flow-focusing geometries and a representation of the flow characteristics generated using the hydrodynamic flow focusing technique. a) Flow-focusing geometry with a smaller central inlet channel and two larger side channels entering at an acute angle. b) Flow-focusing geometry with a 4-way cross formation, all inlet channels have an equal diameter and the two side channels enter at right angles. c) A representation of the flow characteristics observed when using the 4-way cross geometry. The IPA + Lipid flow is tightly focused into a central stream with no evidence of widening. Adapted from [146].

The technique involves the introduction of two fluid streams into the staggered herringbone mixer device. A water-miscible solvent phase (containing lipids and any molecules to be encapsulated) and an aqueous phase. The two phases meet at a Y-junction and achieve laminar flow conditions before passing through the staggered herringbone mixer chamber. Within the mixing chamber, the two streams enter a chaotic mixing environment where the solvent phase is diluted below the lipid solubility limit and liposome self-assembly is initiated.

Fig 1.8: A schematic of a staggered herringbone mixer chamber showing the asymmetric herringbone ridges. Adapted from [135].

Kastner *et al*. used this device to successfully produce liposome nanoparticles drug-loaded with a poorly water-soluble drug, propofol [135]. The liposomes produced

had a diameter varying between 40 – 450 nm which could be accurately controlled by changing the flow rate ratio. Flow rate ratios of 1:1 produced the biggest liposomes and increasing the flow rate of the aqueous phase produced smaller liposomes. However, it was noted that smaller liposomes displayed increased polydispersity. Increasing the total flow rate, whilst maintaining the flow rate ratio, was shown to have no effect on the size of the liposomes, thus showing the potential of this technology for high-throughput, bulk manufacturing. When the low solubility drug was added to the system an encapsulation of approximately 50% was observed at a concentration of 1 mg/mL in liposomes of varying sizes. This is significantly higher than the drug loading seen when using other techniques [135].

One outstanding issue for the use of this technology in a manufacturing environment is purification of the finished product. This can be easily achieved by filtration or ultra-centrifugation, but these techniques do not lend themselves to high-throughput, continuous flow manufacturing. Dimov *et al.* presented a novel lab-on-a-chip device which incorporated both a staggered herringbone mixer and tangential flow-filtration device [98]. This device was able to generate purified liposomal products in less than four minutes and facilitated the purification of a range of formulations with changeable membranes. This modular approach to microfluidics holds great value and could lead to a new wave of microfluidic devices able to be configured to carry out a wide range of functions.

Chapter 2

Materials and Methods

This chapter collates and discusses the materials, equipment and methods used in the completion of this work. This chapter contains details of materials and methods that are used in multiple chapters throughout the thesis to avoid repetition, some methods that are only used in a single chapter may be described separately within that chapter. Information on the proteins, solvents and other chemicals used can be found in the Materials section. The Methods section is split into multiple sub-sections discussing the equipment and techniques used throughout this report. The first sub-section details the techniques used to prepare protein solutions. The second sub-section details techniques used to prepare CCP microparticles. The third sub-section discusses techniques used for the characterisation of CCP microparticles, including imaging techniques along with particle size and distribution measurements. The fourth sub-section discusses the techniques used to analyse protein formulations after rehydration. Finally, the last sub-section details the statistical analyses used within this thesis.

2.1 Materials

Proteins

Native BSA (i.e., BSA in solution that had never been dehydrated to a solid form) was purchased as a 35% solution in sodium chloride and native HSA was purchased as a 20% solution in sodium chloride, both from Merck Life Sciences. BSA, HSA, lysozyme, horseradish peroxidase, catalase and glucose oxidase lyophilised powders were also purchased from Merck Life Sciences. Insulin lyophilised powder was purchased from Sigma. HSA Prime and HSA Elite formulations were provided by Albumedix Ltd. as aqueous solutions at 300 mg/mL and 150 mg/mL respectively.

These two HSA formulations are proprietary products of Albumedix Ltd. and no further details were provided.

Solvents

2-methyl-1-propanol, pentanol, benzyl alcohol, methyl acetate, heptanol, 4-methyl-2-pentanol, octanol, decanol, ethyl acetate and 2-ethyl-1-hexanol were purchased from Sigma, Fisher Scientific and VWR at ACS reagent grade. All solvents were stored in glass vials over 4Å molecular sieve for at least one week prior to usage to remove any bound water. Ultra-pure deionised water (dH_2O) was obtained from the laboratory water supply consisting of a large water de-ionising system and a secondary system for further purification and polishing.

Other chemicals/reagents

Guanidine hydrochloride (GdnHCl) solution was purchased from Sigma at 8M, pH 8.5 in aqueous buffer and used as received. PBS tablets were purchased from Sigma and made into solution as per the manufacturer directions. Hexamethyldisilazane was purchased from Merck Life Sciences at ≥ 97.0% purity. Dilute hydrochloric acid was obtained from laboratory stocks (originally purchased from Fisher Scientific). Molecular sieves (4Å) were purchased from VWR and were heated to 200°C overnight in a vacuum oven prior to use to activate the sieves.

2.2 Methods

2.2.1 Sample Preparation Techniques

Protein Solution Preparation

BSA, HSA and lysozyme solutions were prepared directly in dH_2O. The required mass of lyophilised protein was weighed out in a 20 mL vial and the required volume of dH_2O was pipetted carefully into the vial. Vials were then left to stand until the protein powder had fully dissolved. Peroxidase, catalase and glucose oxidase solutions were prepared in 0.1 M phosphate buffer prepared from dissolvable PBS tablets; protein dissolution was carried out in the same manner as above. Insulin solutions were prepared in dH_2O and adjusted to pH2 with dilute hydrochloric acid.

The pH of the solution was measured using a desktop pH probe, dissolution was carried out in the same manner as above. For proteins supplied in solution, samples were prepared at the desired concentration by dilution with dH_2O. Protein solutions were prepared and used on the same day and were not stored for later use.

If the protein concentration was required to be known more accurately then the sample concentration was measured using a NanoDrop 2000 UV-Vis Spectrophotometer (Thermo Fisher Scientific) using the Protein A280 method that comes built into the instrument software (NanoDrop 2000 Operating Software, version 1.6.198). This method calculates the protein concentration using known values for the measured absorbance, the extinction coefficient of the protein and the pathlength of the sample.

Denatured Protein Solutions

BSA and HSA samples were also prepared and purposefully denatured to act as negative controls when studying protein structure. Protein solutions were prepared as described above and were then added to a volume of 8M GdnHCl to give a 4:1 ratio (GDnHCl:protein solution). Mixtures were then sealed and covered with aluminium foil to block sunlight and left in a vial shaker overnight. GdnHCl is a strong denaturant and functions as a chaotropic agent, capable of disrupting hydrogen bonds with aqueous solutions and weakening the hydrophobic effect, a key driver of protein folding [149].

2.2.2 CCP Techniques

Single Particle Technique

To study the CCP process in detail, a dual-micropipette system was used as described by Utoft [150]. The technique relies upon the use of two handcrafted glass micropipettes with an opening of approximately 5 µm. The micropipettes were prepared from 6” glass capillaries with internal diameter of 0.4 mm. A pipette puller (Sutter Instrument Co., P-97) was used to heat the capillary in the centre and pull it apart to create two long tapered pipettes. The capillary was then mounted into a

micromanipulator and introduced to a micro forge (Narishige, MF-830). The focusing and micropipette placement were adjusted until both the forge bead and the micropipette were in focus. The forge bead was then heated until melting, and the pipette was moved inside the molten glass. The heating was then removed to allow the glass bead to cool and harden. The pipette holder was then gently tapped until the pipette "broke" off. If this produced a pipette with a rough edge, then this could be smoothed by re-heating the forge bead and gently moving the rough edges into the molten bead. After cooling, the pipette would break off with smooth edges.

After preparing a pair of glass micropipettes the surface was modified with hexamethyldisilazane, to provide a hydrophobic surface. This avoided the spreading of aqueous media over the hydrophilic glass surface of the micropipette. 2-3 drops of hexamethyldisilazane were placed into a 1 mL HPLC vials and the non-tapered ends of the pipette were pushed through the septum and suspended (tapered end down) inside the vial with the lid tightly sealed. Vials were left overnight for vapor coating. The hexamethyldisilazane evaporated within the vial and interacted with the alcohols of the glass surface to produce a hydrophobic surface in a process known as silanization, as shown in in figure 2.1.

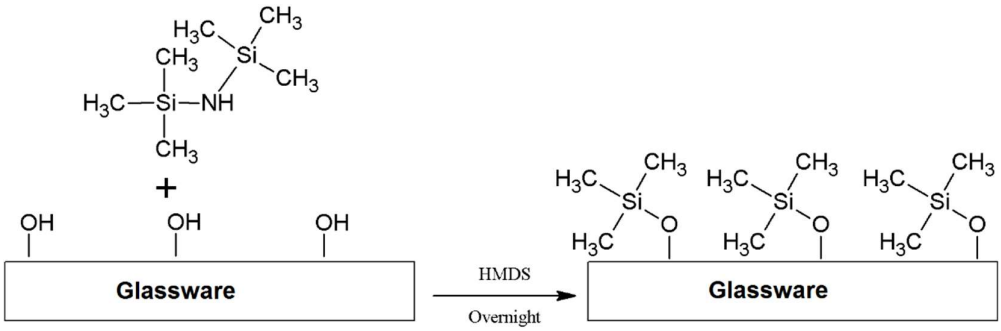

Fig 2.1: Schematic of the silanization process showing hexamethyldisilazane binding to the hydrophilic surface of the glass to form a hydrophobic surface. From [150].

With the micropipettes prepared the experimental setup could be completed. A glass chamber with an opening on either end was held in place on a microscope stage (Axiovert 100) and filled with pentanol. The pentanol was held within the chamber

by surface tension. One micropipette was filled with aqueous protein solution and the other was left empty. Both pipettes were placed into micromanipulators, one either side of the microscope, and manoeuvred into the glass chamber (Fig. 2.2). The microscope focusing and position of the micropipettes were adjusted until both micropipettes were in focus in the centre of the glass chamber.

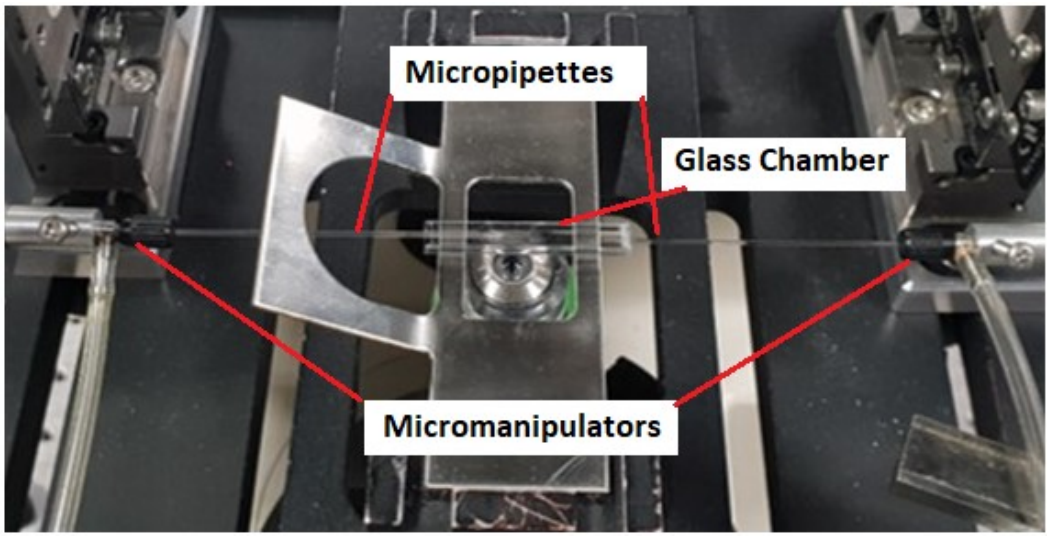

Fig 2.2: Experimental setup for the single particle technique.

With the micropipettes in position, a single droplet of aqueous protein solution was pushed out of the filled micropipette via the use of a 10 mL plastic pipette attached via tubing to the back of the micropipette (Fig. 2.3). The second micropipette was then used to remove the droplet from the first via the application of mild vacuum pressure via a second 10 mL pipette. The droplet was transferred to the second pipette to remove it from the aqueous source within the first pipette. This removed the possibility of protein solution flowing into and out of the droplet. With the droplet attached to the second pipette the process of CCP could be observed and recorded using a digital camera (Allied Vision Technologies, Pike) attached to the microscope and controlled using a customised version of the Labview software.

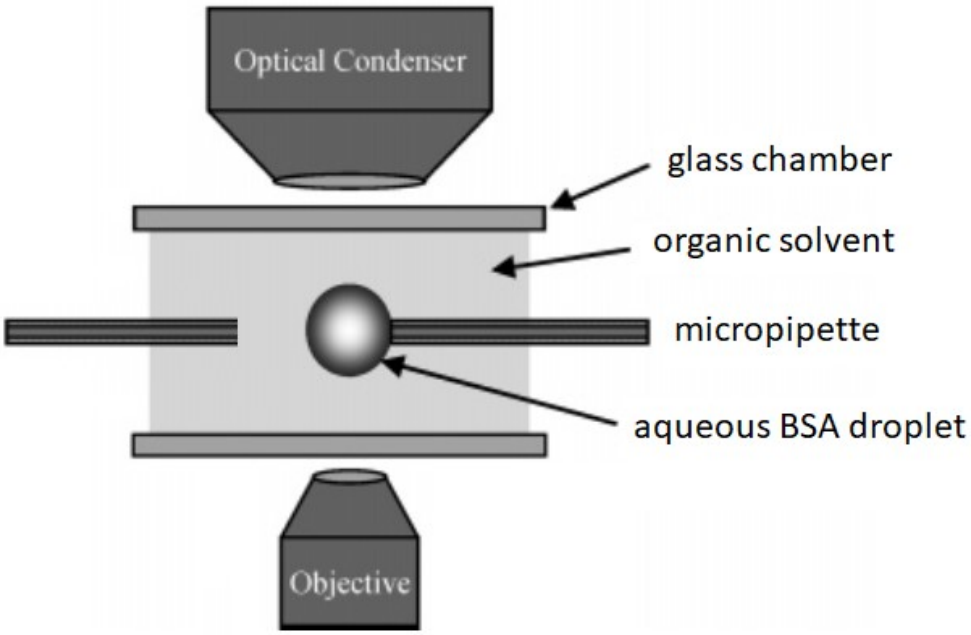

Fig. 2.3: Schematic of the micropipette system used for single particle studies. The left-hand micropipette contains aqueous solution and an aqueous droplet is formed through the application of pressure. The right-hand micropipette is then used to remove the droplet from the aqueous solution source through the application of a weak vacuum. The water within the droplet then dissolves into the surrounding medium and dehydration of the droplet takes place. Image adapted from [151]

Small Scale Vortex Mixing Technique

Aqueous protein solutions were prepared as described and 50 µL of the aqueous solution were added to 1 mL of pentanol in a 1.5 mL microcentrifuge tube. The fluid mixture was vortex mixed at maximum mixing speed for one minute to form a dispersion of aqueous droplets within the organic solvent and allow the CCP process to complete. Samples were then centrifuged at 10,000 rpm for one minute in a microcentrifuge and the supernatant was removed and retained for drying and re-use. Samples were vortex mixed again to resuspend the particulate material in a slurry before being placed under vacuum overnight to evaporate off the residual solvent. A process schematic can be seen in figure 2.4.

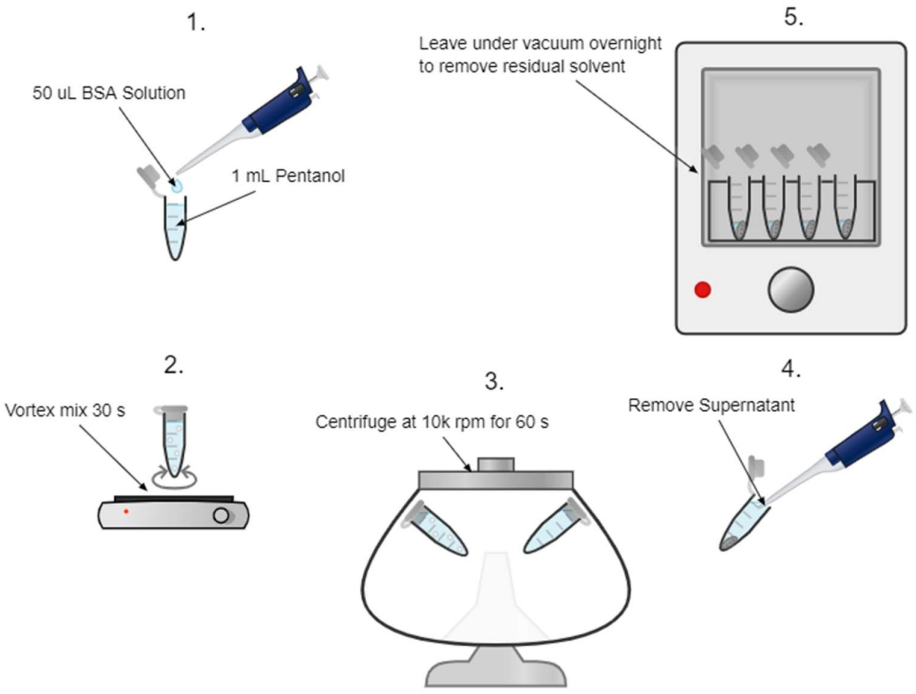

Fig 2.4: Illustration of the 5 steps to producing CCP BSA microparticles. 1. 50 µL of aqueous BSA solution is added to 1 mL of dried pentanol. 2. The fluid mixture is vortex mixed for 1 minute to disperse the aqueous solution throughout the pentanol as droplets and keep them suspended whilst the dehydration process completes. 3. The sample is centrifuged at 10,000 rpm for 1 minute to pelletise the microparticles. 4. The supernatant is removed to leave only residual solvent. 5: The sample is stored under vacuum over night to remove residual solvent, leaving a dried microparticle powder.

Batch Scale Up Techniques

Aqueous protein solutions were prepared as described and 5 mL of the aqueous solution were added to 100 mL of pentanol in a 250 mL glass beaker. The fluid mixture was mixed at high speed using either an overhead stirrer or overhead homogeniser for one minute to form a dispersion of aqueous droplets within the organic solvent and allow the CCP process to complete. Samples were then transferred to 50 mL centrifuge tubes and centrifuged at 6,000 rpm for one minute, the supernatant was removed and retained for drying and re-use. Samples were then vortex mixed to resuspend the particulate material in a slurry before being placed under vacuum overnight to evaporate off the residual solvent.

Single Flow Technique

Aqueous protein solutions were prepared as described above and loaded into a 10 mL syringe placed in a syringe pump. A length of FEP tubing with internal diameter of 250 μm was connected to the syringe, with the other end of the tubing placed into a pentanol reservoir. The tubing was suspended as necessary, and a luer-lock ferrule was fitted over the tube ending to ensure it was held away from the side of the reservoir receptacle and droplets did not adhere to the side of the glass vial. Figure 2.5 shows the experimental setup for this technique.

Fig. 2.5: Experimental setup for the single flow continuous production method. Aqueous protein solution was pumped through a single piece of FEP tubing directly into the stirred solvent reservoir.

The syringe pump was set at the desired flow rate causing the protein solution to travel through the tubing to form an aqueous droplet at the terminus. The droplet would grow as the aqueous phase flow continued and would eventually break off from the tubing into the solvent reservoir which was stirred using either an overhead stirrer or magnetic stirrer and bead. The stirring action suspended the droplet in the solvent reservoir, enabling the droplet to undergo the CCP process. After a predefined length of time, the aqueous flow was stopped and the tubing removed from the reservoir. The reservoir would then be either covered and left for the suspended microparticles to fall to the bottom of the container or transferred to 50

mL centrifuge tubes and centrifuged at 6,000 rpm for 1 minute. The supernatant was removed, and any residual solvent was removed under vacuum overnight.

Flow Focusing Microfluidics

Aqueous protein solutions were prepared as described above and loaded into a 10 mL syringe to act as the dispersed phase. The drying solvent (pentanol unless otherwise stated) was loaded into two further 10 mL syringes to act as the continuous phase. A length of FEP tubing with internal diameter of 250 μm was connected to each syringe, whilst the other ends of tubing were connected to the inlet ports on a 3D Flow Focusing microfluidic chip (Dolomite Microfluidics) with 100 μm channel diameter and a hydrophobic coating on the channel walls. A fourth piece of tubing was then connected to the outlet port of the microfluidic chip and terminated in the solvent reservoir. Tubing was connected via the H Interface and linear connectors (Dolomite Microfluidics). The tubing was suspended as necessary to ensure it was held away from the side of the reservoir receptacle so that droplets did not adhere to the side of the glass vial. Figure 2.6 shows the experimental setup for this technique.

The Microfluidic chip was placed on the stage of an inverted microscope (Nikon Instruments, Eclipse Ti-U), controlled by the Nikon Elements AR software (v 4.60.00 (Build 1171)), allowing for observation of droplet formation at the flow focusing junction using a digital camera (QImaging, OptiMOS). Syringes were placed on syringe drivers and flow rates were then set individually for the continuous phase (two inlets with the same flow rate) and dispersed phase. Flow rates were varied to enable the generation of dispersed phase droplets at the chip junction which then flowed along the outlet tubing and into a stirred reservoir of drying solvent. After a predefined length of time, both flows would be stopped, and the tubing removed from the reservoir. The reservoir would then be either covered and left for the suspended microparticles to fall to the bottom of the container or transferred to 50

mL centrifuge tubes and centrifuged at 6,000 rpm for 1 minute. The supernatant was removed, and any residual solvent was removed under vacuum overnight.

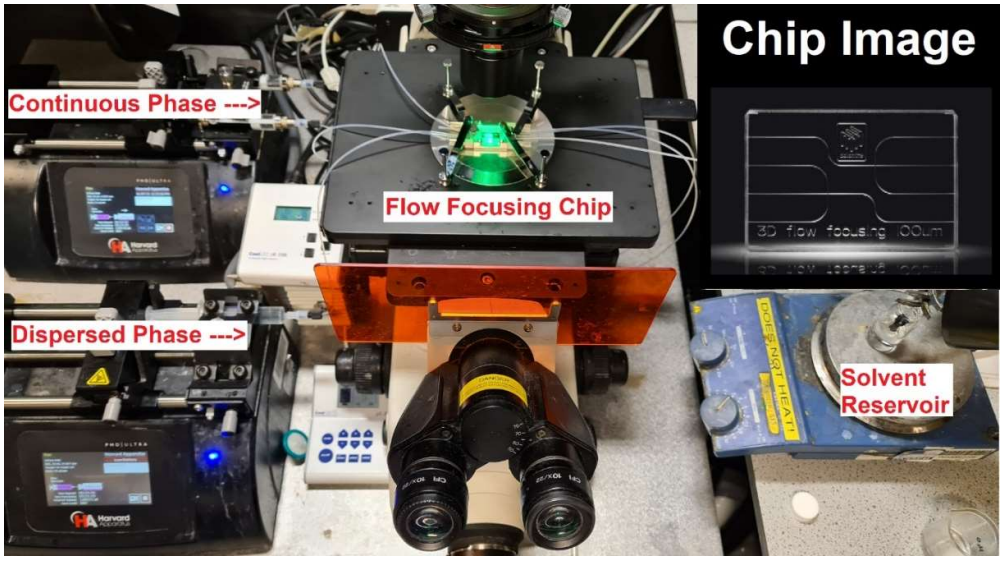

Fig 2.6: Experimental setup for the microfluidic flow focusing method. Aqueous protein solution flowed into the central inlet channel, and drying solvent flowed into the two outer inlet channels. Droplets of dispersed phase were formed at the flow focusing junction which then travelled to the stirred reservoir where the CCP process could occur.

T-reactor Technique

Aqueous protein solutions were prepared as described above and loaded into a 10 mL syringe (dispersed phase). The drying solvent was loaded into a second 10 mL syringe (continuous phase). A length of FEP tubing with internal diameter 250 μm, was connected to each syringe and both syringes were loaded into syringe pumps. The ends of the two lengths of tubing were connected to perpendicular ports on a PTFE T-junction. A third piece of tubing was then connected to the remaining port on the T-junction and terminated in the solvent reservoir. The tubing was suspended as necessary to ensure it was held away from the side of the reservoir receptacle so that droplets did not adhere to the side of the glass vial. (Fig. 2.7).

Flow rates were set individually for the continuous phase and dispersed phase and were varied to enable the generation of aqueous droplets within the T-junction. The aqueous phase then travelled along the outlet tubing as discrete droplets within the

continuous phase. The droplets flowed into a stirred reservoir of drying solvent, where the CCP process could take place. After a predefined length of time, both flows would be stopped, and the tubing removed from the reservoir. The reservoir would then be either covered and left for the suspended microparticles to fall to the bottom of the container or transferred to a 50 mL centrifuge tube and centrifuged at 6,000 rpm for 1 minute. The supernatant was removed, and any residual solvent was removed under vacuum overnight.

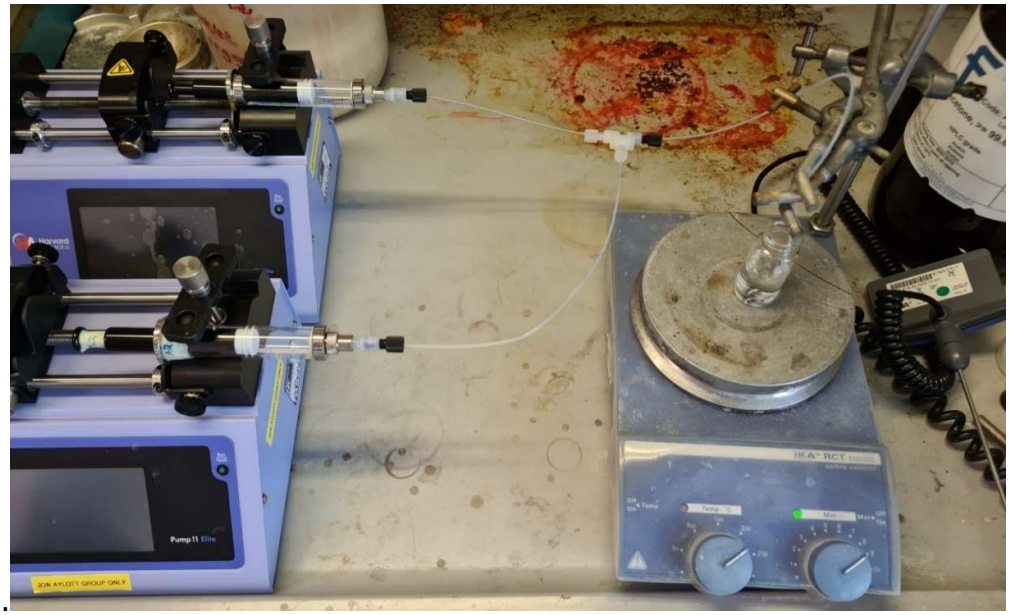

Fig 2.7: Experimental setup for the dual flow continuous production method. Aqueous protein solution (bottom pump) and pentanol (top pump) were flowed into the T-connector where aqueous droplets were formed and travelled into the stirred solvent reservoir via the outlet tubing.

Reservoir Designs

Stirred Reservoir

The stirred reservoir was used with the continuous flow systems described above to act as the drying solvent reservoir for the CCP process to take place. The stirred reservoir consisted of either 10 mL of pentanol in a 20 mL scintillation vials stirred by a magnetic bead, or 100 mL of pentanol in a 250 mL beaker stirred by an overhead stirrer. The stirring action worked to suspend the aqueous droplets within the reservoir whilst the CCP process could take place (Fig. 2.8 Left).

Unstirred Reservoir (Solvent Drop Technique)

The unstirred reservoir was used with the continuous flow systems described above to act as the drying solvent reservoir for the CCP process to take place. The reservoir consisted of 100 mL pentanol within a 100 mL measuring cylinder with no stirring. The aqueous droplets formed in the continuous flow systems entered to reservoir and fell through the tall reservoir whilst the droplets dehydrated and the CCP process finished before the droplets reached the bottom of the vessel (Fig. 2.8 Right).

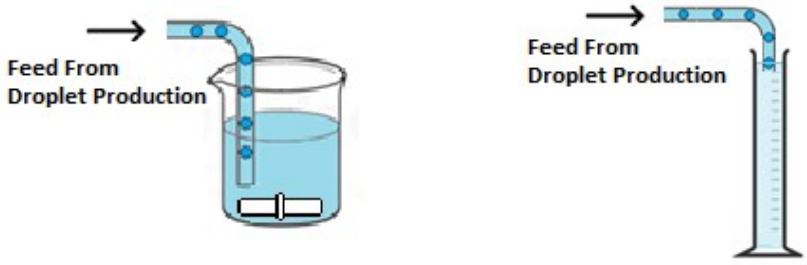

Fig. 2.8: Diagrams showing the two reservoir designs used with the continuous flow production techniques. (Left) The stirred vessel reservoir which uses the stirring action to suspend the aqueous droplets with the CCP process completes. (Right) The unstirred reservoir which allows the aqueous droplets to fall through a column of solvent with the CCP process completes.

2.2.3 Particle Analysis Techniques

Digital Imaging

All non-microscopic digital images were obtained using a smart phone camera (Galaxy S20+, Samsung). If a scale bar were required, this would be supplied by use of a 30 cm rule at held at the edge of the image.

Brightfield Microscopy

Microparticle samples for brightfield microscopy were taken immediately after the CCP process had completed and before centrifugation of the sample. 20 µL aliquots were placed onto clean microscope slides which were then covered with a non-airtight covering and left to dry overnight under a fume hood. Once dried, samples were observed using an inverted Nikon Eclipse Ti-U microscope with a motorised

stage and a CoolLED pE-100 brightfield light source. The microscope was controlled by a PC running the Nikon Elements AR software. Images were obtained using the QImaging OptiMOS camera at 4x magnification in a 3x3 grid and stitched together with a 15% overlap to create a large, high-resolution image showing a large portion of the dried sample. Images were also obtained at 20x magnification using a random movements function within a defined radius. Images shown in the thesis main body are representative images only with the full image repository found online.

Scanning Electron Microscopy (SEM)

Microparticle samples for SEM imaging were taken immediately after the CCP process had completed and before centrifugation of the sample. 20 µL aliquots were placed onto a SEM stub which had been pre-prepared with the attachment of a circular glass cover slip. Samples were covered with a non-airtight covering and left to dry overnight under a fume hood. Once dried the samples were first prepared for SEM analysis by sputter coating with gold at 2.2 mA for 75 seconds to produce a coating of approximately 15 nm (SEM Coating Unit PS3). Samples were then placed into the SEM chamber of a JEOL 6060LV SEM and observed at a working distance of 30 mm with an operating voltage of 5 kV and a spot size of 45 nm. Images shown in the thesis main body are representative images only with the full image repository found online.

Image-based Particle Sizing

Image-based particle sizing was carried out on both bright field light microscopy and SEM images using the Fiji image processing package [152]. Many images were obtained using these techniques and so images were selected both as representative samples and to provide the optimum imaging parameters for the sizing procedure. This involved selecting images with minimal particle overlap to allow for measuring algorithms to identify and measure particles. Where possible, multiple images were selected from each sample to increase the particle count. Figure 2.9 shows the sizing process on a single brightfield image. First a

thresholding process was applied to the images to allow for digital processing, thresholding algorithm was chosen manually although the default algorithm was most often used. Next, a Find Edges process was applied to the image which generated an image of the particle outlines, this was followed by a Hough Circle Transform [153] with a minimum search radius of 6 pixels. A minimum value of 6 pixels was applied as values below this would find continuous overlapping circles within the lines produced by the Find Edges process (Fig. 2.10). The Hough Circle Transform would identify circles found within the image and automatically measure the circle diameter.

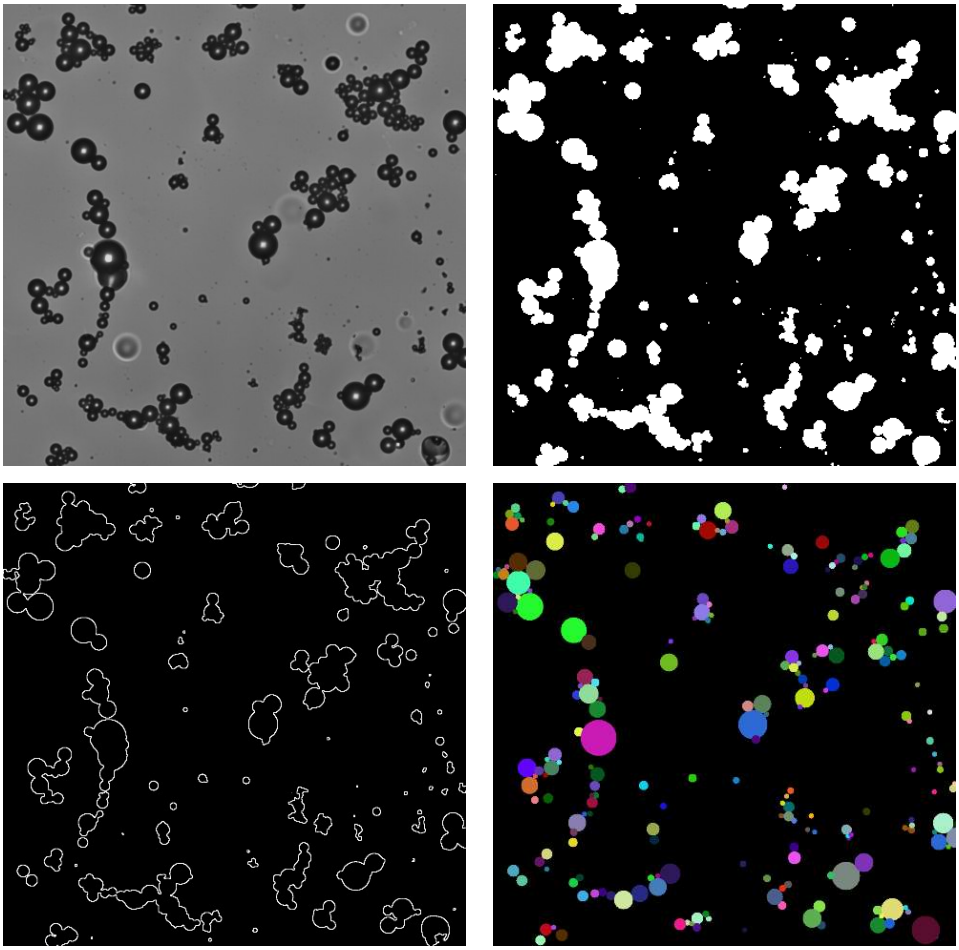

Fig. 2.9: Image processing using Fiji to identify and size particles in a brightfield microscope image. (Top Left): Raw image before any processing. (Top Right): Image after application of a thresholding process. (Bottom Left): A Find Edges process is applied to show particle outlines. (Bottom Right) Output from Hough Circle Transform, all coloured circles were found by the algorithm and are automatically measured.

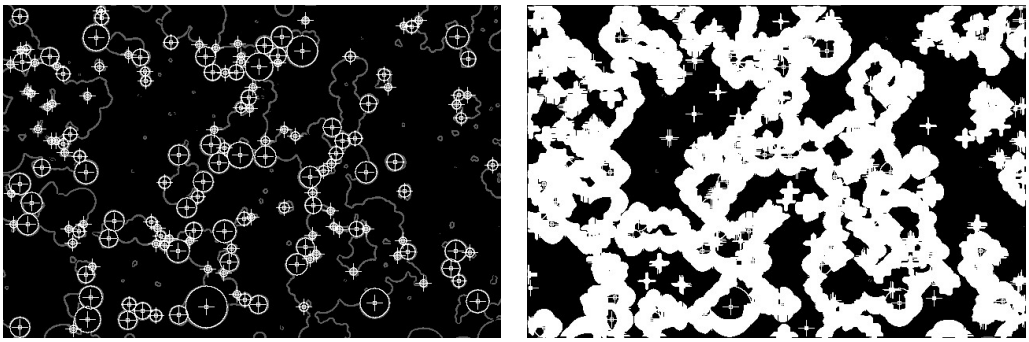

Fig. 2.10: (Left) Hough Circle Transform results showing identified circles overlaid on the processed sample image, minimum radius set to 6 pixels. (Right) The same image with minimum radius set to 5 pixels, this image shows continuous overlapping chains of circles identified within the lines of the image.

Laser Diffraction

Laser Diffraction particle sizing was carried out using the Horiba Partica LA-960 Laser Diffraction Particle Sizer connected to a PC running the LA-960 software package (v 8.10) and equipped with a fraction cell (a 10 mL quartz cuvette designed for use in the instrument). First, 10 mL of pentanol was added to the fraction cell, this was carried out within a fumehood and the cell was covered with parafilm to minimise evaporation and exposure to pentanol vapour. The blank pentanol in the fraction cell was placed into the instrument and the background measurement was taken. Next, samples were concentrated within the solvent reservoir by centrifugation and removal of the supernatant. The concentrated protein microparticle suspension was then added to the fraction cell in 1 mL aliquots and stirring was enabled and adjusted to provide a homogenous suspension within the cell. The laser absorbance measurements were observed on the software panel and 1 mL aliquots of the microparticle sample continued to be added until the absorbance measurements were within the optimal range (as shown in the software) at which point particle size was measured by the instrument.

Laser diffraction particle sizing is distinct from image-based particle sizing as it does not rely on the analysis of microscopic images. Instead, laser diffraction works by measuring the scatter of a laser beam from interactions with a particle. Larger particles will scatter the laser at a larger angle, and these scatterings can be

measured and analysed to provide a particle size distribution. As this technique is not dependent upon particle images, errors due to the Hough Circle Transform or image resolution are not an issue, furthermore the technique can measure an entire sample in one run and is not restricted to the measurement of sampled particles. However, errors can be introduced to the measurement from the use of an incorrect refractive index or by the sample containing too few or too many particles. Too few particles in the sample results in too few scattered photons to achieve a reliable reading. Too many particles in the sample results in too many photons experiencing multiple scattering events after interacting with multiple particles. These potential errors are minimised by calculating an estimate of the refractive index and by slowly adding sample 1 mL at a time to ensure the photon transmission value remains at the optimum value.

2.2.4 Protein Analysis Techniques

Fluorescence Spectroscopy

Fluorescence Spectroscopy can be used to study the tertiary structure of a protein due to the intrinsic fluorescence properties of the tryptophan (Trp) amino acid residue. Protein samples were prepared at 2 mg/mL in the same solvent as the original protein solution was prepared in and transferred to a 1.0 cm pathlength quartz cuvette. Fluorescence spectra were measured using an Agilent CaryEclipse Spectrometer (Scan software v1.2(147)) with slit widths set at 5 nm. Emissions scans of the samples were recorded between 300-400 nm with an excitation wavelength of 295 nm. Results processing, including spectral smoothing, averaging and normalisation were carried out using the SpectraGryph software (v1.2.15.3) [154].

Fluorescence spectroscopy can be used in this manner due to the intrinsic fluorescence properties of the amino acid residues tryptophan (Trp), tyrosine (Tyr) and phenylalanine (Phe). Trp is the most commonly used residue for intrinsic fluorescence analysis due to both the high quantum yield of proteins obtained during

fluorescence analysis and its sensitivity to changes in the local environment [155]. Trp excitation is achieved using an excitation wavelength of 295 nm. Figure 2.11 shows diagrams of both HSA and BSA with each Trp residue highlighted. Both HSA and BSA contain a single Trp residue buried deep within the protein structure (Trp-214 and Trp-212, respectively) and so when a molecule of HSA or BSA undergoes a conformational change, such as a denaturation event, the unfolding of the molecule can cause the environment around the inner Trp residue to become more hydrophilic as the inner residues are exposed to the aqueous environment [156]. Due to the sensitivity of Trp fluorescence to changes in the local environment this will cause a redshift in the peak emission wavelength due to solvent quenching effects [13], allowing the intrinsic Trp fluorescence to be used as an optical probe to analyse any structural changes to the protein.

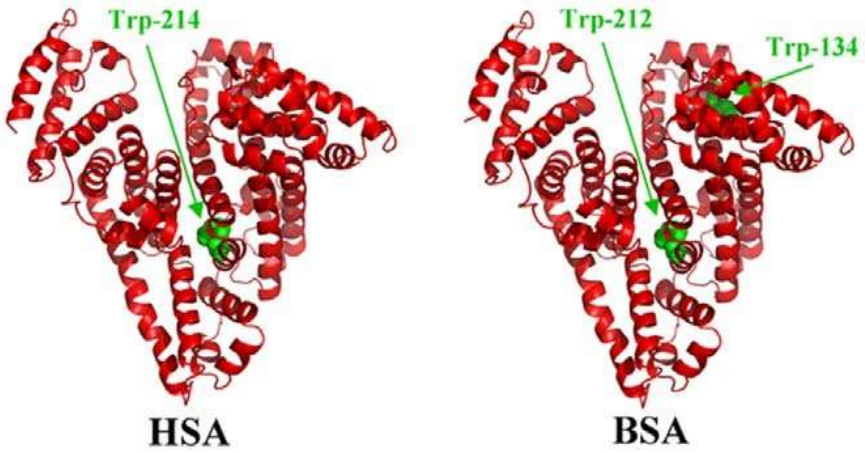

Fig. 2.11: 3-dimensional diagram of the tertiary structure of HSA and BSA showing the location of tryptophan residues within the protein. Adapted from: [157]

Fluorescence analysis of Tyr and Phe residues is less commonly used due to fluorescence quenching caused by ionisation of the Tyr residues by adjacent residues[158] or the transfer of excitation energy to Trp residues [159]. Tyr residues are more abundant then Trp in both HSA and BSA, with the proteins containing 17 and 21 Tyr residues, respectively, which are distributed along the polypeptide chain [160], [161]. This makes Tyr fluorescence less sensitive than Trp

fluorescence to conformational changes in the protein structure. However, several studies have demonstrated that protein denaturation may lead to an increase in the intensity of Tyr fluorescence due to the structural changes brought about by denaturation leading to a reduction in the quenching mechanisms mentioned above [162]–[165]. Throughout this work, Trp excitation was achieved using an excitation wavelength of 295 nm

Fourier-Transform Infrared Spectroscopy (FT-IR)

FT-IR spectroscopy can be used to interrogate the secondary structure of a protein by observation of the Amide I vibrational band. Dehydrated protein samples were rehydrated to 50 mg/mL in the same solvent as the original protein solution was prepared in. 20 µL samples were analysed using an Agilent Cary630 FT-IR spectrometer fitted with a 3-bounce diamond ATR sampling accessory and controlled by MicroLab PC version 5.6.2135.

FTIR-ATR analysis was carried out with 256 scans at a resolution of 4 cm^{-1} and a zero-fill factor of 4 as per the method published by the Shimadzu Corporation [166] and a background spectrum was automatically subtracted from each sample spectrum. Spectrum manipulation was carried out using SpectraGryph software and curve-fitting was carried out using a custom designed Microsoft Excel worksheet.

To prepare the data for curve-fitting, the protocol by Dong *et al*. was followed [167], [168]. First, a scaled subtraction of water was carried out on the sample spectrum to create a resultant spectrum with a straight baseline between 1800-2200 cm^{-1}. The Amide I peak, found between 1600-1700 cm^{-1}, was isolated, a linear baseline applied and the spectra normalised for peak height. The second derivative spectra were then calculated and smoothed using a Savitzky-Golay algorithm and then inverted by division by -1. The spectra were then baselined using an adaptive baseline algorithm and normalised to peak height.

For curve-fitting of the Amide I band, the 2nd derivative spectra were loaded into the custom curve-fitting spreadsheet (Fig. 2.12). The Amide I peak spectra (experimental data) were loaded into Section 1, the third column then calculated normalised data which was plotted on the chart in the centre of the spreadsheet. The peak values of multiple Gaussian curves were then defined in Section 4 as the same values as the peaks noted from the 2nd derivative curve. Section 2 automatically sums the Gaussian curves and plots them on the chart as the experimental model. Section 3 calculates the error between the experimental data and the experimental model. The Microsoft Solver Add-in is then used to manipulate the relative area and standard deviation of the Gaussian curves to provide the lowest possible error and the closest match of the model to the experimental data. The spreadsheet then automatically reports the relative area of each peak in Section 5, allowing for assignment to a specific secondary structural element, as per the literature convention [169], [170]. The protein secondary structure elements could then be quantified as the relative abundance of each element corresponded to the relative area of each Gaussian peak.

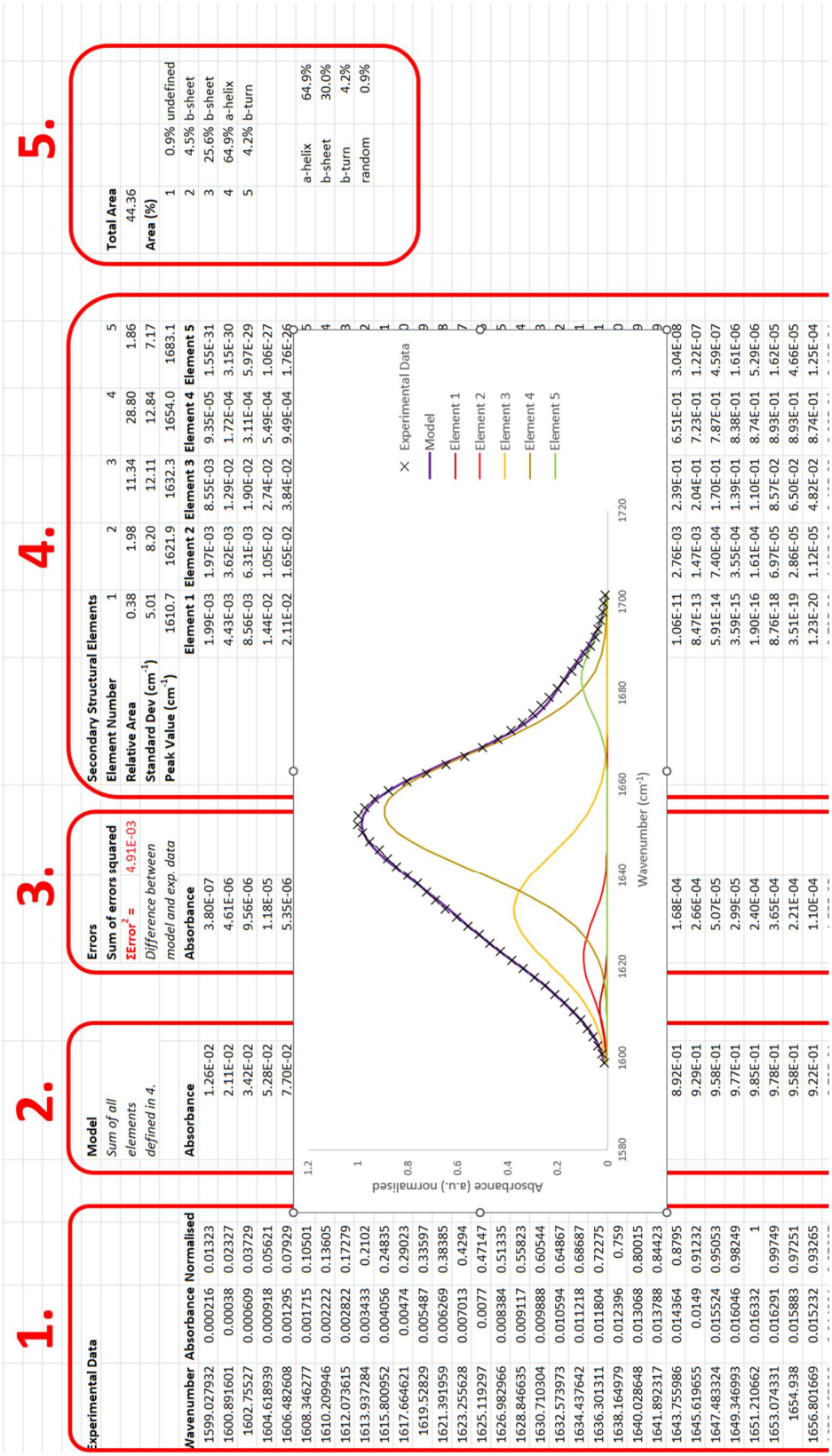

Fig 2.12: Screenshot of the custom-curve fitting spreadsheet used for protein secondary structure determination. Numbered sections are discussed above.

The Amide I band of the infrared spectrum of proteins is associated with C=O bond stretching within the molecule. C=O bonds play an important role in the hydrogen bonds within a protein, which link the secondary structural units and dictate the overall protein structure. As such, the position and shape of the Amide I band are sensitive to the secondary structure composition. The Amide I band is a small section of the entire infrared spectra, with multiple overlapping peaks resulting in a single broad peak instead of multiple resolved peaks for each secondary structural [168]. Using a curve-fitting algorithm it is possible to recreate the multiple overlapping peaks which can then be related to the different secondary structure elements, with the relative area under each curve corresponding to the relative abundance of the corresponding structural element [169]. The relative abundance of the two most common elements: α-helices and β-sheets, are usually reported when comparing protein structures. This is due to the other elements, such a β-turns, being involved in intermolecular hydrogen bonds if protein aggregation occurs [169].

Infrared spectroscopy has been used for protein secondary structure determination for over seven decades, since the early work in this field by Elliott and Ambrose in the 1940s and 50s which found that many characteristic bonds found in protein molecules (such as C-O, C=O and N-H) possess unique, identifying vibrational bands [171]. Later works in the 1980s identified nine characteristic vibrational bands arising from amide groups within the protein structure, of these the Amide I band (1600-1700 cm^{-1}) has been shown to be the most useful for determining the secondary structures of proteins in aqueous solution [172]. The Amide I band is composed, almost entirely, from C-O stretch vibrations and each type of secondary structure gives rise to a unique vibration within the band [172], [173]. In the intervening years, researchers have worked to attribute these vibrational bands to the secondary structural elements, whilst many of these works have shown good agreement with other techniques, such as circular dichroism, more recent studies

are still examining these allocations to improve the determination of secondary structural elements [173]–[175].

UV-Vis Spectroscopy

UV-Vis spectroscopy was used to measure the Aggregation Index (A.I.) of a protein solution. A.I. is a measure of non-soluble, sub-visible protein aggregates and can be used to compare different samples and formulations [176]. Dehydrated protein samples were rehydrated to 1 mg/mL and measured on an Agilent Cary Multicell Peltier UV-Vis spectrometer controlled by Cary UV workstation version 1.1.298, using the initial protein solvent for the blank measurement. Spectra were recorded and the absorbance measurements were taken directly from the raw data.

A.I. is a dimensionless number calculated using the following equation:

$$A.I. = \left(\frac{OD350}{OD280 - OD350}\right) \times 100$$

Where OD350 and OD280 represent the absorbance (%Abs) at 350 nm and 280 nm, respectively.

This method utilises the fact that absorbance at 280 nm can be used to quantify protein concentration in solutions and that proteins do not absorb light above 320 nm. Therefore, any absorbance measured above 320 nm can be attributed to light scattering by undissolved particles. In this case, undissolved particles can be attributed to sub-visible, non-soluble aggregates. Utilising the equation above, it can be shown that as the absorbance at 350 nm increases, so too does the value of the A.I., meaning that a higher A.I. value indicates a higher abundance of non-soluble aggregated particles.

Dynamic Light Scattering

Dynamic light scattering (DLS) is a technique used for measuring the size and size distribution of molecules and particles in the submicron size range. For the work described in this thesis a Malvern Zetasizer Nano DLS, controlled by version 7.12 of

the Zetasizer software, was used to measure the size distribution of protein molecules within an aqueous solution. Samples were prepared at 2 mg/mL and filtered through a 0.45 μm filter into a plastic cuvette. The DLS instrument was setup to run at 25°C with the material setting set on Proteins and the dispersant set as water. If other dispersants were used then the refractive index was measured using an Abbe refractometer. The sample was placed into the DLS and was measured automatically after pressing start.

Typically, DLS is used for the characterisation of particles, emulsions or molecules dispersed or dissolved in a liquid. The technique utilises a single frequency laser which is directed into the liquid sample contained within a cuvette. The laser beam passes into the sample and, if particles are present in the sample, the incident light is scattered in all directions. A detector placed at a known angle from the sample detects any photons which scatter in that direction. The signal received from the detector can then be used to determine the diffusion coefficient and the Stokes-Einstein equation can then be used to calculate particle size. Fig. 2.13 shows a basic representation of a DLS instrument setup.

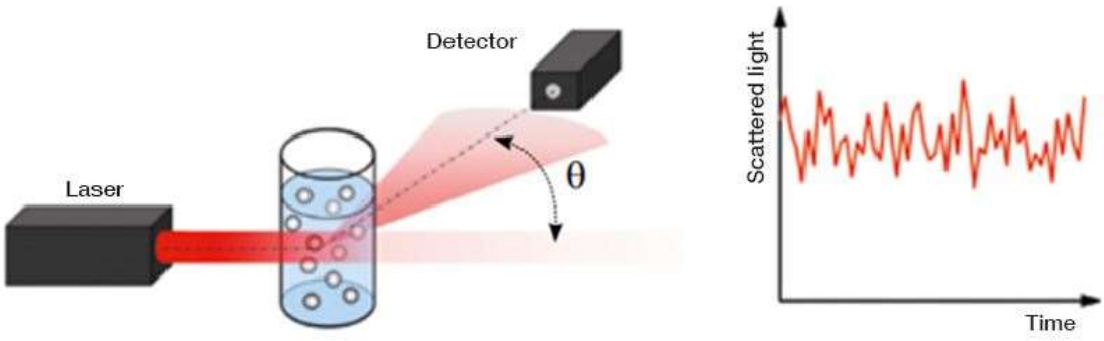

Fig. 2.13: Basic setup of a DLS measurement system. The sample is contained in a cuvette. The scattered light of the incident laser can be detected at different angles. From: [177].

DLS relies upon the random Brownian motion of particles dispersed within a liquid caused by collisions between the particles and the solvent molecules. These collisions induce random particle movement with smaller particles moving at higher speeds than larger particles. As such, assuming knowledge of all other parameters affecting particle movement, the hydrodynamic diameter of a particle can be determined by measurement of the particle speed using the Stokes-Einstein equation. Any non-random movement of particles within the liquid, such as sedimentation, leads to inaccurate results and so the onset of sedimentation indicates the upper size limit for DLS measurements. As larger particles scatter the incident light to a greater degree than smaller particles, the lower size limit of a DLS instrument is defined by loss of signal, becoming indistinguishable from the instrument noise.

To interpret the signal received by the detector into usable data, the intensity signal is plotted as a function of time. Due to the random movement of particles, the intensity is not constant and fluctuates over time, with smaller particles fluctuating more rapidly whilst larger particles generate greater amplitudes between the minimum and maximum intensity (Fig. 2.14 Top). The intensity plot is then used to generate a correlation plot (Fig. 2.14 Bottom). The correlation plot describes a particles position, relevant to its previous position, as a function of time. The plots in figure 2.14 show that, initially, the particles remain localised, but this then decays as Brownian motion moves the particles around in a random fashion. As can be seen, the small particles localised position decays away relatively rapidly due to their faster movement, whilst the larger particles take a longer time before the localised position decays due to their relatively slower movement. The correlation plot is a useful tool to check the "goodness" of the data and whether the sample is suitable for analysis via DLS.

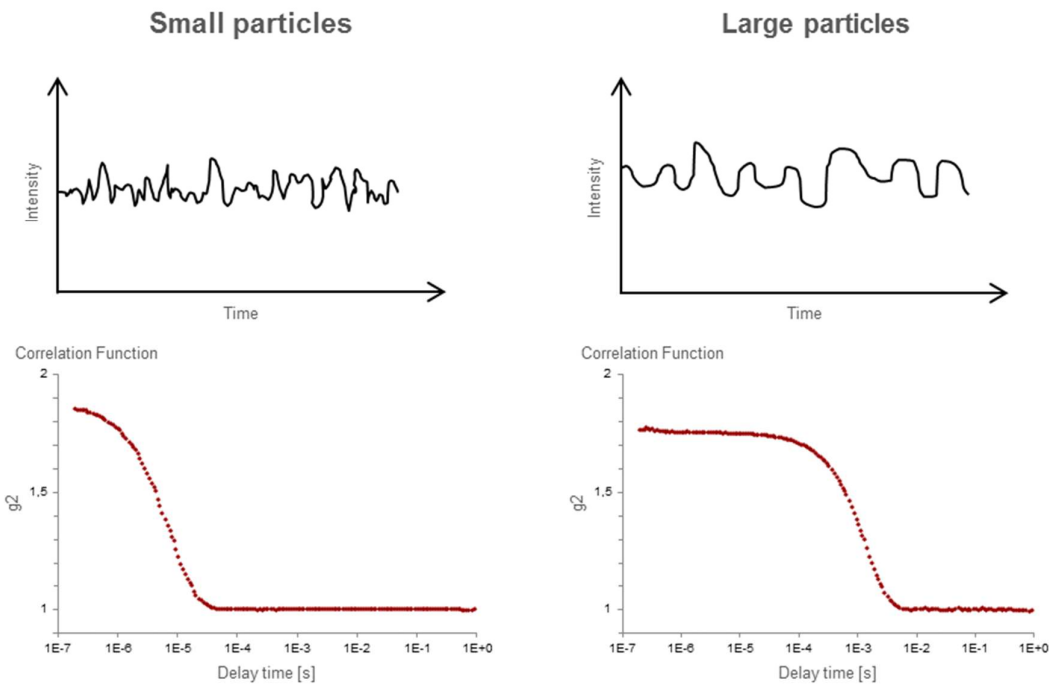

Fig. 2.14: Differences in the intensity trace and correlation function of large and small particles. Smaller particles show faster fluctuations of the scattered light and a faster decay of the correlation function. From[178]

Rheometry

Rheometry measurements were carried out using an Anton Paar MCR302 rheometer controlled by the RheoCompass software (version 1.22.466).

2.2.5 Statistical Analysis

Averaging

Unless otherwise discussed, data were expressed as mean ± 1 S.D. for all experiments. Statistically significant variations in the data were confirmed using a Student's *t*-test with *p*-value < 0.05 being considered statistically significant.

Particle Size Distribution

Particle size distributions were reported using multiple descriptors to provide a clear understanding of the distribution. Mean diameter ± 1 S.D. was provided, along with the D(10), D(50) and D(90) measurements, to provide an understanding of the spread of the data (Fig. 2.15).

To allow for easy comparison of particle distributions, the polydispersity index (PDI) measurement was also reported. PDI is calculated as the standard deviation divided by the mean all squared and gives a value between 0 and 1. The lower the value the more uniform a particle distribution, with values below 0.3 usually defined as monodisperse.

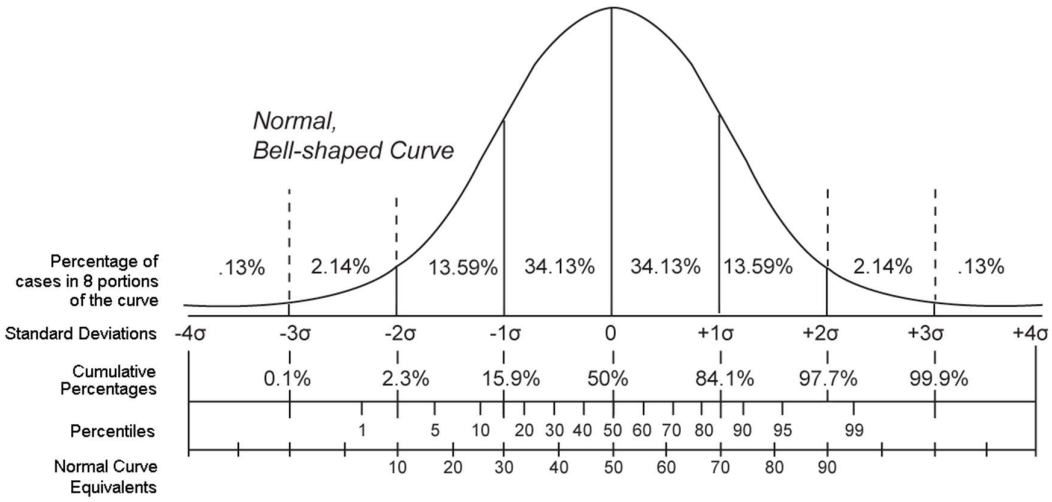

Fig. 2.15: Diagram showing how standard deviation of the mean and percentile measurements match up to describe a normal distribution.

Chapter 3

CCP Technology and Scale Up

3.1 Chapter Introduction

This chapter explores and discusses the technique of CCP and the potential for scale up of the technology for use as an alternative to current industrial processes for protein dehydration. Firstly, the mechanism that underlies the CCP technique was explored by use of a dual-micropipette technique able to generate individual microparticles. This was followed by characterisation of the dehydrated microparticles produced using a small-scale batch production technique. Scale up was then investigated through the use of two medium-scale techniques designed to imitate current industrial practices. Particle size distribution and any protein structural changes were measured to demonstrate the feasibility of large-scale production.

CCP is a technique used for the production of dehydrated protein microparticles via the dehydration of aqueous protein microdroplets by long-chain alcohols. The technique is carried out at room temperature without the requirement for protective additives. CCP was first described in a research paper by Rickard (from the research group headed by D. Needham) in 2010 [151]. This research documented the formation of individual aqueous lysozyme microparticles from aqueous droplets, produced manually via a micropipette system, when held within a reservoir of decanol. Further work carried out by this research group over the following years demonstrated both a batch manufacturing technique for CCP protein microparticles using both pentanol and decanol as the drying solvent, as well as the wider potential of this technology by the use of several different proteins and enzymes with various long-chain organic solvents [13], [79]. The work presented in these research

papers showed a dehydration technology with excellent potential as an industrial technique for dehydrating proteins, enzymes and potentially other biologics.

Since the last of these papers were published, in 2015, there has been no reported work following up on the potential of CCP microparticles for use within the pharmaceutical industry. However, the research has been made use of in other fields in interesting and varied ways, such as the use of CCP within a microfluidic system to prepare cross-linked BSA microparticles [26]. Also work to prepare dye-doped, CCP microparticles for use as biolasers, used for biosensing and biointegration [179]. As such, the work described herein aims to refocus this technology into the field of biopharmaceutics and explore the potential of CCP for industry-scale protein dehydration.

3.2 CCP Technology

CCP is a dehydration technique based upon the formation of aqueous droplets containing a solution of the material to be dried into a solid-state form. The droplets are dispersed within an "infinite-acting" reservoir containing a second fluid which must be immiscible with water, yet capable of dissolving water. In this scenario, an infinite-acting reservoir describes a reservoir of sufficient size that it acts as though it is of infinite size, with the dissolution limit of the solvent having no effect on the droplet dissolution when at the reservoir boundary. The work discussed here used pentanol as the reservoir fluid and generated an aqueous droplet dispersion by vortex mixing a fluid mixture, as per the works described in literature [13], [79]. As the droplets are suspended within the solvent reservoir, the water within the droplets dissolves into the surrounding solvent, causing the aqueous droplets to shrink in size and the concentration of BSA to increase, until the BSA molecules precipitate out of solution to form a solid microparticle with reported BSA concentration of greater than 1000 mg/mL and water content below monolayer coverage [13].

3.2.1 Single Particle Analysis

To further explore the formation of CCP microparticles, the micropipette technique demonstrated by Rickard was employed to observe the dehydration of a single aqueous droplet to form a glassified BSA microparticle [151]. Whilst the full description of this technique can be found in the Materials and Methods chapter, briefly, the technique relies upon the use of two glass micropipettes which are hand forged to provide an opening approximately 5 μm in diameter. Both micropipettes were held by micro-manipulators and manoeuvred into place within a glass chamber containing the organic solvent, the glass chamber was open at either end and the fluid was held within the chamber by surface tension. The setup was constructed on a microscope stage equipped with a 40x objective. Micropipettes were previously coated with hexamethyldisilazane to provide a hydrophobic coating on the glass pipette to prevent wetting and spreading of the aqueous droplet. Once prepared, one micropipette was filled with aqueous BSA solution and manoeuvred into position inside the glass chamber in the field of view of the microscope. Through the application of pressure by the depression of an empty syringe connected to the micropipette, individual aqueous droplets were formed within the solvent medium. The second micropipette was then used to remove the droplet from the original micropipette through the application of a weak vacuum and held the droplet in place within the glass chamber. Removing the droplet from the first micropipette ensured that fluid was not transferring from the pipette into the droplet, or vice-versa. With the droplet held in place within the solvent chamber, the CCP process could be recorded digitally and studied in detail.

Aqueous BSA solution was prepared at 2 mg/mL and then accurately measured using the NanoDrop UV-Vis spectrometer with the built in Protein A280 method for protein quantification, giving the accurate concentration as 1.65 mg/mL. The solution was loaded into one of the micropipettes and a single aqueous droplet was formed at the end of the micropipette, transferred to the second micropipette and

then held in place whilst the CCP process completed. Figure 3.1 shows a timelapse montage of the droplet as it reduces in size and ultimately forms into a solid microparticle. The first six images in this series (reading left to right and top to bottom) show a droplet which is steadily reducing in size as expected. However, in the 7th image (bottom left) the droplet cannot be seen, but returns for the 8th image, and has solidified in the 9th. This disappearance of the droplet in image 7 is due to the optical properties of the droplet as it changes in concentration. As the water in the droplet dissolves into the surrounding solvent, the size of the droplet reduces and the concentration of BSA increases. As the concentration of solute within a solution increases, so too does the refractive index (RI) of the solution. At a specific point in the dehydration period the RI of the droplet and the surrounding medium match, and the droplet boundary effectively disappears from view [151].

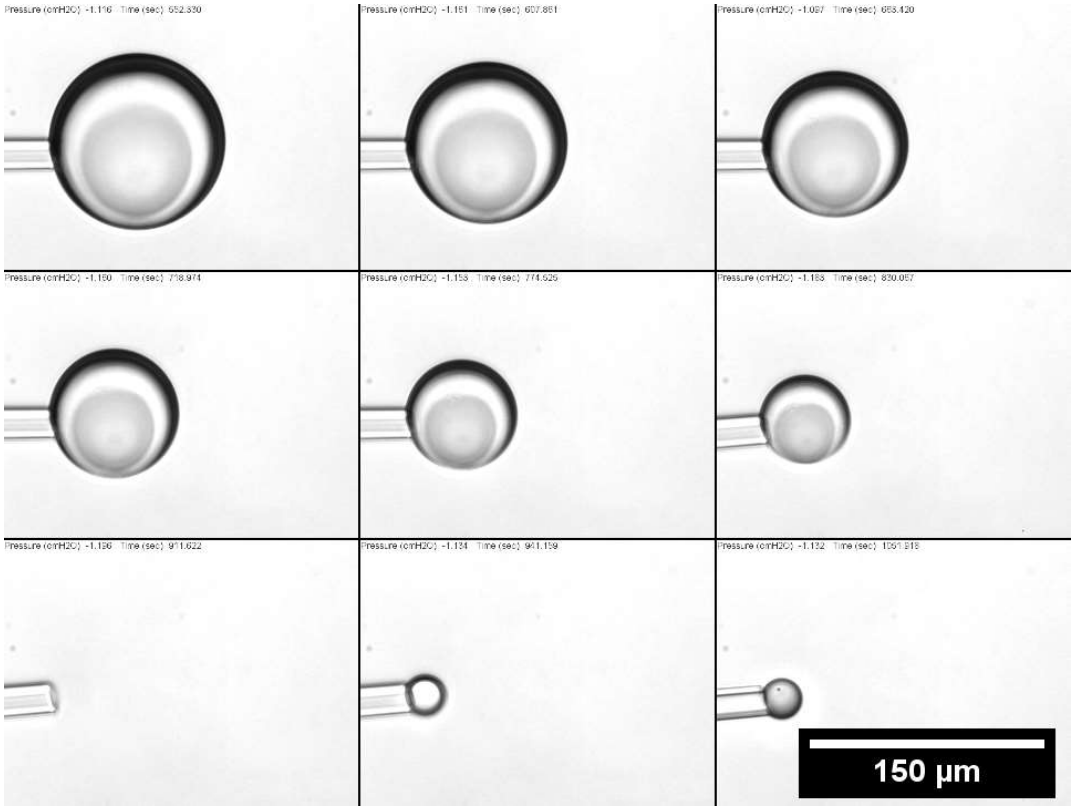

Fig. 3.1: Timelapse montage of an aqueous BSA droplet undergoing CCP to become a solid BSA microparticle. First the droplet shrinks in size and then disappears due to a match in the RI of the two fluids and then returns to view before solidifying.

To characterise the drying process, the radius of the droplet or particle was measured using Fiji at every time point and was plotted as a function of time (fig. 3.2). The blue section of the plot shows measurements of the aqueous droplet, which reduced in size over time, whilst the orange section shows the dehydrated microparticle, at which point the radius remained constant with relation to time. A red circle was added to the plot to show where no measurements could be made due to the droplet losing visibility at the point where the RI matched the surrounding solvent and a quadratic trendline (coloured green) was added to the droplet data, with a coefficient of variance (R^2) value of >0.999. By measuring the RI of BSA solutions at varying concentrations and plotting a calibration chart, it is possible to calculate the BSA concentration of the aqueous droplet at the point where the refractive indices matched. An Abbe refractometer was used to measure the RI of pure water, pentanol, and a series of aqueous BSA solutions. All concentrations were made up manually using a balance and auto-pipette and the concentration was then measured accurately using the NanoDrop UV-Vis spectrometer as above. Using this method, the RI of water was measured as 1.33 and pentanol as 1.41. The series of BSA concentrations was shown to possess a linear relationship of increasing RI with increasing concentration with R^2 > 0.999 (data not shown). However, the highest concentration solution used in the calibration was 154.9 mg/mL, which measured a RI of 1.36, significantly lower than that of pentanol. Assuming that the linear relationship continues at higher concentrations, it was calculated that the BSA concentration at the point where the fluids RIs matched was 387.0 mg/mL. This is similar to the result obtained by Aniket *et al*. who calculated this value at 383 mg/mL using the same method [13].

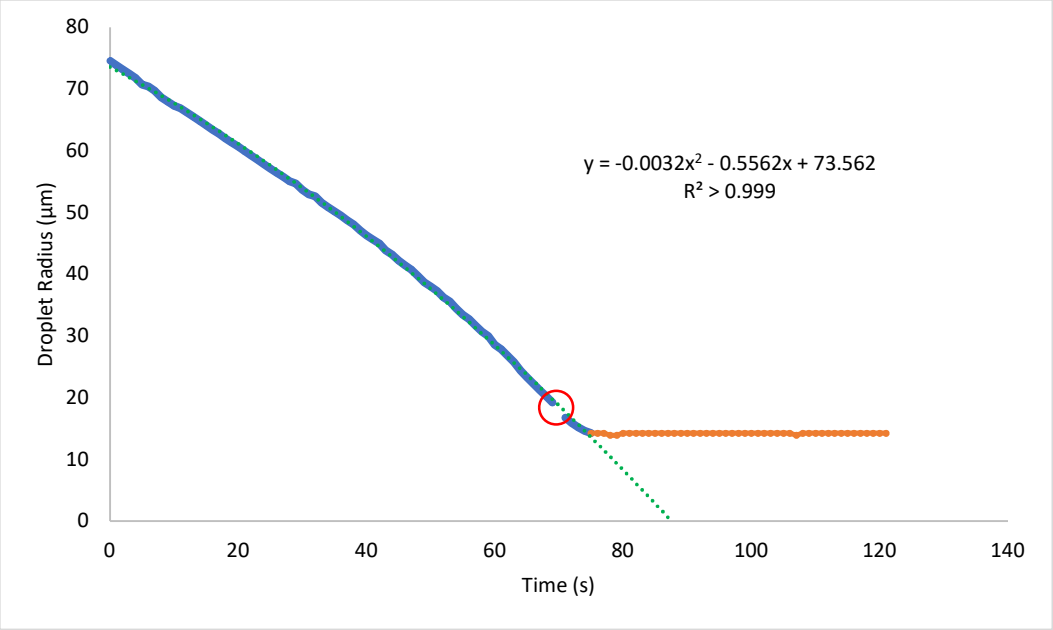

Fig 3.2: A plot of droplet/particle radius as a function of time. The trend line (green) shows a quadratic function for the droplet shrinkage (blue) which then levels off when dehydration completes (orange).

With knowledge of both the BSA concentration and the size of the droplet at a single timepoint it is possible to calculate the mass of BSA present within the droplet. Assuming the loss of BSA from dissolution into the pentanol reservoir is negligible, it is then possible to calculate the concentration at any point within the experiment. The concentration of BSA within the droplet at the point of the RI match was calculated as 387 mg/mL and the droplet size was measured as 18 µm, giving a mass of BSA within the droplet of 9.45 ng. Using this result, the concentration of the droplet at time zero was calculated as 5.6 mg/mL. This is higher than the initial known concentration of the BSA solution of 1.65 mg/mL and can be explained by the time taken to set the experiment up. Manipulation of the micropipettes within the chamber and control of the pressure on the syringes was difficult and it took time to swap the droplet from one micropipette to the other, position the droplet correctly and start the experiment. During this time, water would be diffusing out into the surrounding solvent causing the droplet to shrink and the concentration to increase before the start of the experiment. The concentration of the solidified microparticle was also calculated, giving a concentration of 788.2 mg/mL. This is

lower than that found by Aniket *et al*. who found a maximum concentration 1147 mg/mL [13]. This result implies that the particles formed in this study contained a greater concentration of water or other contaminants than those published in literature. Although further experimentation is required to confirm these measurements and calculations, the difference in results may be due to the water content of the reservoir, the successful experiment occurred after multiple failed attempts, which introduced their own aqueous droplets into the chamber to be dissolved into the surrounding solvent. As such the pentanol used to dehydrate the droplets may have no longer acted as an infinite reservoir, reducing the capacity to dissolve water. Through repetition of this experiment with variation in protein concentration and initial droplet size it should be possible to create a model describing both the microparticle size and time taken for the process as functions of initial droplet size and concentration.

3.2.2 Batch Production of CCP Microparticles

To scale up from the production of single microparticles, CCP microparticles can be obtained using a 5-step process as described in Chapter 2. Step 1: 50 µL aqueous BSA solution is added to 1 mL dry pentanol in a 1 mL Eppendorf tube. Step 2: The Eppendorf tube is vortex mixed at high speed for 30 seconds. This step both creates a droplet dispersion throughout the fluid mixture and acts to keep the droplets in suspension whilst dehydration occurs. Step 3: The suspended, CCP microparticles are centrifuged at 10,000 rpm for 1 minute to pelletise the material. Step 4: The supernatant is removed leaving only a small amount of residual solvent. At this point the sample can be vortex mixed again to produce a slurry of suspended particles within the residual solvent. Step 5: The microparticle sample is stored under vacuum (< 10 mbar) overnight to allow the residual solvent to evaporate from the sample leaving behind a dried microparticle pellet or powder. Multiple samples were prepared from 10 mg/mL BSA solution and prepared for SEM imaging as described earlier. The images showed that the process resulted in a microparticle

distribution with particle size measuring approximately 5 – 75 µm in diameter (fig. 3.3).

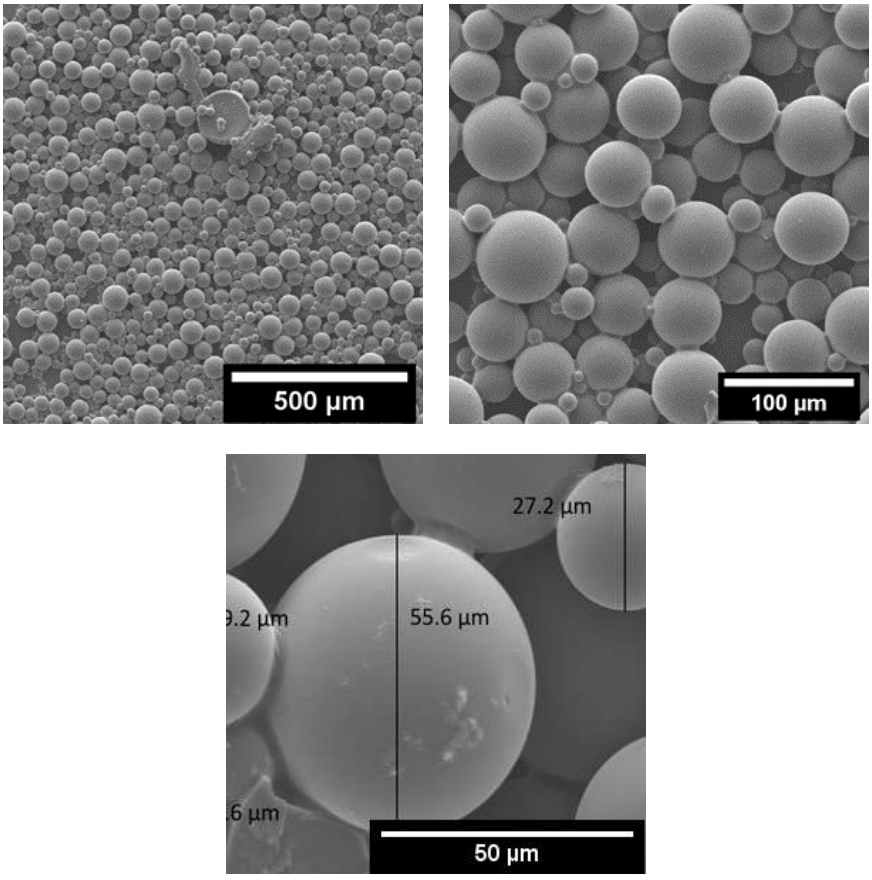

Fig. 3.3: SEM images of BSA microparticles prepared using the CCP vortex mixing method.

3.2.3 Varying BSA Concentration

Through consideration of the CCP process, it is clear that the particle size of the resultant microparticles must be a function of both the initial droplet size and the concentration of the source BSA solution. As droplet size cannot be controlled using the vortex production method, variation of the source BSA concentration was investigated to assess the potential for mean size tunability of CCP microparticles. Aqueous BSA solutions were prepared at 2, 10, 50, 100 and 200 mg/mL and used to prepare CCP microparticles using the vortex mix method described above. Figure 3.4 shows SEM images obtained from three of the samples, top left: 2 mg/mL, top right: 50 mg/mL, bottom: 200 mg/mL. From simple observation of these images,

it is obvious that the average particle size was increasing with increasing concentration. It also clear that with increasing concentration and particle size there is an increase in the abundance of damaged particles. At 2 mg/mL particle size ranged approximately 5 – 40 μm and there were no damaged particles visible. At 50 mg/mL particle size ranged approximately 5 – 95 μm and there was visible damage to some of the particles measuring greater than approximately 50 μm diameter, which appear to have split in half exposing a hollow core. At 200 mg/mL there are many larger particles visible, up to nearly 150 μm diameter with many of the larger particles displaying the same damage. In both the 50 and 200 mg/mL samples there were also visible "pinpricks" in the outer surface of some of the larger particles, in the 200 mg/mL sample it was also evident that these pinpricks were channels into the hollow core of some particles. It is possible that the hollow core seen in the split particles may have contained liquid BSA solution that had not fully dehydrated and become trapped within the centre of the particle. If the trapped aqueous solution was then subjected to an outside force causing it to expand, such as the high vacuum environment used during sample preparation for SEM imaging, then it may escape via a pinhole channel or even rupture the particle as seen.

Particle size was measured using Fiji and the median particle diameter as a function of concentration is shown in figure 3.5, error bars are 1 S.D. of the mean. The dotted line represents a linear trendline with R^2 of 0.8955. The graph shows that average particle size did increase with increasing BSA concentration but that the size distribution also increased with the S.D. reaching over 50% of the measured value at 200 mg/mL. PDI values for the samples under discussion were calculated as 0.131, 0.184, 0.134, 0.224 and 0.353 for the 2, 10, 50, 100 and 200 mg/mL sample respectively. Using this measure of a particle size distribution shows that all samples except for the 200 mg/mL sample would be classified as monodisperse particle distributions.

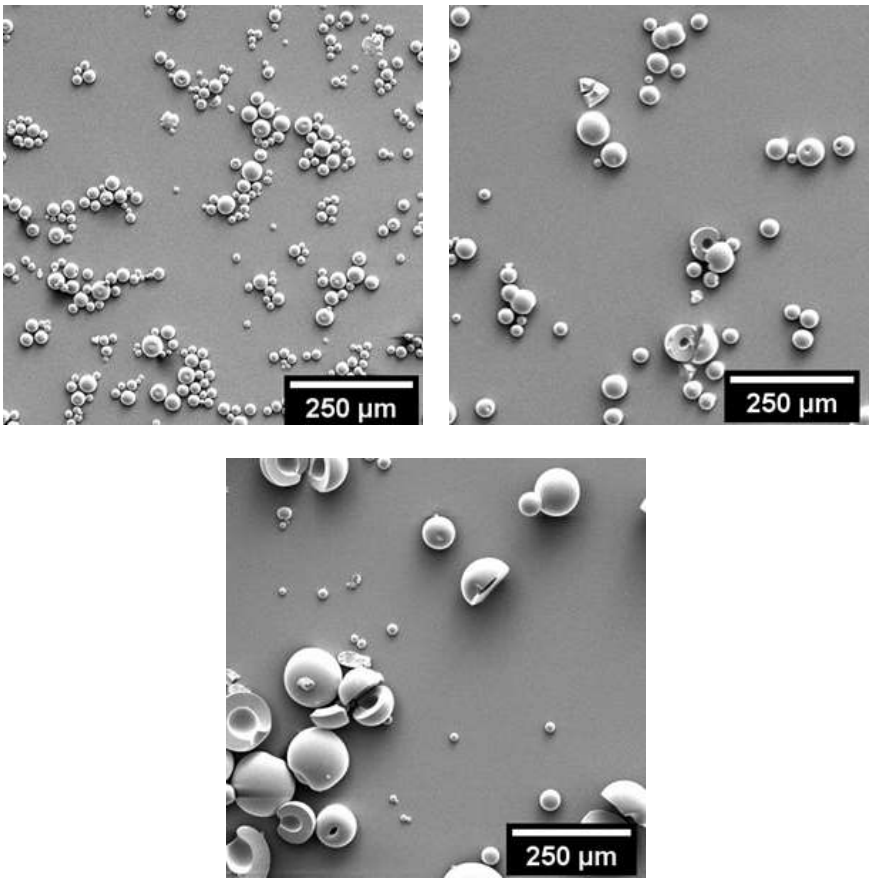

Fig 3.4: SEM images obtained from BSA microparticles prepared using the CCP vortex method from BSA solutions of varying concentration. (Top Left) 2 mg/mL (Top Right) 50 mg/mL (Bottom) 200 mg/mL

This study showed that average particle size could be controlled by variation in the concentration of the BSA source solution. Particles with a median diameter ranging between 26.4 – 52.3 µm were obtained by variation between 2 – 200 mg/mL. However, increasing particle size did also increase the size dispersity of the particles. Depending upon the real-world usage scenario, this may or may not be an issue. If the technology were being used to create a dried product for storage, similar to how lyophilisation is used, then particle size and topography is not important and protein solutions would be used at the highest concentration possible to increase product yield.

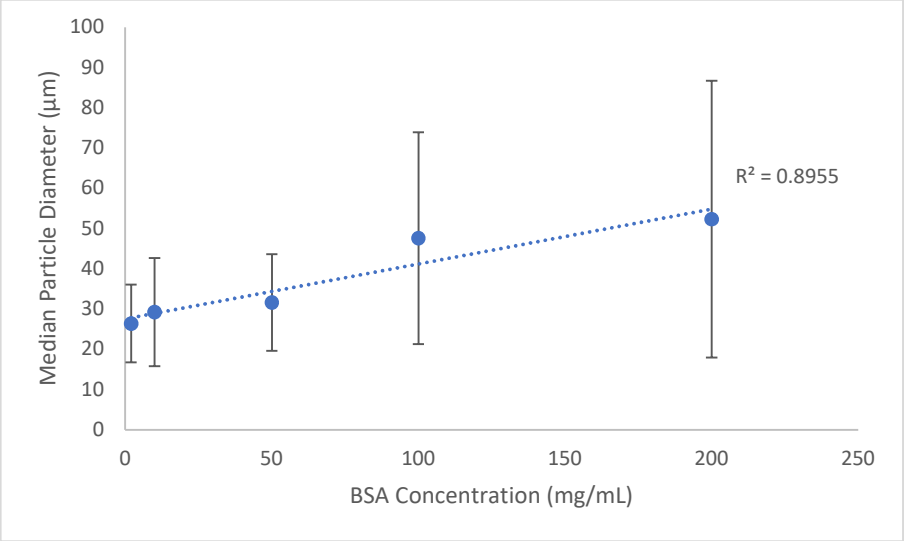

Fig 3.5: Plot showing the median particle diameter as a function of BSA concentration of the aqueous phase. Error bars = 1 S.D. of the mean

3.2.4 Protein Analysis

Proteins can be very sensitive to changes in their local environment, potentially inducing conformational changes in the protein structure. However, rehydration of the protein can often reverse these changes and so the effect of CCP and subsequent rehydration on the structure of BSA was investigated. Fluorescence spectroscopy was used to interrogate the tertiary structure of the protein in order to assess whether any unfolding of the protein was detectable after reconstitution. Dynamic light scattering (DLS) was used to measure the particle size distribution of the reconstituted protein to assess levels of aggregation. CCP samples were prepared from 10 mg/mL BSA solutions, using both native BSA and lyophilised BSA, using the vortex mix method described in Chapter 2 and then reconstituted in 1 mL of deionised water to give solutions of 10 mg/mL. Control samples, for use as comparison materials, were prepared directly from native and lyophilised BSA as purchased from manufacturers. All control samples were prepared at 10 mg/mL in dH_2O.

Bulk Observations

BSA microparticles were prepared using the CCP vortex mixing method as described earlier and the additional vortex mixing step was employed in step 4 to resuspend the centrifuged pellet prior to the final drying under vacuum to prepare powder samples. Multiple samples were prepared and collected together in a glass vial for visual comparison with lyophilised BSA (fig. 3.6). Whereas the lyophilised sample presented as flakes of white material, the CCP sample appeared as a fine powder which appeared free-flowing when shaken. Being a powder formulation, the CCP sample had a much greater surface area than the lyophilised samples, potentially granting more rapid dissolution when reconstituting the product.

Fig 3.6: A visual comparison of purchased lyophilised BSA powder (left) and glassified BSA powder (right).

Fluorescence Spectroscopy

Samples were diluted to 2 mg/mL and analysed using fluorescence spectroscopy with excitation wavelength set at 295 nm and measuring emission intensity between 305 – 450 nm and results are shown in figure 3.7 with emission peak maxima shown below in table 3.1. These results show that the control solution prepared from native BSA measured a peak maximum at 340.9 nm, whereas the control solution prepared from lyophilised BSA measured a peak maximum at 349.8 nm, a difference of approximately 9 nm. A shift in the fluorescence peak emission wavelength as seen here is known as a blue or red shift depending on whether the

peak wavelength shifts towards lower energy (red shift) or higher energy (blue shift). Red or blue shifts in the peak emission wavelength of a protein can often be an indicator of structural degradation of the protein resulting in unfolding or aggregation. As a protein unfolds or aggregates it can expose previously buried sections of the internal structure (and vice versa) to a differing local environment, potentially exposing buried chromophores to a more hydrophilic environment as they are exposed to an aqueous solvent or burying previously exposed chromophores within an aggregated structure. Such changes act to change the polarity of the local environment resulting in changes to the electrostatic interactions between the amino acid residues and thus the fluorescence emission profile. In general, a red shift in the peak corresponds to an increase in environment polarity caused by unfolding of the protein, whereas a blue shift in the data may imply aggregation of the protein as chromophoric residues become buried within an aggregated structure, resulting a less polar environment [156]. In the literature, the fluorescence emission peak wavelength is usually reported as between 340 – 350 nm and therefore the variation between these two samples may be explained by natural variation of the protein with the native sample likely containing more aggregated forms of the protein than the lyophilised sample. Further analysis of this data showed that the peak emissions values obtained from the CCP samples did not show any peak shift from their non-CCP controls. This result indicates that there was a difference in tertiary structure between the native and lyophilised samples but no difference between the CCP and non-CCP samples.

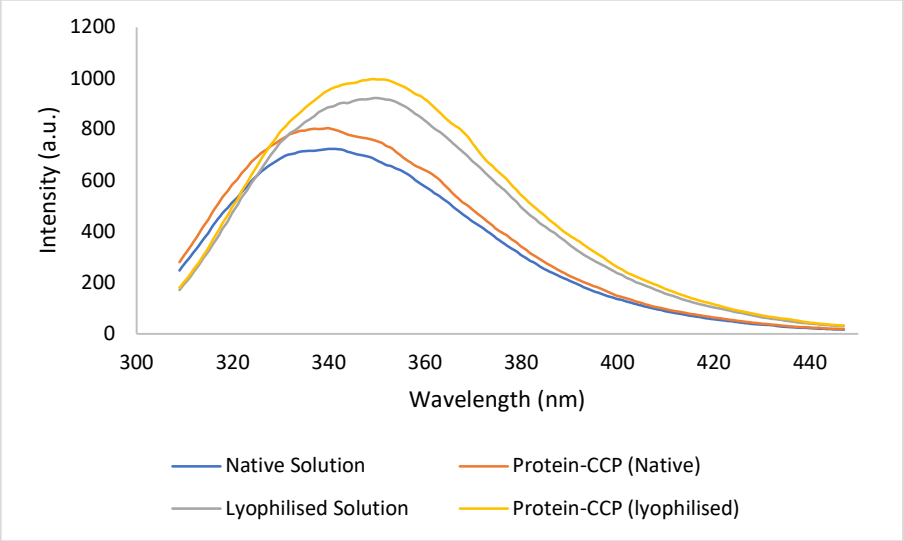

Fig 3.7: Fluorescence spectroscopy results showing fluorescence emission spectra of BSA solutions prepared from native and lyophilised BSA, both CCP and non CCP. This plot shows that there was a spectral shift between the native and lyophilised samples but none but CCP and non CCP samples.

Table 3.1: Emission peak maxima measurements of BSA solutions prepared from native and lyophilised BSA, both CCP and non CCP.

Sample	Emission Peak Maxima (nm)
Native	340.9
CCP (Native)	339.8
Lyophilised	349.8
CCP (Lyophilised)	348.9

Dynamic Light Scattering

The BSA solutions described above were also analysed using DLS to assess the level of protein aggregation found in each sample. Samples were prepared to 2 mg/mL. CCP samples were prepared and measured in triplicate whilst non CCP samples were prepared and measured singly. Figure 3.8 shows the DLS results of aqueous samples produced from native BSA solution, both from CCP formulation and native solution. These results both show a peak at < 10 nm, corresponding to the unaggregated BSA molecule, and a second peak at approximately 58.7 nm, relating to an aggregated form of the protein. In the non-CCP sample the < 10 nm peak

was not detected by the software due to the low intensity but it can still be seen visibly in the plot. For both samples the 58.7 nm peak was dominant when reporting distribution by intensity, but the 6.5 nm peak was dominant when reporting distribution by mass. This difference is due to intensity measurements being weighted towards larger particles due to their increased scattering, but when this is converted to distribution by mass it is clear that the smaller particles made up the majority of the material within the solution. These results show that a large amount of aggregated protein molecules were found within the native BSA samples with 25.3% by mass of the CCP (Native) samples being an aggregated form. When this is considered along with the fluorescence spectroscopy results this implies that the native protein samples may have produced a blue shifted spectra due to aggregation of the protein. When multiple BSA molecules are bound together to form aggregates then the tryptophan residue usually found on the hydrophilic outer surface of the protein molecule may find itself in the hydrophobic interface between protein molecules, resulting in a blue shifted emission. Unfortunately, the peak at 6.5 nm was not detected in the native sample so this cannot be compared numerically, but by visual analysis it is clear that the results from the CCP (Native) samples look very similar to the native samples implying that the CCP process did not result in greater levels of aggregation.

Figure 3.9 shows the DLS results of the samples produced from lyophilised BSA, both rehydrated CCP samples and solution prepared directly from lyophilised powder. Again, two peaks were measured, one at 8.7 nm corresponding to the unaggregated form of the protein and the other at 255 nm corresponding to larger aggregates or contaminants. However, unlike the results from the native samples the 8.7 nm peak is dominant in both the intensity and mass distributions, making up 99.9% and 100.0% of the population by mass for the CCP and non CCP samples respectively. However, the intensity measurements show that for the non CCP samples the unaggregated form of the protein accounted for 59.1% of the

distribution, whereas for the CCP samples this was measured as 49.0% of the distribution. This implies that CCP and subsequent reconstitution of lyophilised BSA did increase the amount of aggregation within the product, however, when accounting for mass this was only an increase of 0.1%.

Taken together, these two results showed up two interesting results. 1. The solutions made up from native BSA appeared to contain a higher degree of aggregation than the lyophilised samples. This was evidenced by both the blue shift in the fluorescence emission wavelength, indicating that more of the tryptophan residues were experiencing a localised hydrophobic environment than in the lyophilised sample, and the DLS data showing a high abundance of larger particles. 2. There appears to be very little impact to the protein structure and aggregation due to the CCP process and subsequent reconstitution into deionised water. Fluorescence spectroscopy showed no evidence that the process had affected the tertiary structure of the protein, whilst DLS measurements showed only a very small increase in aggregation of 0.1% when measuring the mass distribution of the samples.

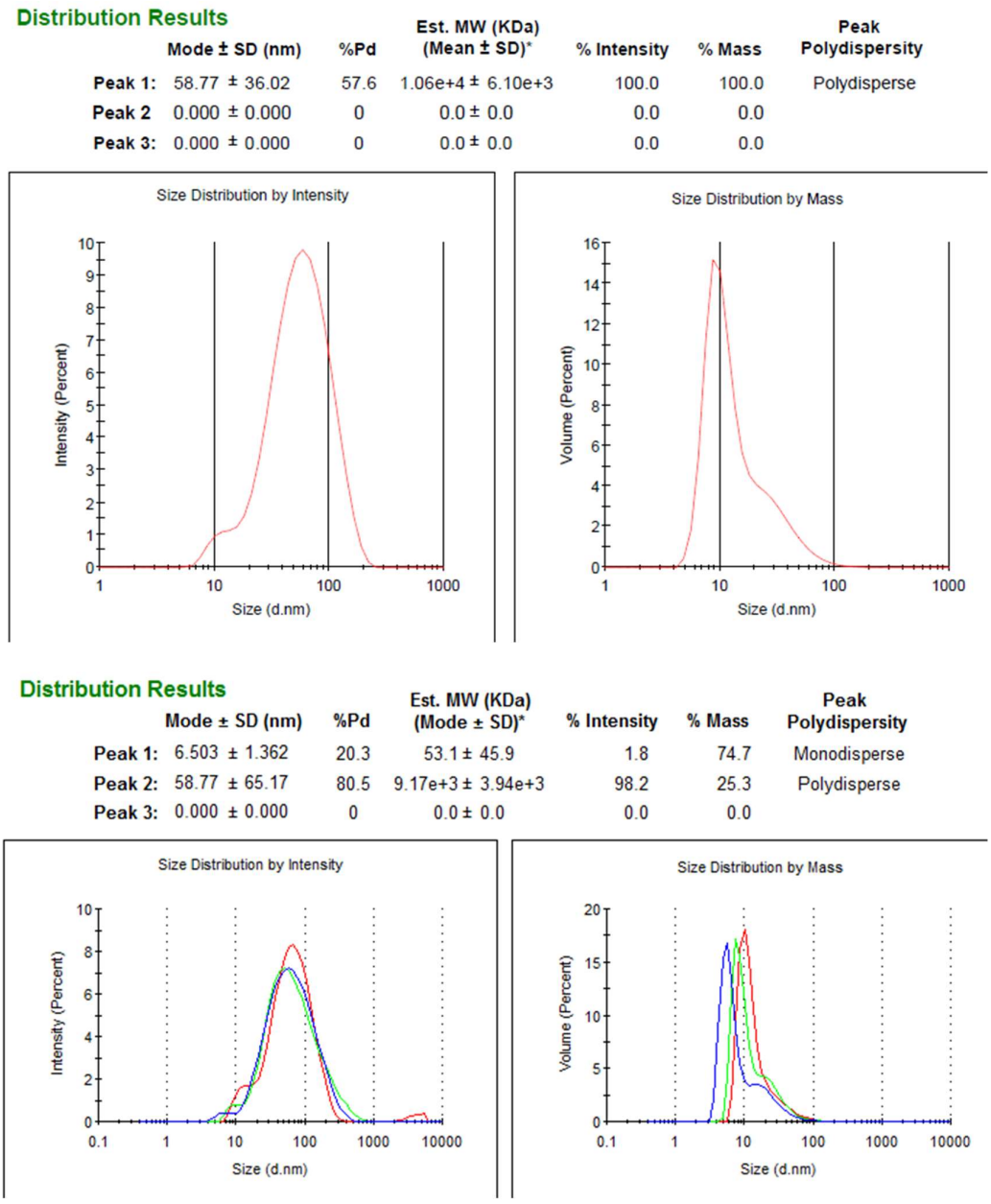

Fig 3.8: DLS results obtained from comparison of aqueous solutions prepared from CCP BSA (prepared from native BSA solution) and directly from native BSA solution. Both samples were prepared at 10 mg/mL and diluted to 2 mg/mL prior to analysis. (Top) Native BSA solution. (Bottom) CCP-BSA solution from native BSA. (Left) Size distribution based on intensity measurements. (Right) Size distribution based on mass.

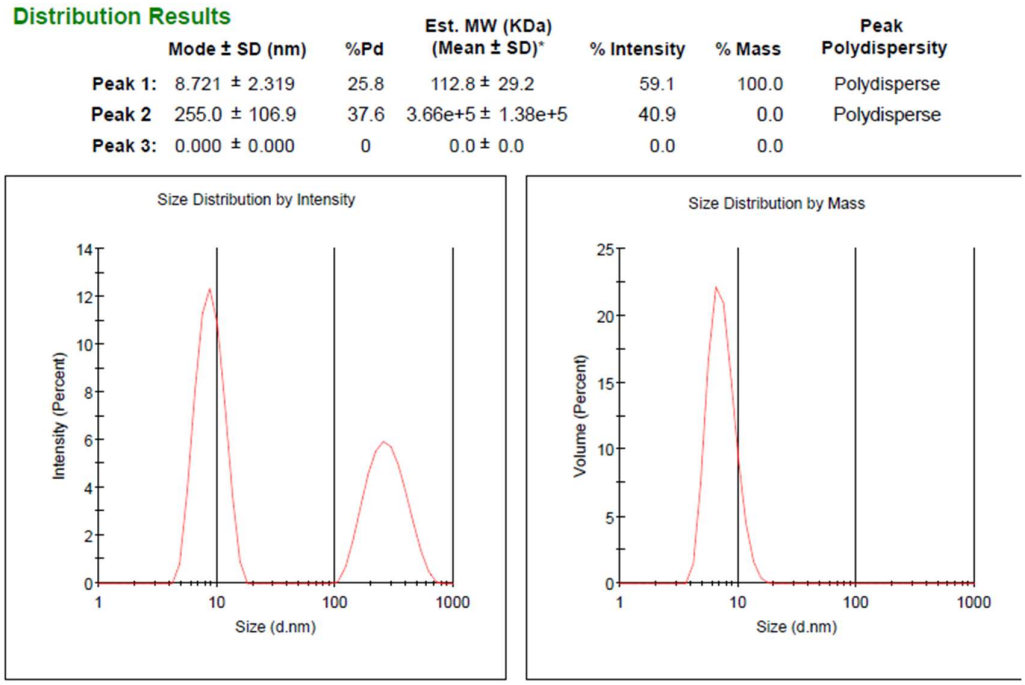

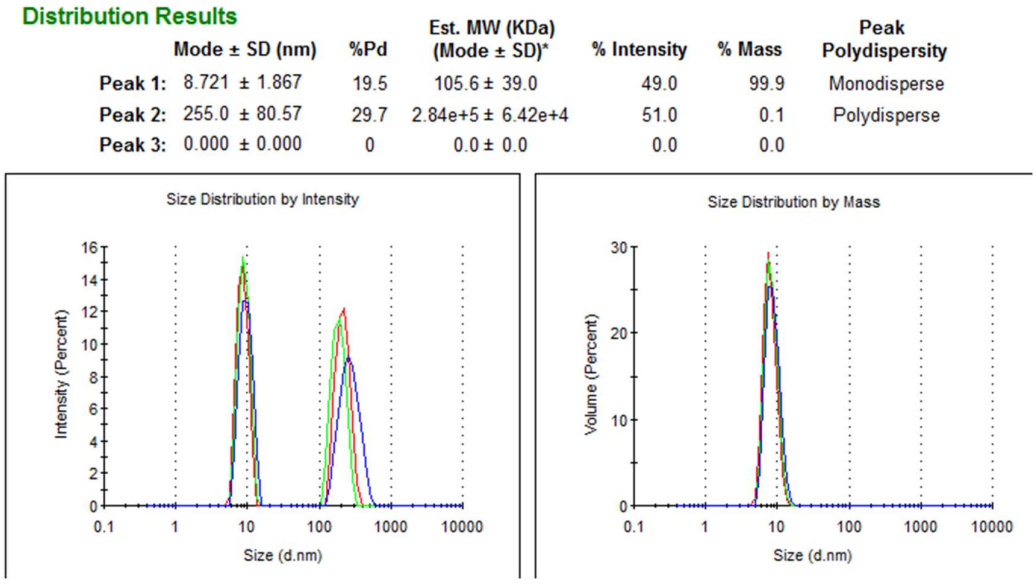

Fig 3.9: DLS results obtained from comparison of aqueous solutions prepared from CCP BSA (prepared from lyophilised BSA solution) and directly from lyophilised BSA solution. Both samples were prepared at 10 mg/mL and diluted to 2 mg/mL prior to analysis. (Top) Lyophilised BSA solution. (Bottom) CCP-BSA solution from lyophilised BSA. (Left) Size distribution based on intensity measurements. (Right) Size distribution based on mass.

3.3 CCP Technology Scale Up

3.3.1 Experimental Setup

This second part of this study was intended to investigate the scale up potential of CCP technology. In an industrial setting, this process would likely be carried out using large batch mixing processes to maximise output and to be compatible with existing biopharm technology. Such a change would clearly provide a difference in environment for the process and so, to approximate this process, the screening method used previously was scaled up to run inside a 250 mL glass beaker. The ratio of BSA solution to solvent was retained in the scale up, with 5 mL of BSA solution being added to 100 mL pentanol. However, running the process inside a beaker or vat makes mixing via vortex difficult and dangerous. Therefore, mixing was achieved using both an overhead stirrer and an overhead homogenizer. These two mixing technologies were selected as each process can be scaled up easily and are already widely used in pharmaceutical production processes.

Samples were prepared from lyophilised BSA powder in deionised water at 10, 50 and 100 mg/mL, the solvent beaker and the mixing device were held in place and the mixing was initiated immediately upon adding the BSA solution to the solvent. Mixing was conducted for one minute after which 20 µL aliquots of the resultant suspension were taken for microscopic observation. The beaker was then covered and left under a fumehood for the suspended material to settle before removal of excess solvent and final evaporation of the residual solvent.

3.3.2 Microscopic Observations

Immediately after the mixing step, 20 µL aliquots of the resultant suspension were placed onto prepared SEM stubs, covered, and left to dry. Samples were then prepared for SEM analysis as described previously.

Overhead Stirrer

Samples that were prepared with the use of an overhead mixer were created using both a fast stir and slow stir speed. A fast stir speed defined as the speed required

to induce a vortex within the beaker reaching to near the stirring head, and a slow stir speed was defined as the speed required to agitate the surface of the liquid to and create a 1 cm deviation in surface position. BSA solutions were prepared at 10, 50 and 100 mg/mL. Figure 3.10 shows the obtained SEM images with the fast stirred samples on the left and slow stirred samples on the right, top to bottom shows increasing concentration. The fast stir samples show the smooth, spherical particles seen when using the vortex mix method, including the damage to larger particles. However, the slow stir samples also exhibited large non-spherical particles, measuring up to approximately 250 μm. The inclusion of these large and irregular particles within slow stir samples may indicate that the droplet formation process had less of a homogenisation effect compared to the fast stir and vortex methods. It is possible that either non-spherical droplets were being generated and undergoing CCP or that droplets were merging before the CCP process completed. However, when discussing the use of CCP as a dehydration technique to act as an alternative to current industrial processes to produce solid-form proteins, the topography of the particles is not important if it does not affect the structure and function of the protein.

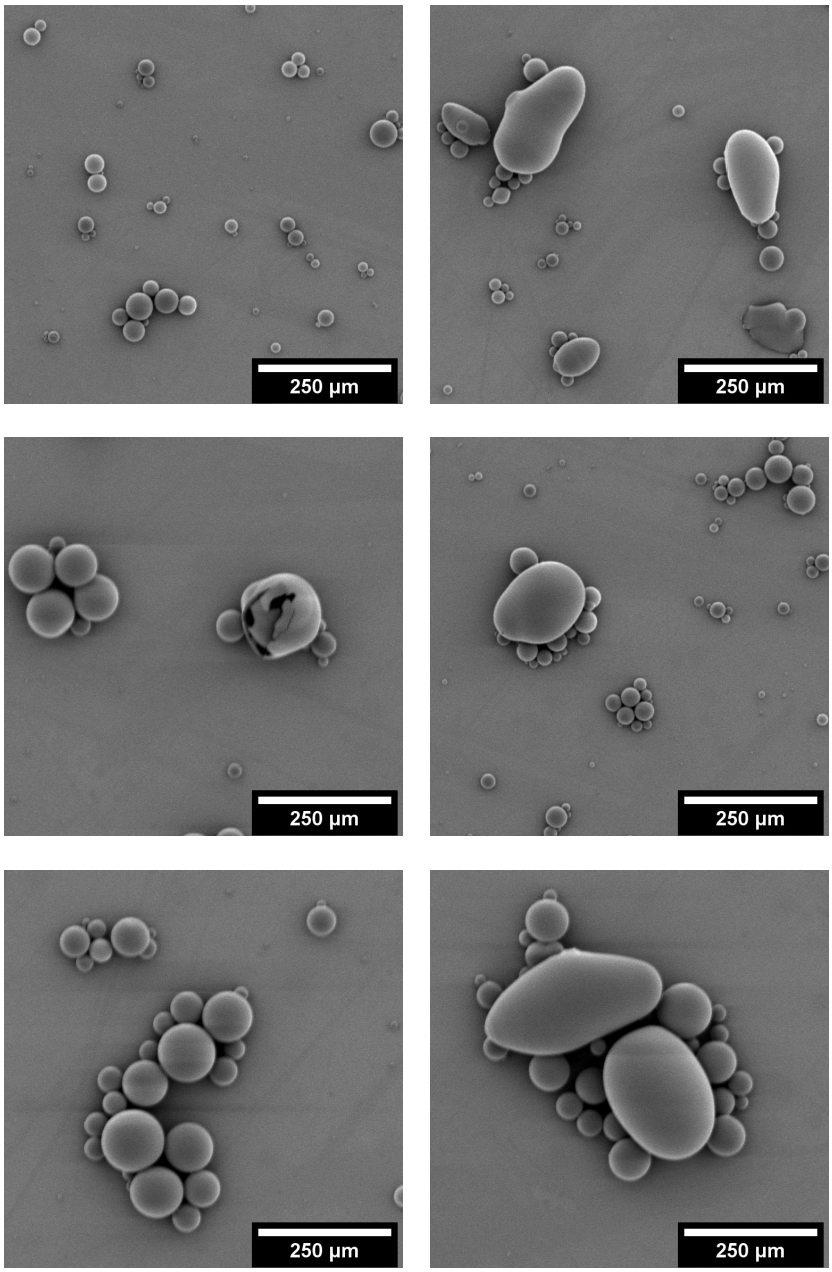

Fig. 3.10: SEM images of BSA samples prepared using the CCP method with an overhead stirrer. (Left) Samples produced with a fast stir speed. (Right) Samples produced with a slow stir speed. (Top to Bottom) 10 mg/mL BSA, 50 mg/mL BSA, 100 mg/mL BSA.

Overhead Homogeniser

Samples that were prepared with the use of an overhead homogeniser were created using both a fast stir (24,000 rpm) and slow stir speed (10,000 rpm) and with BSA concentration at 10, 50 and 100 mg/mL. As with previous samples, 20 µL aliquots were taken and prepared for SEM imaging. Figure 3.11 shows a single SEM image

obtained from each sample with the fast speed samples on the right, the slow speed samples on the left, and concentration increasing from top to bottom. It is immediately apparent that the particles generated using the homogeniser were much smaller than those seen with previous techniques, with diameters in the range approximately 1-5 μm (measured manually using Fiji). Larger, non-spherical particles and damaged particles were visible throughout the samples but there were no obvious differences between fast and slow speed or the samples prepared from different concentration solutions. These observations may be explained by the method of action of a homogeniser. Mixing with a homogeniser has a different effect from either vortex mixing or overhead stirring. Whereas the vortex mixer and stirrer create rotating flows within a fluid, causing dispersion and mixing to take place passively, homogenisation uses mechanical force to mix the fluids by forcing them through small openings under high pressure. This provides a mixing action by forcing fluid away from the mixing head at high pressure, causing fluid flow. This action also has the effect to break down a suspended substance into smaller particles and distribute the reduced particles throughout the medium. This size reduction action would affect the aqueous droplet dispersion, creating smaller droplets and thus smaller particles.

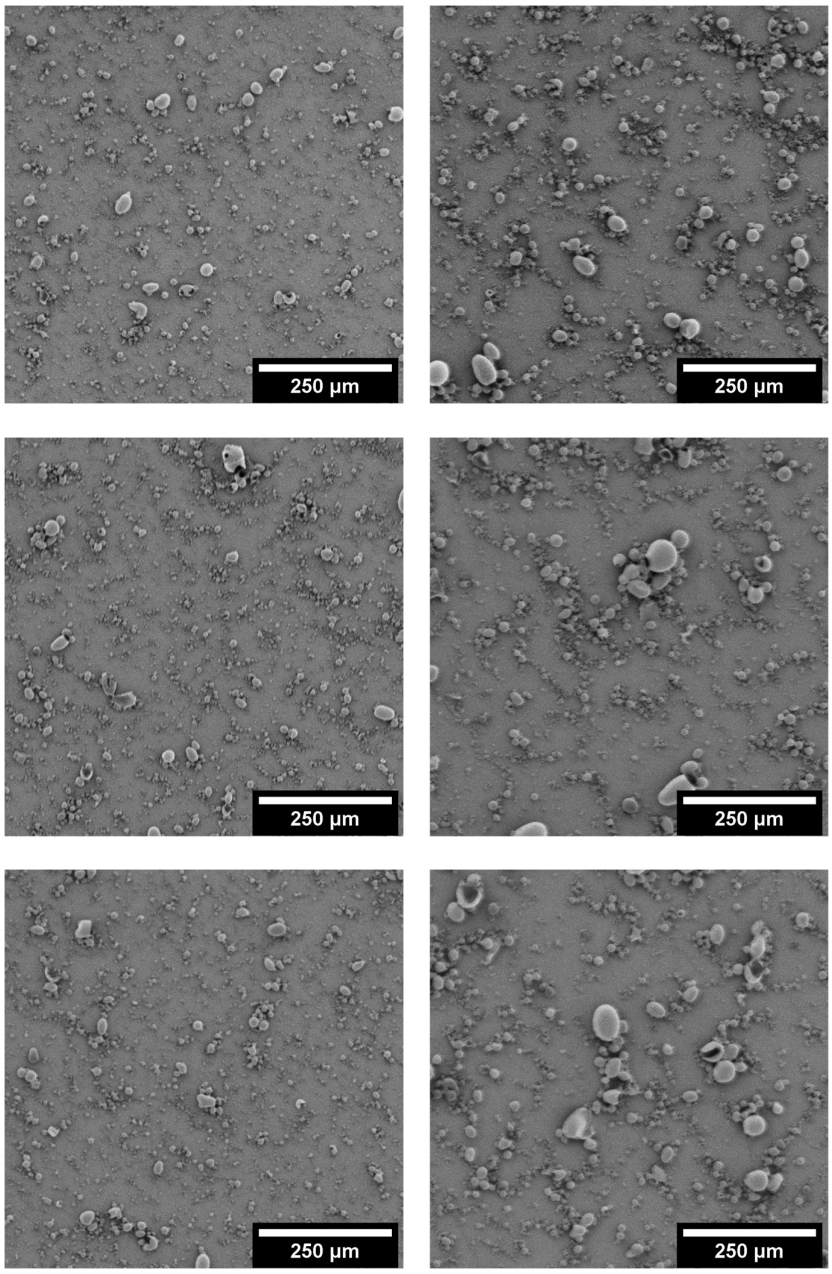

Fig. 3.11: SEM images of BSA samples prepared using CCP and an overhead homogeniser. (Left) Samples produced with a fast speed. (Right) Samples produced with a slow speed. (Top to Bottom) 10 mg/mL BSA, 50 mg/mL BSA, 100 mg/mL BSA.

3.3.3 Protein Analysis

Fluorescence Spectroscopy

As per previous analyses, dehydrated samples were rehydrated and diluted to 2 mg/mL and measured using a fluorescence spectrometer with excitation wavelength set at 295 nm and scanning for emission between 300-400 nm. Both the stirred and

homogenised samples were prepared from 10 mg/mL BSA solution and were mixed at the high-speed setting for each mixing technology. Lyophilised BSA solution at 10 mg/mL was used as the positive control whilst a denatured BSA solution, prepared from 8M GdnHCl as described in the Materials and Methods chapter, was used as a negative control sample. Blank solutions were prepared from the appropriate solvent, dH_2O for the experimental samples and positive controls and a mixture of GdnHCl and dH_2O (4:1 ratio GdnHCl:dH_2O) for the negative control samples.

Fig 3.12 shows the averaged, smoothed and normalised spectra from each sample. It can be seen that the homogenised, stirred and positive control samples all had emission peak maxima of approximately 349 nm whilst the denatured negative control sample had a peak maximum at approximately 359 nm. These results match with those observed previously from the vortex mixed samples, showing that the lyophilised positive control gave a peak emission maximum at 349 nm and that the process of CCP and rehydration did not produce a shift in the measured wavelength. The negative control experienced a red shift in the spectral emission data showing evidence that the protein had begun to denature, exposing the buried tryptophan residue to a more hydrophilic environment.

Dynamic Light Scattering

Samples were also analysed using dynamic light scattering to assess the level of aggregation in rehydrated samples. Only samples produced using the overhead stirrer were analysed in this manner, along with lyophilised BSA solution as a positive control and a denatured BSA solution, prepared from 8M GdnHCl as described in the Materials and Methods chapter, was used as a negative control sample. All samples were prepared at 2 mg/mL and analysed. Results of DLS analysis are shown below in figure 3.13. The positive control result shows the dominant peak measured at 10.23 nm, corresponding to the unaggregated form of the protein. Whilst larger particles were also measured in the intensity distribution,

they were not apparent in in the mass distribution. The negative control result showed the dominant peak at 40.93 nm, corresponding to aggregated forms of the protein. In both the intensity and the mass distributions these forms represented 100% of the distribution. The results obtained from the CCP samples (produced from the overhead stirring technique) also showed a dominant peak representing the unaggregated protein with smaller peaks present at higher sizes. Similar to the results seen earlier from the vortex mix method, the CCP sample did show a decrease in the relative abundance of unaggregated protein forms with the intensity distribution measurements showing a reduction from 87.4% in the positive control, to 49.0% in the CCP sample. However, this related to a 0.1% reduction when calculating the mass distribution of the particles. These results show that, similar to CCP carried out using the vortex mix method, the overhead stirring technique does not cause a large degree of protein aggregation with the abundance of aggregated particles increasing by 0.1% compared with the source material (rehydrated lyophilised powder).

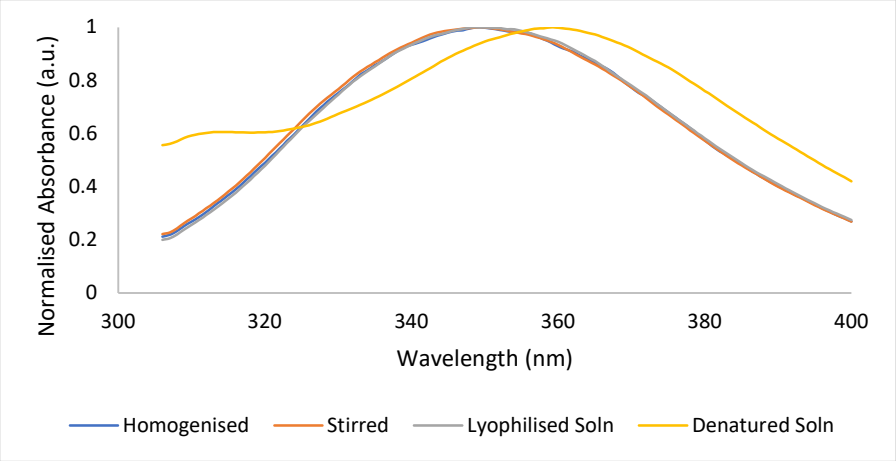

Fig. 3.12*:* Smoothed and normalised fluorescence spectra of rehydrated glassified BSA produced using a scaled-up method with stirring and homogenisation in place of vortex mixing. Sample were excited at 280 nm to measure the innate fluorescence of tryptophan residues. Rehydrated lyophilised BSA powder was used as positive control whilst GdnHCl-denatured BSA was used as the negative control (marked with a dotted line).

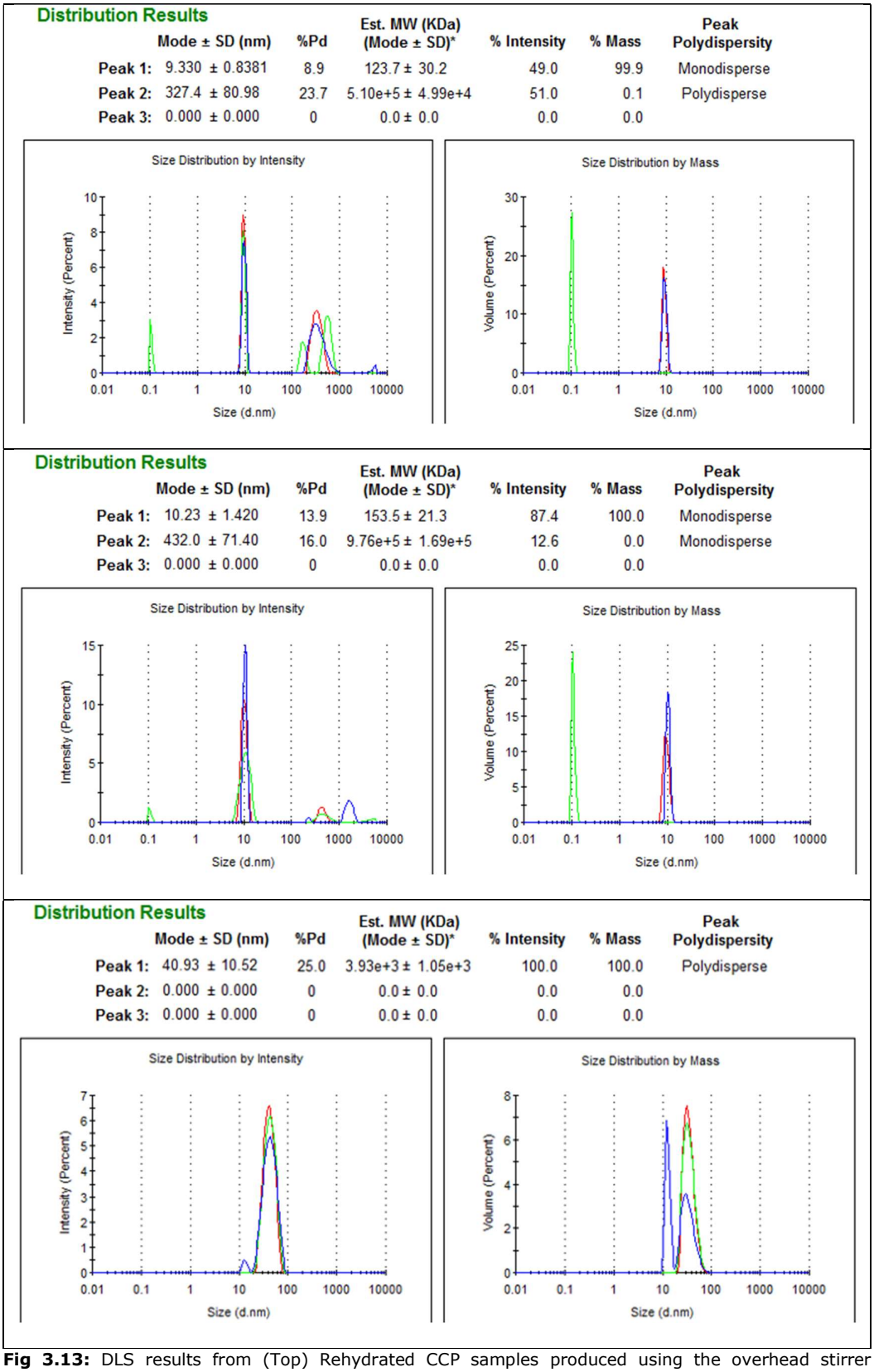

Fig 3.13: DLS results from (Top) Rehydrated CCP samples produced using the overhead stirrer technique. (Middle) Positive control of rehydrated lyophilised BSA powder. (Bottom) Negative control of BSA solution purposefully denatured using GdnHCl.

3.4 Conclusions and Further Work

This chapter aimed to investigate the mechanics behind the CCP process, compare CCP with lyophilisation and to assess the potential for scale up towards an industrial process. One of the more obvious industrial uses for CCP technology would be as an alternative to lyophilisation as a means to dehydrate protein solutions to create dry powder formulations for long-term storage. CCP has a number of advantages over lyophilisation: 1. Lyophilisation often requires the addition of protective additives and stabilisers to protect the protein from the lyophilisation process, whereas CCP has been demonstrated to produce a dried BSA formulation without any requirement for additives or any damaging effect to the protein. 2. Lyophilisation is an energy intensive process, especially when carried out at large scale, due to the requirements to vacuum seal the drying chamber. CCP promises lower energy usage as the only energy requirements for the formation of CCP particles is a mixing technology. However, there is also a solvent removal step requirement for CCP particles which has so far been achieved using vacuum evaporation, to reduce energy usage even further a replacement final drying step would be required such as air drying, perhaps with the careful application of heat to ensure maximum evaporation. Despite these advantages, there is also one drawback of the use of CCP at an industrial level. CCP requires large amount of organic solvent to act as the drying agent, providing both a cost and health and safety impact. The cost factor may be reduced by recycling of the pentanol through removal of the dissolved water, yet this adds further steps, complexity and cost itself.

To study the process of CCP, the micropipette technique was employed to allow the production of a single aqueous microdroplet within the solvent reservoir and to observe the droplet undergoing the CCP process. Observation of the process showed the droplet shrinking over time, as water dissolved into the surrounding pentanol, followed by a brief time where the droplet become invisible due to a match in the

RI of the two fluids. By measuring the droplet diameter as a function of time it was possible to then calculate the diameter of the droplet at the point where the RI match occurred, furthermore, it was also possible to calculate the concentration of the droplet at the RI match by calibrating RI measurements as a function of concentration. With the droplet size and concentration at a known point, it was then possible to calculate the mass of BSA present within the droplet. If it is assumed that the loss of BSA to the surrounding pentanol is negligible then the mass of BSA should remain unchanged as the droplet shrinks over time, allowing for calculation of the protein concentration at any time point. If these experiments were to be repeated multiple times with varying initial concentration and droplet size then it may be possible to model the CCP process and predict the final droplet size and process time based on the initial droplet size and concentration.

Further study of the CCP process was conducted using a small-scale batch technique, in which 50 µL of BSA solution was added to 1 mL of pentanol and the mixture was vortex mixed for 60 seconds to disperse the aqueous phase and suspend the droplets until the process had completed. This process generated smooth, spherical particles ranging in diameter from approximately 5 µm to over 100 µm, with the average size depending upon the concentration of the aqueous BSA source. Increasing the concentration also increased the dispersity of the particle size, with the smallest particles produced regardless of the BSA concentration and the larger particles increasing in size with concentration. Observation of these samples under SEM also showed that the larger particles (above approximately 50 µm diameter) started to show interesting topographical features, such as pin hole indentations. As particle size increased further, particle damage or even particles split open to reveal a hollow core became more abundant and observation of some of the split open particles showed that the pinhole indentations may have acted as a pore through to the central hollow. Although further investigation would be required to understand the hollow core, such as

cryogenic freezing and shattering to observe the hollow core in a frozen state which could then be characterised by a technique such as SEM-EDX, it is possible that the core contained liquid BSA solution that had become trapped within the particle and burst out during SEM sample prep when exposed to a high vacuum.

To investigate the potential of CCP to act as an alternative technique to lyophilisation, fluorescence spectroscopy and DLS were used to characterise both the protein structure and to assess any protein unfolding and aggregation caused by CCP and reconstitution in deionised water. Native and lyophilised BSA solutions were analysed, along with CCP samples prepared from both native and lyophilised BSA. Analysis of the results showed that whilst the native and lyophilised samples exhibited differences in both structure and aggregation, with the native BSA solution showing potential aggregation issues, the CCP samples showed no difference from the non CCP samples. These results show that CCP technology had only a minimal effect on both the tertiary structure of the BSA molecule and the level of aggregation observed and demonstrate that CCP does have potential to be used as a protein dehydration technique

The final aim of this chapter was to investigate the scale up potential of CCP technology. Whilst direct scale up of the vortex mixing technique was not possible without access to industrial scale vortex mixers, the technique was approximated using both an overhead stirrer and an overhead homogeniser to provide the mixing action. The technique was scaled up from 0.5 mL of BSA solution added to 1.0 mL of pentanol in a 1 mL Eppendorf tube to 5 mL BSA solution added to 100 mL pentanol in a 250 mL beaker. This setup was designed to model an industrial-sized stirred vat or homogeniser system. Through microscopic observation and fluorescence spectrometry measurements, as per above, it was shown that both overhead stirring and homogenisation were suitable techniques to produce BSA microparticles prepared via CCP. SEM observation of the particles showed that production via overhead stirrer produced the same smooth, spherical microparticles

observed previously with the inclusion of large, non-spherical particles. It its likely that the inclusion of these particles is due to the lower energy stirring of the overhead stirrer allowing greater random movement of the aqueous droplets, resulting in collisions and larger, non-spherical droplets to be created. Observation of the homogenised samples showed distributions of very small particles with the majority measuring less than 5 μm diameter. This is likely due to the homogenising effect of the homogeniser acting to reduce the droplet size to a smaller scaler than those produced with vortex or overhead mixing. Protein characterisation using fluorescence spectroscopy and DLS showed very similar results to those seen in the vortex mixed samples. Fluorescence spectroscopy showed change in the tertiary structure of the protein whilst DLS measurement showed only a marginal increase in aggregation of 0.1% when measuring the distribution by mass.

Two examples of further work that have come out of these investigations have already been discussed above, the continuation of the micropipette work to model the CCP process and allow for the prediction of particle size and time for CCP to occur, as well as further investigation into the hollow core observed in some of the larger particles. However, there are multiple other avenues of work which could also be explored. An analysis of the concentration of residual solvent left within the microparticles would be a requirement of pharmaceutical regulations. According to the ICH guideline Q3C published by the European Medicines Agency, pentanol is a class 3 solvent, classified as a "solvent with low toxic potential" and whilst efforts to minimise the solvent within a final product should be taken, it is considered acceptable for pharmaceutical products to contain pentanol at a level that equates to 50 mg per day without any further justification [180]. If the daily dose is not known then this can be assumed as 10 mg administered daily, equating to a solvent concentration of not more than 5000 ppm.

Other work which could follow on from these studies include further characterisation of the reconstituted protein. Analysis techniques such as FT-IR or X-ray

crystallography could be employed to further study the protein structure in greater detail. Other techniques such as gel electrophoresis or size exclusion chromatography could also be employed to assess protein aggregates at the smaller scale, such as BSA dimers and trimers, which DLS is not sensitive enough to differentiate. Finally, studies into the reusability of the solvent reservoir could be used to demonstrate the cost saving potential compared to lyophilisation. Solvent drying techniques such as evaporation or tangential flow filtration could be investigated and explored on the larger scale to demonstrate the potential of CCP to succeed lyophilisation as the go-to technique to produce solid-state protein formulations.

Chapter 4

CCP Microparticle Stability

4.1 Chapter Introduction

This chapter aims to investigate the stability of BSA and HSA protein microparticles prepared via CCP through comparison with lyophilised protein powder. One of the primary uses of protein dehydration technologies in industry is to create solid protein formulations for increased long-term stability. As described earlier, many proteins are not naturally stable in aqueous solution and localised environmental changes can cause degradation of the protein product in terms of structural unfolding and aggregation.

Currently, lyophilisation is the most commonly used technique for the dehydration of proteins into solid-state formulations. The technique has long been used in industry and is a well-understood process. However, the lyophilisation process does have drawbacks. It is an energy intensive process requiring a high vacuum chamber where water sublimation can occur, this is especially true at scale where the vacuum chamber can be very large to improve output. Lyophilisation also generally requires the inclusion of protective additives to ensure the process itself does not damage the protein.

CCP offers the promise of a low energy alternative to lyophilisation, requiring energy only to drive the mixing process. CCP also does not require the addition of additives, although investigation into this topic could provide interesting further work, potentially improving the structural integrity or stability of the protein formulation. However, CCP technology also has a number drawbacks including the requirement for organic solvent as the drying medium. As the process requires a high ratio of solvent to protein solution, this requirement will become expensive if the solvent cannot be reused. The use of solvent also raises the question of solvent content in

the final product, potentially requiring additional steps to remove the solvent. Finally, the current process does require the use of a vacuum chamber to dry the residual solvent from the particles. As such, an alternative drying technique may be required to reach the energy efficient process that CCP could become.

To carry out this study, CCP microparticles were produced from native BSA and HSA solution, as well as from two proprietary HSA formulations supplied by Albumedix Ltd. Samples were also prepared directly from lyophilised BSA and HSA. Samples were stored for up to one year at 5°C, 25°C or 40°C and were rehydrated and analysed at defined time points. Samples were analysed to assess protein structure and aggregation.

4.2 Experimental Design

This study was designed to provide an investigation into the long-term stability of dehydrated BSA and HSA formulations prepared using CCP along with a comparison to lyophilised BSA and HSA stored under the same conditions. The European Medicines Agency (EMA) provides guidance on stability testing of new pharmaceutical products [181]. As per these guidelines, samples were stored at 5°C ± 3°C for 12 months as the primary storage condition. Further samples were stored at both 25°C ± 2°C and 40°C ± 2°C for 12 months and 9 months respectively, exceeding the minimum requirement of the EMA of 6 months for accelerated storage conditions. Table 4.1 show the testing regime devised for this study with the testing time points coloured blue, green or red and the non-testing timepoints coloured dark grey.

Table 4.1: The testing regime employed in this study over 52 weeks. Coloured cells indicate an analysis time point and grey cells represent no analysis at that time point.

Temp	Testing time points (weeks)									
	0	1	2	3	4	8	12	26	40	52
5 ± 3°C										
25 ± 2°C										
40 ± 2°C										

Six protein formulations were prepared for this study, four of these formulations were prepared from materials purchased from suppliers as per the Materials and Methods chapter, whilst the other two formulations were proprietary native HSA products provided by Albumedix Ltd. and supplied as an aqueous solution. Formulation 1: Lyophilised powder BSA purchased from the manufacturer (Lyophilised BSA). Formulation 2: BSA microparticles prepared from native BSA solution via CCP (CCP BSA). Formulation 3: Lyophilised powder HSA purchased from the manufacturer (Lyophilised HSA). Formulation 4: HSA microparticles prepared from native HSA solution via CCP (CCP HSA). Formulation 5: HSA microparticles prepared from HSA Prime solution provided by Albumedix Ltd. via CCP (CCP HSA Prime). Formulation 6: HSA microparticles prepared from HSA Elite solution provided by Albumedix Ltd. via CCP (CCP HSA Elite).

At each analysis time point, each protein sample was analysed in triplicate and so the study required the preparation of 72 samples from each of the six protein formulations for a total of 432 samples. To deal with the large number of samples the start of the study was staggered with the samples being stored at different temperatures starting at different times. This meant that a maximum of 30 samples per protein formulation were required at any one time. However, this approach still required up to 180 samples to be prepared in a single day and so samples were prepared using a larger scale version of the vortex mixing technique, in which 1 mL

of 15 mg/mL aqueous BSA was added to 14 mL pentanol in a 50 mL Eppendorf tube and vortex mixed for 60 s. This produced a 15 mL suspension of CCP microparticles at a concentration of 1 mg/mL, this was then split into fifteen 1 mL samples and dried and harvested as per the standard vortex mix method. This method ensured that fifteen samples were prepared per batch, significantly reducing the preparation time. The lyophilised BSA and HSA samples did not require to be processed using the CCP technique and so 1 mg samples were weighed directly into 1 mL Eppendorf tubes. This proved more difficult than anticipated due to static issues, and so a relatively large error of ± 0.1 mg (± 10%) was deemed acceptable.

Samples were prepared as described and one triplet of samples from each formulation was kept aside for analysis immediately for the time zero measurements. The remainder of the samples were stored at the selected temperatures, 5°C, 25°C, 40°C, in a laboratory specification fridge or incubator and triplicate samples were removed and analysed at each timepoint.

To analyse the protein samples and asses the stability of the protein formulations, samples were first reconstituted in 1 mL deionised water to produce a 1 mg/mL solution. Fluorescence spectroscopy was used to assess any non-reversable unfolding of the protein molecules. To assess any increases to the level of aggregation in the samples, UV-Vis spectroscopy was employed to measure the aggregation index (A.I.) of the solution and size exclusion chromatography (SEC) were used to directly measure the size and abundance of aggregated forms. All techniques, except for the SEC method, are described fully in Chapter 2. SEC analysis was carried out at Albumedix by their staff.

4.3 Results and Discussion

4.3.1 Fluorescence Spectroscopy

In this study, fluorescence spectroscopy was used to infer details about the tertiary structure of the various BSA and HSA formulations stored at multiple temperatures over one year. At each analysis timepoint, a triplet of each sample was removed

from the temperature-controlled environment and dissolved in deionised water to 1 mg/mL. Denatured protein solutions were prepared from 8M GdnHCl, as described in the Materials and Methods chapter, as negative control samples. Samples were excited 295 nm and emission spectra were recorded between 300 – 400 nm. Blank solutions were prepared from the appropriate solvent, dH_2O for the experimental samples and positive controls and a mixture of GdnHCl and dH_2O (4:1 ratio GdnHCl:dH_2O) for the negative control samples.

BSA samples stored at 5°C

Figure 4.1 shows two bar charts detailing the peak emission wavelengths of the BSA formulations stored at 5°C at each time point with the excitation wavelength set at 295 nm. The measurement obtained from the GdnHCl-denatured control samples are also plotted on the chart to act as a negative control. Analysis of these data show that the GdnHCl-denatured BSA (negative control) sample measured peak emission at a significantly higher wavelength than the CCP or lyophilised samples across all time points, indicating that neither formulation experienced structural unfolding to the extent of the control sample. It can also be seen that there were no obvious trends in the peak wavelength with increasing storage time, with the final measurements of each sample measuring less than 1% deviation from the initial value. These results indicate that the proteins were not experiencing any trend in structural unfolding of the structure over 52 weeks of storage at 5°C.

BSA samples stored at 25°C

Figure 4.2 shows two bar charts detailing the peak emission wavelengths of the BSA formulations stored at 25°C at each time point with the excitation wavelength set at 295 nm. The measurement obtained from the GdnHCl-denatured control samples are also plotted on the chart to act as a negative control. Analysis of these data showed that the measured peak wavelength of samples remained significantly lower than that of the negative control across all samples and time points, except for the Week 26 data points, and that there were no trends in the data with the final

measurements of each sample measuring less than 1% deviation from the initial value. These results indicate that the proteins were not experiencing any trend in structural unfolding of the structure over 52 weeks of storage at 25°C. As commented above, the Week 26 data points measured significantly higher than all other data points for both BSA formulations, after which time the following data points returned to their previous values, as such the data points are considered to be spurious, likely caused by sample contamination during sample analysis or preparation.

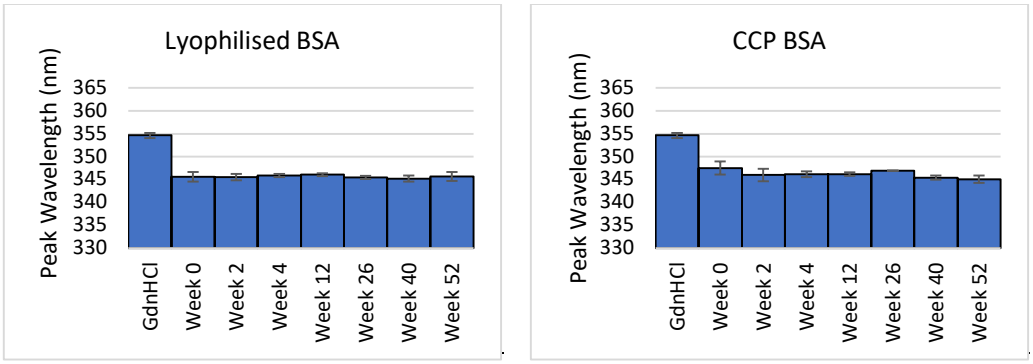

Fig. 4.1: Chart showing peak emission wavelength of rehydrated lyophilised BSA and BSA microparticles prepared via CCP samples stored at 5°C at each time point with the excitation wavelength set at 295 nm. Samples were recorded in triplicate and error bars = 1 S.D. of the mean.

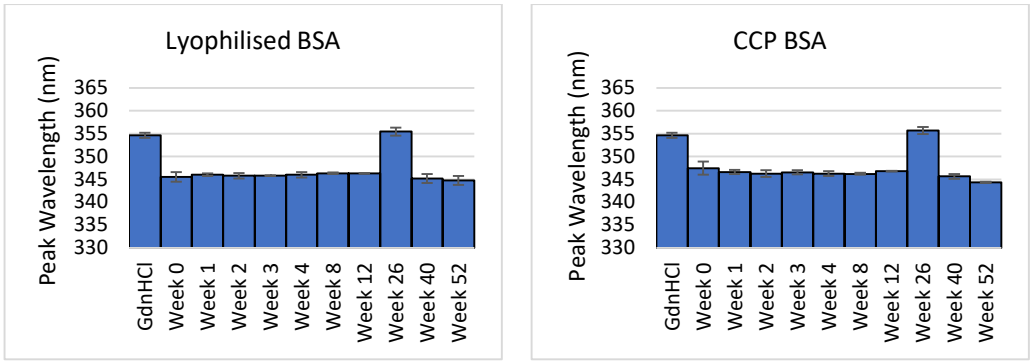

Fig. 4.2: Chart showing peak emission wavelength of rehydrated lyophilised BSA and BSA microparticles prepared via CCP samples stored at 25°C at each time point with the excitation wavelength set at 295 nm. Samples were recorded in triplicate and error bars = 1 S.D. of the mean.

BSA samples stored at 40°C

Figure 4.3 shows two bar charts detailing the peak emission wavelengths of the BSA formulations stored at 40°C at each time point with the excitation wavelength set at 295 nm. The measurement obtained from the GdnHCl-denatured control samples are also plotted on the chart to act as a negative control. Analysis of the data showed all time points measuring significantly lower than the negative control and no clear trend in the peak emissions. As with the samples at lower temperatures the final measurements of each sample measured less than 1% deviation from the initial value, indicating that the protein was not experiencing any non-reversible unfolding throughout the experiment.

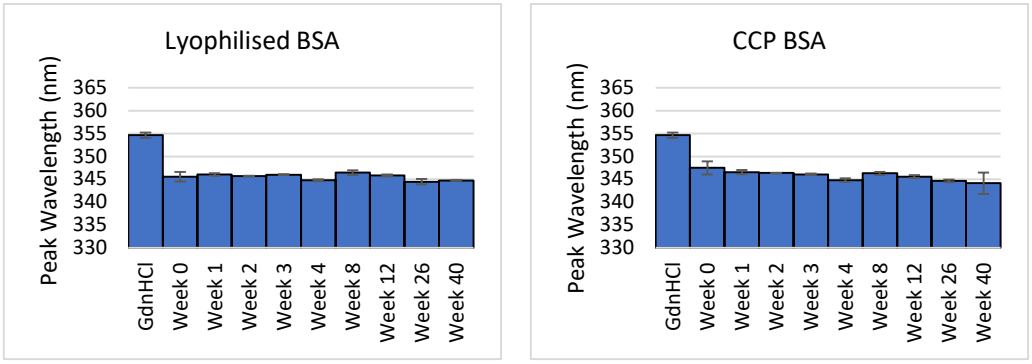

Fig. 4.3: Chart showing peak emission wavelength of rehydrated lyophilised BSA and BSA microparticles prepared via CCP samples stored at 40°C at each time point with the excitation wavelength set at 295 nm. Samples were recorded in triplicate and error bars = 1 S.D. of the mean.

HSA samples stored at 5°C

Figure 4.4 shows four bar charts detailing the peak emission wavelengths of the HSA formulations stored at 5°C at each time point with the excitation wavelength set at 295 nm. The measurement obtained from the GdnHCl-denatured control samples are also plotted on the chart to act as a negative control. Analysis of the HSA CCP sample did appear to show a trend towards increasing peak emission with increasing storage time over the first four weeks of the study, after which time it remained at the higher value. However, the difference between the measured wavelength values of the week 0 result and the week 52 result was less than a 1%

deviation, indicating that the apparent trend may be natural variation. Analysis of the other formulations showed no statistically significant trends or deviations, with the exception of the HSA Elite Week 4 samples which showed a significant decrease in the peak wavelength. However, as this decrease was not observed at later time points it was regarded as an outlier. These results show that the final measurements of each sample measured less than 1% deviation from the initial value, implying that none of the formulations experienced non-reversible protein unfolding during storage at 5°C.

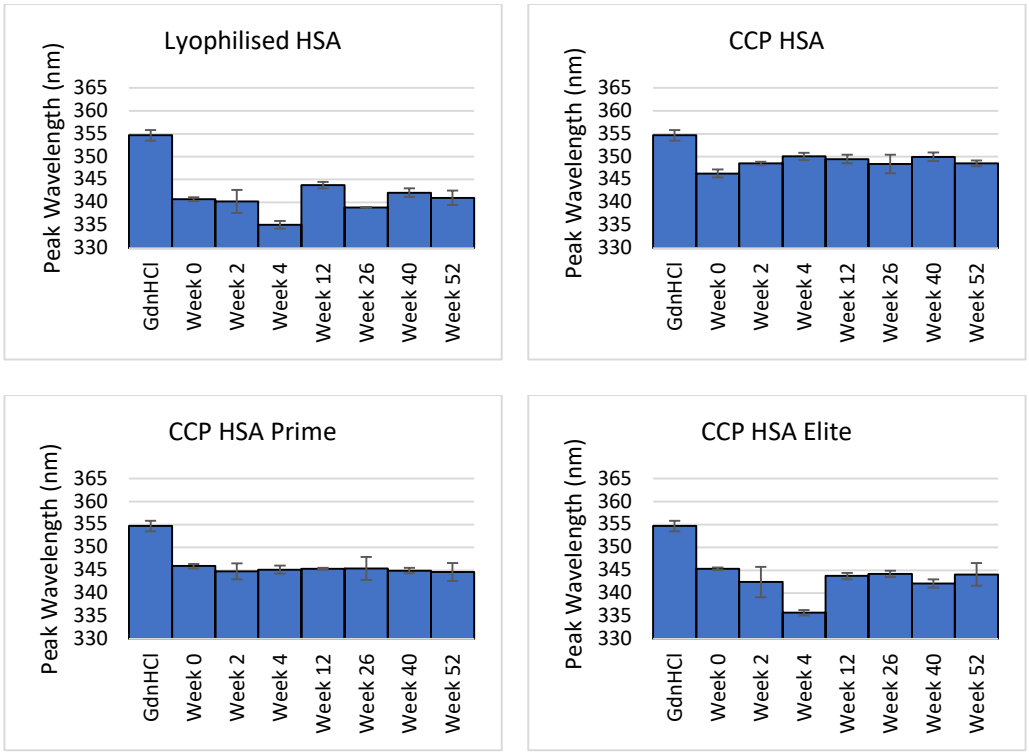

Fig. 4.4: Chart showing peak emission wavelength of rehydrated lyophilised HSA and HSA microparticles prepared via CCP samples stored at 5°C at each time point with the excitation wavelength set at 295 nm. Samples were recorded in triplicate and error bars = 1 S.D. of the mean.

HSA samples stored at 25°C

Figure 4.5 shows four bar charts detailing the peak emission wavelengths of the HSA formulations stored at 25°C at each time point with the excitation wavelength set at 295 nm. The measurement obtained from the GdnHCl-denatured control samples are also plotted on the chart to act as a negative control. Analysis of these

results show that none of the formulations experienced any trend in the peak wavelength values with the final measurements of each sample measuring less than 1% deviation from the initial value. This implies that the proteins were not experiencing any non-reversible unfolding. All samples did, however, measure a large spike in the value at week 26, as was seen in the BSA samples. This reinforces the decision to ignore these results as a sample prep or sampling error.

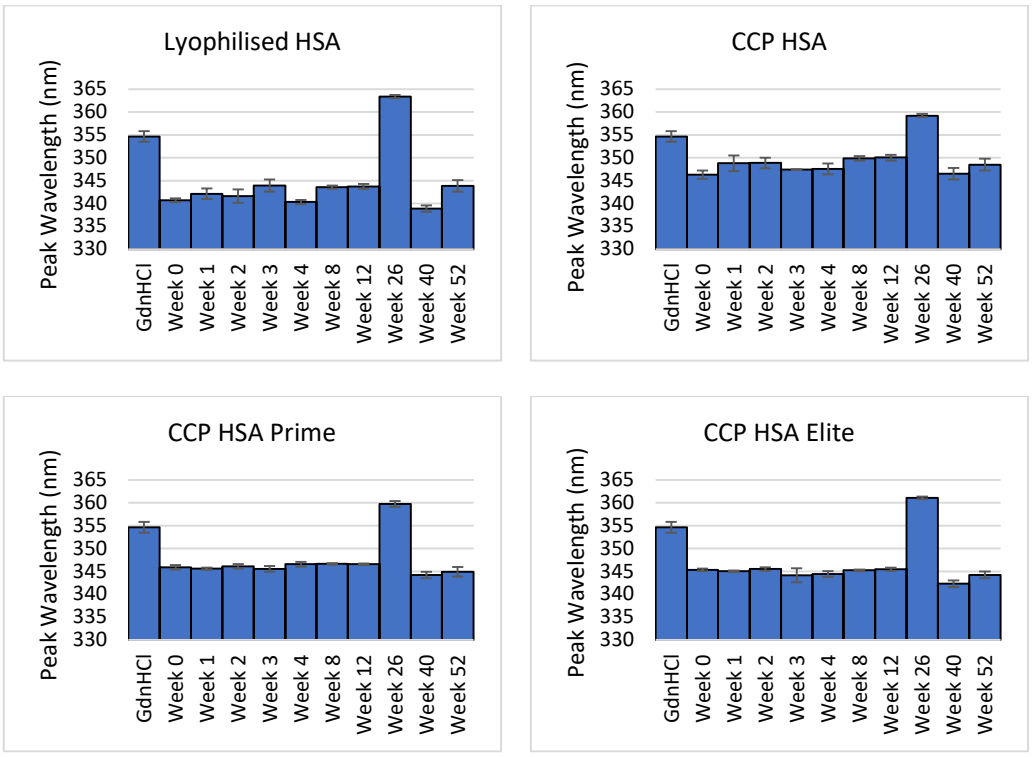

Fig. 4.5: Chart showing peak emission wavelength of rehydrated lyophilised HSA and HSA microparticles prepared via CCP samples stored at 25°C at each time point with the excitation wavelength set at 295 nm. Samples were recorded in triplicate and error bars = 1 S.D. of the mean.

HSA samples stored at 40°C

Figure 4.6 shows the results obtained the peak emission wavelengths of the HSA formulations stored at 40°C at each time point with the excitation wavelength set at 295 nm. The measurement obtained from the GdnHCl-denatured control samples are also plotted on the chart to act as a negative control. Analysis of these data showed that the CCP HSA formulation showed an increase in peak wavelength after the first week of storage, decreasing to 98.9% of the initial value, after which the

measurements remained high. This increase in the measured peak wavelength may indicate an increase in non-reversible unfolding, however, the overall change in the peak value over 40 weeks remained low, reaching 100.64% of the initial value and remaining significantly lower than that of the negative control. The other three HSA formulations did not show any trend in the measured values showing that there was no evidence of non-reversible unfolding throughout the lifetime of the study.

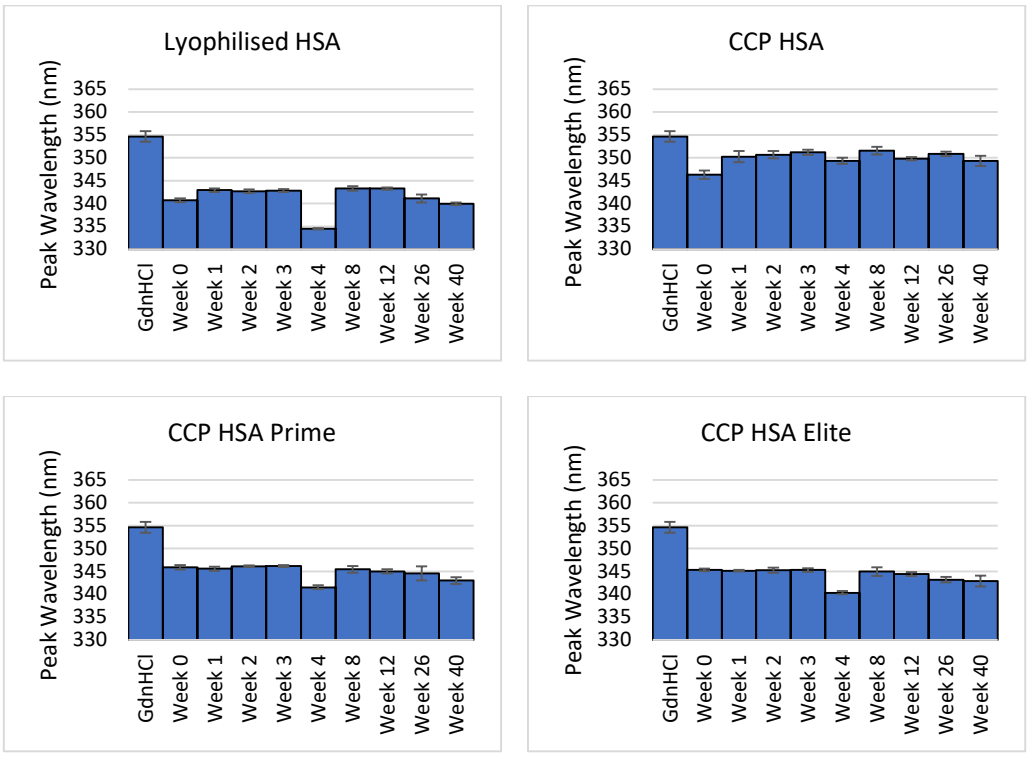

Fig. 4.6: Chart showing peak emission wavelength of rehydrated lyophilised HSA and HSA microparticles prepared via CCP samples stored at 40°C at each time point with the excitation wavelength set at 295 nm. Samples were recorded in triplicate and error bars = 1 S.D. of the mean.

4.3.2 UV-Vis Spectroscopy

The Aggregation Index (A.I.) of a protein solution is a measure of non-soluble, sub-visible protein aggregates and can be used to compare different samples and formulations. The technique utilises UV-Vis spectroscopy and was carried out as described in the Materials and Methods chapter. As a brief description of the technique, the rehydrated BSA samples were measured using UV-Vis spectroscopy. This method utilises the fact that absorbance at 280 nm can be used to quantify

protein concentration in solutions and that proteins do not absorb light above 320 nm. Therefore, any absorbance measured above 320 nm can be attributed to light scattering by undissolved particles. In this case, undissolved particles can be attributed to sub-visible, non-soluble aggregates. By taking the ratio of the absorbance measurement at 350 nm to the absorbance measurement at 280 nm minus the absorbance at 350 nm, and multiplying the result by 100, one can calculate the A.I. Using this calculation, one obtains a result that increases in value as the absorbance at 350 nm increases or the absorbance at 280 nm decreases and is a useful tool to compare the relative degree of aggregation between protein samples. This technique cannot distinguish between different polymeric aggregates of the protein but is a useful screening tool to test the relative abundance of non-soluble aggregation.

During the analysis of the data obtained using this technique, multiple outlying data points were discarded based upon the UV-Vis absorbance spectra. The calculated A.I. of the rejected data points were all significantly higher than the other data points in the triplicate and the data from the adjacent time points and skewed that data points towards high A.I. with very large error margins. To decide which data points were rejected the UV-Vis absorbance spectra were interrogated and outlier data points showed a significant reduction in or complete absence of the absorbance at 280 nm compared with other samples in the triplet. Figure 4.7 shows an example of spectra that were accepted (left) and rejected (right). The rejected spectra show very limited or no absorbance peak at 280 nm and it is believed this is due to sample preparation errors which resulted in uneven quantities of protein in each sample, with some samples containing very little protein resulting in very low concentration samples once reconstituted.

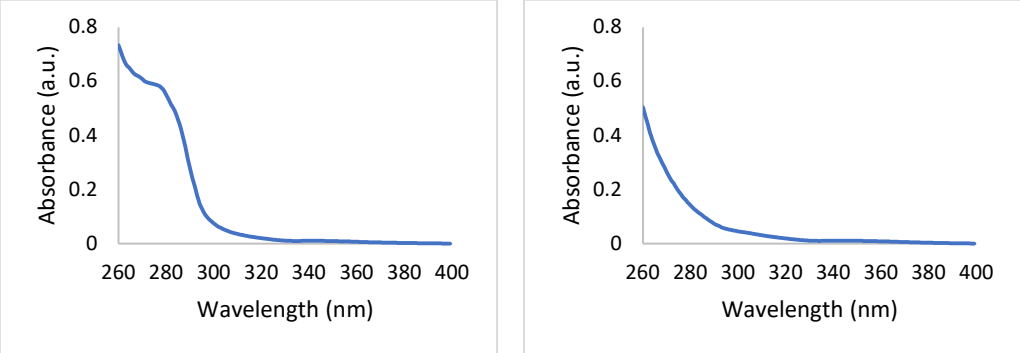

Fig. 4.7: UV-Vis spectra showing accepted (left) and rejected (right) samples for the purpose of calculating the A.I. of the sample. The accepted spectrum had a clear peak at 280 nm which was attributable to protein in solution. The rejected spectrum had no clear peak at 280 nm indicating a low concentration of protein.

BSA samples stored at 5°C

Figure 4.8 shows the A.I. results obtained from the BSA samples stored at 5°C. Analysis of these data show that the BSA lyophilised samples experienced an increase in A.I. value from 1.05 at Week 0 to 1.96 at Week 40 (186.7% of initial measurement), whereas the CCP samples started with a value of 2.44 at Week 0 and experienced no increasing trend to end with a value of 2.64 (108.2% of initial measurement) at Week 40. These results imply that the lyophilised samples did experience an increase in non-soluble aggregates over the course of 40 weeks stored at 5°C. Whilst this implies that the lyophilised sample may have performed less well than the CCP samples, with increasing aggregation over time, it should be noted that the CCP sample measurement at Week 0 was greater than that of the lyophilised sample at Week 40. Interestingly, the week 52 samples gave A.I. measurements very close to zero for both BSA formulations. This highly significant reduction was caused by a depression in the spectral data centred at approximately 345 nm in these samples (Fig. 4.9). This caused the absorbance at 350 nm to be very close to zero, and thus the A.I. calculation also being very close to zero. Whilst it is unclear what caused this difference in the spectra of the week 52 samples, it is likely that these values are spurious and due to some form of measurement or sample preparation error.

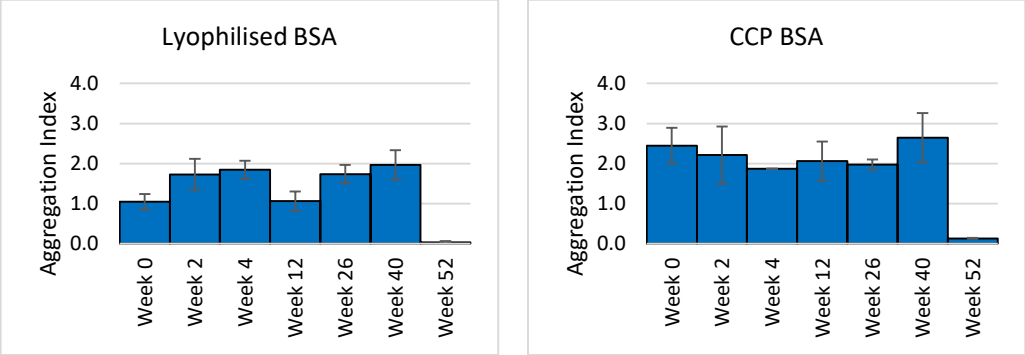

Fig. 4.8: Plots of the Aggregation Index of BSA samples stored at 5°C and tested at time intervals over 52 weeks, errors bars = 1 S.D. of the mean.

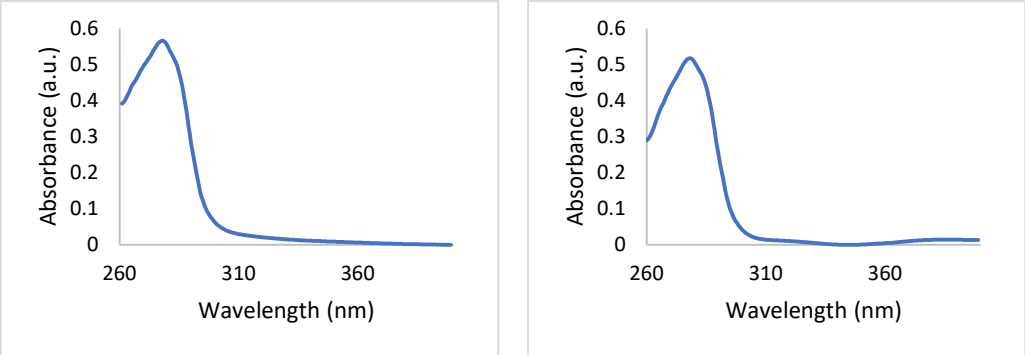

Fig. 4.9: UV-Vis spectra obtained from BSA microparticles prepared using CCP samples stored at 5°C (Left) Data from week 40. (Right) Data from week 52. Comparison of the two spectra shows that a depression in the spectra is evident in the week 52 spectra at approximately 345 nm.

BSA samples stored at 25°C

Figure 4.10 shows the A.I. results obtained from the BSA samples stored at 25°C. Analysis of the data showed that the mean A.I. values of both lyophilised and CCP BSA samples increased significantly by week 2 of the study, ending the study with A.I. measurements of 3.53 (336.2% of initial measurement) and 3.45 (141.4% of initial measurement) respectively. These results imply that the abundance of non-soluble aggregates increased significantly for both BSA formulations after two weeks of storage at 25°C. However, after week 2, the A.I. values did not increase significantly for either formulation for the remainder of the study (with two exceptions as discussed below). This further implies that after two weeks of storage at 25°C no further aggregation took place within the protein samples.

It is clearly seen in the data plot that the CCP BSA samples at week 26 gave a highly significant, large increase in the value of A.I. compared to the previous and following data points. This data point matches with that seen in the fluorescence spectroscopy data and supports the suggestion that this is due to contamination of some description to the sample resulting in either increased aggregation or non-soluble particulate contamination. Calculation of the A.I. from the lyophilised BSA samples at week 52 resulted in a significantly lower value than the week 40 samples. Similar to the results seen in the samples stored at 5°C, this resulted from a depression in the spectral data centred at approximately 345 nm, the cause of which is unclear.

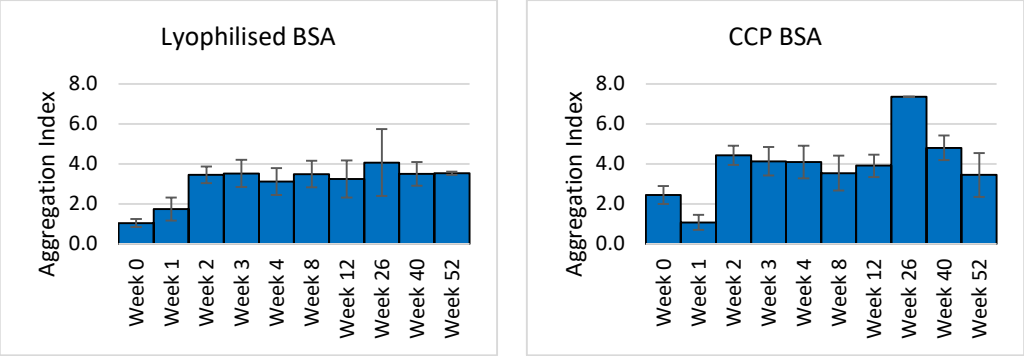

Fig. 4.10: Plots of the Aggregation Index of BSA samples stored at 25°C and tested at time intervals over 52 weeks, errors bars = 1 S.D. of the mean.

BSA samples stored at 40°C

Figure 4.11 shows the A.I. results obtained from the BSA samples stored at 40°C. Analysis of these data shows a clear trend of increasing A.I. with increasing storage time at 40°C for both formulations, with mean A.I. values increasing from 1.05 to 5.94 (565.7% of initial measurement) and 2.44 to 12.73 (521.7% of initial value) for lyophilised and CCP samples respectively. Statistical analysis showed that the A.I. of the lyophilised sample increased significantly after one week of storage at 40°C whilst the A.I. of the CCP samples increased significantly after two weeks of storage at 40°C. These data imply that both BSA formulations began to form additional non-soluble aggregates within the first week of storage at 40°C and continued to form further aggregates throughout the lifetime of the study. Whilst

the A.I. of both BSA formulation increased by over 500% during the 40 week study, the CCP samples showed a slightly lower overall increase. However, as noted above, the CCP samples started at a higher A.I. value which may have impacted on aggregate formation.

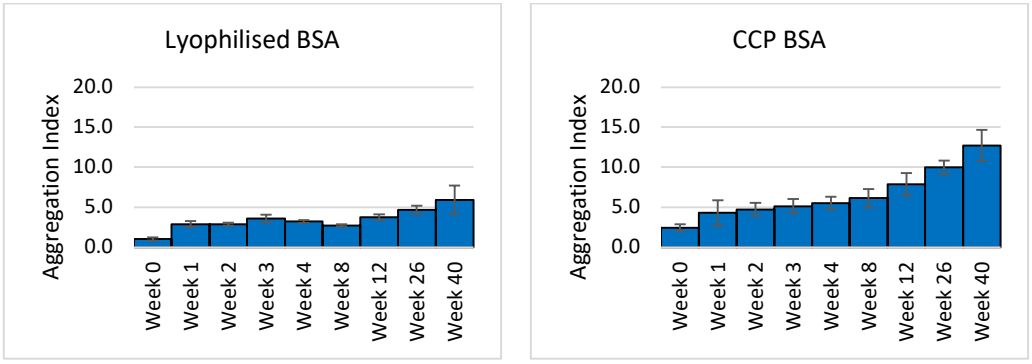

Fig. 4.11: Plots of the Aggregation Index of BSA samples stored at 40°C and tested at time intervals over 40 weeks, errors bars = 1 S.D. of the mean.

HSA samples stored at 5°C

Figure 4.12 shows the A.I. results obtained from the various HSA formulations stored at 5°C. As with the results from the BSA formulations, the Week 52 samples measured near-zero results and were ignored. These data showed that the lyophilised samples experienced an increasing A.I. value ranging from 2.77 at Week 0 to 4.97 at Week 40 (179.4% of initial measurement). The CCP HSA results measured variable data throughout the study with high values recorded at Week 4 and Week 26, although the mean A.I. value only deviated from 2.21 to 2.37 between Week 0 and Week 40 (107.2% of initial measurement). The results from both the HSA Prime and Elite formulations showed that the A.I. value did trend towards increasing A.I. with increasing time, however, the Week 0 samples from both formulations measured significantly higher than the Week 2 samples, implying that there may have been an issue with the Week 0 samples causing additional aggregation. Taking the week 2 measurements as the initial values, the Prime formulation increased from 2.10 at week 2 to 3.02 at week 40 (143.8% of initial

measurement) and the Elite formulation increased from 4.04 to 6.97 (172.5% of initial measurement).

Overall, these results show that all samples experienced increased levels of non-soluble aggregates over the course of 1 year stored at 5°C. Both the lyophilised and CCP samples showed evidence of significantly increased aggregation by Week 4 whilst the CCP Prime and Elite formulations did not experience significant increases until Week 26 and Week 40 respectively. As with the BSA samples stored at 5C, the week 52 samples showed a dramatic reduction in the A.I. value over all samples due to a localised depression in the spectral data centred at approximately 345 nm.

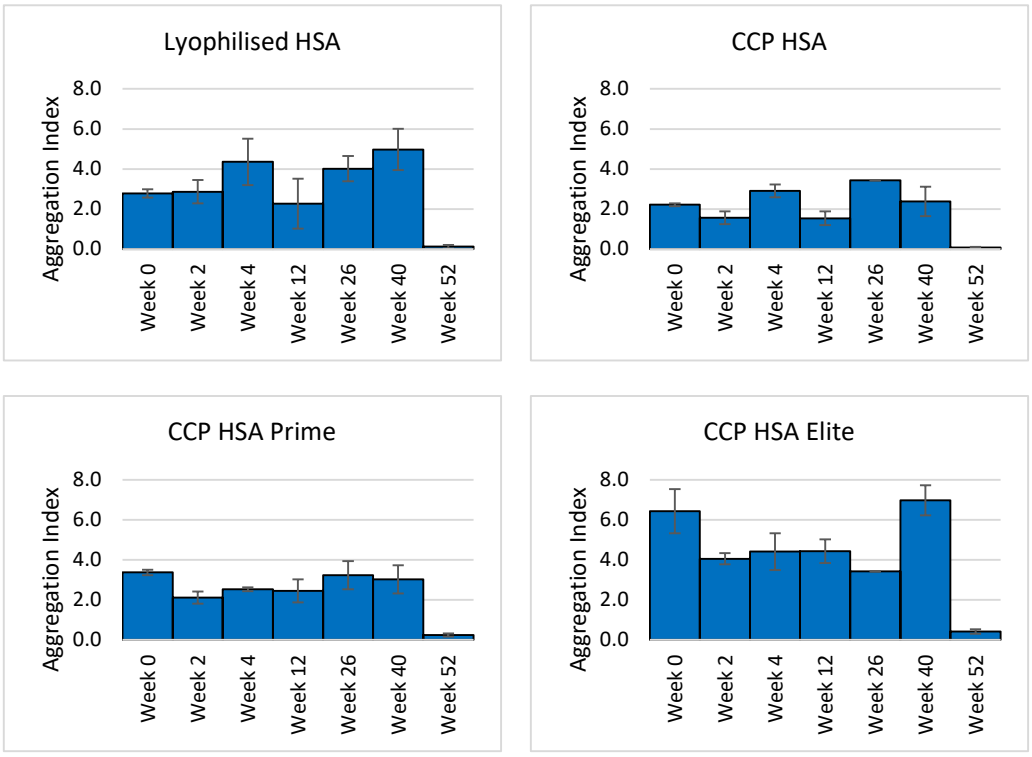

Fig. 4.12: Plots of the Aggregation Index of HSA samples stored at 5°C and tested at time intervals over 52 weeks, errors bars = 1 S.D. of the mean.

HSA samples stored at 25°C

Figure 4.13 shows the A.I. results obtained from HSA samples stored at 25°C, for the three CCP samples the y-axis was truncated to cut off the result from Week 26. As discussed above, the Week 26 samples stored at 25C all reported high levels of structural unfolding and aggregation leading to the conclusion that these samples were contaminated at some point in the sample or analysis preparation steps. Analysis of these data showed that the lyophilised HSA samples reported a sharp increase in the A.I. measurements over the first two weeks of the study, after which time it continued to increase over the course of the study, reaching 8.27 at Week 40 (298.6% of initial measurement). The CCP HSA samples also experienced a significant increase in the measured A.I. values by the second week of the study, however after the second week the A.I. value the reduced consistently until a final increase again at Week 40 to 6.71 (303.6% of initial measurement). Both the CCP Prime and Elite formulations showed similar, but less pronounced, results to the CCP HSA samples. Both sets of results saw an increase in the A.I. measurements over the first two weeks, followed by a gradual reduction and a final increase at Week 40. The measured A.I. values increased from 3.36 to 6.08 (181.0% of initial measurement) for the Prime formulation and 6.42 to 8.56 (133.3% of initial measurement) for the Elite formulation.

These results indicate that all formulations experienced an increase in non-soluble aggregate formation over the lifetime of the study. The lyophilised and CCP samples both experienced an approximate three-fold increase in the A.I. measurements, whereas the Prime and Elite formulations experienced lesser increases.

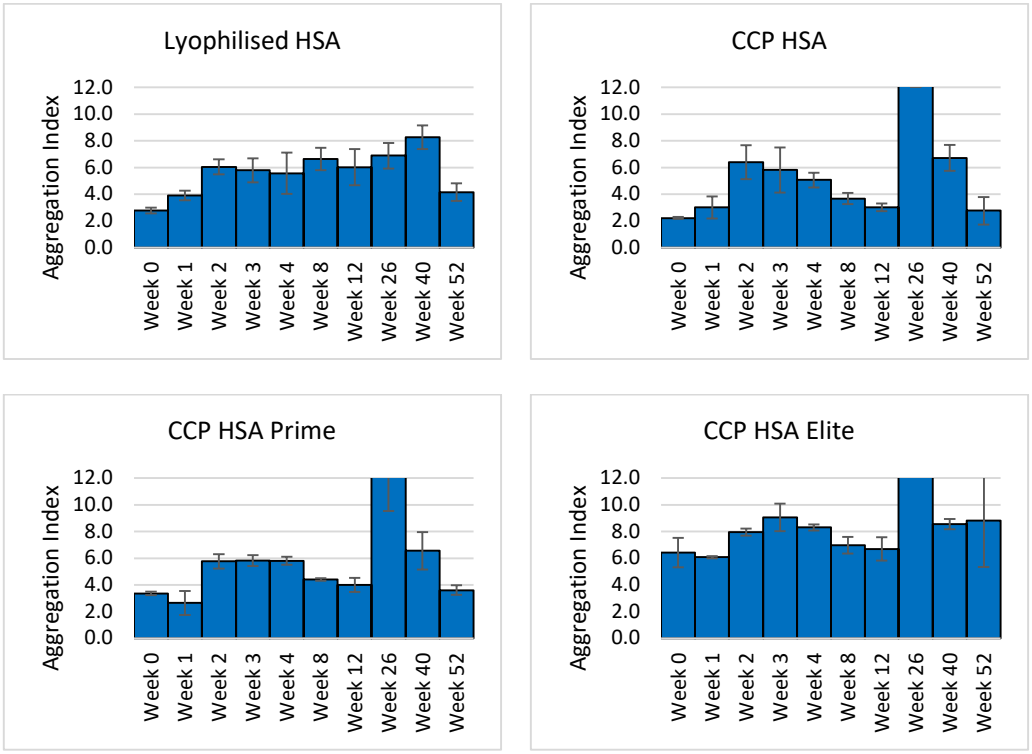

Fig. 4.13: Plots of the Aggregation Index of HSA samples stored at 25°C and tested at time intervals over 52 weeks, errors bars = 1 S.D. of the mean.

HSA samples stored at 40°C

Figure 4.14 shows the A.I. results obtained from HSA samples stored at 40°C. Analysis of the data showed a clear trend towards increasing A.I. with increasing storage time for all samples. This result shows that all protein samples experienced increasing levels of aggregation whilst being stored at 40°C. The lyophilised samples experienced an increase in A.I. value from 2.77 to 12.68 (457.8% of initial measurement), the CCP HSA samples experienced an increase from 2.21 to 10.36 (468.8% of initial measurement), the HSA Prime samples measurements increased from 3.36 to 14.52, (432.1% of initial measurement), and the HSA Elite samples measured from 6.42 to 12.60 (196.3% of initial measurement).

These results indicate that all HSA formulations experienced an increase in non-dissolvable aggregates beginning in the first week of the study and continuing to increase throughout the study lifetime.

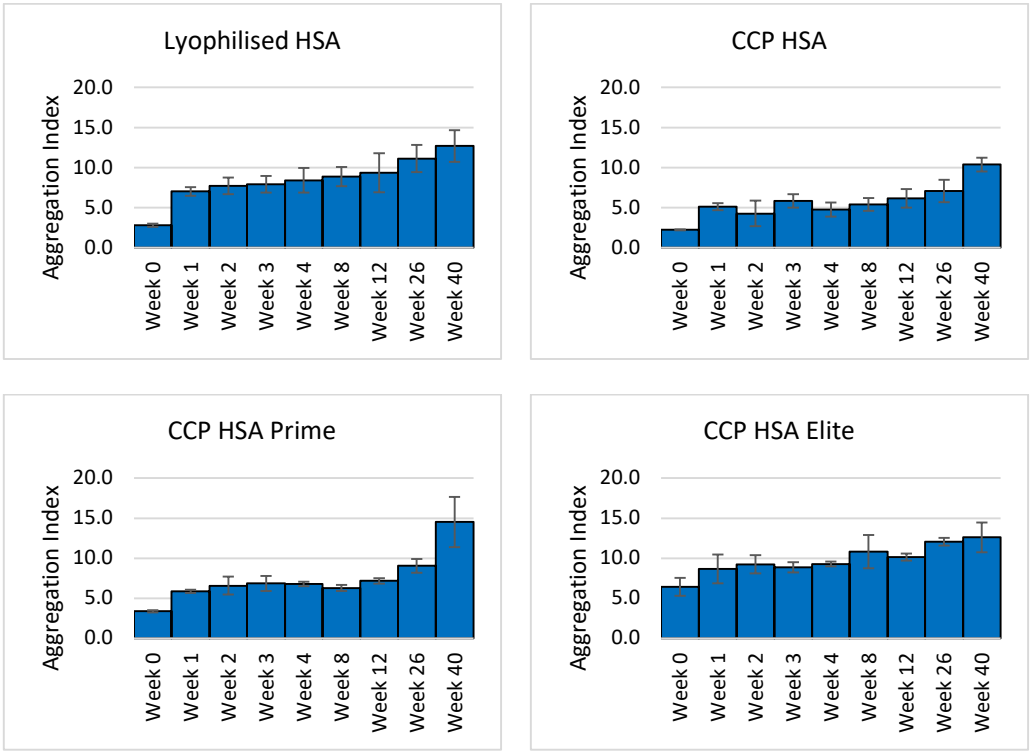

Fig. 4.14: Plots of the Aggregation Index of HSA samples stored at 40°C and tested at time intervals over 40 weeks, errors bars = 1 S.D. of the mean.

4.3.3 Size Exclusion Chromatography

Size exclusion chromatography is an industry standard technique for the quantitative assessment of protein aggregation and is capable of separating and quantifying aggregated protein forms, including the original monomer, dimers, trimers and larger polymers. The technique involves passing a protein solution through a HPLC column containing porous polymers or silica beads with a pre-determined pore size. Separation of protein aggregates is achieved as smaller particles will be able to move into or through the porous stationary phase, slowing their passage through the column. The larger a particle, the less pores it will be able to pass into and thus the faster it will elute through the column.

All SEC measurements were prepared and carried out by staff at Albumedix Ltd. using their equipment and protocols. Unfortunately, due to instrumentation issues at Albumedix Ltd., multiple data points were missed throughout the study as

discussed below. As the analysis was carried out at Albumedix, I was unable to repeat missed measurements.

BSA samples stored at 5°C

Figure 4.15 shows the results obtained from the SEC analyses carried out on the BSA samples stored at 5°C, providing the relative abundance of monomer, dimer, trimer and polymer within the protein solution at each time point in the study. Analysis of the data showed that a clear trend of reducing monomer abundance over time, and an accompanying increase in aggregated forms, existed in the CCP samples with the relative abundance of monomer forms reducing from 72.5% to 61.2%. Whilst any such trend was less easy to confirm in the lyophilised sample due to missing data points, it can be seen that a similar reduction in monomer abundance and increase in dimer forms was seen from Week 26 onwards with the relative abundance of monomer forms reducing from 89.3% to 88.4%. The results imply that both BSA formulation experienced increasing levels of non-soluble aggregation throughout the lifetime of the study and that the CCP BSA formulation experienced a greater increase.

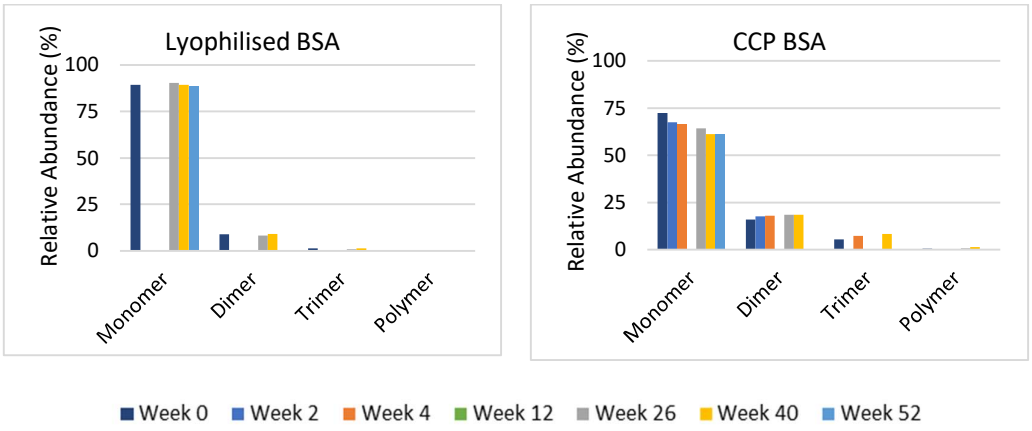

Fig. 4.15: SEC data obtained from BSA samples stored at 5°C showing relative abundance of monomer and aggregated forms of the protein. (Left) Lyophilised BSA (Right) CCP BSA.

BSA samples stored at 25°C

Figure 4.16 shows the results obtained from the SEC analyses carried out on the BSA samples stored at 25°C. These results show that the CCP samples experienced

a continuous reduction in monomer abundance throughout the study, reducing from 72.5% to 58.9%. However, the results from the lyophilised samples, although missing data, seem to show a trend of stable monomer abundance until Week 26, after which a trend towards a reduction in abundance can be seen. Between Week 0 and Week 26, the CCP sample experienced a reduction in monomer abundance of only 89.3% to 87.0% but this then reduced to 73.5% by Week 52. Overall, these results show that both BSA formulations experienced a decrease in monomer forms of the protein at the end of the 52 week study, with the relative abundance of monomer forms dropping by approximately 15% for each formulation. However, it appears that the lyophilised samples did not begin to experience a large reduction in monomer forms until after Week 26, whereas the CCP samples showed a trend towards reducing abundance from the first week of the study.

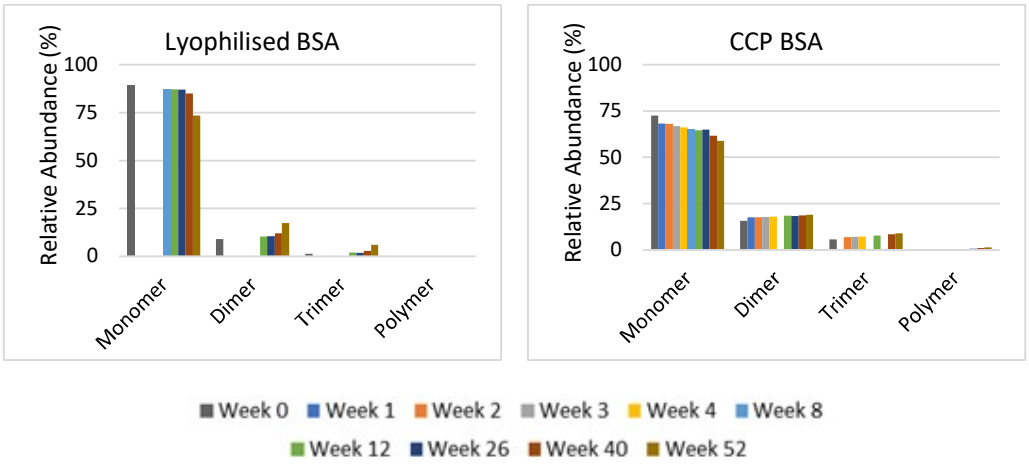

Fig. 4.16: SEC data obtained from BSA samples stored at 25°C showing relative abundance of monomer and aggregated forms of the protein. (Left) Lyophilised BSA (Right) CCP BSA.

BSA samples stored at 40°C

Figure 4.17 shows the results obtained from SEC analyses carried out on the BSA samples stored at 40°C. As with the samples stored at lower temperatures, visual analysis of the data showed that both lyophilised and CCP samples experienced a decreasing abundance of monomer, along with an accompanying increase in aggregated forms, with increased storage time. Analysis of these results shows that

both formulations experienced a clear trend of reducing monomer abundance over time, this was clear even with the missing data from the lyophilised samples. The lyophilised samples measured a reduction in monomer abundance from from 89.3% to 67.5%, whilst the CCP samples experienced a reduction from 72.5% to 41.4%. These results demonstrate that both formulations experienced a high degree of aggregation over the lifetime of the study, reporting a greater reduction in monomer abundance than was experienced at lower temperatures.

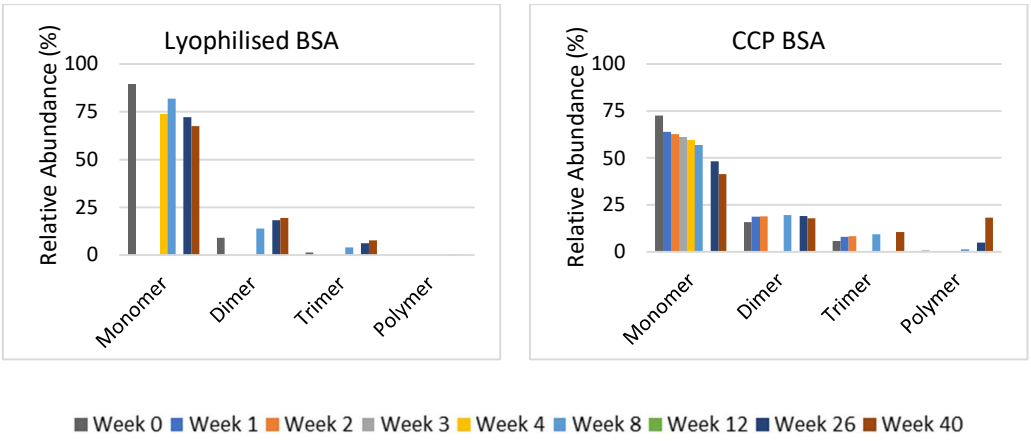

Fig. 4.17: SEC data obtained from BSA samples stored at 40°C showing relative abundance of monomer and aggregated forms of the protein. (Left) Lyophilised BSA (Right) CCP BSA.

HSA samples stored at 5°C

Figure 4.18 shows the SEC data obtained from the four HSA samples stored at 5°C. Analysis of these results shows that the lyophilised samples showed no clear trend in the abundance of monomer forms of the proteins with only a very minor reduction after week 26. However, all three CCP formulations did exhibit evidence of decreasing abundance of monomer forms over the study. Furthermore, it can be seen for all samples that the decrease in monomer forms was accompanied by a primary increase in the abundance of dimer forms and a minor increase in trimer forms. There was no evidence of an increase in larger aggregated forms. Over the lifetime of the study the lyophilised formulation experienced a reduction in monomer abundance from 84.1% to 83.2%, the CCP HSA formulation experienced a reduction in monomer abundance from 86.4% to 79.7, the CCP Prime samples experienced a

reduction in monomer abundance from 91.9% to 74.5%, and the CCP Elite samples experienced a reduction in monomer abundance from 88.8% to 74.1%. These observations imply that that all the samples experienced increased aggregation throughout the study with the HSA Prime and Elite formulations experiencing the greatest levels of aggregation whilst the lyophilised HSA samples experienced the least.

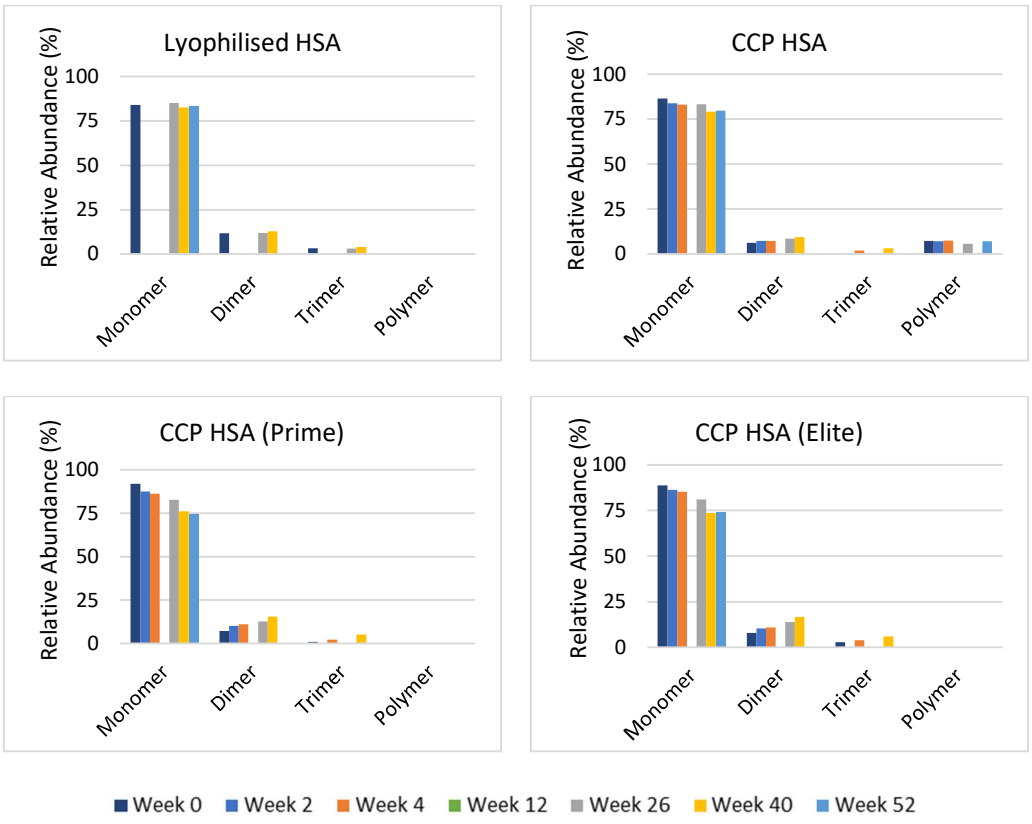

Fig. 4.18: SEC data obtained from HSA samples stored at 5°C showing relative abundance of monomer and aggregated forms of the protein. (Top Left) Lyophilised HSA (Top Right) CCP HSA (Bottom Left) CCP HSA Prime (Bottom Right) CCP HSA Elite

HSA samples stored at 25°C

Figure 4.19 shows the SEC results obtained from HSA samples stored at 25**°**C. Analysis of these data showed that all four formulations exhibited a trend of decreasing abundance of monomer as storage time increased, along with an associated increase in dimer and trimer forms of the protein. Interestingly, the week 26 sample showed a large and unexpected decrease in monomer abundance in the

lyophilised samples and smaller, unexpected increases in the CCP samples. These data points are likely attributable to sample contamination as seen in other 25°C Week 26 samples discussed in this report. The data show that the lyophilised samples experienced a reduction in monomer abundance from 84.1% to 73.5%, the CCP HSA samples experienced a reduction in monomer abundance from 86.4% to 75.7%, the CCP Prime samples experienced a reduction in monomer abundance from 91.9% to 69.5%, and the CCP Elite samples experienced a reduction in monomer abundance from 88.8% to 71.4%. These observations imply that all four HSA formulations experienced increased aggregation over the lifetime of the study with reductions in monomer abundance corresponding with increase in dimer and trimer forms of the protein. The lyophilised and CCP HSA samples experienced the least aggregation, whilst the Prime and Elite formulations experienced the greatest.

HSA samples stored at 40°C

Figure 4.20 shows the HPLC-SEC data obtained from HSA samples stored at 40°C over 40 weeks. These results show a clear trend, across all formulations, of reducing monomer and increasing dimer and trimer forms of the protein as storage time increased. Unfortunately, missing data points means it was not possible to observe any effects on the lyophilised samples over weeks 1, 2 and 3, but the week 4 data showed no decrease in monomer forms of the protein. However, the abundance of monomer then dropped off rapidly after week 4. All other formulations experienced a large reduction in the abundance of monomer after one week of storage followed by a gradual reduction in the following weeks until the end of the study. Analysis of this data shows that the lyophilised samples experienced a reduction in monomer abundance from 84.1% to 49.1%, the CCP HSA samples experienced a reduction in monomer abundance from 86.4% to 62.5%, the CCP Prime samples experienced a reduction in monomer abundance from 91.9% to 55.0%, and the CCP Elite samples experienced a reduction in monomer abundance from 88.8% to 61.9. These results indicate that all protein formulations experienced a high degree of aggregation when

stored at 40°C over 40 weeks with an associated increase in aggregated forms of the protein.

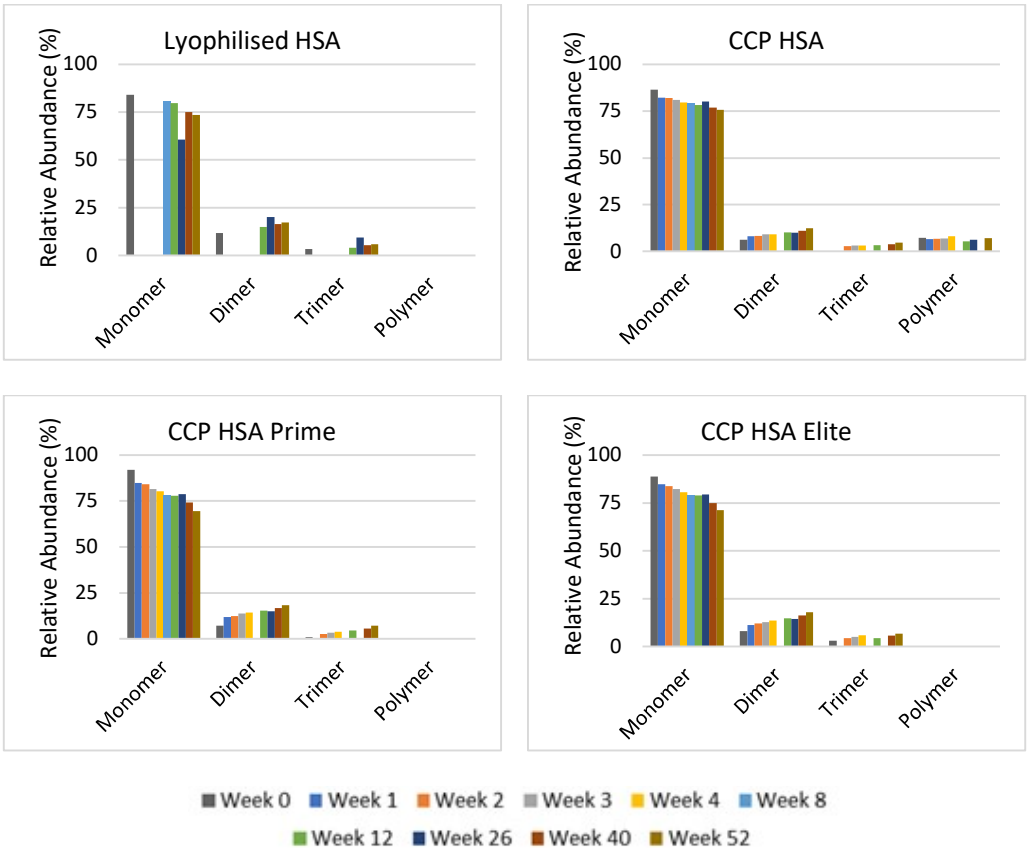

Fig. 4.19: SEC data obtained from HSA samples stored at 25°C showing relative abundance of monomer and aggregated forms of the protein. (Top Left) Lyophilised HSA (Top Right) CCP HSA (Bottom Left) CCP HSA Prime (Bottom Right) CCP HSA Elite

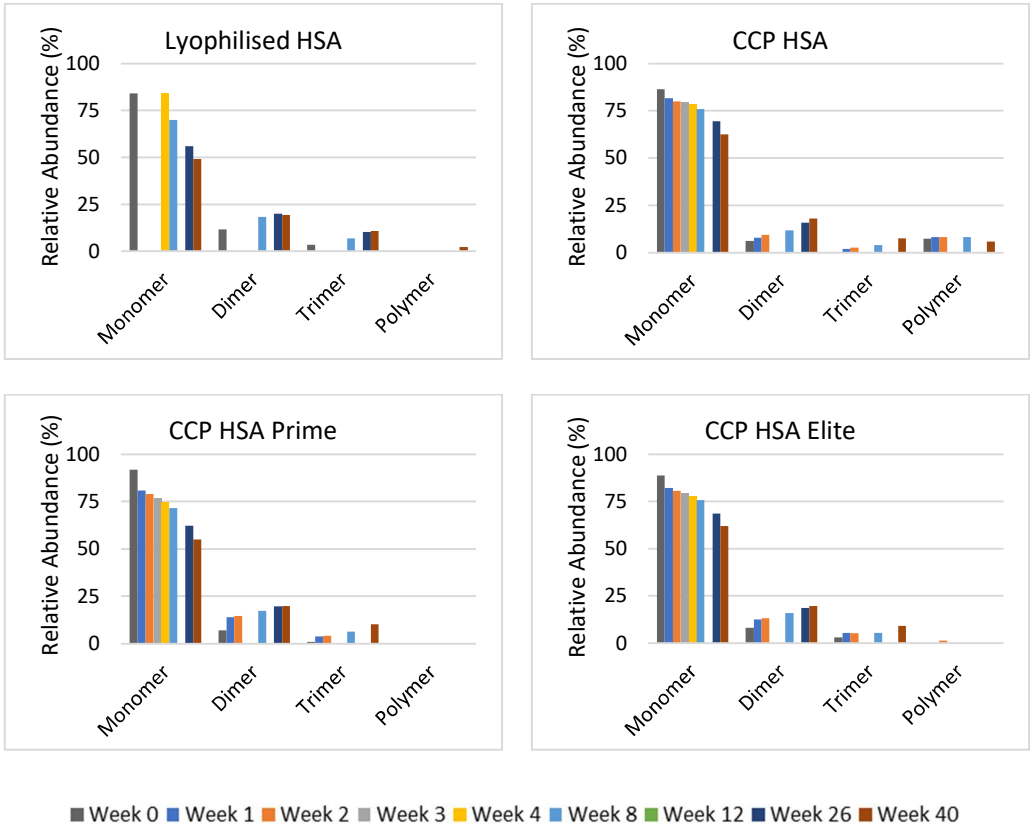

Fig. 4.20: SEC data obtained from HSA samples stored at 40°C showing relative abundance of monomer and aggregated forms of the protein. (Top Left) Lyophilised HSA (Top Right) CCP HSA (Bottom Left) CCP HSA Prime (Bottom Right) CCP HSA Elite

4.3.4 Protein Analysis Comparison

To allow for direct comparison of the results from the various analyses and protein formulations, the results were tabulated and heat-mapped to allow for quick visual comparison (Table 4.2). The fluorescence spectroscopy results were tabulated as absolute deviation of the final measurement from the initial measurement and cells were heat mapped with dark green highlighting the lowest values and deep red the highest values. This table shows how each formulation increased in final deviation with increasing storage temperature (with the exception of the lyophilised HSA result which showed a large spike in the 25°C data). This table also shows that the two lyophilised samples performed better than the CCP samples with final peak emission deviations less than 1 nm across all temperatures (with the exception noted above). The CCP samples, meanwhile, measured larger deviations in the

measured data with all formulations measuring deviations greater than 1 nm over nearly all temperatures. Whilst these measured deviations are still relatively small, remaining significantly lower than the GdnHCl-denatured negative control sample, the result does imply that CCP dehydrated BSA and HSA does not retain structural integrity long-term as well as lyophilised formulations.

Table 4.2: Heat-mapped results comparison. Fluorescence Spectroscopy results are shown as absolute deviation of the final measurement form the initial measurement. A.I. and SEC results are shown as the final measurement expressed as a percentage of the initial measurement. All cells are heat-mapped to allow for easy visual comparison with green indicating smaller changes and red indicating larger changes.

	Fluorescence Spec.			**Aggregation Index**			**SEC**		
	Absolute deviation of final measurement from initial measurement (nm)			**Final measurement expressed as a percentage of initial measurement (%)**			**Final measurement expressed as a percentage of initial measurement (%)**		
Sample	**5°C**	**25°C**	**40°C**	**5°C**	**25°C**	**40°C**	**5°C**	**25°C**	**40°C**
Lyophilised BSA	0.08	0.78	0.82	186.7	336.2	565.7	99.0	82.3	75.6
CCP BSA	2.44	3.08	3.36	108.2	141.4	521.7	84.4	81.2	57.1
Lyophilised HSA	0.29	3.17	0.77	179.4	298.6	457.8	99	87.4	58.4
CCP HSA	2.23	2.15	2.98	107.2	303.6	468.8	92.2	87.6	72.4
CCP HSA Prime	1.27	0.99	2.88	143.8	181	432.1	81.1	75.6	59.9
CCP HSA Elite	1.23	1.1	2.45	172.5	133.3	196.3	83.5	80.4	69.7

The results from the A.I. measurements show that the CCP BSA and CCP HSA samples performed extremely well when stored at 5°C with each formulation, recording very minor increases when compared to the other formulations. The lyophilised samples performed worst when stored at 5°C with the A.I. measurements nearly doubling by the end of the study. At higher temperatures, all samples saw large increases in the measurements across the board. These results imply that the lyophilised samples experienced greater increases to the relative abundance of non-soluble aggregates than the CCP when stored at 5°C over the lifetime of the study.

The SEC results show that the lyophilised formulations performed extremely well when stored at 5C with the final measurement for each formulation reporting 99% of the initial measurement of monomer abundance. This value ranged between 81.1 – 92.2% for the CCP formulations. However, when stored at 25C or 40C for one year, all formulation tested responded more equally. This implies that the CCP formulations experienced more aggregation overall than the lyophilised formulations when stored at 5C over the course of the study. However, the results from the A.I. measurements showed that the lyophilised formulations experienced increased non-soluble aggregation when stored at 5C. As non-soluble aggregates are generally larger polymeric forms of the protein, these two results can be taken together and imply that the CCP formulations may have experienced greater aggregation overall but likely into smaller aggregate forms, such as dimers and trimers, which tend to remain soluble. Meanwhile, the lyophilised formulations experienced less aggregation overall but tended to form larger, non-soluble aggregates as recorded by the A.I. measurements.

4.4 Conclusions and Further Work

During this study, dehydrated BSA and HSA powder formulations prepared by CCP and lyophilisation were stored at 5°C, 25°C and 40°C and analysed at pre-determined time points to assess the protein stability in the solid-form. Protein structure was characterised using fluorescence spectroscopy to assess levels of non-reversible protein unfolding. This was compared against negative controls of BSA and HSA solutions that had been denatured using 8M GdnHCl to disrupt hydrogen bonds and weaken the hydrophobic effect and cause the protein molecules to unfold, as described in the Materials and Methods chapter. Protein aggregation was studied using UV-Vis spectroscopy to calculate the aggregation index and size-exclusion chromatography to measure the relative abundance of low molecular weight aggregates.

Analysis of the BSA formulations by fluorescence spectroscopy showed no evidence of disruption to the protein structure throughout the length of the study, regardless of the temperature at which they were stored. Whilst minor variations in the emission wavelength were measured, these were all non-significant changes and may be due to natural variation in the samples or equipment. Overall, analysis of BSA structure using fluorescence spectroscopy showed that there was no clear advantage between the use of lyophilisation or CCP as a stability enhancer for long-term storage with both dehydration techniques measuring significantly lower than the negative control sample.

Analysis of protein structure of the HSA formulations showed no evidence of protein unfolding when stored at 5°C and 25°C for 52 weeks. The results did show statistically significant variations in the measured values of peak emission wavelength but this can be attributed to the small errors measured for the Week 0 samples and does not necessarily imply significant unfolding of the protein. However, analysis of the samples stored at 40C showed that the CCP-HSA formulation did show a potential increase in the peak emission wavelength over the course of the study with a maximum increase of approximately 5 nm from the Week 0 result. Overall, these results demonstrate that the CCP-HSA did show evidence of non-reversible unfolding when stored at 40C whereas the lyophilised samples did not. However, the Elite and Prime HSA formulations provided by Albumedix Ltd. did not show any evidence of non-reversible aggregation, regardless of storage temperature. This implies that CCP-HSA formulations can be prepared that have equal stability (in terms of protein unfolding) to lyophilised formulations.

The rehydrated protein formulations were also analysed using UV-Vis spectroscopy to calculate the aggregation index and assess the levels of non-soluble aggregates present in the samples. The aggregation index of a fluid is not a direct measure of aggregation, instead measuring light scattering from suspended aggregates. As such the technique is not capable of distinguishing between different size

aggregates but is often used as quick screening assay to identify the presence of larger aggregates before other techniques, such as SEC are used. When comparing these data it should be noted that the Week 0 measurements from the CCP samples were more than double those of the lyophilised samples. This may indicate the CCP and rehydration process resulted in greater levels of aggregation than the lyophilisation and rehydration process, however, results from Chapter 3 indicate that this is not the case. As such, it is likely that the increased A.I. measurements at Week 0 are a result of the formulations being prepared from differing source material. The lyophilised powder was purchased directly from a supplier, whereas the CCP samples were prepared in-house from a native solution.

Analysis of BSA samples stored at 5°C showed that the lyophilised formulation exhibited significant variations in the result of the course of the study whilst following an increasing trendline. Conversely, the CCP formulation did not exhibit any significant changes or trends from the week 0 measurements. At 25°C, measurements from both formulations showed that the A.I. increased significantly in the first two weeks of the experiment. After this time point both formulations measured constant A.I. values for the remainder of the study. At 40C, both formulations exhibited increasing A.I. measurements over the course of the study. These results imply that all BSA samples, except for the CCP samples stored at 5C, experienced an increase in non-soluble aggregation over the course of the study. This increase was minimal at 5°C but more pronounced at 25°C and 40°C. Comparing lyophilised samples to CCP samples, it can be concluded that when stored at 5°C or 25°C there is minimal difference between the two formulations, however, when stored at 40°C the CCP samples experienced a greater degree of aggregation than the lyophilised samples.

The analysis of the HSA formulations showed that all samples, across all temperatures, reported increasing A.I. values over the course of the study. Analysis of the three CCP formulations showed that each the Week 0 measurements were

significantly higher than the Week 2 measurements, implying that the Week 0 samples may have been contaminated. As such, A.I. measurements were compared with the Week 2 results instead of the Week 0 results. Furthermore, the Week 52 results from, the samples stored at 5°C showed near-zero results, as with the BSA samples, and were also ignored.

Comparison of the formulations stored at 5°C showed that the lyophilised samples reported the largest increase in A.I. measurements, experiencing an increase of nearly 100% of the A.I. value over the study lifetime. Meanwhile, the A.I. values of the CCP formulations only increased by approximately 50%. For the samples stored at 25°C, both the lyophilised and CCP samples recorded an increase in the A.I. value of nearly 200% whilst the Prime and Elite samples recorded lower increases of less than double. At 40C, all formulations showed a very clear trend towards increasing A.I. value with increasing storage time. The lyophilised, CCP-HSA and Prime formulations all experienced an A.I. increase of approximately 350% whilst the Elite formulation increased by approximately 100%. These results show that the different formulations of HSA reacted in different ways to long-term storage, when stored at 5°C, the CCP samples showed less evidence of increasing abundance of non-soluble aggregates than the lyophilised samples. At 25°C and 40°C, the CCP and lyophilised samples behaved equally,

The final analysis used in this study was SEC, to characterise the aggregation within each sample. Unfortunately, many data points from the lyophilised samples were missed during this study, making comparison difficult. However, the A.I. measurements discussed above make for good comparison data whilst the SEC measurements allow for further characterisation of the aggregated protein forms within a sample. Analysis of BSA samples stored at 5C showed that the lyophilised samples did not experience much increase in aggregated forms of the protein, with the relative abundance of monomer dropping by only 1%, whereas the CCP samples experienced a greater reduction in monomer forms of 15.6%. It was also shown

that the aggregation in the lyophilised samples produced a small increase in dimer forms only, whereas the CCP sample reported an increase in both dimer and trimer forms of the protein. At 25C, it appeared that the lyophilised sample retained high levels of monomer forms until week 26, at which point the abundance of monomer dropped off rapidly along with an increase in both dimer and trimer forms of the protein, however it should be noted that much of the early data is missing. In contrast, the CCP samples showed a rapid reduction in monomer abundance from Week 1 of the study, then following a reducing trend over time along with an increase in dimer and trimer forms and even some larger polymer forms by the end of thew study. Despite the apparent difference in the early stagtes of the study, both the lyophilised and CCP formulations reported equal reductions in monomer abundance of 18.8% and 17.7%, respectively. With BSA stored at 40C, the reduction in monomer forms of the protein were readily apparent in both formulations with the lyophilised samples reporting a drop of 24.4% in monomer abundance and the CCP samples reporting a 42.9% reduction. Both of these reducing monomer levels were accompanied by increases in dimer, trimer and polymeric forms of the protein. The CCP samples may even have started to measure a reduction in the number of dimer forms towards the end of the study as the abundance of polymeric forms increased rapidly.

Analysis of the HSA samples showed very similar results to those observed from the BSA formulations. When stored at 5C, lyophilised samples did not show much evidence of increased aggregation, although missing data points makes this difficult to confirm. A small reduction in monomer abundance of 1% was visible by the end of the study, along with a small increase in dimer and trimer forms of the protein. By contrast, the CCP samples all showed clear evidence of increased aggregation with increasing storage time, reporting decreases in the monomer form of 7.8% for the CCP-HSA samples, 18.9% for the Prime HSA and 16.5% for the Elite HSA samples. These decreases were all accompanied by corresponding increasers in the

dimer and trimer forms of the protein. At 25C, again all samples showed a clear trend of decreasing monomer content over time along with increasing dimer and trimer count. However, all formulations reported a more equal reduction in monomer than was seen in the 5C samples, with the lyophilised and CCP samples reporting 12.6% and 12.4% reduction whilst the Prime and Elite formulations reported a 24.4% and 19.6% reduction respectively. Finally, the samples stored at 40C also reported large decreases in monomer abundance with all three CCP formulations reporting a rapid reduction during the first week. As with previous results, all decreases in monomer abundance were associated with increases in dimer and trimer forms. Polymeric forms of the protein did not appear to increase during the study. Overall, these data show that all formulations tested during this study reported increases in aggregation When stored at 5C the lyophilised samples reported only minor increases to aggregation, whereas the CCP samples reported significant increases in aggregation. At higher temperatures the lyophilised and CCP samples reported similar levels of aggregation increases.

Taken altogether, these results imply that the CCP formulations may have experienced greater aggregation overall but likely into smaller aggregate forms, such as dimers and trimers, which tend to remain soluble. Meanwhile, the lyophilised formulations experienced less aggregation overall but tended to form larger, non-soluble aggregates as recorded by the A.I. measurements.

Future work stemming from this study would include repetition of such a study using alternative proteins to study the stability of more pharmaceutically relevant materials. This study could include further protein analyses including X-ray crystallography or FT-IR spectroscopy to provide more sensitive measurements of protein structure. If proteins are selected which have an activity assay available, then biological activity could also be measured to assess the functionality of the protein after storage and rehydration. Finally, a study could be performed to assess the use of stabilising additives within the aqueous protein solution. Such additives

could provide even greater advantages to the CCP technology, potentially resulting in the technology outperforming other dehydration techniques.

Chapter 5

Continuous Manufacture of CCP Microparticles

5.1 Chapter Introduction

This chapter discusses the continuous manufacture of CCP microparticles and the potential of the technology to produce size tuneable particles with a monodisperse size distribution. A continuous production system can be defined as a production system in which the materials and product are continuously charged into and discharged from the system throughout the duration of the process [182]. This is in contrast to a batch production system in which materials are charged into the system at the start of the process, and the product is discharged all at once sometime later with no materials entering or exiting the system between these times [182]. The majority of pharmaceutical manufacturing is carried out using batch methodologies, but recent advances in continuous manufacturing technologies are making the approach more feasible [183]. Continuous manufacture processes are generally considered an improvement over batch production systems, providing advantages in product quality and safety, as well as economic benefits [184]. With much of the pharmaceutical industry remaining tied to batch production techniques, there is an opportunity for new and agile businesses to incorporate continuous manufacturing into their productions lines and benefit from the advantages such a move can bring.

Continuous manufacture is generally carried out within a flow of fluids, where solid or liquid ingredients are pumped into a system where processing is conducted (often referred to as a reactor), before flowing out of the system as a final product or product precursor. A further advantage of fluid-flow continuous manufacture is the potential to manufacture highly uniform, size tuneable particles. This property of fluidic particle production has been well known and documented for many years

with size of the particle being controlled by manipulation of flow rates. If such properties were demonstrated using CCP technology within a fluid-flow continuous manufacturing system, then many new avenues of pharmaceutical research are opened. For example, a highly uniform distribution of CCP microparticles could be used to prepare high concentration protein suspensions in non-aqueous carriers for high dosage injections. Alternatively, CCP microparticles could be used as a dissolution aid or delivery vehicle for low solubility drugs. These new avenues of research are discussed further in Chapter 7 of this thesis.

The work presented in this chapter studies three techniques for the continuous manufacture of the aqueous droplet precursors to CCP microparticles. Droplets were formed and measured and parameters such as flow rate ratio and total flow rate were adjusted whilst looking for any change to droplet size. After the characterization of droplet production, the droplets were allowed to exit the continuous system into a solvent reservoir to allow the process to complete and the resultant particles were also characterized.

5.2 Continuous Production Techniques

Continuous production of microparticles or nanoparticles is generally performed with the use of a fluidic system in which droplets and/or particles are formed within the system and exit the system within a flow of fluid to be harvested for use. This concept is fundamentally different to the batch production techniques discussed in this thesis so far, in which the aqueous phase was introduced to the solvent reservoir as a single event and the stirring action was used to create a droplet suspension in which the CCP process could take place. The formation of droplets by vigorous stirring is a chaotic process and does not allow for control of droplet size or uniformity, thus resulting in a polydisperse distribution of microparticles. However, under a continuous manufacturing regime the generation of individual droplets allows for the potential to control the droplet size and distribution, producing a size-controlled, mono-disperse distribution of microparticles.

Three droplet generation techniques were investigated, along with two different reservoir types. Figure 5.1 shows representations of each droplet generation technique and reservoir configurations used in this study. The top three diagrams represent the droplet generation techniques. 1: The single flow technique, in which aqueous protein solution flowed through a length of tubing (internal diameter 250 μm) which terminated within the solvent reservoir. Droplet generation took place at the terminus of the tubing as the aqueous phase flowed out, which then sheared away from the tubing upon reaching a specific size. 2: A microfluidic technique known as flow-focusing, in which the aqueous and organic phases meet at a cross junction where the aqueous phase is restricted and forced to disperse into individual droplets by a local pressure build up, which travel down the outlet tubing to the reservoir. 3: The T-reactor technique, in which both aqueous protein solution and the drying solvent flow along tubing, intersecting within a T-connector of internal diameter 500 μm. Within the T-connector the two fluids meet under high pressure and aqueous droplets are formed which travel down the outlet tubing and exit into the solvent reservoir, unfortunately it was not possible to observe the mechanism by which droplets were formed using this technique. The bottom two diagrams show representations of the two solvent reservoirs: 4: The stirred vessel reservoir, in which the aqueous droplets are suspended by stirring of the reservoir to allow the CCP process to take place. 5: The unstirred reservoir system, named the solvent drop technique, which does not rely on stirring to facilitate CCP. This reservoir design allows for the aqueous droplets to fall though a column of drying solvent, undergoing CCP as they travel, collecting as CCP microparticles at the bottom of the vessel.

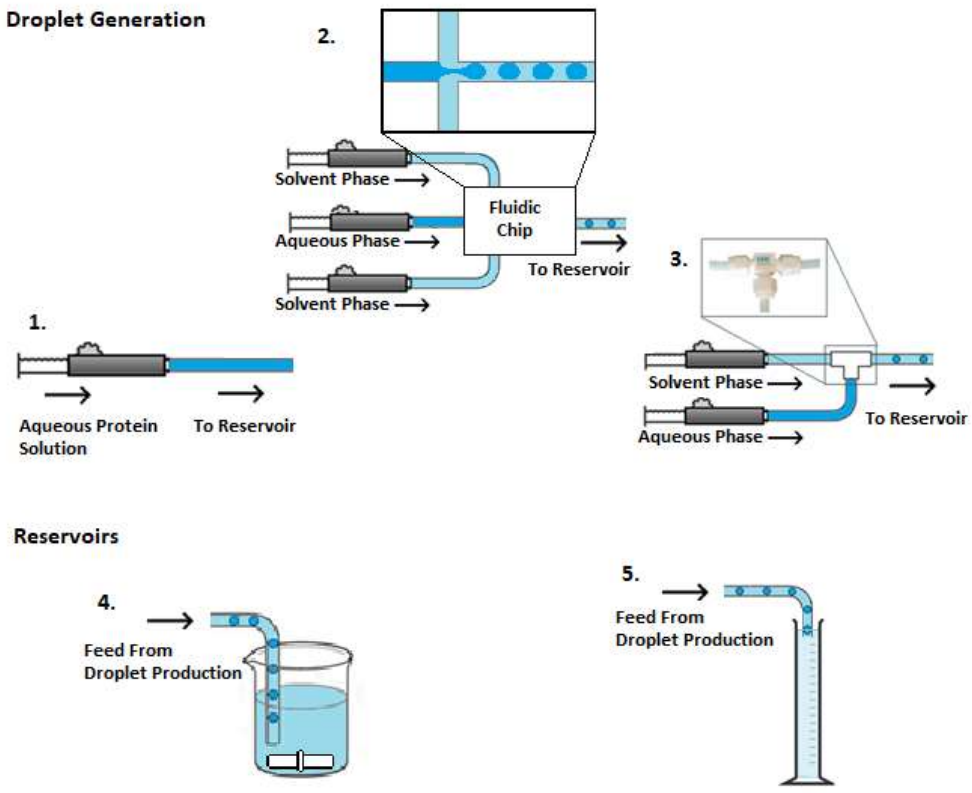

Fig. 5.1: Diagrams of each droplet generation technique and reservoir configuration. 1: The Single Flow technique. 2: Microfluidic Flow Focusing. 3: The T-reactor technique. 4: Stirred reservoir. 5: Unstirred reservoir.

5.3 Results and Discussion

5.3.1 Droplet Generation

To understand the processes involved in the continuous production of CCP microparticles, droplet formation was first investigated. BSA solution at 50 mg/mL was prepared and used as the aqueous phase to form droplets and dry pentanol was used as the organic phase. Droplets produced by each technique were observed and measured and the effects of varying the flow rates were investigated for each technique. In order to collect images of the droplets for comparison and sizing, no stirring was applied to the reservoir.

Single Flow Continuous Production

The single flow technique was distinct from the other techniques discussed in this chapter as droplets were not formed upstream of the reservoir. Instead, droplets were formed at the terminus of the tubing as the aqueous phase was deposited into the solvent reservoir (Fig. 5.2). The droplets formed at the end of the tubing were imaged using a digital camera and measured using Fiji. The aqueous flow rate was set at either 10, 50 or 100 μL/min and 10 droplets were imaged from each flow rate. Droplet images were measured using Fiji. These measurements showed that variation of the aqueous flow rate did not affect the droplet size, which was measured with a mean diameter of 1.8 ± 0.1 mm. As the aqueous phase exits the terminus of the tubing a droplet forms at the end of the tube due to the surface tension of the fluid. As the droplet increases in size, it also increases in mass until the effect of gravity overcomes the attractive force of the surface tension and pulls the droplet away from the tubing. Varying the flow rate of the aqueous phase did not affect the surface tension or gravity and so did not affect the droplet size. However, increasing the flow rate did increase the rate at which droplets were formed. It should be noted that this measurement was made with no stirring applied to the reservoir, if stirring were applied to the reservoir then additional shear forces would be acting upon the droplet, potentially causing the droplet to shear away from the tubing earlier in the growth stage, resulting in smaller droplets being produced.

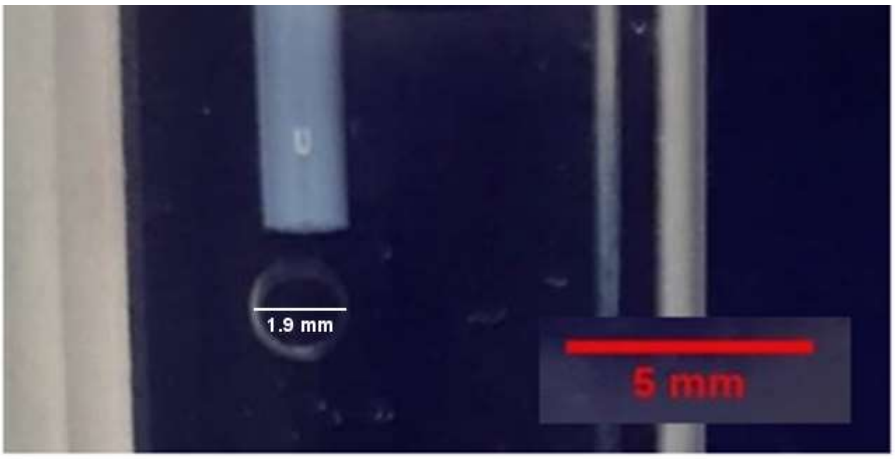

Fig. 5.2: Image showing a droplet of aqueous phase formed using the single-flow technique after it has detached from the tubing end with no stirring applied to the solvent reservoir.

Flow Focusing Microfluidics

The flow focusing continuous production technique made use of a 3D Flow Focusing microfluidic chip purchased from Dolomite Microfluidics (Fig. 5.3). The chip was purchased with a hydrophobic coating on the inside of the fluid channels to reduce the hydrophilicity of the glass surfaces and reduce the risk of side wetting, where the aqueous flow adheres to the glass surface and inhibits the formation of aqueous droplets. The chip is reversible, containing two flow focusing junctions (Fig. 5.3 pop-out), each with three inlets and one outlet. The continuous phase was introduced via inlets 1 and 3, whilst the dispersed phase was introduced via inlet 2. The phases meet at the flow focusing junction, where droplets are generated due to constriction of the dispersed phase resulting in droplets being forced through the junction as the pressure in the inlet phase builds up.

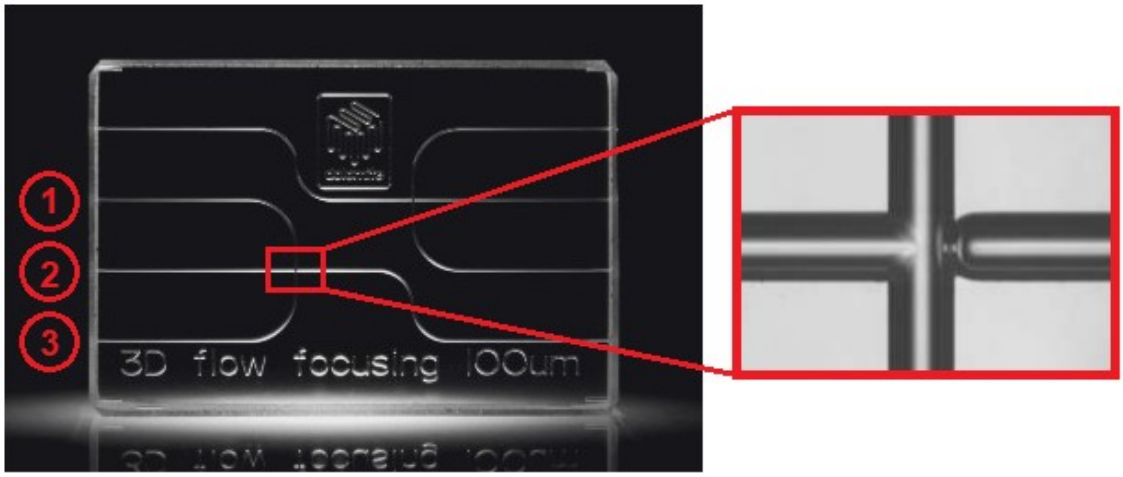

Fig. 5.3: Image of the Dolomite Microfluidics 3D Flow Focusing microfluidic chip. The chip contains two flow focusing junctions and can be reversed to allow access to either junction. The inlets and outlets of the chip were connected to PTFE tubing allowing the introduction of the two fluid phases. For aqueous droplet generation, the continuous phase (solvent) is connected to the top and bottom inlet (labelled 1 and 3), whilst the dispersed phase (aqueous) is connected to the middle inlet (labelled 2). The fluids intersect at the flow focusing junction and, if conditions are correct, droplets are formed by constriction of the dispersed phase and droplets of dispersed being forced through the junction by the local pressure build up. Images from [185].

The formation of droplets within a flow focusing junction relies upon one of two methods (Fig. 5.4): 1. Dripping: in the dripping regime, the dispersed phase is fully constricted by the continuous phase causing a local pressure build up in the inlet channel. Once the local pressure in the system overcomes the surface tension of the dispersed phase a droplet of the dispersed phase is forced into the stream of continuous phase which then travels along the outlet channel as another droplet is forced out of the junction [186]. 2. Jetting: in the jetting regime, the dispersed phase is partially constricted to force a thin jet of the dispersed phase to travel down the center of the outlet channel. Further downstream, the jet experiences fluctuations induced by the Rayleigh-Plateu instability, eventually breaking down and producing droplets with a diameter larger than the width of the jet stream [186]. Both of these mechanisms can be controlled by variation in the flow rate ratio between the two phases and the total flow rate of the system.

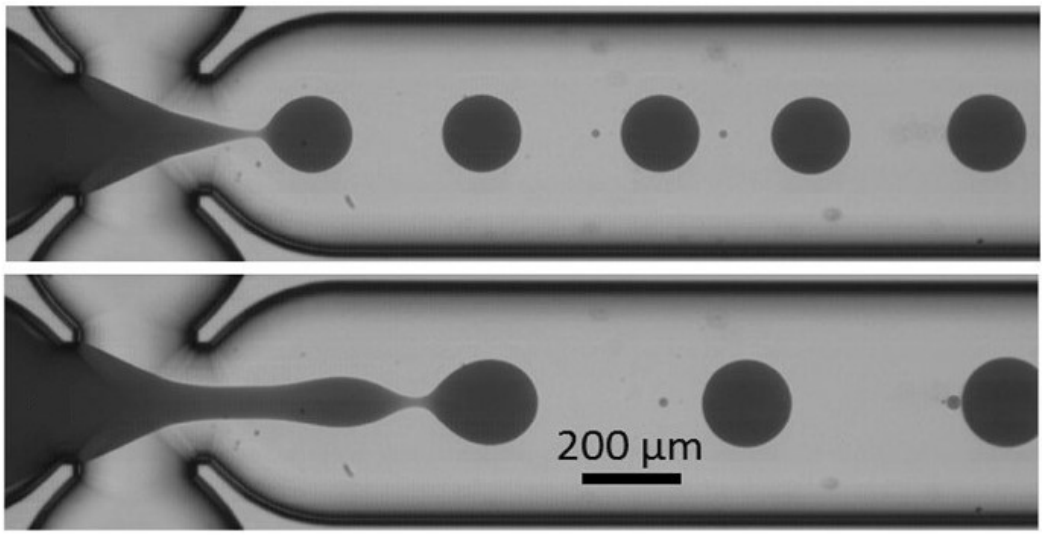

Fig. 5.4: (Top) Flow focusing operating in the dripping regime. (Bottom) Flow focusing operating in the jetting regime. Adapted from [187]

To investigate droplet production using the microfluidic flow focusing technique, the system was set up as described in Chapter 2 with the continuous phase flow rate (Qc) set at 100 µL/min (total flow rate over both inlets, ie 50 µL/min per inlet) and the dispersed phase flow rate (Qd) initially set at 20 µL/min to give a flow rate ratio of 5:1 (Qc:Qd) resulting in a co-flow of fluids along the outlet channel. The dispersed phase flow rate was then reduced incrementally until droplet generation was achieved. After each change to flow rates, 10 minutes were allowed for stabilisation of flow rates and pressures, as per the directions provided by Dolomite Microfluidics [185]. Utilising this method, stable droplet production was achieved in a jetting regime at Qd = 5 µL/min, giving a flow rate ratio of 20:1 (Qc:Qd). Figure 5.5 shows two brightfield microscopy images of droplets being formed at the flow focusing junction by the jetting method using a high-speed camera. The top image was recorded at at 20,000 frames per second with a resolution allowing for visualization of both the droplets and the width of the outlet channel. The bottom image was recorded at 50,000 frames per second and allow for visualization of the droplets with very little motion blur. Once droplet formation had been achieved, the system remained stable with droplet formation observed for over one hour without any

breakdown of the system. Multiple images were obtained using the high speed camera at 50,000 frames per second and droplets diameters were measured manually using Fiji. As the droplet images were blurred in the horizontal plane, all diameters were measured using the vertical plane. In total, 68 droplets were measured, providing a mean diameter of 12.5 ± 0.84 µm.

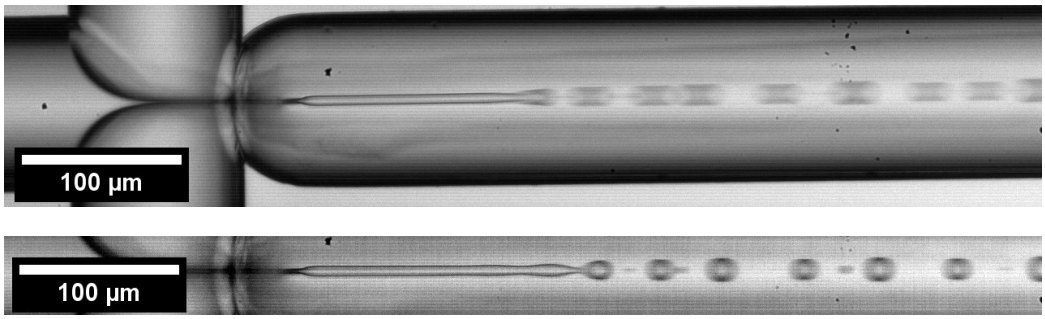

Fig 5.5: Two light microscopy images recorded using a high-speed camera of droplet production achieved via microfluidic flow focusing. Qc = 100 µL/min, Qd = 5 µL/min to give a flow rate ratio of 20:1 (Top) image recorded at 20k fps. (Bottom) image recorded at 50k fps

Variation of Qd away from 5 µL/min by as little as 1 µL/min resulted in unstable droplet production or complete breakdown of droplet generation. At Qd = 4 or 6 µL/min droplet production became unstable with droplet formation stopping and starting and large variation in droplet size. At Qd = 3 µL/min the dispersed phase flow was completely restricted, and solvent was observed travelling into the syringe containing the aqueous phase, at Qd = 6 µL/min the jetting stream extended much further into the outlet channel with no visual evidence of droplet formation when the jet ended. Whilst difficult to confirm, it appeared that when the jetting stream was extended over a long distance it increased the propensity for the aqueous stream to interact with the side of the channel, resulting in side-wetting which inhibited droplet generation.

Despite the breakdown of droplet generation when Qd was varied from 5 µL/min, droplets were observed exiting the outlet tube into the drying reservoir regardless of the flow rate settings. To investigate this, the outlet tubing was observed directly using light microscopy. However, this did not reveal the presence of aqueous

droplets travelling along the outlet tubing. This may imply that droplets were not being generated within the microfluidic system and were instead being generated at the terminus of the outlet tubing similar to the mechanism used by the single flow technique. The aqueous phase could travel along the channel sides to the outlet tubing terminus at which point a droplet would begin to form due to the surface tension of the aqueous phase. However, unlike the single flow technique, the outlet tubing contained both the aqueous phase and continuous phase, resulting in both contact area between the droplet and the aqueous phase within the tubing and an additional downward force acting on the droplet from the continuous phase exiting the tubing. As such the droplet would likely shear away from the tubing at a smaller size.

T-reactor Continuous Production

The T-reactor design utilised a plastic T-connector as a "millireactor" in which the aqueous and organic phases mixed to form aqueous droplets upstream of the solvent reservoir. The droplets then travelled through the outlet tubing carried by the solvent flow and exited into the solvent reservoir. Unfortunately, it was not possible to observe the droplet formation within the T-connector due to the opaque material it was made from. However, droplets were observed exiting the outlet tubing into the reservoir and, furthermore, droplets were observed under magnification whilst travelling along the outlet tubing.

Figure 5.6 shows a digital camera image of aqueous droplets exiting the outlet tube and entering the solvent reservoir. Both images were collected with Qc set at 100 µL/min and Qd set at 25 µL/min in the left image and 100 µL/min in the right image. Unfortunately, the resolution of the obtained images was too low to obtain accurate measurements, but it was clear through visual observation of the images that there was a size difference between the two samples. To measure the droplets more accurately the outlet tubing was held in place on a microscope stage and brightfield microscopy was employed to observe the droplets moving within the tubing. The

clear FEP tubing used for this technique allowed for observation of the droplets within the tubing. Figure 5.7 shows two images of aqueous droplets within the outlet tubing obtained via brightfield microscopy. For these samples, both images were obtained with the continuous phase flow rate set at 300 µL/min whilst the dispersed phase flow rate was set at 1 µL/min in the left image and 50 µL/min in the right image. Measurement of these droplets showed an increase in droplet size with increasing aqueous flow rate. It can also be seen that, even with the continuous to dispersed flow rate ratio set at 60:1 (Qc = 300 µL/min, Qd = 5 µL/min), the droplet diameter was larger than the internal diameter of the tubing, resulting in a squashed, elongated "slug" of fluid.

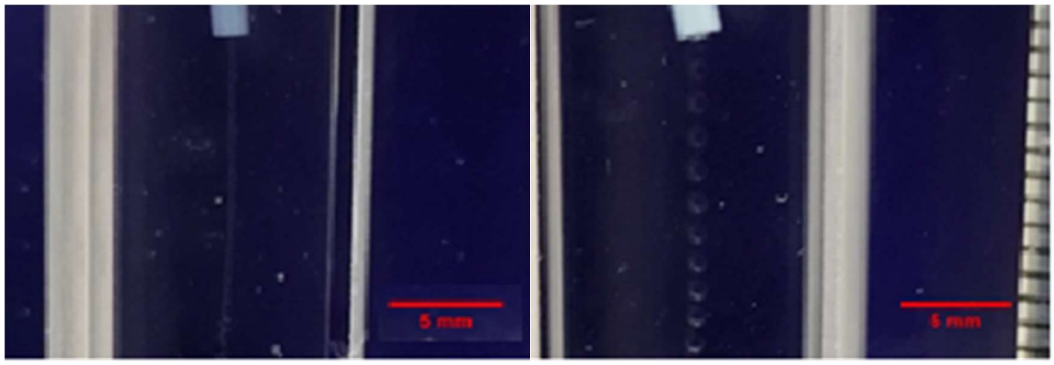

Fig 5.6: Images of droplets produced using the dual-flow technique showing a clear size difference with varying conditions. Left: solvent phase: 100 µL/min, aqueous phase: 25 µL/min. Right: solvent phase:100 µL/min, aqueous phase: 100 µL/min.

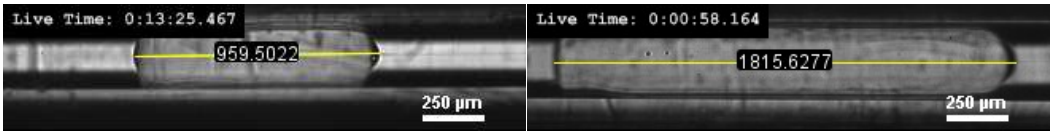

Fig 5.7: Light microscopy images of droplets produced using the dual-flow continuous production technique. Images were obtained of droplets within the outlet tubing. (Left) Continuous phase: 100 µL/min, Dispersed phase: 5 µL/min. (Right) Continuous phase: 300 µL/min, Dispersed phase: 50 µL/min.

To quantify the effect of varying the flow rates on the droplet size the solvent flow rate (continuous phase flow rate, Qc) was set at 100, 200 or 300 µL/min and the

aqueous flow rate (dispersed phase flow rate, Qd) was varied between 1 – 50 µL/min. Droplet images were collected from within the outlet tubing and droplet size was measured using Fiji. Droplet size was reported as the diameter of the sphere of equal volume to the observed droplet. For this calculation the droplet was assumed to be a perfect cylinder within the tubing and the volume was calculated as the cross-sectional area of the tubing multiplied by the droplet length. The field of view of the microscope allowed for a maximum droplet length of approximately 1,750 µm (560 µm diameter) so droplets larger than this could not be measured. Results of this experiment are plotted below in figure 5.8 where the droplet diameter is calculated as the diameter of the sphere with equivalent volume, error bars shown are ± 1 S.D. of the mean.

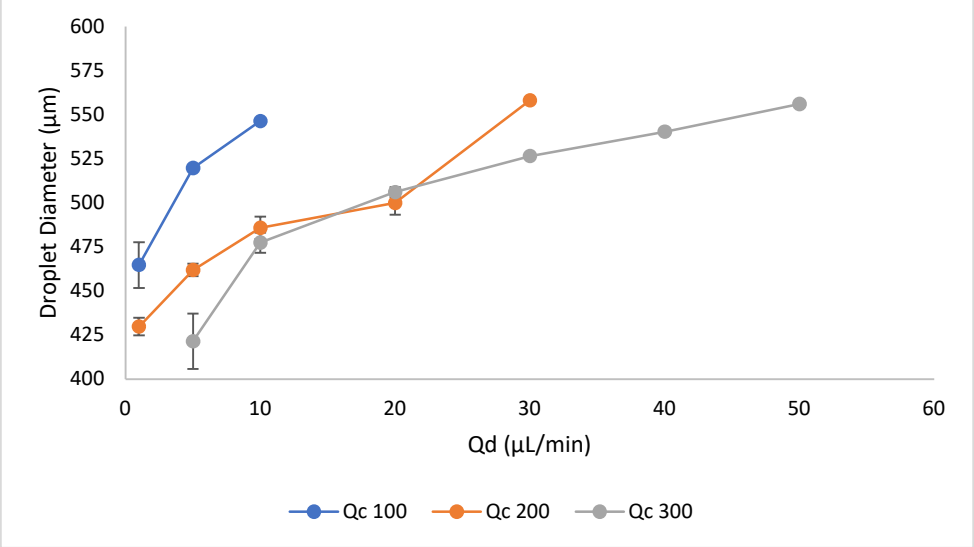

Fig 5.8: Droplet diameter (of sphere of equivalent volume) as a function of flow rates of both Qc and Qd. Error bars = 1 S.D. of the mean.

These results showed that an increase in Qd resulted in an increase in droplet size, whilst an increase in Qc resulted in a decrease in droplet size. It is also notable that the droplets displayed increasing size uniformity as Qd was increased, as demonstrated by the reducing error bars. Unfortunately, it was not possible to measure droplets with diameter greater than approximately 560 µm, therefore it was not possible to assess the maximum droplet size achievable using this

technique. However, it is likely that when the ratio between Qc and Qd reached a critical point, droplet generation would cease or become chaotic as the dispersed phase would be completely restricted by the continuous phase. The minimum size achievable was approximately 420 μm diameter as observed with Qc set to 300 μL/min and Qd set to 5 μL/min. Attempting to increase Qc any further resulted in excessive back pressure and leakage from the syringe whilst decreasing Qd further resulted in the continuous phase overcoming the pressure from the aqueous phase and backflowing into the aqueous phase syringe.

5.3.2 Particle Formation and Characterisation

To complete the process of CCP and form microparticles, the droplets of aqueous BSA studied above were required to undergo dehydration as water diffuses into the drying solvent, this causes the concentration of BSA within the droplet to increase until a critical point is reached and the BSA precipitates out of solution to form solid microparticles. To achieve this, the generated droplets were deposited, via the outlet tubing, into a stirred vial containing pentanol as the drying solvent. Later experiments made use of an alternative, non-stirred, reservoir system utilising a 100 mL measuring cylinder filled with pentanol. The stirred vessel reservoir utilized the stirring action to keep the aqueous droplets suspended within the pentanol whilst the CCP process completed, meanwhile the non-stirred reservoir utilized a long column of pentanol that the droplets fell through whilst the CCP process completed. To characterize these systems, experiments were conducted to study the effects of varying flow rates and BSA concentration. Particle samples were prepared and 20 μL samples taken for observation via light microscopy and measurement via Fiji. The remainder of the sample was concentrated by centrifugation and removal of the supernatant.

Varying Protein Concentration

Previous chapters studying batch production techniques showed that the average particle size could be modelled as a function of protein concentration and so this relationship was tested using a continuous flow technique. Consideration of the technique and previous works leads to the hypothesis that the particle size will remain a function of protein concentration with increasing concentration resulting in increasing particle size. To investigate this hypothesis, experiments were conducted using the single flow technique with samples produced from BSA solutions at 2, 50, and 200 mg/mL. The flow rate was set at 30 μL/min using a 10 mL stirred reservoir. The system was left to run for 10 minutes before the tube was removed from the solvent reservoir and samples taken for microscopic analysis. Figure 5.9 shows a single brightfield microscopy image obtained from each sample.

A visual inspection of the images indicates an obvious trend towards larger particles with increasing BSA concentration, with the 200 mg/mL sample also displaying a number of very large particles (larger than 100 μm). Particle sizing was carried out using the Fiji image analysis method as described previously. Figure 5.10 shows the sizing result from each sample displayed as histograms with axes unified for direct comparison, whilst table 5.1 shows the sizing data in numeric form. For this study only one sample was produced from each concentration of BSA solution.

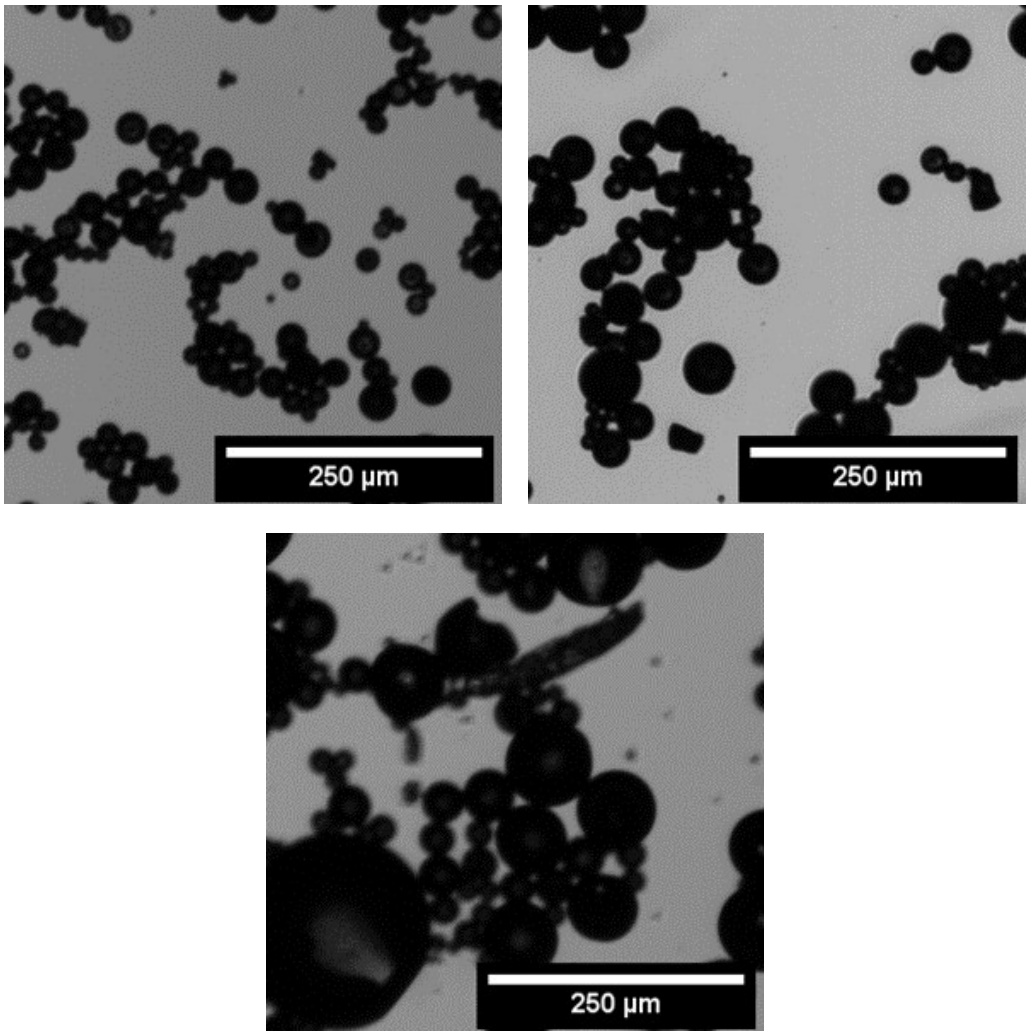

Fig 5.9: Brightfield microscope images of particle samples produced using the single tube continuous production method with a fast stir speed and flow rate at 30 µL/min. (Top Left) BSA solution at 2 mg/mL (Top Right) BSA solution at 50 mg/mL (Bottom) BSA solution at 200 mg/mL

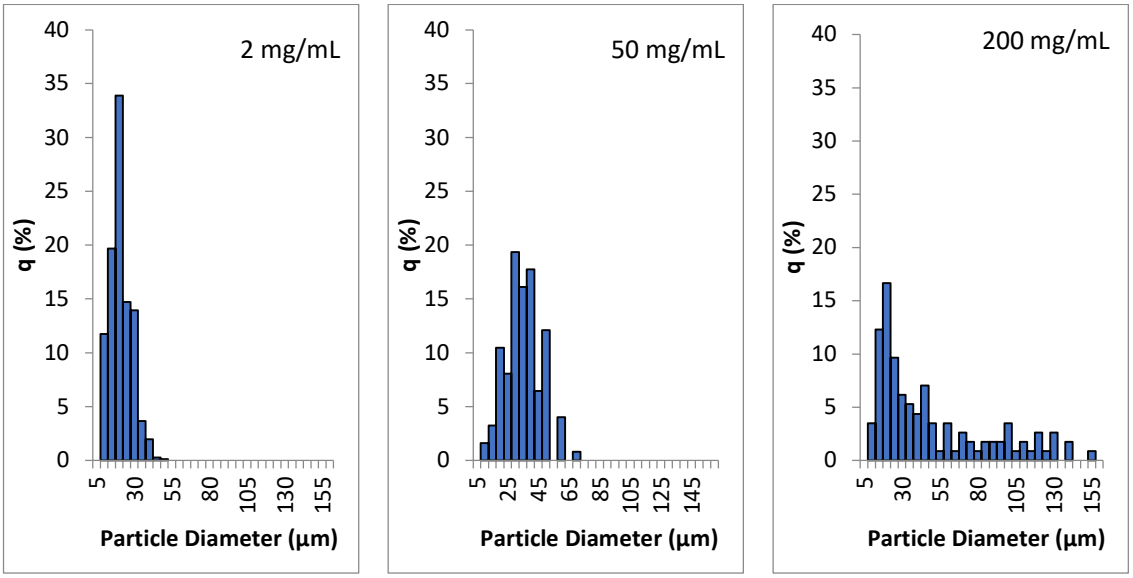

Fig. 5.10: Particle size measurements carried out using Fiji showing the diameter of BSA microparticles created using the single flow continuous production method with varying BSA concentration. (Left) 2 mg/mL BSA solution. (Middle) 50 mg/mL BSA solution (Right) 200 mg/mL BSA solution

Table 5.1: Values for the median, 10th and 90th percentiles and PDI of the particle distribution measured using image-based particle sizing

	Particle Diameter (µm)				
Sample	**Mean**	**D(10)**	**D(50)**	**D(90)**	**PDI**
2 mg/mL	20.0	10.0	18.0	28.8	0.13
50 mg/mL	30.0	18.0	32.0	50.0	0.12
200 mg/mL	46.7	14.0	32.0	107.4	0.64

These data show that the mean particle diameter increased from 20.0 µm to 30.0 µm when the BSA concentration was changed from 2 mg/mL to 50 mg/mL with similar measurements of PDI of the distribution. Increasing the concentration to 200 mg/mL saw the mean diameter increase to 46.7 µm along with a large increase in PDI to 0.64, indicating a polydisperse distribution. The D(10) measurements were similar amongst all samples, whereas the D(90) measurements increased with increasing concentration. This shows that the increase in average particle size was driven by increasing number of and size of the largest particles in the sample. This

trend towards larger particles with increasing BSA concentration fits with the data from earlier chapters and the assumptions about the mechanics of the process.

Vary Flow Rates – Flow Focusing Technique

Investigation into droplet size using the flow focusing technique showed that the generation of highly uniform aqueous droplets was possible at the flow focusing junction but that deviation away from either Qd or Qc resulted in breakdown of the production. However, it was also observed that droplets were exiting the outlet tubing regardless of whether droplets were being formed at the flow focusing junction. Furthermore, droplets were not visible travelling along the outlet tubing, as they were with the T-reactor technique. These observations lead to the conclusion that the droplets may be being formed at the outlet tubing terminus in a similar fashion to the mechanism controlling droplet production in the single flow technique. As it was not possible to measure the size of the droplets, except in the single instance of formation at the flow focusing junction, it was also not possible to assess whether droplet size could be controlled by variation in the flow rates. As such the technique was instead used to produce CCP microparticles using the stirred vessel reservoir at varying values of Qd and constant Qc. Particles were then measured using both the image-based and laser diffraction methods. Particles were prepared using 50 mg/mL BSA solution, and a 10 mL pentanol reservoir stirred at high speed. Qc was set at 100 µL/min (50 µL/min at each inlet) whilst Qd was varied with the following values: 5, 10, 20, 30, 40, 50 µL/min. Run times were calculated to allow for 0.5 mL of aqueous phase to enter the reservoir. At the end of the run, the tubing was removed from the reservoir, which was left stirring for a further minute to allow the CCP process to complete. 20 µL samples were then taken for microscopic observation and wet samples were retained for laser diffraction measurements. Figure 5.11 shows a single brightfield microscope image obtained from each sample. Visual analysis of these images shows no clear difference in

particle size between samples and also there was no evidence of large, irregular structures or large amounts of small "debris" particles.

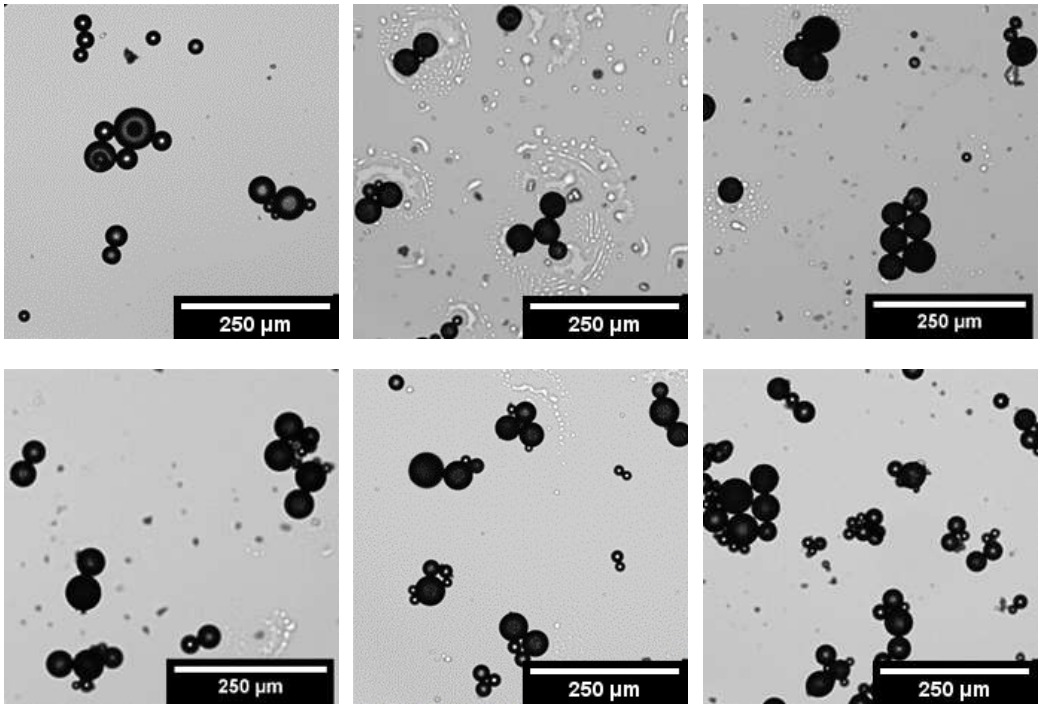

Fig. 5.11: Brightfield microscope images of BSA microparticles created with the flow focusing continuous production method. Qc was set at 100 µL/min and Qd was varied. (Top Left) Qd = 5 µL/min (Top Middle) Qd = 10 µL/min (Top Right) Qd = 20 µL/min (Bottom Left) Qd = 30 µL/min (Bottom Middle) 40 µL/min (Bottom Right) Qd = 50 µL/min

Image based particle sizing was carried out using both the Fiji image analysis method and the laser diffraction method, both of which were described previously. Figure 5.12 shows the image-based sizing result from each sample displayed as histograms with axes unified for direct comparison whilst table 5.2 shows the sizing data in numeric form. Samples were also retained for laser diffraction measurements and results are shown in figure 5.13 as histograms whilst table 5.3 shows the sizing data in numeric form.

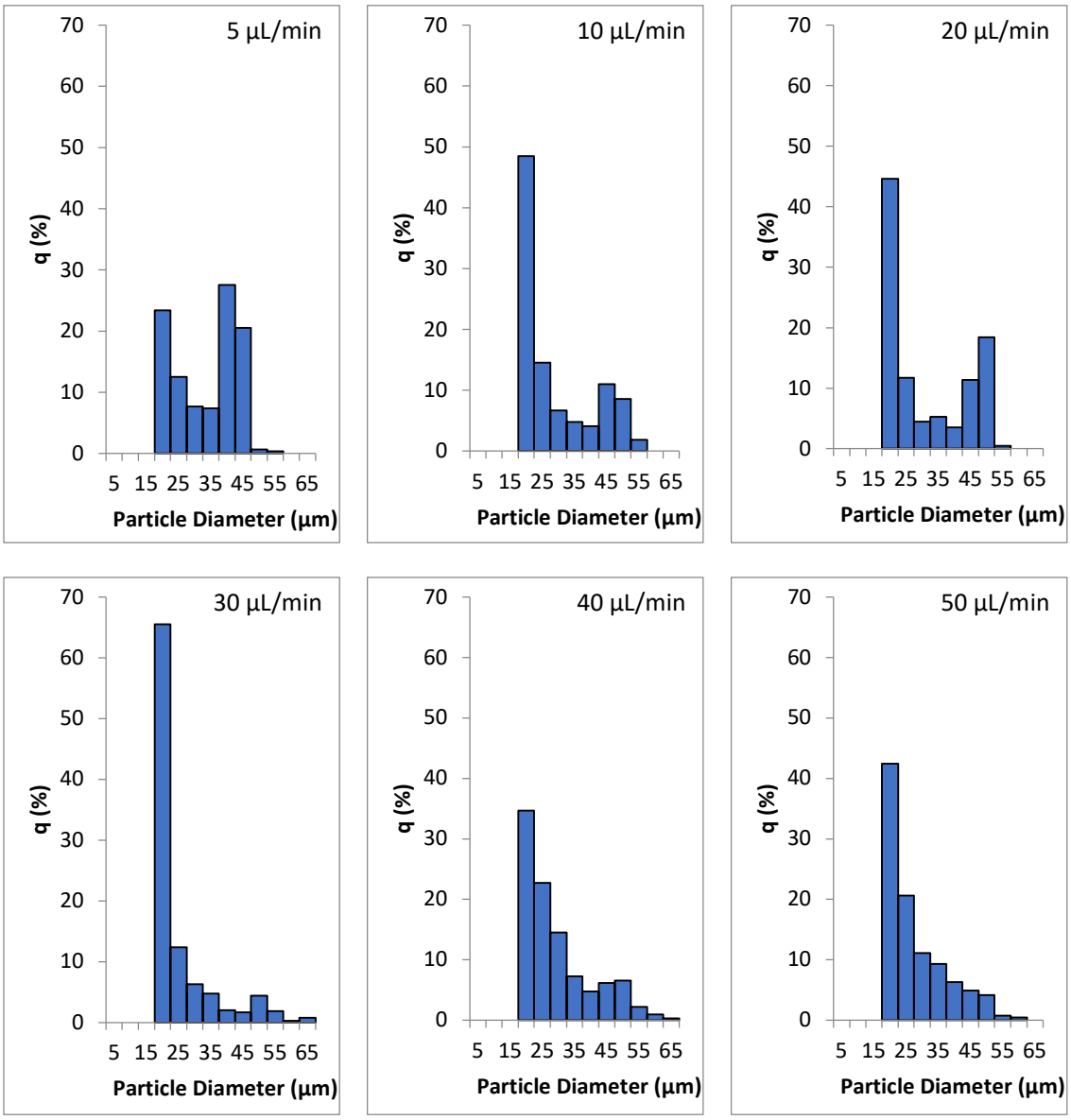

Fig 5.12: Particle size measurements carried out using Fiji showing diameter of glassified BSA particles created using flow focusing microfluidics with Qc set at 100 µL/min and varying Qd. (Top Left) 5 µL/min (Top Middle) 10 µL/min (Top Right) 20 µL/min (Bottom Left) 30 µL/min (Bottom Middle) 40 µL/min (Bottom Right) 50 µL/min

Table 5.2: Values for the median, 10th and 90th percentiles and PDI of the particle distribution calculated using the image-based sizing technique

	Particle Diameter (μm)			
Qd	**Median**	**D(10)**	**D(90)**	**PDI**
5 μL/min	35.0	16.8	40.2	0.10
10 μL/min	20.7	15.5	45.4	0.19
20 μL/min	22.0	15.5	46.6	0.19
30 μL/min	16.8	15.5	37.6	0.21
40 μL/min	23.3	15.5	44.1	0.16
50 μL/min	22.0	15.5	40.2	0.15

These results of the image-based sizing show that with Qd set to 5 μL/min a bi-modal size distribution was measured with peaks at 20 μm and 40 μm. As Qd was increased, the peak at 40 μm reduced in size until at Qd = 30 μL/min the peak was largely non-existent and only the peak at 20 μm was present. This implies that, at lower values of Qd, two differently sized populations of droplets were present within the reservoir, resulting two differently size particle distributions. However, as Qd increased, the relative amount of larger droplets reduced until only the droplets which resulted in 20 μm particles were being produced. Laser diffraction sizing also showed a bi-modal distribution for the 5 μL/min samples with a primary peak at 45 μm and a smaller shoulder peak visible at 15 μm. As with the data from the image-based sizing, the smaller of the two peaks reduced in size with increasing Qd and was no longer visible at Qd = 20 μL/min. Whilst the values of the two peaks seen at lower Qd were consistent between techniques, the primary and secondary peaks were inverted, with the image-based measurements reporting the peak at 20 μm becoming dominant whilst the laser diffraction measurements indicated that the 45 μm particles became the dominant species. Further to these discrepancies between the two measurement techniques it was noted that both peaks, from either technique, measured particles that were significantly larger than the droplets formed at the flow focusing junction. The droplets generated from the flow focusing

junction were measured at 12.5 ± 0.84 μm which is smaller than the 15-20 μm peaks seen in the sizing data. This strongly implies that the microparticles were not formed directly from these droplets and that larger droplets were formed within the system before CCP took place.

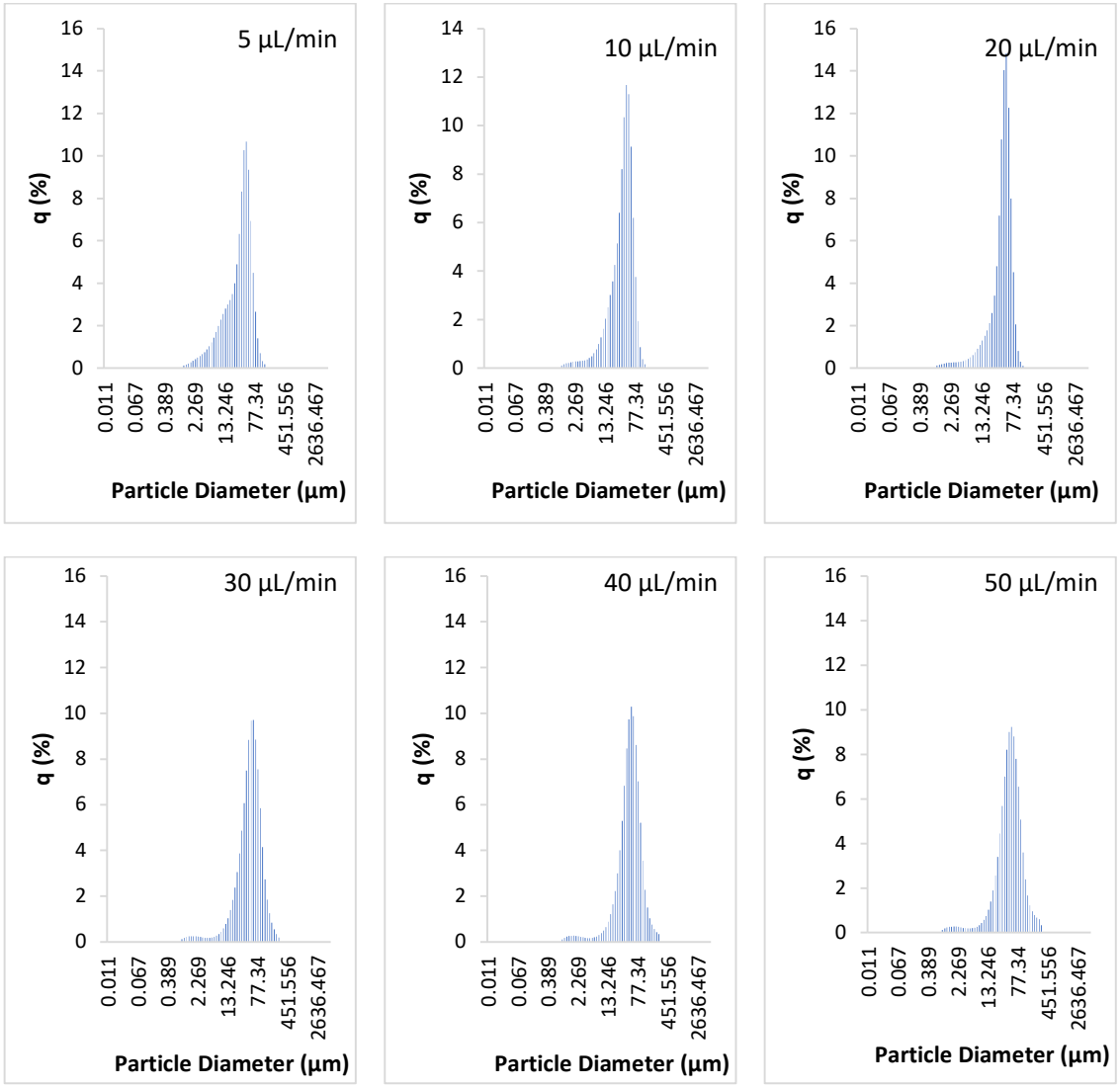

Fig 5.13: Particle size measurements carried out using laser diffraction showing diameter of BSA microparticles created using flow focusing microfluidics with Qc set at 100 μL/min and varying Qd. (Top Left) 5 μL/min (Top Middle) 10 μL/min (Top Right) 20 μL/min (Bottom Left) 30 μL/min (Bottom Middle) 40 μL/min (Bottom Right) 50 μL/min

Table 5.3: Values for the median, 10th and 90th percentiles and PDI of the particle distribution calculated using the image-based sizing technique

	Particle Diameter (µm)			
Qd	**Median**	**D(10)**	**D(90)**	**PDI**
5 µL/min	32.5	7.5	58.7	0.38
10 µL/min	36.9	12.2	63.4	0.28
20 µL/min	42.0	14.7	65.0	0.21
30 µL/min	47.2	17.5	94.3	0.42
40 µL/min	45.8	18.5	90.2	0.43
50 µL/min	44.7	17.4	96.4	0.56

Consideration of the flow focusing system and the CCP process leads to the conclusion that the aqueous droplets must have been forming into larger droplets before the process completed in order to form particles larger than the original droplets. This process likely occurs within the flow focusing system as the droplets are transported through the microfluidic channels.

One location in which this process may have taken place would be at the point where the outlet channel within the microfluidic chip terminates and the fluid mixture enters the plastic tubing. The internal channel diameter within the microfluidic chip was 100 µm, whereas the internal diameter of the outlet tubing was 250 µm. As such, when the fluid mixture leaves the microfluidic chip, it would experience a reduction in the pressure causing it to move through the system. This reduction in pressure would result in a reduction in the fluid velocity and may cause the aqueous droplets to collide and coalesce into larger droplets. Alternatively, when the droplets reach the larger outlet tubing, they may break down into an aqueous stream and undergo side wetting, resulting in the aqueous phase travelling down the side of the tubing, to form droplets at the terminus of the tubing similar to the mechanism seen in the single flow technique.

Varying Flow Rates - T-reactor

It was demonstrated above that the T-reactor technique produced droplets with a high degree of size uniformity whilst allowing size tunability of the droplets through manipulation of the fluid flow rates. Based on the assumption that the final particle size is a function of initial BSA concentration and droplet size, it was hypothesized that the use of the T-reactor technique would result in a monodisperse distribution of CCP microparticles whose size would a linear function of the droplet size controllable through manipulation of the flow rates. To investigate this hypothesis, the T-reactor system was setup using 50 mg/mL BSA solution and a 10 mL stirred pentanol reservoir. Qc was set at 200 µL/min whilst Qd was varied with the following values: 10, 20, 30, 100, 150 µL/min. Run times were calculated to allow for 0.5 mL of aqueous phase to enter the reservoir. At the end of the run, the tubing was removed from the reservoir, which was left stirring for a further minute to allow the CCP process to complete fully. 20 µL samples were then taken for microscopic observation and wet samples were retained for laser diffraction measurements. Figure 5.14 shows a single brightfield microscope image obtained from each sample. Observation of these images did not show any obvious trend in particle size with variation in Qd. All images showed particle distributions which appeared similar under visual analysis. To quantify this observation, particles were sized using both Fiji and laser diffraction.

Image-based particle sizing was carried out using the Fiji image analysis method as described previously. Fig. 5.15 shows the sizing result from a single sample prepared using each flow rate displayed as a histogram with y-axis unified for direct comparison, whilst table 5.4 shows the mean values obtained from each triplicate. From the image-based sizing data it can be seen that there was no clear relationship between Qd and particle size with all samples measuring a mean particle diameter between 25.0 – 30.6 µm, and all PDI calculations staying below 0.2, indicating a

highly monodisperse population. These results disagree with the earlier hypothesis that particle size was a function of flow rate.

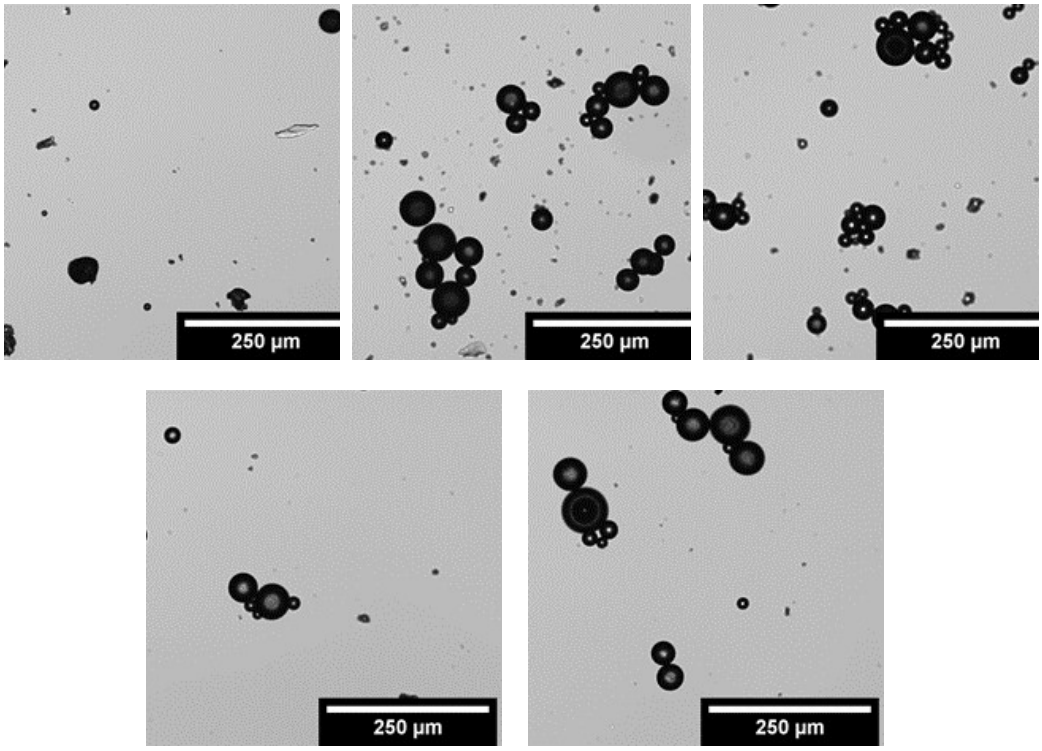

Fig 5.14: Brightfield microscope images of BSA microparticles created with the T-reactor continuous production method. Qc was set at 200 µL/min and Qd was varied. (Top Left) Qd = 10 µL/min (Top Middle) Qd = 20 µL/min (Top Right) Qd = 30 µL/min (Bottom Left) Qd = 100 µL/min (Bottom Right) Qd = 150 µL/min

The remainder of the particle suspensions were concentrated via centrifugation and removal of the supernatant and measured using the Horiba Partica LA-960 Laser Scattering Particle Size Distribution Analyzer as per the method described earlier. Figure 5.16 shows the sizing result from a single sample prepared using each flow rate displayed as a histogram with y-axis unified for direct comparison, whilst table 5.5 shows the mean values obtained from each triplicate. The laser diffraction data show again there was no clear trend towards increased median particle size with increasing Qd. The results also show that when Qd was set at 10 µL/min and 20 µL/min the measured PDI was relatively large (> 0.5), indicating that the particles exhibited a polydisperse size distribution. However, at 30 µL/min the PDI reduced

to 0.26 and at both 100 µL/min and 150 µL/min the PDI was measured at 0.18, indicating monodisperse particle distributions. These results also disagree with the stated hypothesis that particle size would be a function of flow rate.

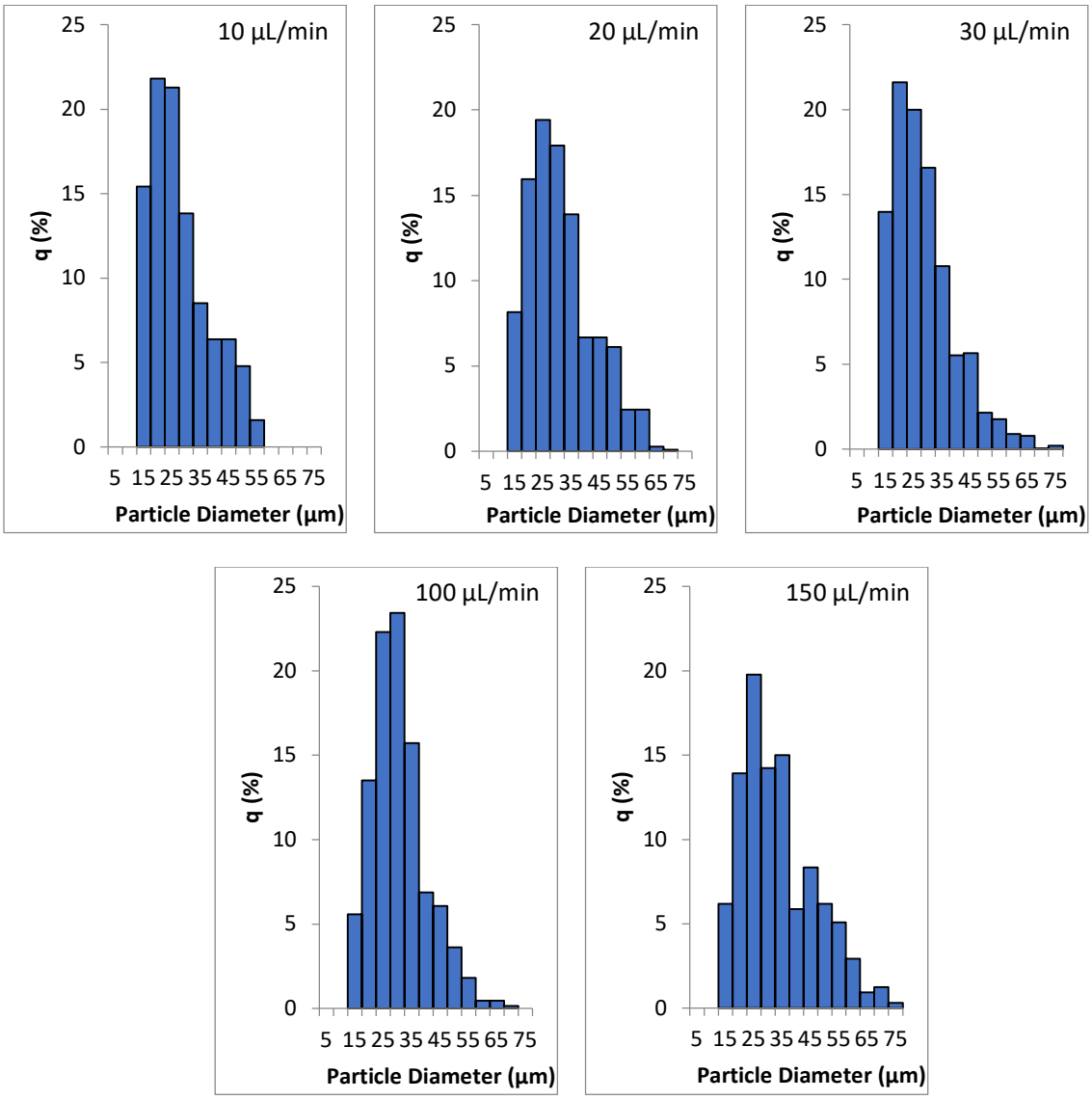

Fig 5.15: Particle size measurements carried out using Fiji showing diameter of BSA particles created using the T-reactor technique with Qc set at 200 µL/min and varying Qd. (Top Left) 10 µL/min (Top Middle) 20 µL/min (Top Right) 30 µL/min (Bottom Left) 100 µL/min (Bottom Right) 150 µL/min

Table 5.4: Mean values for the median, 10th and 90th percentiles and PDI of the particle distribution calculated from triplicate samples and measured using image-based particle sizing

	Particle Diameter from Triplicate Measurements (µm)				
Qd	**Mean**	**D(10)**	**D(50)**	**D(90)**	**PDI**
10 µL/min	25.0 ± 10.4	12.3 ± 0.9	23.3 ± 0.0	40.2 ± 5.5	0.19 ± 0.03
20 µL/min*	28.9	15.5	27.2	45.4	0.15
30 µL/min	25.6 ± 10.5	13.8 ± 0.7	22.9 ± 2.0	41.0 ± 2.7	0.18 ±0.01
100 µL/min	29.6 ± 10.9	17.7 ± 0.7	28.1 ± 1.5	43.6 ± 3.7	0.12 ±0.00
150 µL/min	30.6 ± 10.8	16.8 ± 0.0	28.5 ± 1.3	48.7 ± 2.2	0.15 ±0.15

*Sample only measured singly

Comparison of the image-based results to the laser diffraction results shows that the mean sizes reported by the laser diffraction measurements were significantly larger than those obtained from the image-based technique, almost double the reported size for some samples. This difference may be due to multiple sources. Firstly, in the calculation used to calculate the median average. The image-based technique counts individual particles, so the median is that of a numerical distribution where all particles are counted equally. The laser diffraction technique measurement counts a volumetric distribution, so the median value is the volume median where larger particles provide a larger signal. This causes the volume median to report a higher value than the number median. Other experimental parameters may also have an effect on the reported median size, such as the sampling technique for image-based sizing, or issues surrounding the use of the Hough Circle Transform algorithm. Issues surrounding the Hough Circle Transform and microscopic images have been discussed earlier, with the algorithm tending to find an excess number of smaller particles and reduced number of larger particles. Despite this difference between techniques, there were also similarities in the results. Both measurement techniques reported large diameter particles for the samples produced at 10 µL/min and 20 µL/min that did not fit any obvious trend. However, the remaining samples (30 µL/min and greater) did show a potential trendline of increasing diameter with increasing Qd.

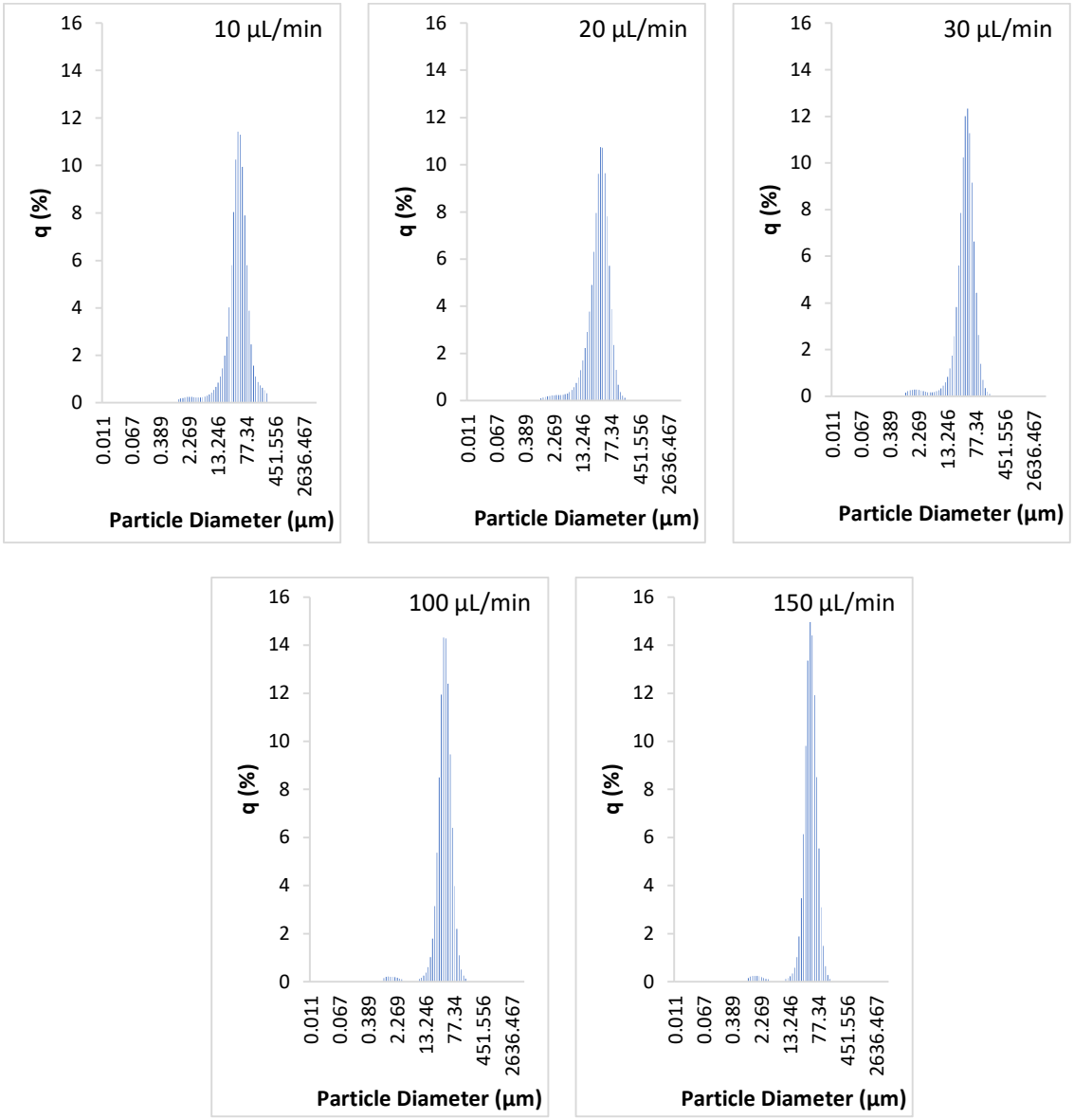

Fig. 5.16: Particle size measurements carried out using Laser Diffraction showing diameter of BSA particles created using the T-reactor technique with Qc set at 200 µL/min and varying Qd. (Top Left) 10 µL/min (Top Middle) 20 µL/min (Top Right) 30 µL/min (Bottom Left) 100 µL/min (Bottom Right) 150 µL/min

Table 5.5: Mean values for the median, 10th and 90th percentiles and PDI of the particle distribution calculated from triplicate samples

	Particle Diameter from Triplicate Measurements (µm)				
Qd	**Mean**	**D(10)**	**D(50)**	**D(90)**	**PDI**
10 µL/min	51.9 ± 2.2	17.1 ± 3.0	42.4 ± 1.0	91.4 ± 8.9	0.63 ± 0.17
20 µL/min	38.6 ± 12.5	15.0 ± 0.9	40.3 ± 10.6	106.5 ± 35.4	0.57 ± 0.29
30 µL/min	41.0 ± 3.3	18.6 ± 2.0	38.2 ± 3.0	66.5 ± 5.3	0.26 ± 0.01
100 µL/min	42.4 ± 2.6	23.6 ± 0.8	39.7 ±1.9	64.7 ± 4.9	0.18 ± 0.03
150 µL/min	46.2 ± 3.3	26.0 ± 0.5	43.4 ±0.1	70.6 ± 1.5	0.18 ± 0.02

Use of the Unstirred Reservoir

The results obtained from this study disagreed with the hypothesis stated earlier, that particle size could be modelled as a linear function of droplet size. As this contradicts the basic assumption made about the mechanism that drives the CCP process, an alternative hypothesis was devised to explain this behavior. This hypothesis stated that the aqueous droplets within the stirred vial reservoir were being homogenized by the stirring action, resulting in similarly sized droplets within the stirred suspension regardless of the initial droplet size when entering the reservoir. This would then result in uniformly sized particles as observed. To test this hypothesis, an alternative reservoir design was trialed in which aqueous droplets were allowed to fall through a long column of solvent, dehydrating as they fall and completing the CCP process before reaching the bottom of the vessel, resulting in dehydrated microparticles collecting at the bottom of the vessel.

To assess this technique for the production of CCP particles, the T-reactor technique was employed with the outlet tubing exiting into a 100 mL measuring cylinder filled with 100 mL pentanol to act as the solvent reservoir. For this study, the BSA source solution was prepared at 100 mg/mL to produce droplets with a high BSA content and reduce the time take for the CCP process to complete and ensure particles had formed before the droplets reached the bottom of the cylinder. The continuous phase flow rate was set at 200 µL/min and the dispersed phase flow rate at 30

μL/min. The experiment was allowed to run for 10 minutes. After this time the tubing was removed from the reservoir and any droplets falling through the column were allowed to reach the bottom of the cylinder. Excess solvent was removed from the cylinder and the sample was transferred to a 20 mL scintillation vial for ease of access before 20 μL samples were taken for microscopy. The remainder of the sample was left under pentanol for laser diffraction measurements.

Figure 5.17 shows a brightfield light microscope image of the sample obtained from the unstirred vessel technique showing large and uniform particles with no evidence of irregular, cracked structures or small, debris-like material. Particle sizing was carried out using both the image-based technique and laser diffraction and results are shown in figure 5.18 as histograms and in table 5.6 in numerical form. These results showed that, in agreement with the microscope image, the particles obtained using this technique appeared to have formed as large (~100 μm) particles with a very high degree of uniformity, as evidenced by PDI measurements of 0.003 and 0.06 from the image-based and laser diffraction techniques, respectively. It can also be noted that the particles produced using this technique were much larger than the particles produced using the stirred reservoir technique, regardless of the droplet production system used. Particles were measured with a median diameter of 143.0 μm when measured with image-based sizing and 92.3 μm when measured with laser diffraction. These measurements are significantly larger than the particles produced using the single flow technique and stirred vessel reservoir with the source BSA solution at 100 mg/ml, indicating that the increased particle size was not from the increased concentration alone. This result implies that the particles were produced from larger droplets and, therefore, that no homogenization effect had taken place.

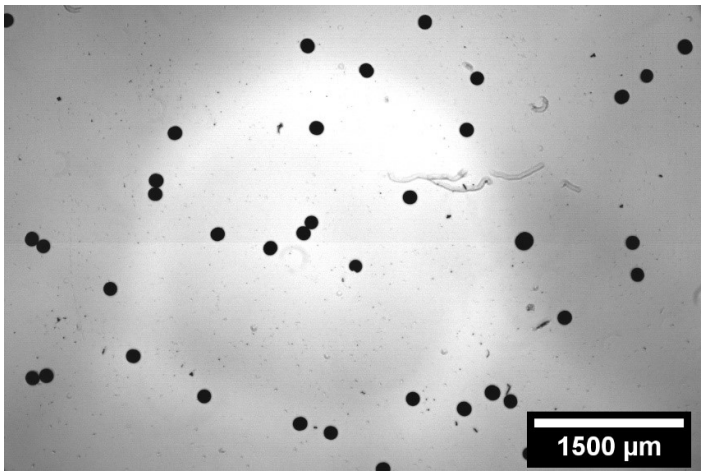

Fig. 5.17: Brightfield microscopy image of particles produced using the unstirred vessel technique. Visual analysis shows that the particles observed were highly uniform.

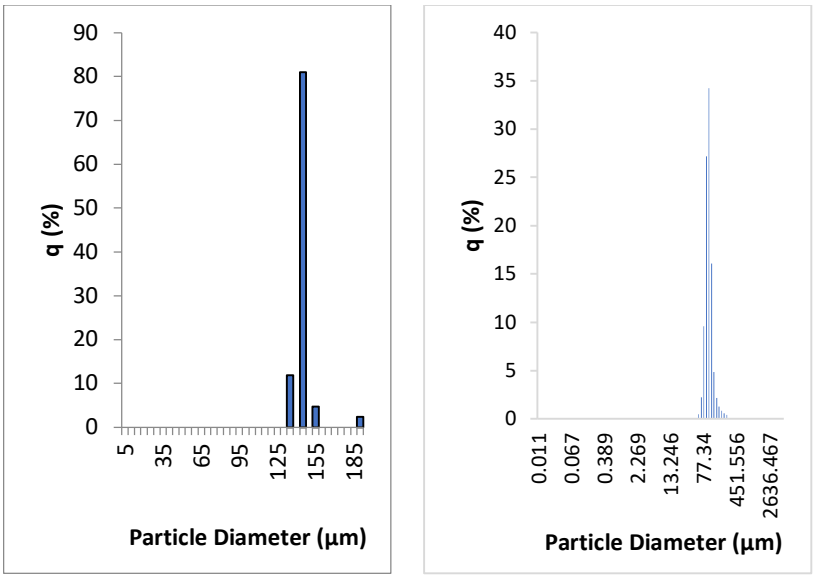

Fig. 5.18: Particle size measurements carried out using image-based sizing and laser diffraction sizing, showing diameter of BSA particles created using the unstirred vessel technique with Qc set at 200 µL/min and Qd set at 30 µL/min. (Left) Sizing from image-based technique (Right) Sizing from laser diffraction

Table 5.6: Values for the mean, 10th, 50th and 90th percentiles and PDI of the particle distribution calculated using both the image-based sizing technique and laser diffraction

Measurement Technique	Particle Diameter (μm)				
	Mean	**D(10)**	**D(50)**	**D(90)**	**PDI**
Fiji	143.3	133.1	143	143.0	0.003
Laser Diffraction	96.1	74.8	92.3	116.7	0.06

5.4 Conclusions and Further Work

The aims of the studies discussed in this chapter were to investigate the possibility of continuous manufacture of CCP microparticles as well the potential for size tunablility through variation in the system parameters, such as flow rates and protein concentration. Three continuous manufacture techniques were tested, the single flow technique, the T-reactor technique and the microfluidic flow focusing technique. All three systems were intended to continuously introduce aqueous BSA droplets into a solvent reservoir wherein the CCP process would take place and protein microparticles would be formed.

The single flow technique consisted of the aqueous solution flowing directly into the solvent reservoir via single tube with internal diameter of 250 μm. This setup resulted in relatively large aqueous droplets of approximately 2 mm to be formed at the terminus of the tubing before breaking away and falling to the bottom of the vessel. The T-reactor system utilised a T-connector, internal diameter 500 μm, in which the dispersed phase intersected with a flow of the continuous phase. The T-connector acted as a "millireactor" to form aqueous droplets which were carried along the flow of solvent to exit into the solvent reservoir. The method resulted in the formation of aqueous droplets whose size could be controlled by variation in the fluid flow rates. A thorough investigation into droplet size with variation in flow rate ratio and total flow rate was not conducted, nevertheless, it was demonstrated that droplet size could be varied from approximately 420 μm to at least 560 μm, at which point the droplets were too large to measure. The microfluidic flow focusing technique made use of a commercially available microfluidic flow focusing chip in

which the continuous and dispersed phases intersect at a cross junction to form aqueous droplets. Using this technique, it was only possible to form aqueous droplets within a very small window of flow rates. Droplets measuring 10.9 μm were formed when the continuous phase flow rate was set at 100 μL/min and the dispersed phase set at 5 μL/min to give a flow rate ratio of 20:1. Deviation from these flow rates resulted in unstable droplets production or complete breakdown of droplet generation.

These results showed that size tuneable aqueous BSA droplets could be formed within the T-reactor system through variation in the flow rates and therefore it followed that the microparticles produced using this technique should also be size tuneable. However, production of CCP particles via the stirred reservoir resulted in particles with similar size distribution, regardless of technique used. Median particle diameter was measured as approximately 15 – 35 μm with image based sizing and 30 – 55 μm using laser diffraction particle sizing. This was similar to the size of particles produced using the batch techniques explored earlier and implies that the stirred solvent reservoir may have been having a homogenization effect on the droplets similar to the vortex mixing of the batch technique. However, the flow focusing technique generated droplets smaller than the resultant particles, meaning that the droplet size must have increased prior to the CCP process taking place. This may have occurred within the reservoir due to the homogenization effect of the stirring or it may have occurred within the microfluidic device due to droplet instability.

To remove the stirring from the solvent reservoir, a new system was devised in which aqueous droplets exit the microfluidic device and fall through a column of drying solvent, dehydrating as they fall, to form particles before they reach the bottom of the vessel. To test this technique, the T-reactor system was employed, creating a droplet measuring approximately 558 μm diameter. When collected and measured, the resultant particles were sized at approximately 100 μm diameter,

significantly larger than the particles produced using the stirred reservoir, with an extremely high degree of uniformity. This result implies that these larger particles were formed from droplets that had not been homogenized and that this system may provide the basis of a continuous production system with variable particle size. Whilst this study does demonstrate the continuous production of CCP particles, it also poses many further questions. Firstly, the solvent drop system should be explored further to assess whether variation in the flow rates of the two liquid phases does indeed result in variation of particle size and to find the limits of the size variation. If this is shown to be the case the system could be used to further probe the CCP process and calculate the relationship between droplet size, aqueous phase concentration and particle size. This could be used in conjunction with the micropipette technique discussed earlier to corroborate the results from the two techniques. The solvent drop system could also be used to explore what is happening to the droplets within the microfluidic system. If particles produced using these two systems continue to measure larger than the droplets generated at the flow focusing junction, then it can be assumed that the droplets are merging within the microfluidic device. If the particles produced are the predicted size, then it implies that the homogenizing effect from the stirred reservoir acted to increase the droplet size. Flow focusing as a technique should also be explored further to find if more optimal parameters exist. The use of alternative solvents as the continuous phase will alter the interfacial tension between the fluids, potentially allowing for more stable variations in droplet size. To further increase the possibility of creating stable droplets within the microfluidic device the use of a surfactant could be introduced to the aqueous phase. Surfactants act to lower the surface tension of a material, increasing the stability of a discrete droplet, however, it is likely that the surfactant will remain attached to the microparticle when the process is complete, causing an impurity in the product.

Chapter 6

Solvent and Protein Screening

6.1 Chapter Introduction

This chapter describes two screening studies designed to investigate the extent to which CCP technology can be expanded through exploration of alternative drying solvents and additional proteins. For this technology to translate from a laboratory-based interest to an industry accepted method, it must be shown to work with a wide range of proteins (and potentially other biologics) and to provide an advantage over existing technologies. The scale up potential of this technology has been discussed earlier in this thesis which brings with it advantages to both power usage and cost, as well as reducing the time per batch. Additionally, it has been demonstrated that this technology can be used in a continuous production regime which has the potential to reduce costs and processing times even further.

To date there is still limited research on CCP, with the majority of research being carried out by a single research group which have tended to focus on the science underlying the technology and modelling the behaviour of individual microdroplet dehydration [13], [79], [151], [188]. Only one of these studies reported on the use multiple proteins and drying solvents and utilised a pre-treatment method to control the water saturation levels of the solvents [79]. The study found that a dried powder formulation was formed from all combinations of reagents, and that analysis of the protein secondary structure and biological activity showed comparable results to analysis of lyophilised protein powders.

The study presented here aimed to build upon this work, working with a larger and more diverse group of proteins and solvents. In addition, further analysis and characterisation of the dehydrated product was undertaken. As well as analysis of protein structure after reconstitution, the dried microparticles were characterised

microscopically for topographical features and used for calculation of particle size and distribution.

6.2 Experimental Design

This study comprised of two screening experiments utilising the small-scale vortex mixing batch technique carried out in 1.5 mL microcentrifuge tubes. This method uses only very small quantities of reagents, allowing it to be used as an effective screening technique. The solvents used in this study all possessed differing water absorption values, meaning they had the capacity to dissolve differing volumes of water. As a solvent becomes near saturated with water, the rate of water absorption reduces, thus reducing the ability of the solvent to induce the CCP process. Furthermore, if the solvent reaches complete saturation, the absorption of water stops entirely and the process would be unable to proceed.

The small-scale vortex mixer method was used to run the screening study with the 1 mL pentanol reservoir replaced with 1 mL of the solvent to be screened. However, as each solvent had a different water absorption, it followed that the volume of aqueous BSA solution added to the reservoir should be varied for each solvent. To decide the volume of aqueous phase to add to each solvent, the maximum theoretical volume of water that could be dissolved in 1 mL of the solvent was calculated from the water absorption value. This was rounded down to the nearest 5 µL and used as the initial volume of BSA solution to add to the 1 mL reservoir. After the first screening run using the initial volume of aqueous phase, the second screening run was completed with the volume of aqueous phase reduced by 25%. A third screening run was also completed with the volume of aqueous reduced by a further 25%. This approach was designed to ensure that CCP was not being hindered or prohibited by water saturation and that only the properties of the solvent were affecting the process. The protein screening experiments were carried out in a similar way to the solvent screening described above. Four solvents were selected based upon the results of the solvent screening experiments. Aqueous

solutions of each protein were prepared, added to 1 mL of each of the four drying solvents and dehydrated as per the method. The volume of aqueous solution added to the drying solvent was obtained from the results of the previous experiments.

Table 6.1: Water absorption and density values of each solvent taken from literature and the calculated maximum volume of aqueous BSA solution to add to 1 mL of solvent.

Solvent	Water absorption at 20°C (%w/w)	Initial vol. of aqueous BSA solution (µL)	Aq. BSA added for 2nd rep. (-25%, µL)	Aq. BSA added for 3rd rep. (-25%, µL)
2-Methyl-1-propanol	33.2	330	247.5	185.6
Pentanol	10.21	90	67.5	50.6
Benzyl alcohol*	8	80	60	45.0
Methyl acetate	8	75	56.25	42.2
Heptanol	6.63	50	37.5	28.1
4-Methyl-2-pentanol	5.9	45	33.75	25.3
Octanol	4.35	35	26.25	19.7
Decanol**	4.3	35	26.25	19.7
Ethyl acetate	3.3	25	22.5	16.9
2-Ethyl-1-hexanol	2.4	20	15	11.3

*no temp given in reference

**value at 25°C

6.2.1 Material Selection

Choice of Drying Solvents

Solvents were selected based upon their water absorption value. Water absorption is a measure of the maximum volume of water that can be dissolved into a given volume of solvent and has been shown to be proportional to the dissolution rate of an aqueous droplet within the solvent [189]. As such, the water absorption value of a solvent would affect the time taken for an aqueous droplet to dissolve into the solvent, and thus the speed at which CCP will occur. Previous work carried out by Aniket *et al*. showed that varying the water absorption value of a solvent (in this case pentanol) by pre-treating the solvent with water affected the hydration level of the resultant protein powder, with greater water absorption resulting in a drier

powder formulation [13]. Due to the known effect of water absorption on the final product of CCP, and the ease of finding these values in literature, this characteristic was considered to be a useful selection criterion.

Whilst solvents were selected based upon their water absorption values, it should be noted that this is not the only factor that affects the dissolution of aqueous droplets into another fluid. Properties such as the polarity of the fluids, the availability of hydrogen bonding and the surface area of the droplets, which is further influenced by factors such as the droplet generation method, fluid densities and relative surface tensions of the two fluids, will all also affect the dissolution rate of the aqueous droplets. As such, the water absorption value of any given solvent should not be expected to be the only predictor of the solvent's potential for use in CCP.

Water absorption values of various solvents were taken from literature with the values for pentanol and decanol chosen as baseline values due to their extensive use in the study of CCP [190], [191]. Five solvents were selected with water absorption values between that of pentanol and decanol, one with a water absorption value greater than that of pentanol, and two with water absorption values lower than that of decanol. This provided ten solvents in total, eight of which were alcohols with the other two being esters. The chosen solvents and their reported water absorption values can be seen in table 6.1.

Choice of Proteins

Six proteins were chosen for this study, representing a variety of different molecular sizes and biological functions but all having a clinical or industrial use and so would benefit from technologies to produce stable, solid formulations. The proteins chosen were HSA, lysozyme, catalase, horseradish peroxidase (HRP), glucose oxidase (GO) and insulin.

HSA is the most abundant protein in human blood and its biological functions include the transport of hormones, fatty acids and other compounds throughout the vascular system, as well as being involved in pH buffering and maintaining oncotic pressure. HSA has a molecular weight of 66.5 kDa and is a well understood and stable, model protein similar to BSA. HSA was selected for its similarity to BSA which has been the model protein used for CCP in previous studies.

Lysozyme is another well understood, stable protein with a molecular weight of 14 kDa. This protein has an antimicrobial action and forms part of the innate immune system. Lysozyme is commonly used in laboratory setting for the lysing of gram-negative bacteria and in medicine as an antimicrobial agent [192], [193].

Catalase is a very large protein, with a molecular weight of 240 kDa, which acts as a catalyst for the decomposition of hydrogen peroxide to water and oxygen. Catalase is commonly used in microbiology laboratories for the catalase test to aid in the identification of bacterial species. The catalase test provides information as to whether a bacterial strain contains catalase, being known as catalase-positive bacteria, or does not contain catalase, being known as catalase-negative bacteria [194], [195]. Catalase is also of use in the food industry for the removal of hydrogen peroxide from food items such as milk and cheese [196]. More recently, catalase has also been shown to be useful as a biosensor for alcohol determination in beer samples [197].

Horseradish peroxidase is a peroxidase enzyme with a molecular weight of 44 kDa found in the horseradish plant where is it used to catalyse the oxidation of various organic compounds. HRP has found use in laboratories as it can be conjugated to a fluorescent or luminescent molecule and used as a label to determine the presence of a molecular target using western blots or ELISA tests [198]. Recent uses also include the HRP functionalisation of gold nanoclusters for the real time monitoring of hydrogen peroxide [199], [200].

Glucose oxidase is an oxidoreductase found in fungi and insects which catalyses the oxidation of glucose to hydrogen peroxide and displays antibacterial properties when in the presence of oxygen and glucose. GO is a large protein with a molecular weight of 160 kDa. The protein is widely used for glucose monitoring assays in both healthcare settings and in fermentation bioreactors [201], [202].

Insulin is an important protein which regulates carbohydrates, fats and proteins within the metabolic system. Decreased levels of insulin activity results in diabetes mellitus, a metabolic disorder characterised by high levels of blood sugar as the regulatory action of insulin is inhibited. Type 1 diabetes mellitus is managed with injections of insulin, providing a clinical need for the production of insulin. Insulin is the smallest protein involved in this study with a molecular weight of 5.8 kDa.

Water Absorption Calculations

The volume of aqueous protein solution that was added to the drying solvent for CCP was calculated from the water absorption value of each solvent used. The water absorption value represents the volume of water that can be dissolved into a given volume of solvent to reach saturation and, therefore, indicates the maximum theoretical amount of water that can be removed from droplets of aqueous protein solution. However, if adding this maximum theoretical volume of water, it would not be expected for CCP to take place, the rapid absorption of water required for CCP to occur relies upon the assumption that the reservoir acts as an infinite well and does not become saturated with absorbed water. To allow for this, the initial calculation of the theoretical maximum was rounded down to the nearest 5 µL and the method was repeated multiple times with reduced volumes of aqueous solution added. To calculate the maximum theoretical volume of water that could be absorbed by each solvent, literature values of water absorption and solvent density were obtained and converted to calculate the maximum volume of water that could be absorbed by 1 mL of solvent. For this calculation, aqueous protein solutions were assumed to have the same properties as dH_2O.

6.3 Results and Discussion

6.3.1 Visual Analysis

Solvent Screening

Samples were prepared as discussed earlier and after vortex mixing were placed into a rack and left for 5 mins to allow any suspension to settle. After this time, the samples were observed visually, and digital images were captured. Samples were inspected for evidence of a particulate suspension or solid material at the bottom of the tube. Figure 6.1 shows the digital images captured of the samples and table 6.2 shows the tabulated results of the visual inspection. Observation of the samples five minutes after vortex mixing showed a range of different results. Conducting the CCP process using pentanol, heptanol, 4M2P, octanol and decanol all resulted in a hazy suspension with white particulate material collecting at the bottom of the tube at the end of at least one of the experiment replicates (these are marked as green cells in table 6.2). 2M1P samples did produce a hazy white suspension but there was no evidence of particulate material. These samples also produced a clear section of the bottom of the tube, which may have been an undissolved aqueous layer. This would explain the lack of visible particulate material as particles would fall to the bottom of the tube and be redissolved by the aqueous layer. Samples produced with benzyl alcohol also produced a hazy suspension but there was no evidence of particulate matter. Of the two esters used in this study, methyl acetate produced samples containing large masses of white material which collected at the bottom of the tube, as opposed to particulate material. It was also noted that this material formed extremely rapidly when BSA solution was added to the solvent and could be seen moving within the tube during the vortex mixing. However, ethyl acetate showed no sign of particulate material with an undissolved water layer visible in each replicate. Finally, 2E1H did not show any evidence of particulate material during any of the study replicates.

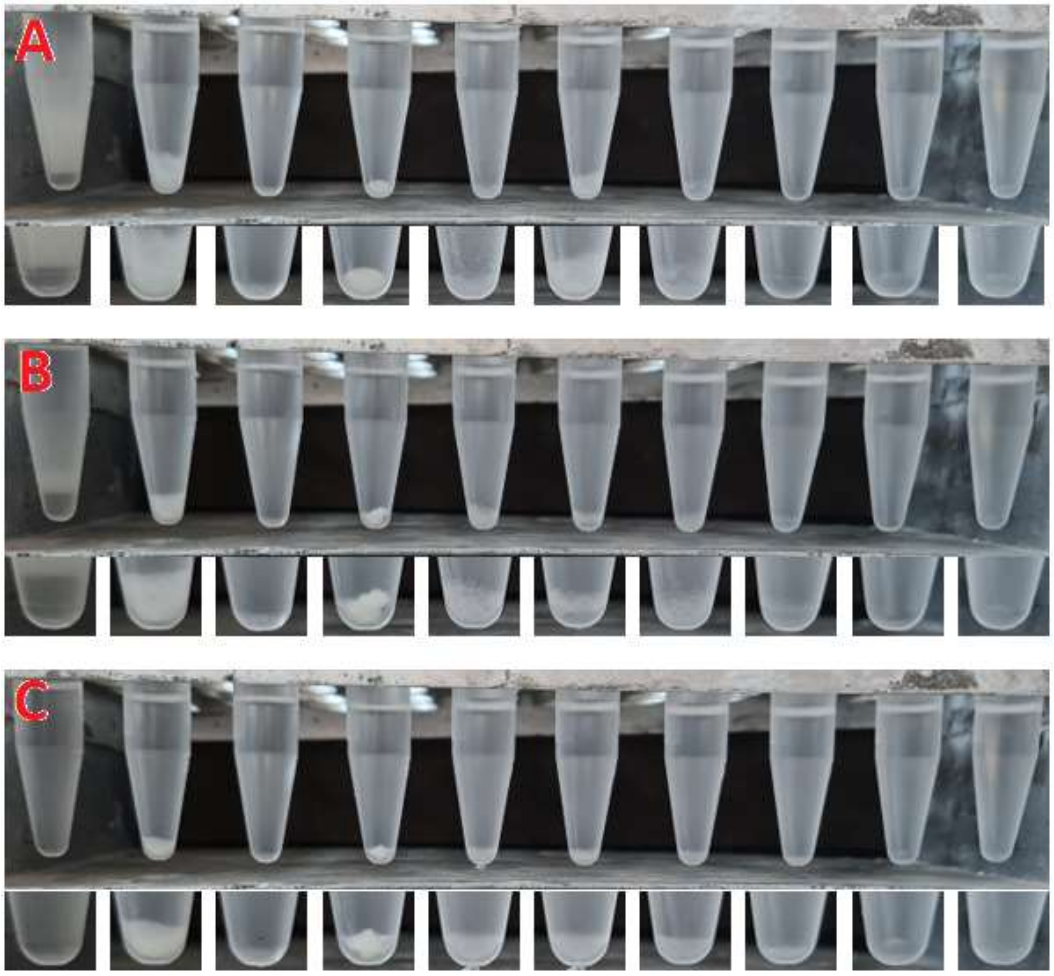

Fig 6.1: Digital images of CCP samples 5 minutes after vortex mixing. Left to right solvents are: 2-methyl-1-propanol, pentanol, methyl acetate, heptanol, 4-methyl-2-pentanol, octanol, decanol, ethyl acetate, 2-ethyl-1-hexanol. (A): Initial volume of aqueous BSA solution added. (B): Volume of aqueous BSA solution reduced by 25%. (C): Volume of aqueous BSA solution reduced by a further 25%.

Based on the results obtained in this analysis, a follow-up investigation into the use of 2M1P was conducted to investigate the apparent aqueous layer formed at the bottom of the vial. The ratio of solvent to protein solution used for CCP in this solvent was approximately three times higher than the next solvent due to the greater water absorption value of 2M1P. Due to the greater volume of aqueous solution added to the solvent it was hypothesised that an increased mixing time may have been required to allow for the water to be absorbed by the solvent. It was also hypothesised that there was simply too much water present for CCP to occur in the volume of solvent used. Both these hypotheses were tested by

producing two more samples utilising 2M1P as the drying solvent. For the first sample, 50 µL aqueous BSA solution was added, and the mixture was vortex mixed for 1 minute as per the previous samples. For the second sample 247.5 µL of aqueous BSA solution was added (the volume used for the middle replicate) and was vortex mixed for two minutes. Fig. 6.2 shows the digital images of the two samples.

Table 6.2: Tabulated representation of the results from visual observation of the fluid mixtures after 5 minutes. Cells are colour-coded as per the legend.

Solvent	Volume of BSA solution added to 1 mL solvent		
2-methyl-1-propanol	330	247.5	185.6
1-pentanol	90	67.5	50.6
Benzyl alcohol	80	60	45.0
Methyl acetate	75	56.25	42.2
1-heptanol	50	37.5	28.1
4-methyl-2-pentanol	45	33.75	25.3
1-octanol	35	26.25	19.7
1-decanol	35	26.25	19.7
Ethyl acetate	30	22.5	16.9
2-ethyl-1-hexanol	20	15	11.3

	Visible particulate
	No visible solid
	Visible secondary liquid layer
	Visible non-particulate solid

Results of this follow up experiment showed that when 50 µL of BSA solution was added to 1 mL of 2M1P, there was no evidence of the clear liquid at the bottom of the tube and white particulate matter was observed instead. The sample that had 247.5 µL of aqueous solution added with an increased mixing time did produce the clear section at the bottom of the tube. However, the size of the clear section did appear reduced compared to the sample using the same volume of aqueous solution with a shorter mixing time, implying that the increased mixing time may have aided

in water dissolution but a longer mixing time may have been required to allow full dissolution of the aqueous phase.

Fig. 6.2: Digital images of the two follow-up tests with 2-methyl-1-propanol. (Left) 50 µL of BSA solution added to 1 mL solvent and mixed for 1 minute. (Right) 247.5 µL BSA solution added to 1 mL solvent and mixed for 2 minutes.

Protein Screening

This experiment was designed to investigate whether proteins other than BSA can be successfully dehydrated using the CCP technique to produce solid protein microparticles. As such, the addition of the maximum volume of aqueous solution was not required and aqueous phase volumes were selected to allow for successful completion of the process. Based upon the results of the solvent screening experiment, four solvents were selected for use in the protein screening experiment. 2M1P, pentanol, 4M2P and methyl acetate were selected for use as drying solvents in this study. 2M1P, pentanol and 4M2P all performed well as drying solvents and had relatively high degrees of water absorption. Methyl acetate was selected for its distinct mode of action, apparently producing large flakes of material instead of spherical microparticles. For this experiment, 45 µL of aqueous protein solution was added to 1 mL of each solvent and vortex mixed for 1 minute as per the method. The mixtures were then placed in a rack for 5 minutes to allow any suspension to settle before being visually observed and imaged digitally.

Figure 6.3 shows the digital images captured from these samples. All samples appeared to produce a solid residue although the samples produced in 4M2P were less consistent with only very small quantities of solid being visible in some samples. Unlike the samples generated in the solvent screening experiments, the solid

material formed in the methyl acetate samples was not easily identifiable as non-particulate ands so microscopic analysis was required to confirm the state of the material. Varying amounts of solid material were also observed between the different proteins across each solvent, this may be attributable to the concentration of the protein solutions used, which varied between 50 mg/mL for HSA and lysozyme and 2 mg/mL for catalase.

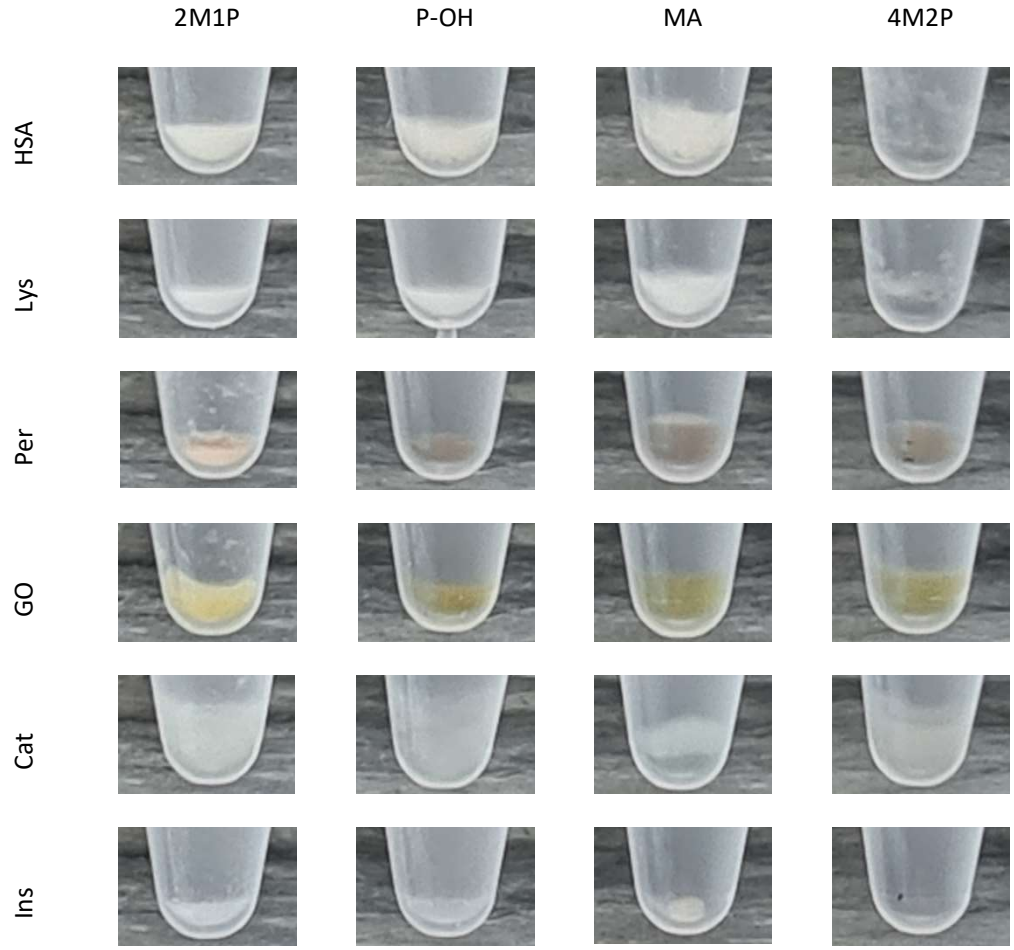

Fig 6.3: Digital images of sample produced during the protein screening study 5 minutes after vortex mixing. showing particulate precipitate was produced with all proteins and all solvents.

6.3.2 Microscopic Analysis

Samples for microscopic analysis were prepared by taking 20 µL aliquots from each sample immediately after vortex mixing and pipetting onto clean microscope slides and aluminium SEM stubs fitted with glass coverslips. Samples were then placed

under a loose covering to prevent dust and other contaminants and were left to dry overnight under a fume hood. Once dried, samples were imaged with brightfield microscopy using 4x and 20x magnification optics. Images taken at 4x magnification allowed for an overall view of the particle population and were analysed for large-scale particle aggregation, whereas images obtained at 20x magnification allowed for the observation and measurement of individual particles. The samples prepared for SEM observation were kept aside until brightfield microscopy analysis had been completed and selected samples were taken forward for SEM. SEM images were recorded at x200 magnification, allowing study of the topography of individual particles. The images shown in this chapter are representative images only and do not account for every sample analysed.

Solvent Screening

Pentanol and Decanol

Pentanol and decanol were used as the baseline solvents for this study as they have been used as the drying solvent for CCP in previous works. Visual observation of the microcentrifuge tubes showed a hazy suspension and the collection of white particulate material about the bottom of the tube. These observations were confirmed with microscopic analysis which revealed uniformly smooth and spherical microparticles across samples produced with both solvents (Fig. 6.4). Brightfield microscopy did not show any evidence of large-scale particle aggregation or irregularities, but the SEM images did show evidence of irregular, cracked structures in the samples produced using decanol, (fig. 6.4 bottom).

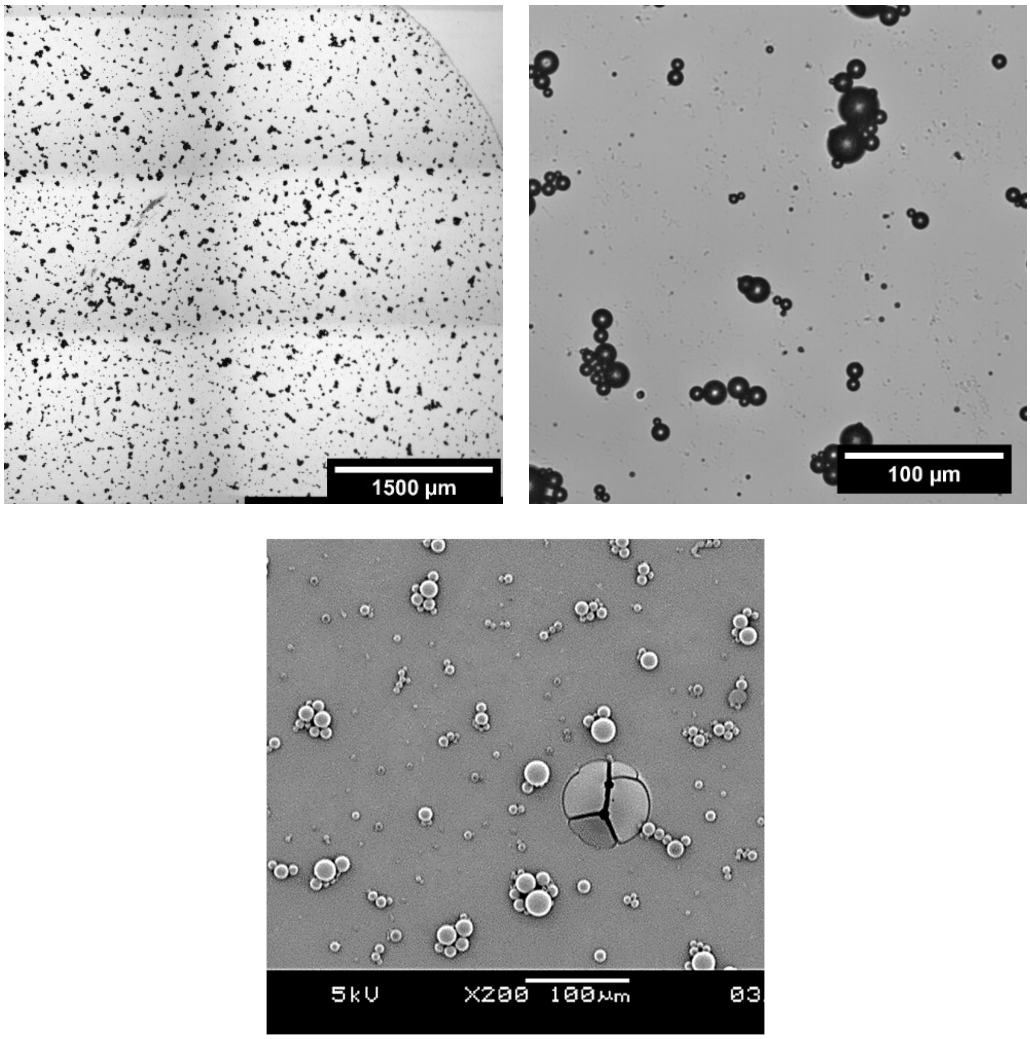

Fig. 6.4: Representative images of CCP BSA microparticles produced using pentanol and decanol. (Top) Light microscope images. (Bottom) SEM image.

2-Methyl-1-Propanol

Whilst visual observation of the initial samples produced in 2M1P were inconclusive, with no visible particulate material, microscopic observation of samples taken from the suspension clearly showed the presence of spherical microparticles. Fig. 6.5 shows images of the sample containing 247.5 µL of aqueous BSA solution obtained from both brightfield microscopy and SEM imaging. The brightfield images again show uniformly smooth and spherical microparticles with no evidence of large-scale aggregation. However, large, cracked structures were visible under SEM similar to those seen in the decanol samples. Unlike the decanol samples, however, the

structures seen in these samples were much larger and were not circular, they appeared reminiscent of a burst or cracked surface.

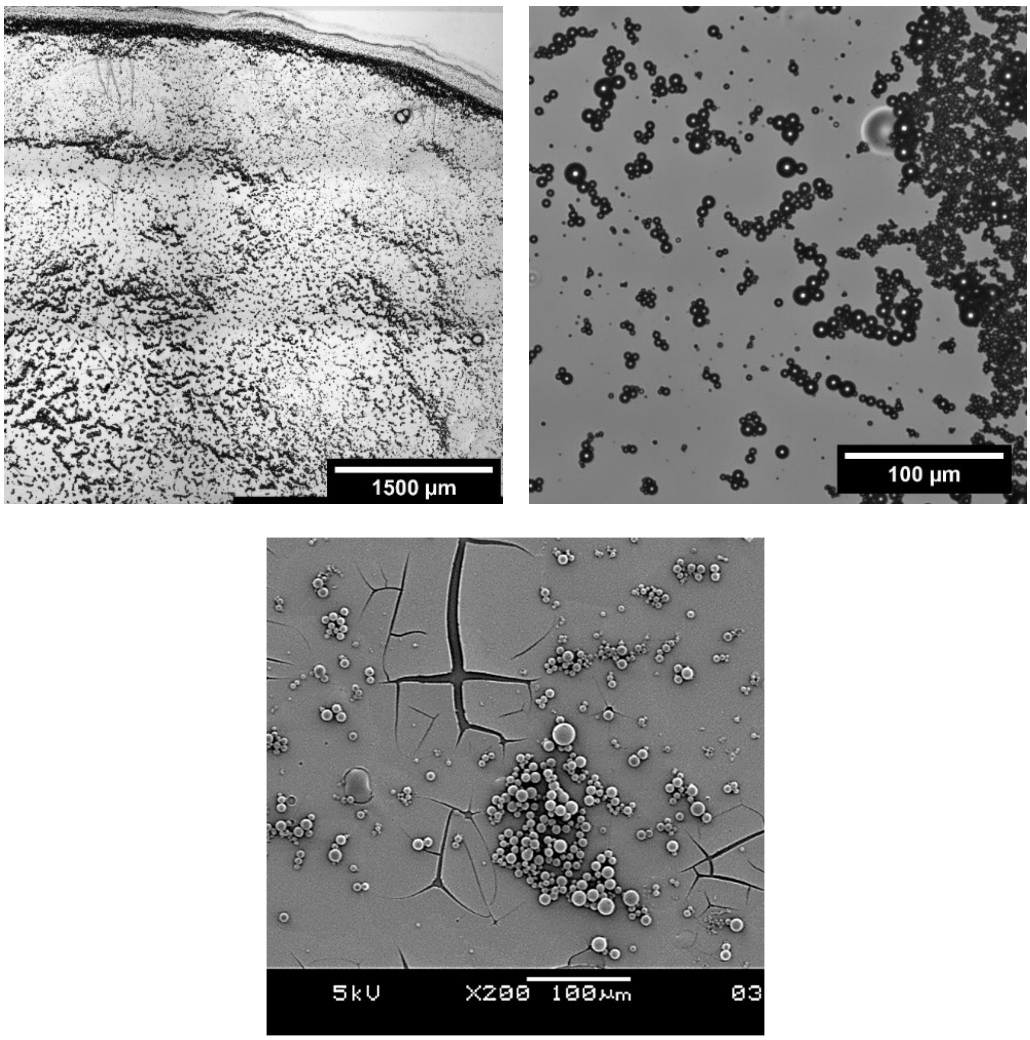

Fig. 6.5: Microscopy images of samples produced using 2-methyl-1-propanol as drying solvent with 247.5 µL of aqueous BSA added. (Top) light microscope images. (Bottom): SEM image.

Heptanol, 4-Methyl-2-Pentanol, Octanol, and 2-Ethyl-1-Hexanol

Visual inspection of samples using these solvents implied that CCP had occurred within these solvents, as evidenced by the generation of suspensions and white particulate matter. Microscopic observation confirmed these results with brightfield microscopy showing particles very similar to those obtained using pentanol and decanol. SEM imaging also showed results similar to those seen with pentanol and decanol, uniformly smooth and spherical microparticles without any evidence of

large-scale aggregation or irregular particles with the exception of samples produced in octanol which did show a small number of large irregular structures similar to those seen in decanol (Fig. 6.6).

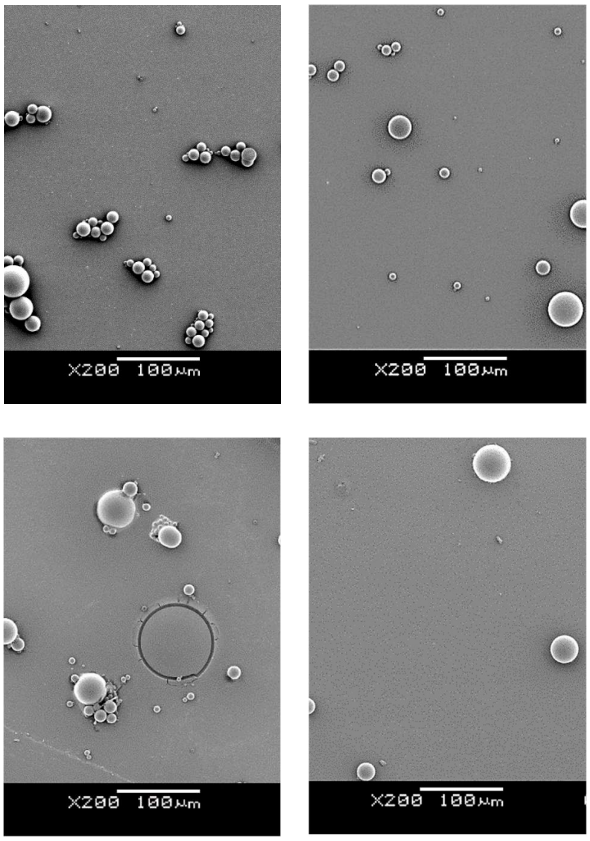

Fig. 6.6: SEM images obtained to x200 magnification. (Top Left) Microparticles produced using heptanol as drying solvent and 37.5 µL aq. BSA solution. (Top Right) Microparticles produced using 4-methyl-2-pentanol as drying solvent and 33.8 µL aq. BSA solution. (Bottom Left) Microparticles produced using octanol as drying solvent and 19.7 µL aq. BSA solution. (Bottom Right) Microparticles produced using 2-ethyl-1-hexanol as drying solvent and 11.2 µL aq. BSA solution.

Methyl Acetate and Ethyl Acetate

Visual observations of methyl acetate and ethyl acetate samples implied that CCP did not occur in any of the samples tested. Methyl acetate samples did appear to produce a solid white material, but the material appeared to be in the form of large flakes as opposed to particulate material. The ethyl acetate samples produced no visual evidence of solid material. However due to the low water absorption of this

solvent, and thus the small volume of BSA solution added, it may be the case that solid material was formed but at a quantity difficult to observe visually.

Microscopic analysis of the samples showed that no solid material was found in the methyl acetate samples taken from the middle of the vial after vortex mixing, whilst a very small number of smooth, spherical microparticles were found in the ethyl acetate samples. As no particles were found in the methyl acetate samples, SEM images of the precipitate were collected instead. Fig. 6.7 shows SEM images obtained of the precipitate found in the methyl acetate samples and a single particle from the ethyl acetate samples. The precipitate material in the methyl acetate sample is clearly not the particulate material expected to be found from CCP, however if the protein retains structure and function once reconstituted it could prove a useful addition to CCP technology.

Methyl acetate and ethyl acetate are chemically distinct from most of the other solvents in this study, being esters not alcohols, but were included based upon the water absorption values. The ester functional group possesses less molecular polarity than alcohols, however they do not form intermolecular hydrogen bonds leaving hydrogen atoms available to form hydrogen bonds with water. This leads to methyl acetate possessing a relatively high degree of water solubility (the opposite of water absorption showing how much of the solvent can dissolve into a given volume of water), over 10 times that of pentanol. This implies that the thermodynamics of the dissolution will favour the solvent phase dissolving into the aqueous droplets, creating an anti-solvent for BSA and causing the BSA molecules to precipitate out into solid precipitate material.

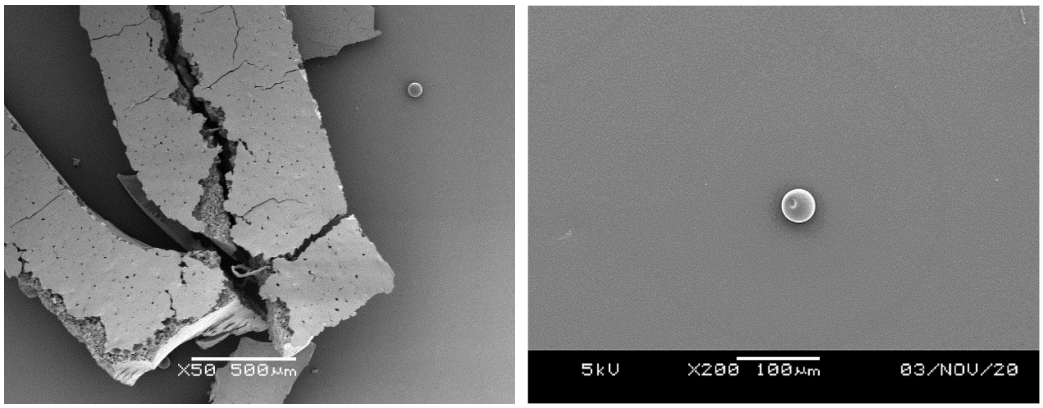

Fig. 6.7: (Left): SEM image taken of material produced when using methyl acetate as drying solvent. (Right): SEM image of a single microparticle produced using ethyl acetate is the drying solvent.

Benzyl Alcohol

Visual observation of the benzyl alcohol samples showed a hazy suspension with no evidence of solid matter. Microscopic analysis showed that a residue or slurry had appeared to form which was pock-marked with spherical microparticles (Fig. 6.8). The clear difference in appearance observed in benzyl alcohol compared to the other solvents tested may be explained by the chemistry of the solvent. Benzyl alcohol is a secondary alcohol consisting of a benzene ring with a single hydroxymethyl functional group. The presence of a benzene ring in the molecule causes a dipole moment within the molecule, leading to increased polarity and, thus, increased water absorption and water solubility. This results in a solvent with lower water absorption than pentanol but greater water solubility. This implies that the solvent will be dissolving into the aqueous droplets at a faster rate than the aqueous droplets dissolve into the solvent reservoir. Whilst further study would be required to understand the effects of this process it seems a fair assumption that the solvent-saturated droplets, also containing dissolved BSA, may create a form of slurry or residue material as observed.

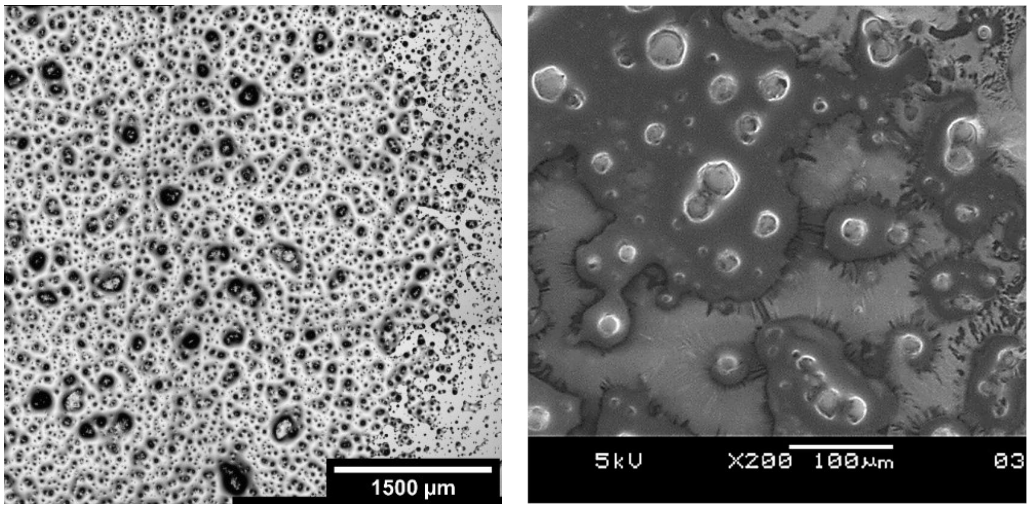

Fig. 6.8: Microscopy images of samples produced using benzyl alcohol as drying solvent with 60.0 µL of aqueous BSA added. (Left): Brightfield image obtained at 4x magnification. (Right): SEM image obtained at 200x magnification.

Protein Screening

Human Serum Albumin and Lysozyme

HSA and lysozyme were prepared in de-ionised water as described earlier. Microscopic observation showed that all samples produced in 2M1P, pentanol and 4M2P generated the smooth and spherical microparticle formulations similar to those seen with CCP of BSA, whilst samples produced in methyl acetate generated the large flake-like material similar to that observed in the solvent screening experiments. Figure 6.9 shows SEM images from each sample where it can be seen that the microparticles produced using these proteins and solvents were visually similar to those seen with BSA in the previous study with little evidence of large-scale aggregation or irregular structures. SEM images of the methyl acetate samples (Fig. 6.9, Top Middle) showed no evidence of microparticle formulations with the lysozyme sample showing no evidence of solid material at all, however, this may be due to the sampling technique failing to capture any material from this sample.

Insulin

Insulin solution was prepared in de-ionised water and adjusted to pH 2 as per the method section above. Brightfield microscopy showed that, similar to previous

samples, spherical microparticles, with no evidence of large-scale aggregation or irregular particles, had been produced in the 2M1P, pentanol and 4M2P solvents but not in the methyl acetate samples. Fig 6.10 shows SEM images from each sample where it can be seen that the average particle size appeared to be smaller than that of HSA and lysozyme and that interesting topographical features were present. In the images obtained from both 2M1P and pentanol samples it can be seen that pinhole-like structures were visible on some of the larger particles and in the 4M2P samples the same cracked structures as seen previously were evident

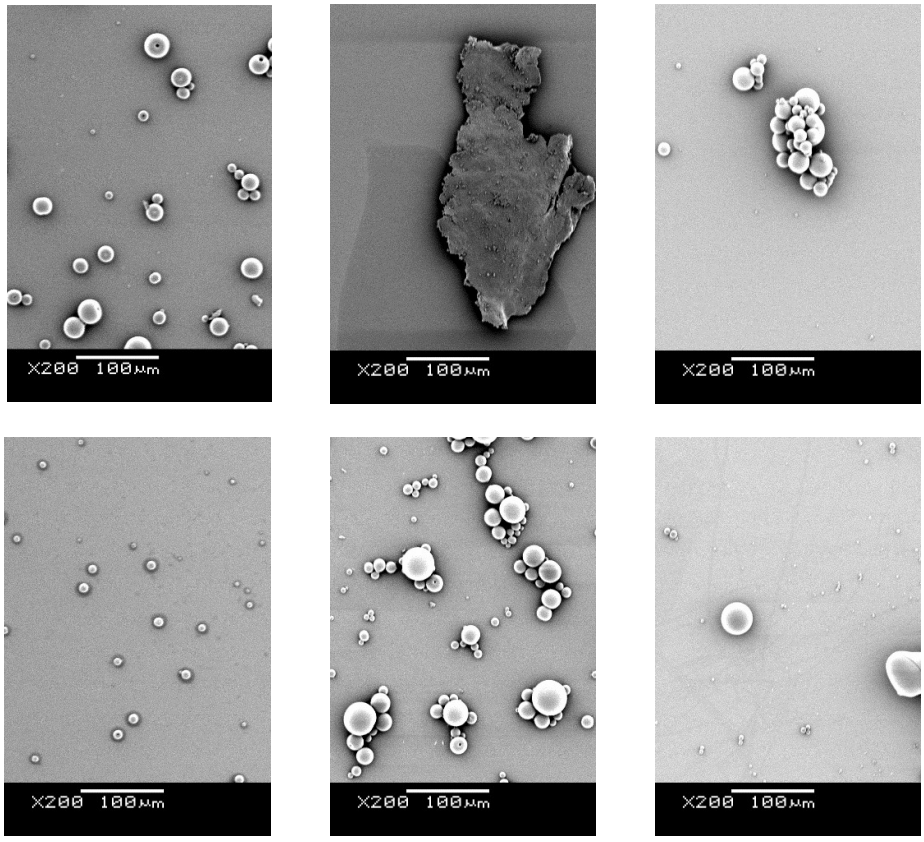

Fig. 6.9: SEM images of CCP material produced from multiple proteins in multiple solvents.
(Top Left) HSA in 2M1P (Top Middle) HSA in methyl acetate (Top Right) HSA in 4M2P (Bottom Left) Lysozyme in 2M1P (Bottom Middle) Lysozyme in pentanol (Bottom Right) Lysozyme in 4M2P

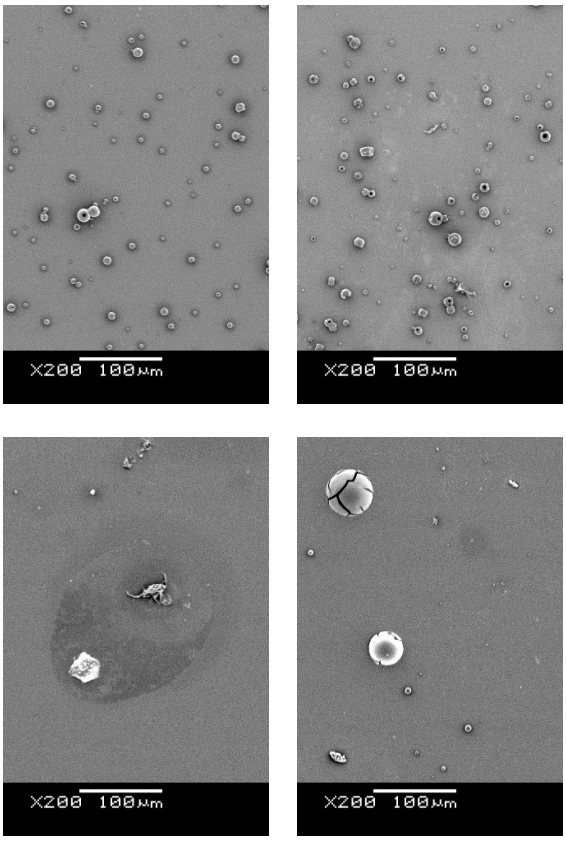

Fig. 6.10: SEM images of material produced from CCP of insulin in various solvents. (Top Left) 2M1P (Top Right) Pentanol (Bottom Left) Methyl acetate (Bottom Right) 4M2P.

Catalase, Peroxidase and Glucose Oxidase

Catalase, peroxidase and glucose oxidase were dissolved in a phosphate buffer, as opposed to simply dH_2O, to achieve an aqueous solution and visual observation of the vortexed mixtures appeared to show that particulate matter had been formed. However, microscopic observation showed that instead of the spherical microparticles observed in previous results, geometric crystalline structures were the most abundant materials present in the samples (Fig 6.11) with only a few spherical microparticles found, primarily in the 2M1P samples. As these proteins were dissolved in salt solution, rather than de-ionised water, the crystalline structures are likely to be precipitated salt crystals from the buffer similar to those seen in the work presented by Bitterfield *et al.* [203]. However, as some spherical particles were observed it follows that CCP did occur with the particles being obscured by the salt crystals, or perhaps even with the crystals forming around the

particles as the aqueous droplets dehydrated leaving the salt crystals and protein particles within the same structure.

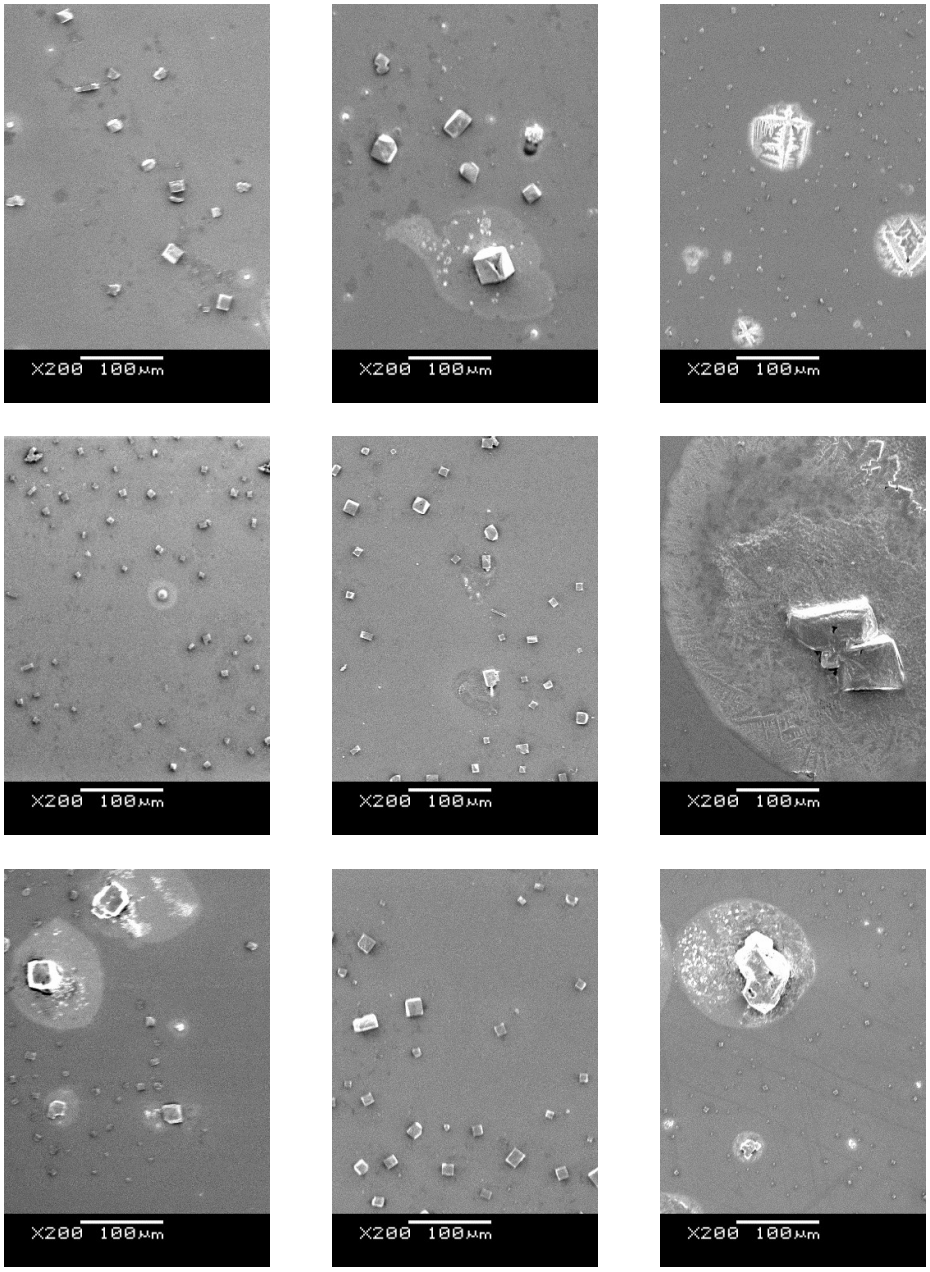

Fig. 6.11: SEM imaging of the result of CCP using various proteins dissolved in phosphate buffer and various solvents. (Top) Catalase in 2M1P, pentanol and 4M2P. (Middle) Peroxidase in 2M1P, pentanol and methyl acetate. (Bottom) Glucose Oxidase in 2M1P, pentanol and 4M2P

6.3.3 Particle Characterisation

Particle sizing was carried out using the image-based technique discussed in the methods section. Brightfield microscopy images taken at x20 magnification were used for this analysis. As multiple images were obtained, with overlap of images, it was decided that size measurements would be obtained from a single image to avoid counting particles more than once. The image used was selected randomly to avoid bias but if the image contained only a very small number of particles or was not representative of the overall particle population then a replacement image was selected at random. Due to the resolution of the images obtained in this study, the minimum particle diameter measurable was 4 μm.

Solvent Screening

Particle sizing of the solvent screening samples was conducted as described above using the same method as that used for the solvent screening samples. However, the image-based sizing method only works for circular structures and requires a large number of particles to provide a meaningful distribution. As such, the samples produced in benzyl alcohol, methyl acetate, ethyl acetate and 2E1H were excluded from this analysis.

Figure 6.12 shows the frequency distribution, shown as a population percentage, of particles in the diameter ranges 0-5 μm, 5-10 μm and >10 μm. The distribution of particle sizes shows that samples produced in both 2M1P and pentanol contained a majority population in the size range 5-10 μm with approximately 40% of particles falling into this size range. All other samples had a majority population in the size range 0-5 μm, with approximately 45-50% of particles in this size range across all solvents. 4M2P samples showed a deviation from the other samples with a very low percentage of particles in the 5-10 μm range and a larger population in the > 10 μm range. However, samples produced using 4M2P only had a low number of countable particles (n = 69) which may have skewed the results compared to the other samples.

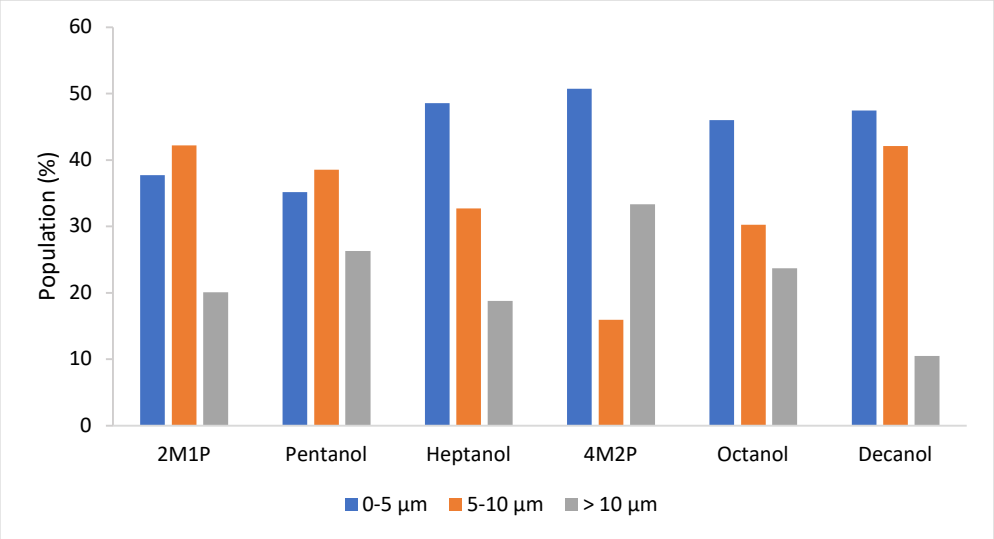

Fig. 6.12: Distribution of particle sizes (measured as particle diameter in µm) observed in samples produced using six different solvents. Particles were split into three different size ranges: 0-5 µm, 5-10 µm and > 10 µm.

However, despite the difference in size populations, the maximum and mean size of the particles remained similar across all samples with a maximum particle size of 24-31 µm and a mean size between 6-8 µm. Again 4-methyl-2-propanol was an outlier in these measurements with a maximum particle size of 48.2 µm and a mean particle size of 12.6 µm (Table 6.3).

Table 6.3: Breakdown of the maximum and mean particle size (as diameter in µm) for particles produced by CCP of BSA using six different solvents.

	Max. Particle Diameter (µm)	Mean Diameter ± 1 S.D. (µm)
2M1P (n = 448)	27.4	7.4 ± 4.0
Pentanol (n = 236)	29.3	7.8 ± 4.7
Heptanol (n = 208)	30.0	6.9 ± 4.2
4M2P (n = 69)	48.2	12.6 ± 13.0
Octanol (n = 152)	30.6	7.3 ± 4.4
Decanol (n = 411)	24.1	6.2 ± 2.8

Protein Screening

Particle sizing of the protein screening samples was carried out using the same method as that used for the solvent screening samples. However, as the image-based sizing method only works for circular structures it was not possible to size the crystalline particles found in the samples produced using catalase, peroxidase or glucose oxidase. As with the solvent screening samples, the samples produced in methyl acetate were also excluded as very few, if any, spherical particles were found.

Figure 6.13 shows the frequency distribution, shown as population percentage, of the measured particles in the diameter ranges 0-5 μm, 5-10 μm and >10 μm. The size distribution data shows that particles produced in 2M1P and 4M2P varied in size between proteins, whereas the samples generated using pentanol produced fairly consistently sized particles regardless of the protein used. In the pentanol samples, the particles sized 5-10 μm accounted for 35-40% of the particle population across all three solvents. HSA and lysozyme samples produced in pentanol also had very similar amounts of particles less than 5 μm and greater than 10 μm. Insulin samples produced in pentanol showed some deviation with an increased number of smaller particles (<5 μm) and a decreased number of larger particles (>10 μm). However, this may be due to the lower concentration of the aqueous insulin solution used. A lower concentration of protein means less protein molecules per volume of water, resulting in less protein molecules per droplet and thus smaller particles once the aqueous droplets have fully dissolved into the solvent. This difference may also be related to the properties of the aqueous solution as the insulin solution was adjusted to pH 2 which may have an effect on the interaction between the aqueous and solvent phase resulting in smaller droplets. Samples produced using both 2M1P and 4M2P generated particles with greater size variability with samples produced from insulin and 4M2P having 100% of the particle population having diameter of greater than 10 μm.

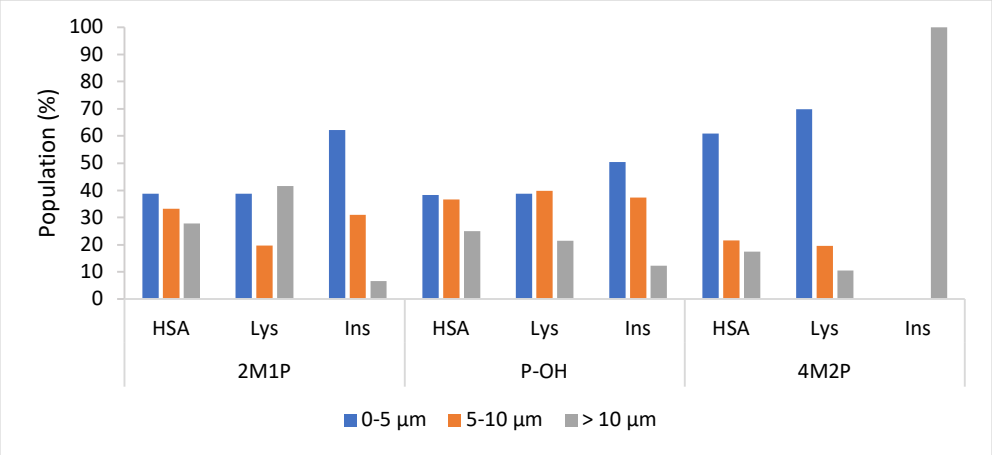

Fig. 6.13: Distribution of particle sizes (measured as particle diameter in µm) observed in protein samples produced using three different solvents. Proteins used were HSA, lysozyme and insulin. Solvents were 2M1P, pentanol and 4M2P. Particles were split into three different size ranges: 0-5 µm, 5-10 µm and > 10 µm.

Table 6.4 shows the maximum and mean diameter of measured particles and agrees with the results above, in that the samples prepared in pentanol had the highest size uniformity with the mean particle diameter varying between approximately 6-8 µm.

Table 6.4: Breakdown of the maximum and mean particle size (as diameter in µm) for particle samples produced using three different solvents. Proteins used were HSA, lysozyme and insulin. Solvents were 2M1P, pentanol and 4M2P.

	Max. Particle Diameter (µm)	Mean Particle Diameter ± 1 S.D. (µm)
HSA in 2M1P (*n* = 631)	39.1	8.5 ± 6.2
Lysozyme in 2M1P (*n* = 697)	36.5	10.3 ± 7.4
Insulin in 2M1P (*n* = 830)	18.9	5.5 ± 2.6
HSA in P-OH (*n* = 709)	38.5	8.1 ± 5.2
Lysozyme in P-OH (*n* = 747)	45.6	7.7 ± 5.0
Insulin in P-OH (*n* = 1342)	21.5	6.3 ± 3.2
HSA in 4M2P (*n* = 545)	48.9	7.6 ± 7.5
Lysozyme in 4M2P (*n* = 348)	50.2	6.1 ± 5.8
Insulin in 4M2P (*n* = 361)	204.3	30.7 ± 20.3

6.3.4 Protein Analysis

Fluorescence Spectroscopy

Solvent Screening Samples

The dehydrated microparticle samples were rehydrated with dH_2O to 2 mg/mL in a quartz cuvette and fluorescence emission spectra were obtained between 300-400 nm with an excitation wavelength of 295 nm. Only samples produced using four of the selected samples were analysed for protein structure: 2M1P, Pentanol, methyl acetate and 4M2P. Solutions prepared from lyophilised BSA powder at 2 mg/mL were prepared and used as positive control samples whilst BSA solution that had been purposefully denatured using 8M GdnHCl solution was used as the negative control. Blank solutions were prepared from the appropriate solvent, dH_2O for the experimental samples and positive controls and a mixture of GdnHCl and dH_2O (4:1 ratio GdnHCl:dH_2O) for the negative control samples. All measurements were obtained in triplicate and the resultant spectra were averaged and smoothed before being replotted (Fig. 6.14).

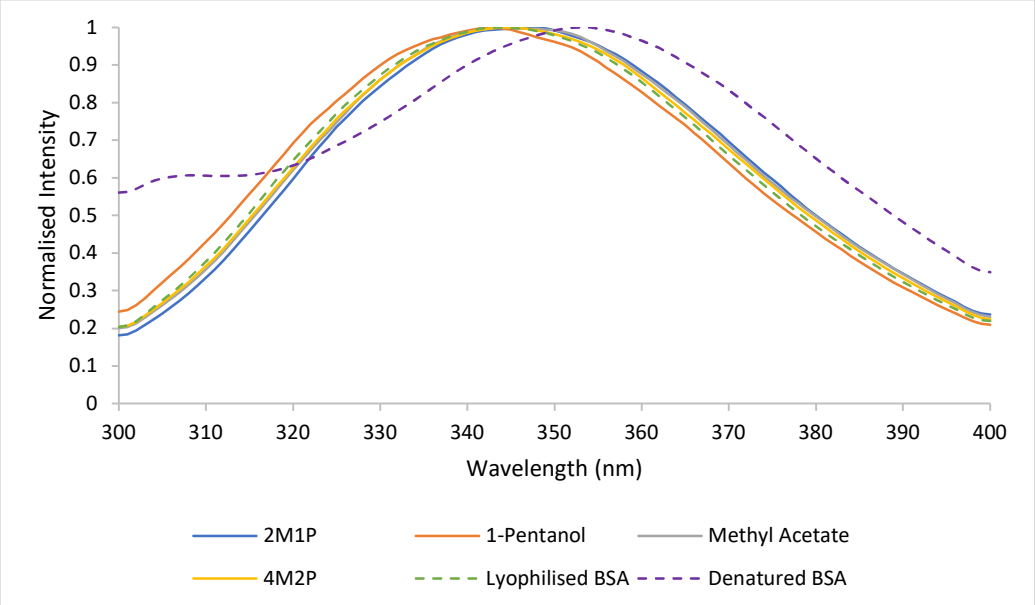

Fig. 6.14: (Left) Averaged and normalised fluorescence intensity spectra showing the peak emission wavelengths of BSA microparticle samples prepared with several organic solvents and reconstituted in

de-ionised water. Control samples were BSA solution from lyophilised powder and denatured BSA. (Right) Mean peak emission wavelength of samples produced with each solvent. Error bars = 1 SD.

The fluorescence emission spectra showed that the positive control sample (aqueous solution prepared from lyophilised BSA) gave a peak emission measurement at 344.0 ± 1.6 nm and the negative control (purposefully denatured BSA solution) gave a peak emission wavelength at 354.4 ± 1.2 nm. All samples prepared using CCP gave an emission maximum measurement between 342.4 – 347.0 nm. Calculation of a Student's t-test between experimental samples and the control samples showed that there was no significant difference between the peak emission wavelength of lyophilised BSA and the CCP BSA samples but that there was significant difference between the negative control and the experimental samples. These results show that no structural difference between the CCP and lyophilised samples could be detected, whereas the negative control sample showed a significant deviation, with the peak emission wavelength being redshifted by approximately 10 nm due to the unfolding of the protein structure. This indicates that the overall tertiary structure of rehydrated CCP BSA microparticles is unchanged from that of the source material, meaning that the CCP process did not act to denature the protein. As lyophilisation is currently the leading technology for the production of dehydrated protein formulations, this data shows that CCP could be used as an alternative technique without impacting the overall protein structure.

Protein Screening Samples

Dry powder samples produced during the solvent screening study were rehydrated to 2 mg/mL and analysed with fluorescence spectroscopy to provide information about their tertiary structure. Solutions made from the lyophilised powders of each protein were also prepared and used as positive controls.

HSA, lysozyme, peroxide, glucose oxidase and catalase all contain tryptophan residues within their structure, providing an intrinsic fluorescence property similar to that of BSA and information about the tertiary structure of the proteins can be

obtained by measuring the emission peak wavelength as per the solvent screening study [165], [204]–[207]. However, insulin does not contain any tryptophan residues within its structure and so this method cannot be used. Instead, the intrinsic fluorescence of tyrosine residues can be used. Insulin samples were excited at 276 nm and the excitation intensity measured between 300-400 nm. Similar to the tryptophan method, any unfolding of the protein creates a redshift in the fluorescence emission [208].

Figure 6.15 shows the fluorescence spectra obtained from the aqueous protein solutions prepared from rehydrated proteins, as well as aqueous solutions prepared from lyophilised powders of each protein to act as a positive control. The spectra show that the HSA samples prepared using CCP measured a peak emission wavelength of approximately 342 nm, whereas the peak maximum of the control sample was measured at approximately 333 nm. This result implies that CCP-HSA sample may have experienced a red shift in the spectral emission of 9 nm. However, a search of the literature shows that the expected peak emission wavelength of aqueous HSA is expected to be between 340 – 345 nm [209]–[211]. This implies that it was the control samples that had experienced a blue shift in the emission spectra and that the CCP-HSA sample was within the expected range.

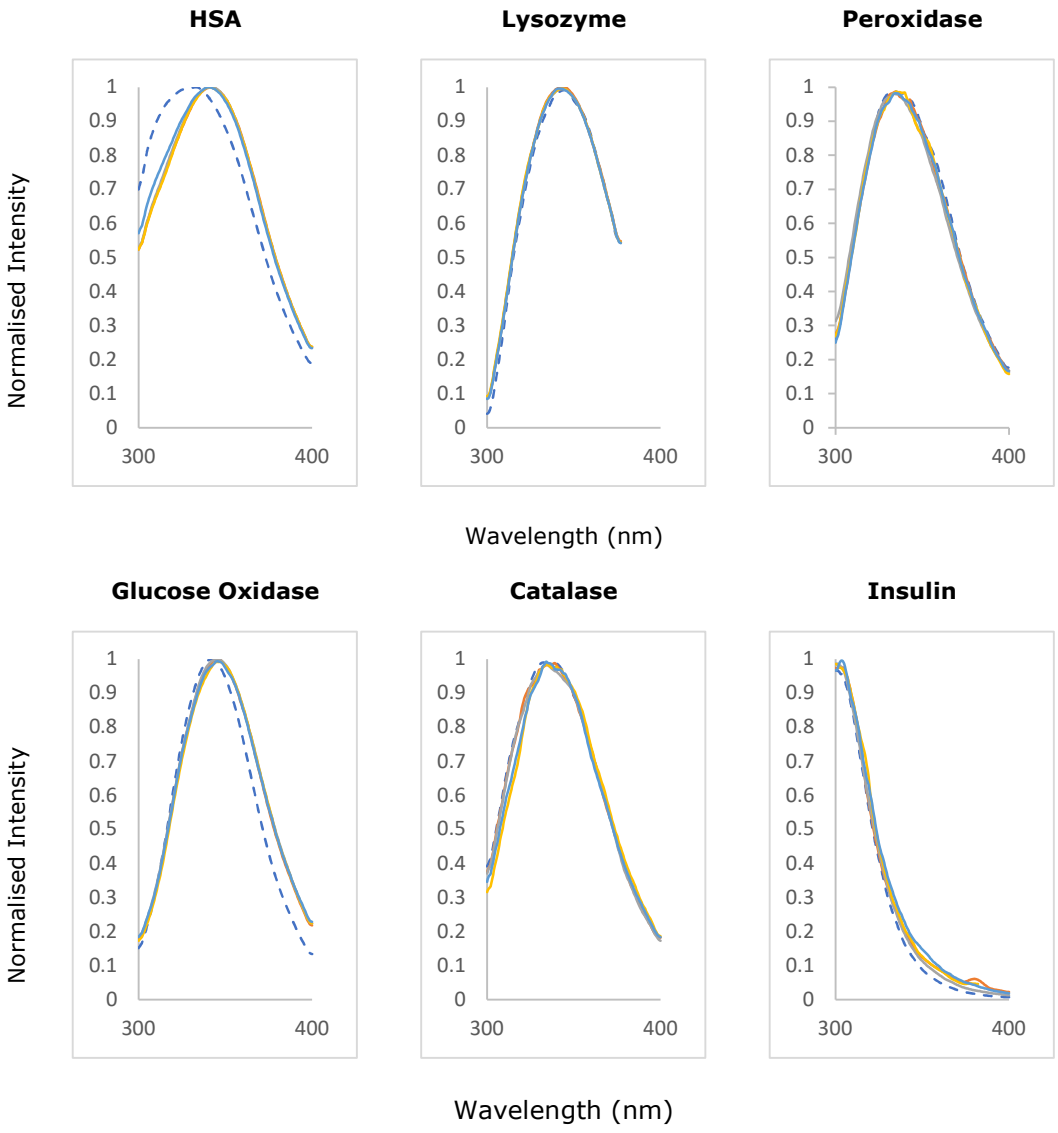

Fig 6.15: Smoothed and normalised fluorescence spectra of rehydrated proteins. HSA, lysozyme, peroxidase, glucose oxidase and catalase were excited at 280 nm to measure the innate fluorescence of Tryptophan residues, whilst insulin was excited at 276 nm to measure the innate fluorescence of Tyrosine. Rehydrated lyophilised proteins powders were also measured as positive control samples (marked with a dotted line).

Secondary Structure Analysis

Solvent Screening

Dehydrated BSA microparticle samples were rehydrated with dH_2O to their initial solution concentration and 20 µL was placed onto the crystal of a FTIR

spectrophotometer fitted with an ATR sampling accessory. Solutions prepared from lyophilised BSA powder were also prepared and used as positive controls. BSA solution that had been purposefully denatured using 8M GdnHCl was used as the negative control. Infrared spectra were obtained and analysed to give data on the secondary structure of the protein.

Figure 6.16 shows the inverted secondary derivative spectra from one sample of native BSA solution showing the largest peak at approximately 1658 cm^{-1}. This peak corresponds to the α-helix secondary structural element, showing that α-helices make up the primary component within the protein. Fig. 6.17 shows the relative abundance of α-helices and β-sheets in the rehydrated CCP BSA samples and control samples with the results displayed numerically below in table 6.5. As predicted from the 2nd derivative spectra, native BSA samples were made up of primarily of α-helices, at approximately 37% of the molecule, with β-sheets making up approximately 18%. The remaining 45% of the molecule would be made up the minor elements and unstructured portions.

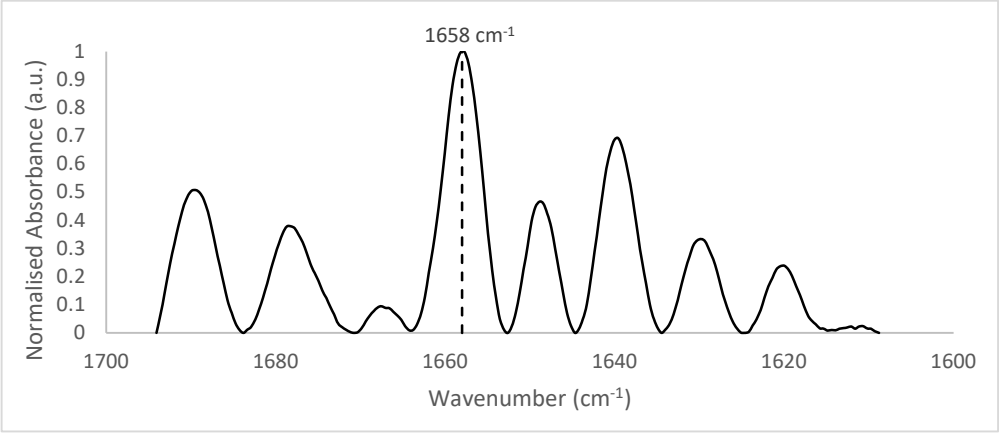

Fig. 6.16: 2nd derivative spectra of the Amide I band measured from native BSA solution showing the largest peak at approximately 1658 cm^{-1}. Comparing to published literature shows that this peak corresponds to the α-helix structural element.

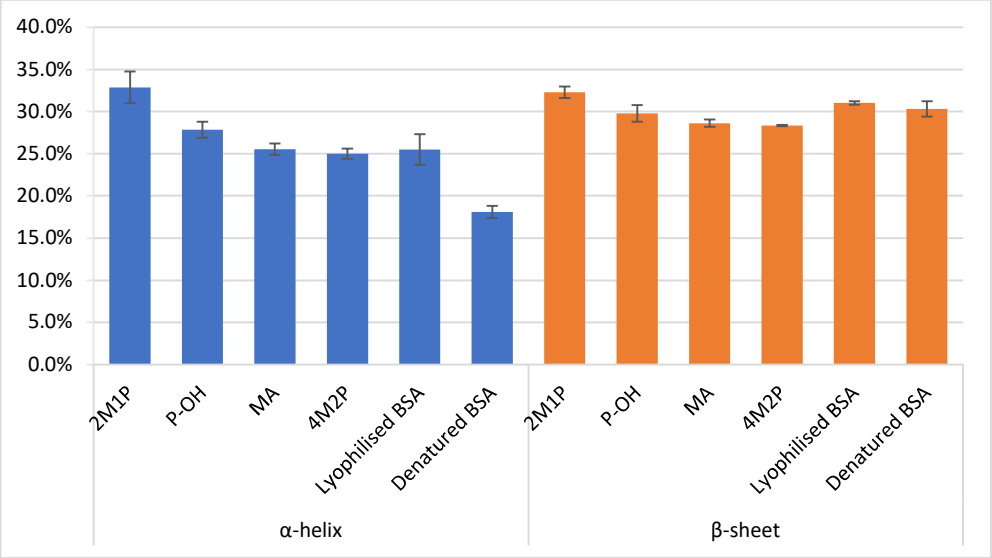

Fig 6.17: Bar chart and table data showing the relative abundance of α-helix and β-sheet structural elements within rehydrated BSA samples. Solutions were prepared from lyophilised BSA and purposefully denatured BSA were also measured as control samples.

Table 6.5: FT-IR results showing relative abundance of α-helix and β-sheet structural elements within rehydrated BSA samples. Solutions were prepared from lyophilised BSA and purposefully denatured BSA were also measured as control samples.

	Relative Abundance (%)	
	α-helix	β-sheet
2M1P	32.9 ± 1.9	32.3 ± 1.0
P-OH	27.8 ± 1.0	29.8 ± 0.4
MA	25.5 ± 0.7	28.6 ± 0.1
4M2P	25.0 ± 0.6	28.4 ± 0.2
Lyophilised BSA solution	25.5 ± 1.8	31.0 ± 0.9
GuHCl-denatured BSA solution	18.1 ± 0.7	30.3 ± 0.9

These results show a significant decrease in a-helix abundance between the positive and negative control samples, indicating that this test is valid for use in determining whether a BSA sample has been denatured by the CCP process. Analysis of the results from the experimental samples show that none of the samples reduced significantly in α-helix abundance, implying that denaturation had not taken place as a result of the dehydration process. However, the 2M1P samples actually showed

a significant increase in the abundance of α-helix from approximately 25.5% in the lyophilised control to 32.9% in the CCP sample. Whilst this increase does not necessarily indicate denaturation or unfolding of the protein tertiary structure, it does show that the protein underwent structural change which did not recover upon rehydration.

Analysis of β-sheet abundance within the rehydrated protein samples showed that there was not a significant difference in the measurements between the two control samples, meaning that this measure was not a useful test for the analysis of denaturation. However, both the 4M2P and MA samples prepared using CCP showed a significant decrease in abundance from approximately 31.0% in the lyophilised sample to 28.4% and 28.6% respectively. As with the results for the α-helix structure, this does not necessarily mean that the protein has undergone denaturation but shows a structural change has taken place.

Protein Screening

Dehydrated microparticle samples were rehydrated with deionised water to 50 mg/mL and 20 µL was placed onto the crystal of a FTIR-ATR spectrophotometer. Solutions prepared from lyophilised protein powders were also prepared and used as positive control samples. Infrared spectra were obtained and analysed to give data on the secondary structure of the protein.

Table 6.6 shows the mean relative abundance of α-helix and β-sheet structures for each sample. These results show that the reconstituted samples prepared from HSA, lysozyme and peroxidase experienced small fluctuations in the measurements of relative abundance of α-helix and β-sheet structures. However, the samples produced from glucose-oxidase, catalase and insulin experienced much larger changes in their secondary structure.

The measured values of α-helix and β-sheet structures for the HSA samples show a small amount of variation between different samples, with α-helix values ranging

96.6% – 103.2% of the control sample values. Application of a student's t-test showed that all changes seen in the HSA samples were non-significant meaning that the data does not support the hypothesis that CCP and reconstitution affected the secondary structure of the protein and that the variations observed were due to noise and error in the measurements. Lysozyme samples also experienced small variations in both α-helix and β-sheet structures across all samples with the abundance of α-helix structures observed in the lysozyme samples ranging 95.2% - 97.6% of the control sample values. Calculation of a student's t-test showed that all of these reductions were significant, with the exception of the 4M2P samples. This result strongly implies that the small reduction in α-helix structures seen in these samples were a real effect and can be attributed to the CCP process. Measured results from the peroxidase samples showed a reduction in α-helix structures across all samples, along with an increase in β-sheet structures. The measured values showed that α-helix values ranged from 89.5% - 91.5% of the control sample measurements. Application of a student's t-test showed that all of these changes were significant, implying that the reduced values were a real effect brought about by the CCP process.

Secondary structure measurements from the samples produced from the other three proteins, glucose-oxidase, catalase and insulin, showed greater deviation from the control sample, with all samples producing highly significant reductions in the relative abundance of α-helix and a corresponding increase in the abundance of β-sheet structures. Measurements of α-helix abundance showed that glucose-oxidase values ranged from 54.2% - 73.5% of the control sample values, catalase values ranged between 35.0% - 42.3% of the control samples value and insulin values ranged 65.7% - 73.3% of the control samples measurements.

Table 6.6: Relative abundance of α-helix and β-sheet structural elements from protein samples prepared in various solvents. Solutions prepared from lyophilised powder were used control samples.

		Relative Abundance (%)	
		α-helix	**β-sheet**
HSA	2M1P	39.5 ± 1.6	22.4 ± 0.3
	P-OH	40.7 ± 0.8	26.5 ± 1.1
	MA	41.3 ± 1.2	25.2 ± 0.7
	4M2P	42.2 ± 0.4	25.1 ± 1.1
	Lyophilised Solution	40.9 ± 0.5	26.2 ± 0.2
Lys	2M1P	36.5 ± 0.2	24.4 ± 0.2
	P-OH	35.6 ± 0.2	24.4 ± 0.6
	MA	35.8 ± 0.5	22.4 ± 0.6
	4M2P	36.3 ± 0.7	23.7 ± 0.3
	Lyophilised Solution	37.4 ± 0.1	23.5 ± 1.5
Per	2M1P	39.1 ± 0.6	12.6 ± 0.3
	P-OH	39.4 ± 0.9	12.2 ± 0.5
	MA	39.2 ± 0.8	12.5 ± 1.1
	4M2P	40.0 ± 0.3	12.5 ± 0.2
	Lyophilised Solution	43.7 ± 1.3	10.5 ± 1.3
G-O	2M1P	21.1 ± 1.6	35.0 ± 5.8
	P-OH	28.6 ± 5.6	25.0 ± 3.1
	MA	22.1 ± 3.9	34.5 ± 6.1
	4M2P	27.0 ± 3.0	32.3 ± 3.7
	Lyophilised Solution	38.9 ± 1.0	11.6 ± 1.3
Cat	2M1P	15.5 ± 2.0	37.5 ± 4.5
	P-OH	14.3 ± 0.5	41.2 ± 8.2
	MA	17.0 ± 0.6	37.1 ± 8.7
	4M2P	14.6 ± 1.4	40.2 ± 3.0
	Lyophilised Solution	40.2 ± 0.7	32.3 ± 1.0
Ins	2M1P	22.6 ± 0.8	39.4 ± 1.9
	P-OH	24.4 ± 1.5	36.5 ± 3.1
	MA	25.2 ± 2.2	33.8 ± 4.6
	4M2P *	23.7	-
	Lyophilised Solution	34.4 ± 4.0	28.6 ± 9.0

* only one sample measured.

Further consideration of these data show that the two proteins that experienced the least change to their secondary structure, HSA and lysozyme, were the only two proteins dissolved directly into de-ionised water. All other protein solutions were prepared from aqueous buffer solutions. Of the proteins prepared in buffer solutions, peroxidase, catalase and glucose oxidase were dissolved in a phosphate buffer and, as discussed earlier, observation of the dried powder revealed that salt crystals appeared to have formed. As such it is possible that the inclusion of these salt crystals affected the secondary structure of the proteins. It can also be noted that these three protein solutions were prepared at different concentrations, with peroxidase at 20 mg/mL, glucose-oxidase at 10 mg/mL and catalase at 2 mg/mL.

6.4 Conclusions and Further Work

6.4.1 Solvent Screening

This study aimed to investigate the applicability of CCP for use with various proteins and solvents with an eye towards the use of this technology an in industrial setting. The initial solvent screening study was designed to attempt dehydration of BSA at close to the maximum theoretical yield of protein for each solvent investigated. This was achieved by calculation of the maximum volume of water that could be dissolved into 1 mL of solvent and attempting the CCP technique using this volume of aqueous protein. Using this calculated volume of aqueous protein solution, protein microparticles were observed in 5 of the 10 solvents selected. Samples prepared in 2-methyl-1-propanol, 1-pentanol, 1-heptanol, 4-methyl-2-pentanol and 1-octanol all contained well-defined, spherical microparticles when prepared at the calculated maximum theoretical yield. As such, these solvents were considered the most promising candidates for industrial use. Samples prepared in methyl acetate also produced a solid form of the protein when the calculated maximum amount of aqueous phase was used, but rather than producing spherical microparticles, the protein appeared to precipitate out into large, flake-like particles.

To continue the study, the volume of aqueous protein solution was reduced by 25% and CCP was attempted again. This process was then repeated a third time, with the volume of protein solution reduced by a further 25%. This process ensured that all solvents were given the opportunity to allow for CCP without becoming saturated by the water in the solution. Of the other solvents used in this study, the use of 1-decanol, ethyl acetate and 2-ethyl-1-hexanol did appear to produce dehydrated BSA microparticles although the yield was low due to the low volumes of aqueous phase used. The use of benzyl alcohol as the drying solvent resulted in a very different outcome. Discreet microparticles were not observed in the dried solid material, instead the material formed a residue which appeared to be pock-marked with solid microparticles. This behaviour is likely explained by the chemistry of benzyl alcohol which results in a chemical with a relatively high water solubility and a relatively low water absorption.

The dehydrated microparticles produced in this first study showed a variety of size distributions with no obvious trends following solvent properties such as the water absorption or density of the solvents. As the BSA concentration of the aqueous phase was constant over all samples, the size distribution of the microparticles must be related to the size distribution of the microdroplets formed when the aqueous/solvent phases were mixed together. The lack of obvious trends in the data shows that the size distribution of microdroplets (and thus microparticles) formed in the solvent reservoir must have a complex relationship with the properties of the two liquids. This relationship is likely to depend upon multiple properties such as the densities of the fluids, the interfacial tension between the fluids and the absorption and dissolution values of the fluids.

Samples produced from four of the ten solvents used were then selected for further characterisation to analyse any structural changes to the protein after CCP and reconstitution. 2-methyl-1-propanol and pentanol were selected for having the highest yield potential of the solvents, methyl acetate was selected due to producing

a different physical form of the protein, and 4-methyl-2-pentanol was selected due to being a secondary alcohol which had not previously been studied in the literature. BSA tertiary structure was analysed using fluorescence spectroscopy with lyophilised BSA solution acting as a positive control and GdnHCl denatured BSA solution as a negative control. Fluorescence spectroscopy showed that the there was no significant difference in the tertiary structure of the protein between the lyophilised protein solution and the CCP protein solution. Furthermore, the negative control sample did show a significant redshift in the peak emission wavelength, showing that the tertiary structure of the negative control sample was significantly different from the experimental samples. Analysis of the protein secondary structure was conducted using FT-IR spectroscopy providing similar results. The negative control sample showed a significant decrease in the relative abundance of α-helix structures compared with the positive control whilst all experimental samples showed no significant changes from the positive control.

The results of this study showed that a range of potential solvents does exist for use with CCP technology, and that choice of solvent can affect the particle size distribution of the resultant microparticles. However, it has also been demonstrated that prediction of the particle size distribution, or even the ability of the solvent to form CCP microparticles, is difficult as many factors are likely to affect the outcome. This study also raises many new questions and potential research areas. A study into the use of solvents with higher values of water absorption could lead to finding solvents which allow for even greater potential yields, and through directed modelling it may be possible to find solvents which maximise the potential yield by dehydrating a large volume of aqueous protein solution in the minimum time and using the minimum amount of energy when mixing. Modelling the relationship between the solvent and yield would be difficult to accomplish in a screening study like this one but may be easier to accomplish using a micropipette setup similar to that demonstrated in Chapter 3 of this thesis.

6.4.2 Protein Screening

This study aimed to investigate the use of CCP with multiple proteins. So far in this thesis, all studies have used BSA as a model protein, however BSA is a relatively large, globular protein with good water solubility and so is not representative of the vast majority of proteins. To explore the extent to which CCP can be used with a wide variety of proteins, six proteins were selected representing a variety of different molecular sizes and biological functions. To explore the dehydration of these proteins, a screening study was established using four of solvents based upon the results of the solvent screening experiments. Proteins selected for this study were: human serum albumin, lysozyme, catalase, horseradish peroxide, glucose oxidase and insulin. Solvents selected for study were: 2-methyl-1-propanol, 1-pentanol, methyl acetate and 4-methyl-2-pentanol.

HSA and lysozyme aqueous solutions were both prepared directly in de-ionised water at 50 mg/mL and observation of the resultant dried material revealed spherical microparticles similar to those observed in the BSA samples above. Furthermore, samples prepared in methyl acetate resulted in large flake-like material as opposed to microparticles. Insulin aqueous solution was prepared in dH_2O and adjusted to pH2. Samples produced from insulin also produced spherical microparticles but they appeared smaller overall and many appeared to have a pinhole structure in their surface. This appears similar to some of the images seen earlier in this thesis which showed microparticles that had been split open revealing a hollow core and a hole from the surface to the hollow core.

The other three proteins: catalase, horseradish peroxidase and glucose oxidase, were all prepared as aqueous solutions in PBS at 20 mg/ml, 10 mg/mL and 2 mg/mL respectively, as opposed to dissolution in de-ionised water. Observation of the solid, dried powder obtained from these proteins revealed crystalline structures instead of the spherical microparticles obtained from the dehydration of previous proteins. The crystalline structures were of a size consistent with CCP microparticles and were

observed in the samples prepared from each of these proteins and each solvent tested, with the exception of samples prepared in methyl acetate. The samples prepared in methyl acetate displayed the large flakes of material seen previously. The crystalline structures seen in these samples were reminiscent of salt crystals, and so it is possible that CCP did occur in these samples but the buffer salts became entrained within or formed crystals around the protein.

Particle sizing was carried out using an image-based measurement technique based on the Hough Circle Transform algorithm which is used to find circles within visual data. As such, sizing could only be conducted on the samples which produced spherical particles, this included particles made from HSA, lysozyme and insulin, using the solvents 2-methyl-1-propanol, 1-pentanol and 4-methyl-2-pentanol. As discussed previously, particle size is dependent upon the protein concentration of the aqueous phase and the size of the microdroplets formed in the solvent reservoir. Results from the solvent screening study showed that the use of different solvents produced particles with a different size distribution, potentially due to the physical interactions between the two phases to form differently sized microdroplet dispersions. The results generated in this study showed that each combination of protein and solvent produced particles with a different size distribution with no obvious trends visible. However, by comparing the particle size distribution of all samples produced within a single solvent it was clear that the use of 1-pentanol produced the most uniformly sized particles. When comparing HSA and lysozyme particles produced in 1-pentanol, they had a very similar size distribution profile. Including particles produced from insulin into the comparison, it was seen that the insulin particles contained a greater quantity of smaller particles (< 5 μm) and a lesser quantity of larger particles (> 10 μm) whilst the percentage of particles with diameter between 5 – 10 μm remained approximately equal at about 35% – 40% of the total population.

Protein tertiary structure analysis was conducted on all combinations or protein and solvent selected for this study. Similar to the solvent screening experiment, solutions prepared from the lyophilised proteins were used as positive control samples and results showed that all samples tested measured a peak emission wavelength that was not significantly different from the positive control. The exception to this was the HSA samples which provided measurements showing that all experimental samples had red shifted by approximately 10 nm, suggesting that the tertiary structure had begun to unfold. This result was surprising as HSA is very similar to BSA in structure and composition, so a similar result was expected. It is possible that these samples became contaminated or were not handled correctly and unfolding occurred after the reconstitution but repeat samples and measurements would be needed to investigate this further

Analysis of the protein secondary structure was carried out using FT-IR spectroscopy with lyophilised proteins acting as positive control samples. The results from these measurements show that both HSA and lysozyme underwent very little conformational change due to the CCP process and subsequent reconstitution. HSA samples showed no significant change in the relative abundance of α-helix structures, lending to the hypothesis that the differences observed in the tertiary structure may have been spurious. Results of the lysozyme measurements showed that all experimental samples experienced a significant reduction in the abundance of α-helix structures, however, the measurement errors were very low for the lysozyme samples, meaning that even very small absolute changes can produce a significant result. The other four proteins experienced much larger changes to their secondary structure, displaying large reductions in the relative abundance of a-helix structures. However, it should be noted that the aqueous solutions of these four proteins contained buffer salts, whereas HSA and lysozyme solutions did not. As such it is possible that the inclusion of buffer salts in the CCP product may have affected the protein structure. It was also noted that the samples

with the lowest concentration of protein in the aqueous phase seemed to have experienced the largest reduction in α-helix structures. When the α-helix abundance was plotted against the concentration of protein in the aqueous phase a linear relationship was seen, which lends credence to the possibility that the presence of salt crystals within the CCP sample may affect the secondary structure of the protein with a greater ratio of salt to protein causing a greater degree of disruption to the structure. However, this link is tenuous at best and further work would be required to investigate this more fully.

As with the solvent screening work, this study has opened up new questions and avenues for research. An investigation into the effects of salts in the aqueous phase should be conducted. If the link suggested above were found to be correct then this could be a setback for the use of CCP as an alternative to freeze drying as many proteins are not readily soluble in water and require salts or other excipients to achieve useful concentrations. However, it may also be the case that the addition of different salts or other excipients may protect the proteins during the CCP process. It would also be interesting to re-run some of these experiments and conduct activity assays on the reconstituted proteins. This could not only confirm the applicability of CCP for the drying of proteins but may also provide further details on the changes seen in the secondary structure of some of the proteins, it is even possible that the changes do not affect the biological activity of the proteins as there was no impact on the tertiary structure, and thus the binding site structures. Finally, the inclusion of salt crystals in the CCP powders suggests that other material may also be dehydrated using this technique. An investigation into the dehydration of other biological material such as mAbs, viral vectors, exosomes, or even larger structures such as cells themselves. If successful CCP and reconstitution of a range of biological structures were demonstrated, then CCP could potentially become a one-size-fits-all technique for the dehydration of biological materials.

Chapter 7

Preliminary Works and Final Conclusions

7.1 Chapter Introduction

This chapter discusses two further potential applications of CCP technology along with some early proof of concept experiments to show feasibility. Final conclusions and further work that has arisen from these studies are also discussed to end the thesis. The experimental data shown in this chapter are early works designed only to show feasibility of the potential applications.

The first potential application discussed in this chapter is the use of CCP to manufacture protein microparticles for use in non-aqueous suspensions for subcutaneous injection. Currently, therapeutic proteins are typically administered by intravenous injection of dilute solution, requiring regular hospital visits by the patient [212]. The use of subcutaneous injections for the delivery of therapeutic proteins would potentially allow for self-administration of the product, removing the need for regular hospital visits and paving the way for many new therapeutic protein products. However, administration via subcutaneous injection has proven problematic due to the need for high doses required for many protein therapeutics, often in the region of hundreds of milligrams [213]. Under US FDA regulations, subcutaneous injection volume must not exceed ~1.5 mL with a viscosity not exceeding ~50 cP [214]. However, protein solutions in the hundreds of mg/mL concentration range tend to have markedly increased viscosities due to interactions in the electrical double layer brought about by the physical proximity of the protein molecules within the solution [215], [216]. This typically increases the viscosity of highly concentrated protein solutions well above 50 cP, making them unsuitable for subcutaneous injection [217]. In addition, protein solutions often display instability

at high concentration which may compromise the clinical safety and efficacy of the product [218]. Strategies have been developed to help reduce the viscosity of highly concentrated protein solutions, in some cases the addition of hydrophobic salts or variation in buffer or pH make it possible to reduce the surface charge on the protein resulting in fewer double layer interactions, reduced viscosity and increased stability [215], [216], [219]. However, the concentration requirements of excipients are generally very high, often up to 20:1 excipient to protein by mass, resulting in reduced space within the solvent for the protein to occupy [213], [215], [216].

An alternative approach to reduce the viscosity of highly concentrated protein formulations is to replace the aqueous solution with protein suspensions. This has been demonstrated with proteins in their crystalline form for a number of marketed therapeutics resulting in lowered viscosities [213], [220]. However, the crystallisation of proteins is time-consuming and unpredictable due to their high molecular weight, abundant glycosylation, and flexible structure [213], [221]. A further approach to reduce the viscosity of high concentration protein therapeutics is to remove the use of aqueous media entirely and to suspend solid protein formulations within a pharmaceutically acceptable non-aqueous media for subcutaneous injection. This concept has been discussed for over a decade now with several studies showing highly concentrated protein powder suspensions with viscosities far lower than an equivalently concentrated aqueous solution [217], [222], [223].

Whilst the use of non-aqueous protein powder suspensions is not an established biopharmaceutical technology, meaning that there are no marketed human therapeutics using the technology, the use of non-aqueous injections is common in farmed cattle. High concentration suspensions of bovine somatotropin formulated in sesame oil and a bovine growth hormone formulated in miglyol oil are both marketed for use in cattle [212], [224]. Furthermore, in work carried out in 2006 by Chen *et al*., pharmacokinetic studies were carried out on cynomolgus monkeys who

were injected with monoclonal antibody formulations prepared either as a powder suspension or an aqueous solution [225]. The results of this study showed that no differences were detected in the plasma profiles between the monkeys given a powder suspension formulation and those given an aqueous solution.

The second potential application of this technology is the use of BSA microparticles produced using CCP as a solubility enhancer for drugs with poor aqueous solubility. Poor aqueous solubility of therapeutic drugs is an increasingly common issue facing formulation scientists. Whilst approximately 40% of current pharmaceutical drugs can be classified as poorly water soluble, it is estimated that up to 90% of in-development drugs share the same classification based on the definition by the biopharmaceutical classification system [226]. Poor aqueous solubility has been shown to cause poor drug absorption and oral bioavailability [227] as well as causing the formulation of volume-limited dosage forms, such as ocular, nasal, intramuscular and subcutaneous delivery, to be challenging due to the limited quantity of drug that can be delivered. For these reasons, developing new technologies and approaches to enhance drug solubility has become a major research drive in the field of drug discovery and development. Over the past two decades many techniques and strategies have been developed to increase the aqueous solubility of poorly soluble drugs. These include micronization and nanonization, formation of solid and particulate dispersions, amorphisation, salt formation, surfactant micellization and polymeric and cyclodextrin complexations [228]–[232]. However, these techniques do not always produce satisfactory results and a combination of multiple techniques is often employed to enhance the solubility to required levels [233]. As such, the cost and complexity required for screening and manufacture of these formulations can become untenable. Therefore, the development of innovative approaches to enhance drug solubility is still a priority research goal as new, poorly water-soluble drugs are discovered and require formulation.

The naturally abundant protein albumin, found in blood plasma, has long been known to exhibit solubility enhancing properties and has been used as a non-toxic, biodegradable and highly stable excipient in numerous pharmaceutical applications [234]–[236]. Albumin has the ability to form reversible binding complexes with ligands, allowing the bound molecule to exist in aqueous systems in higher concentrations than in its unbound state. Albumin contains two positively charged primary binding sites and several secondary binding sites that bind to ligands primarily by hydrophobic, Van der Waals and hydrogen bonding interactions [237], [238]. Anionic and hydrophobic molecules, such as many poorly soluble drugs, show high affinity to albumin molecules and thus create binding complexes, resulting in solubility enhancement. Albumin also possesses many accessible free amino and carboxyl groups with the potential to form salt bridges with acidic or basic drugs, respectively [239]. Khoder *et al*. showed that bovine serum albumin (BSA) could be used as a solubility enhancer for the model drug indomethacin (IND) [240]. IND is a poorly water soluble, non-steroidal, anti-inflammatory drug that has been reported to bind to albumin with high affinity via the creation of salt bridges [241], [242]. Furthermore, it has been shown that using particle engineering techniques (freeze drying and spray drying) it was possible to create BSA:IND solid dispersions that provided significantly higher solubility enhancement, with an enhancement factor of up to 100,000 [240]. As such, it follows that CCP microparticles containing a BSA:IND mixture may follow this trend and also provide a very high level of solubility enhancement. To investigate this possibility, BSA:IND solid dispersions were created from an aqueous solution of the mixture, the solid particles were then reconstituted with dH_2O and analysed using UV-Vis spectroscopy to identify IND within the aqueous solution.

7.2 Preliminary Investigations

7.2.1 High Concentration Protein Injectables

For this preliminary work, benzyl benzoate (BB) and isopropyl myristate (IPM) were used as non-aqueous suspension media. BB is a low viscosity, organic compound used as a topical medication and insect repellent and is approved for parenteral injection by the FDA [222], [243]. IPM is another non-toxic organic compound with lower viscosity than benzyl benzoate and is used in a variety of pharmaceutical products as a skin moisturiser to enhance drug penetration, the active ingredient in a treatment for headlice and as an ingredient for some mouthwash products [244]. However, IPM is not approved for parenteral injection by the FDA [245].

To prepare the suspensions, CCP microparticles were first prepared from lyophilised BSA using the vortex mixer method described in Chapter 2. BSA microparticle powder was then added to BB or IPM and shaken to suspend the particles. Samples were then taken and observed using light microscopy. Initial observations showed large particle aggregates had formed within the isopropyl myristate (Fig. 7.1 Left) which could not be broken up using manual agitation or by vortex mixing. However, the application of sonication broke up the particle aggregates, producing a well dispersed suspension (Fig. 7.1 Right).

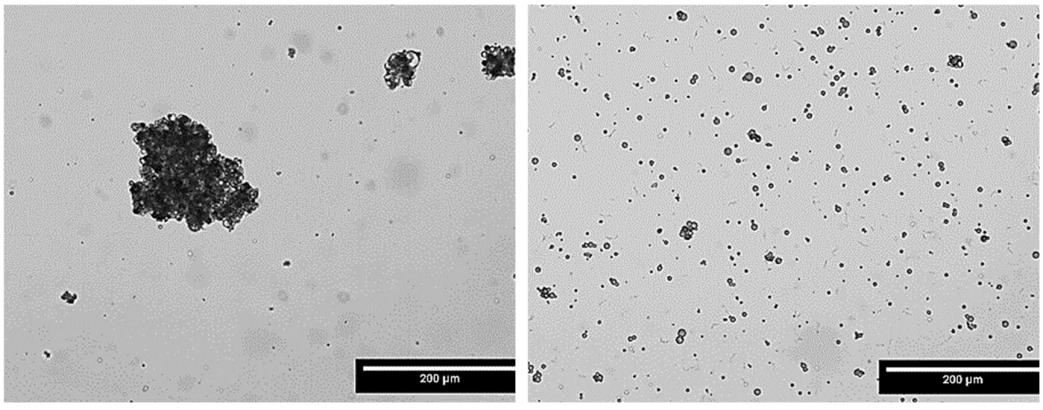

Fig 7.1: Light microscopy images of BSA microparticles prepared via CCP resuspended in isopropyl myristate. Left: Before sonication. Right: After sonication

Viscosity of Non-Aqueous Suspensions

CCP microparticles were added to both BB and IPM and sonicated to create particle suspensions at 200 mg/mL and 300 mg/mL. Fig 7.2 shows the viscosity measurements of these samples as a function of shear rate recorded using a rheometer, along with that of the two fluids containing no suspended material. These results show that the viscosity of the IPM suspensions remained below the 50 cP limit for subcutaneous injections at all concentrations measured, whereas the BB suspensions measured higher viscosity, going above the 50 cP limit at 300 mg/mL.

Viscosity measurements of aqueous BSA solution at varying concentration was not conducted in this small proof-of-concept study, however these measurements have been carried out multiple times and are readily available in literature. Fig 7.3 shows a plot of BSA solution viscosity as a factor of concentration overlaid onto the same plot for both BB and IPM suspensions (solution viscosity plot taken from Hong *et al*. [246]). This plot shows that BB and IPM based suspensions of BSA microparticles have higher viscosity than an equally concentrated aqueous solution at low concentration, however, above approximately 250 mg/mL the viscosity of aqueous solution increases exponentially, whereas suspension viscosity of both BB and IPM suspensions continues to increase linearly within the concentration range tested, resulting in a vastly lower viscosities at 300 mg/mL for the suspension-based formulations.

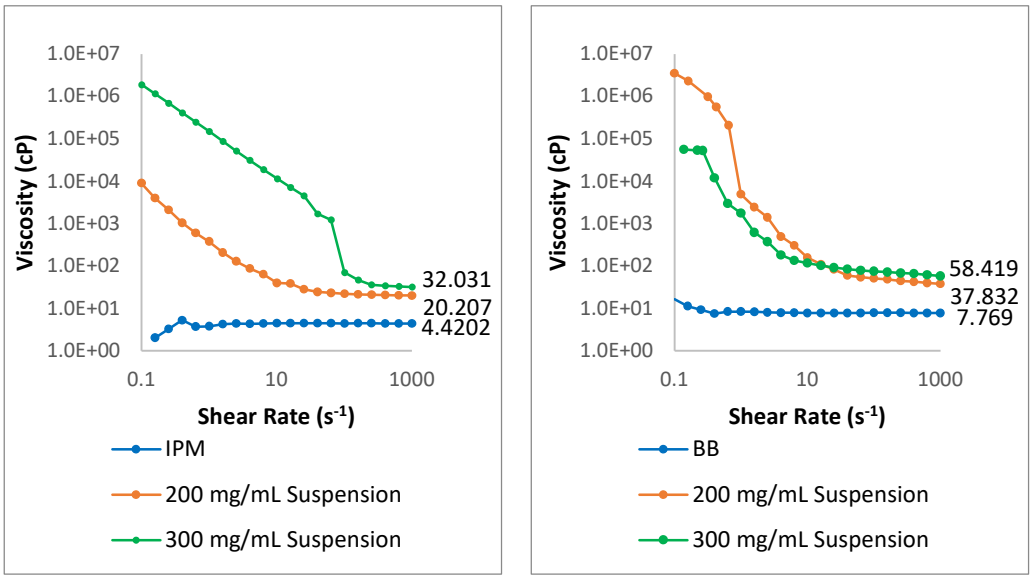

Fig 7.2: Viscosity measurements with increasing shear rate as measured using an Anton Paar Rheometer. (Left): IPM measurements at 0 mg/mL, 200 mg/mL and 300 mg/mL. (Right) BB measurements at 0 mg/mL, 200 mg/mL and 300 mg/mL.

These results show a great potential for the use of CCP microparticles in non-aqueous subcutaneous injections. Preparation of the suspensions, whilst more complex than the production of an aqueous solution, was simple and rapid with no requirement to micronize the powder with milling technologies. After a brief application of sonication, a homogenous suspension was formed of spherical microparticles, similar to the particles obtained by suspension of spray-dried particles. However, the CCP technique produced particles with a higher degree of sphericity than spray-drying which may act to reduce the viscosity and injectability of the suspension. It has been demonstrated that the spherical particles obtained from spray-drying show both a reduced viscosity and reduced tendency to block needles than their lyophilised and milled counterparts, allowing for higher concentration formulations [247]. As CCP microparticles show an even greater sphericity (and size uniformity if prepared via a continuous fluidic system) than spray-dried particles, it follows that they may allow for higher concentration suspensions for administration.

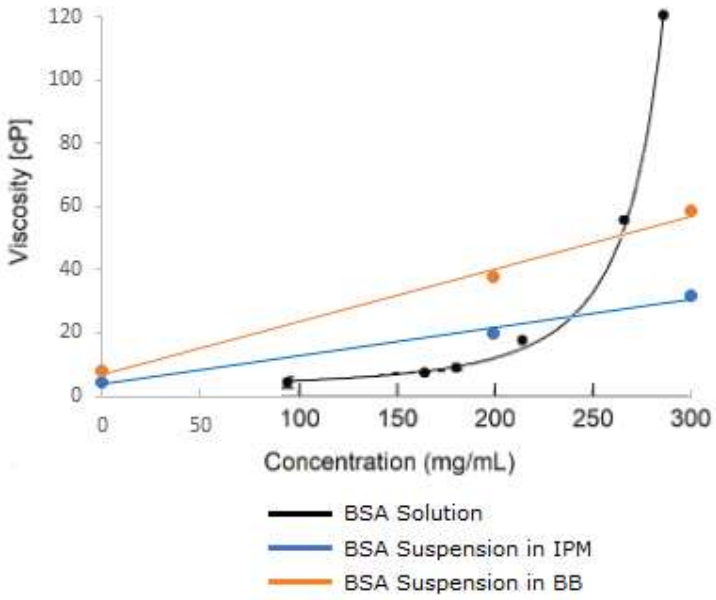

Fig. 7.3: Plot of viscosity of BSA suspensions as a function of concentration superimposed over a plot of aqueous solution viscosity. BSA solution plot adapted from Hong *et al.* [246].

Whilst a great deal more work is required before this technology could become mainstream, the promise of highly concentrated and low viscosity protein suspensions makes this an exciting proposal for future study. To take this work forward there are many further studies that could be carried out. An investigation into the use of different solvents and solvent mixtures, as well as the inclusion of excipients to aid stability or lower viscosity, would help to find the optimal viscosity profile whilst satisfying regulatory guidance. Marschall *et al.* authored an extensive review article on this subject detailing many solvents that have been used for this purpose and discussing the requirements of the suspension vehicle [222].

Further studies into the viscosity of protein powder suspensions would need to be conducted, including measurements of both higher and lower concentration suspensions to gain a greater insight into their properties for short-listing or modelling. The shear rate inside a 27-gauge needle can reach values greater than 200,000 s^{-1}, far greater than the shear rate reached above or with most

conventional viscometers or rheometers [248]. However, specialist viscometers utilising microfluidic channels and arrays of pressure sensors are now available which can measure viscosity at much greater shear rate, such as those found in a needle during injection. Since both solvents selected in this small study displayed shear thinning behaviour, measurement of viscosity at higher shear rate could show further viscosity reduction, allowing for higher concentrations whilst remaining within regulatory guidelines.

It would also be important to study the properties and stability of the suspension and particles within. Developing a suspension which remains stable over the longer term can be challenging with the two phases being prone to instability, resulting in a change to particle size [249]. Such changes to particle size are usually increases, as particles aggregate, which can cause regulatory issues, or even needle blockages [222], [250]. Few studies have investigated the physical stability of non-aqueous protein powder suspensions. Miller *et al.* reported that a suspension of milled lysozyme which was stored at room temperature showed no evidence of change in particle size after 2 months and that the sample was visually resuspendable after 1 year [212]. Furthermore, Yordanova reported on suspensions of milled decapeptide in various non-aqueous vehicles which were stored at an elevated temperature [251]. It was demonstrated that after 1 year of storage the suspensions were still injectable through needles used for veterinary administration.

A thorough analysis of protein stability would also be required. In general proteins show good stability in solid form, as discussed in Chapter 4 of this thesis, and so the main driver of any instability would be from the suspension vehicle [252]. When studying fluids for use as the suspension vehicle it will be important to assess its effects on protein stability. The vehicle must not interact with the protein, or any excipients found within the suspension, in a way to cause structural degradation or reduced activity. These interactions could be caused by the chemical composition of the suspension vehicle itself, such as the poly-unsaturated fatty acids found in

many plant oils, or by impurities such as water or oxygen which will interact with proteins causing degradation [222].

7.2.2 Co-Formulation and Solubility Enhancement

BSA as a Solution Enhancer

For this initial work, IND was used as a model poorly soluble drug with a reported water solubility of 0.937 mg/L at 25°C. IND is a non-steroidal anti-inflammatory drug used for symptomatic relief from arthritis and is classified as a Class II drug, meaning it is poorly soluble and highly permeable [253]. Furthermore, IND binds with high affinity to albumin due to the formation of salt bridges with the albumin amino groups [30], [31].

As per the method by Khoder *et al.*, two IND samples were prepared at 1.2 mg/mL in 10 mL hydro-alcoholic solution (19:1 water:ethanol) and shaken for 24 hours [240]. One sample also contained BSA at 10 mg/mL whilst the other sample did not. Figure 7.4 shows the resultant dispersions, it is clear to see that the left-hand sample (containing BSA) resulted in a clear solution, whereas the right-hand sample (containing no BSA) resulted in an opaque, milky suspension. This implies that, in this instance, the BSA acted as a dissolution enhancer with an enhancement factor of over 1000, allowing the indomethacin to fully dissolve in the hydro-alcoholic mixture.

Sample Preparation

To prepare BSA:IND CCP microparticles, the BSA:IND solution prepared above was used as the aqueous phase and added to a pentanol reservoir before being vortex mixed to produce microparticles. The negative control sample was a BSA CCP particles produced using BSA dissolved in the same hydro-alcoholic solution as the aqueous phase without the addition of IND. The positive control was the BSA:IND solution used to prepare the BSA:IND microparticles. All samples and controls were prepared in triplicate. It was hypothesised that IND molecules would become entrapped within the aqueous droplets and thus become entrained within the

particles as they formed. After being left to dry, samples were redissolved in the hydro-alcoholic solution to 10 mg/mL and analysed using UV-Vis spectroscopy. If IND molecules had become entrained within the BSA microparticles then they would also be present within the redissolved solution and thus be measurable by UV-Vis spectroscopy.

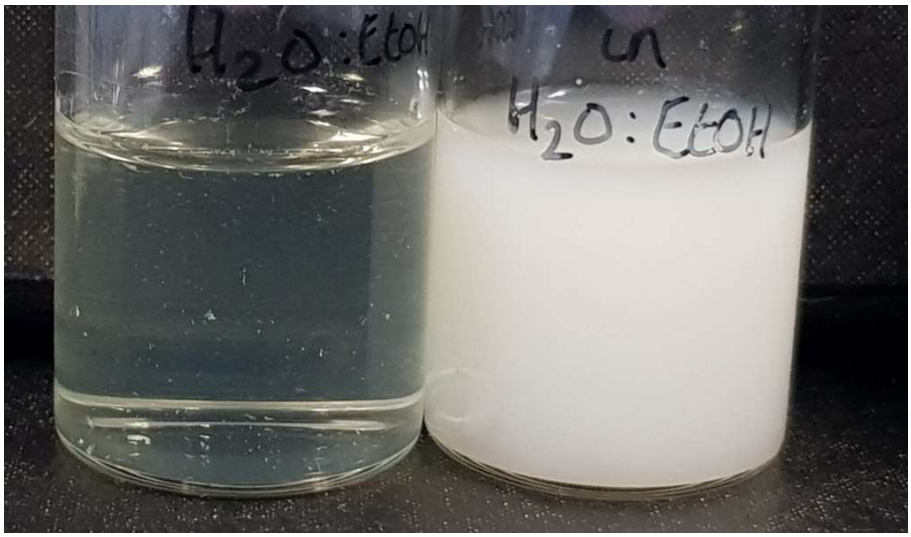

Fig 7.4: IND solutions at 1.2 mg/mL in 10 mL hydro-alcoholic solution (19:1 water:ethanol). Left vial solution also contains lyophilised BSA at 10 mg/mL. Right vial contains no BSA.

Figure 7.5 shows the averaged results of the UV-Vis analysis with the y-axis (absorbance) normalised. This figure shows that all samples produced a peak at approximately 280 nm which corresponds to the BSA molecules in solution. It can be noted that the BSA:IND solution produced a peak closer to 270 nm but this may be attributed to peak shift due to the raw measurements being outside of the linear Beer-Lambert range. It can also be clearly seen that both the BSA:IND solution and the BSA:IND microparticles produced a secondary peak at 320 nm which corresponds to the spectral fingerprint of IND. This result implies that IND was present within the reconstituted BSA:IND microparticle sample.

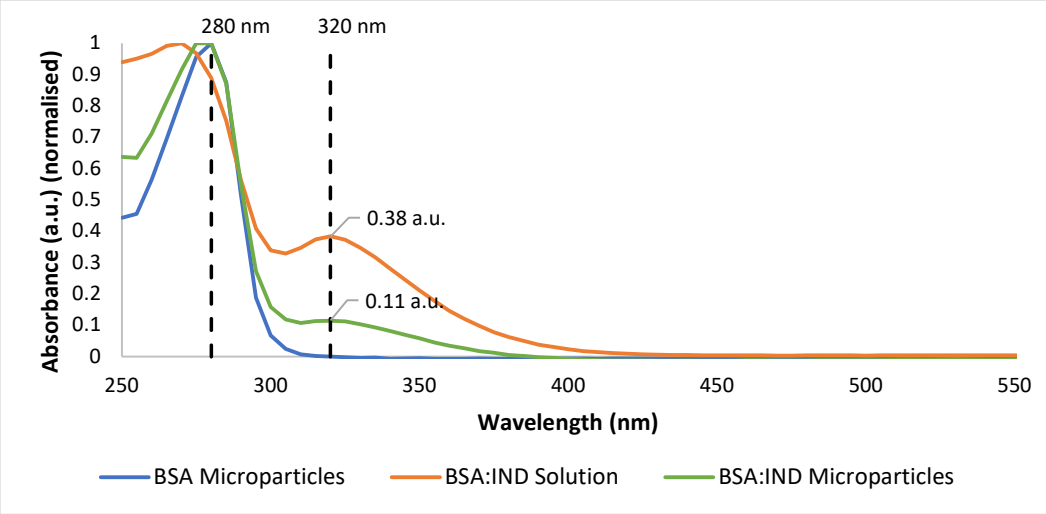

Fig 7.5: UV-Vis spectra of rehydrated BSA formulations. (Blue) Microparticle formulation prepared without IND. (Orange) BSA:IND solution. (Green) Microparticle formulation prepared from IND-doped aqueous phase.

As described above, these data show the potential for CCP microparticles to be used as a scaffold or delivery vehicle for poorly soluble drug products. Whilst this analysis is not a fully quantitative result, the normalisation along the y-axis allows for scrutiny of the ratio between BSA and IND. As the BSA:IND microparticles were formed from the initial BSA:IND solution, it was expected that the BSA to IND ratio would remain constant regardless of the absolute concentration, assuming there were no losses of BSA or IND. However, the results do not show this, indicating that the IND content of the microparticle formulation was reduced by a factor of approximately 3 when compared to the original BSA:IND solution, giving an encapsulation efficiency of approximately 33%. The remainder of the IND is likely to have remained in the drying reservoir having not become entrained in the microparticle formation. It should also be noted that this analysis does not confirm that the IND found within the reconstituted microparticle sample was entrained within the BSA microparticles. It is possible that the IND remained as a separate entity within the dry powder formulation or present within the residual pentanol that was evaporated off in the final drying step. However, it is unlikely that

approximately 33% of the total IND content would have been found within the small volume of residual pentanol.

To continue this study there are several avenues of research that could be explored. Firstly, the stated aim of investigating the ability of CCP BSA microparticles to increase the solubility enhancing effect of BSA could be further investigated. This could be accomplished by preparing bulk quantities of BSA:IND microparticles and preparing a high concentration solution from the microparticles. This may prove difficult to achieve due to the solubility limit of BSA so preparing a stock solution with a higher ratio of IND to BSA may be required, as per Khoder *et al.* [240]. Analysis and quantification of the IND concentration may be achievable using UV-Vis spectroscopy, as demonstrated above, but more accurate measurements may be made using technologies such as HPLC.

It may also be interesting to investigate the "missing" IND. The UV-Vis analysis discussed above implied that only about 33% of the initial IND content was present in the reconstituted microparticle solution. It seems apparent that the remainder of the IND would remain in the pentanol reservoir and removed from the sample with the supernatant. To assess this, further IND quantification should be conducted on the supernatant using UV-Vis spectroscopy or HPLC as discussed earlier.

An investigation into the physical location of the IND molecules when the sample is in the dry powder state would help to understand the processes involved in the formation of such particles. The hypothesis for this study was that the IND molecules would be entrained within the CCP particles, however, this is not clear from the results gathered so far. To investigate this, dry microparticle samples could be analysed using microscope-spectroscopic techniques to analyse the chemical composition of single microparticles. As many of these techniques, such as Energy Dispersive X-Ray (EDX) spectroscopy or Secondary Ion Mass Spectrometry (SIMS), are surface techniques only individual microparticles may require sectioning or crushing prior to analyse to increase the surface area of the sample.

7.3 Final Conclusions

The stated aims of this thesis were to further explore CCP technology with a view towards industrial applicability as an alternative protein dehydration technique. Indeed, during the completion of these studies a US-based company, Lindy Biosciences (Durham, North Carolina), launched Microglassification™ as a "process that gently removes a majority of the water from solutions of proteins, or other biologics, resulting in solid, spherical, amorphous microbeads" [254]. Lindy Biosciences markets the technology as a process which produces "spherical, dense, stable particles of a therapeutic protein" [255] which are ideal for "long-term storage, or for non-standard formulations such as suspension formulations (for high-concentration delivery of antibodies), encapsulation (for sustained/controlled release), or dry powder pulmonary delivery" [255]. The fact that this technology is already being used in industry, for the same uses as explored within this thesis, supports the industrial applicability of the technology, to which the studies found herein add further weight.

In Chapter 3 the underlying physical mechanism of the technique was explored using a dual-micropipette system capable of generating individual aqueous protein droplets within a solvent reservoir and observing the droplet dissolution and eventual solidification into a microparticle. Using this technique, it was demonstrated that the BSA concentration within the droplet could be determined at a specific point in the dehydration process when the RI of the two mediums matched, turning the droplet briefly invisible. This phenomenon occurred due to the variation of the RI in a liquid as the concentration of the solute changes. With the assumption that losses of BSA to pentanol reservoir were negligible, it is then possible to calculate the concentration of the droplet and particle at any time point in the experiment. Under the further assumption that the trigger for precipitation of the protein molecules into a solid particle is driven by the concentration within the aqueous droplet, it should then be possible to model the size of the dehydrated

particle and the time for the CCP process to complete as functions of the initial droplet size and concentration.

Batch production of CCP microparticles prepared from BSA was then explored using a small-scale vortex mixer technique carried out inside a 1.5 mL centrifuge tube. This technique generated polydisperse distributions of spherical microparticles which were characterised and compared with a lyophilised BSA formulation using spectroscopic methods and SEM imaging. Using this technique, it was demonstrated that it was possible to control the average particle size through manipulation of the concentration of the aqueous BSA solution. Through consideration of the CCP process it can be surmised that an increase in the concentration of the BSA solution causes an increase in the concentration of the aqueous droplets, resulting in more BSA molecules per droplet, and therefore larger particles. However, the SEM results also showed that with increasing particle size came increasing particle size dispersity. Furthermore, larger CCP microparticles (above approximately 50 μm diameter) showed increasing tendency to become damaged, resulting in pinhole pores in the surface of the particles or even for the particle to split open revealing a hollow core, to which the surface pores provided a channel. Further analysis of this observation is still required but it is possible that the hollow core was filled with liquid BSA solution which expanded and burst free from the particles when placed under vacuum.

CCP particles were next rehydrated and analysed spectroscopically along with rehydrated lyophilised BSA samples and native BSA samples. Fluorescence spectroscopy was employed to compare the tertiary structure of rehydrated CCP particle against the two control samples and it was demonstrated that the process of CCP dehydration and subsequent rehydration had no impact on BSA tertiary structure. Next DLS was employed to assess aggregation levels within the three BSA solutions. Results from the DLS analysis showed that the CCP process and rehydration did not affect the amount of aggregated protein forms within the

solution. Taken together, these results show that dehydration via CCP and subsequent rehydration does not induce any non-reversible changes in the protein structure or degree of aggregation.

The final study in Chapter 3 investigated the scale up of the technology using two mid-scale laboratory techniques designed to imitate large-scale industrial processes. The 1 mL solvent reservoir held with a 1.5 mL centrifuge tube was replaced with a 100 mL solvent reservoir within a 250 mL beaker to imitate an industrial scale vat. Mixing was provided using either an overhead stirrer or overhead homogeniser to imitate two current mixing techniques widely used in industry. Through SEM observation of the resultant solid material, it was shown that both of these techniques generated solid particle distributions similar to those observed using the smaller scale technique. However, differences were observed with the samples produced with the overhead stirrer also including large, non-spherical particles and the homogenised samples producing much smaller particle distributions with the majority of particles measuring less than 5 μm. Spectroscopic analysis of the rehydrated microparticle formulations showed results similar to those obtained from the scall-scale technique, indicating that the two larger-scale methods did not induce structural degradation or aggregation in the samples.

Results from Chapter 3 demonstrate that CCP does have the potential to act as an alternative industrial technique to lyophilisation for the preparation of dehydrated, solid protein formulations. However, there are still further questions to be answered before the technology could be accepted. As described earlier, the hollow core observed in some larger particles must be characterised, if the hollow core contains liquid protein solution, then this could have long-term storage implications if the protein in the centre is not in a solid form. Furthermore, the residual solvent within the protein microparticles must be quantified in order to be conform with regulatory procedures.

In chapter 4, the long-term stability of CCP microparticles was investigated. Whereas the previous chapter demonstrated the potential of CCP technology to be used as an industrial alternative to lyophilisation for the production of dehydrated protein formulations, it did not account for the long-term stability of the product. As the primary use of protein lyophilisation is to increase storage stability, it is important to assess this characteristic in any new technology. In this study, BSA and HSA formulations prepared from native BSA and HSA, as well two proprietary HSA formulation provided by Albumedix Ltd. Control samples were also prepared directly from lyophilised BSA and HSA powder.

Samples were dehydrated using CCP and stored at either 5°C, 25°C or 40°C for up to one year. At defined time points, samples were removed from storage, rehydrated and analysed to assess changes to protein structure and aggregation. Fluorescence spectroscopy results did not show any disruption to protein structure across all protein formulations and temperatures throughout the lifetime of the study. However, analysis of protein aggregation did show that CCP formulations experienced smaller increases to the aggregation index than the lyophilised samples, indicating that the CCP samples were generating less non-soluble aggregates during storage than their lyophilised counterparts. However aggregate analysis via HPLC-SEC showed that the CCP samples experienced greater aggregation than the lyophilised samples, with larger decreases to the relative abundance of monomer forms and increases to dimer and trimer forms. The HPLC-SEC results also showed that increases in larger aggregated forms were minimal. Taken together these results indicate that protein structure remained largely unaffected by storage, even at elevated temperatures. However, increased levels of aggregation were observed across all protein formulations at all temperatures with the lyophilised samples showing large increases in the A.I. measurements and the CCP samples showing large increases in the HPLC-SEC data. These two results imply that the lyophilised samples experienced increases primarily in larger, non-

soluble aggregates whereas the CCP samples primarily experienced increase in smaller, soluble aggregates.

Further work in this area includes the repetition of this study with alternate proteins. If it was demonstrated that the CCP process can successfully dehydrate multiple proteins with long-term stability on par with lyophilised formulations it would help to elevate the profile of the technology for industrial use. A repeat of this study could also include further analytical techniques, such as X-ray crystallography or circular dichroism, to study structural changes with greater resolution. The inclusion of a biological activity assay would also confirm whether dehydrated CCP particles retain acceptable levels of activity after long term storage.

Chapter 5 of this thesis focused on the production of CCP microparticles using continuous flow systems. Continuous flow systems are generally considered an improvement over batch production systems, providing advantages in product quality and safety, as well as economic benefits. Furthermore, the production of microparticles via continuous, fluidic systems has long been known to provide the capability for highly uniform, size tuneable particle distributions. If these size control properties were to be demonstrated using CCP technology, it would open the door towards numerous alternate uses within the field of biopharmaceuticals.

Three continuous flow techniques were trialled, with the T-reactor method demonstrating the generation of size tuneable aqueous droplets, controlled via manipulation of the flow rates of the two fluids. However, when these droplets were introduced into a stirred reservoir to allow dehydration to take place and subsequently measured, the average particle size did not follow the droplet size, resulting in similarly sized particles regardless of the droplet size. Consideration of the process lead to the conclusion that the stirring of the reservoir was producing a homogenisation effect on the aqueous droplets, leading to the similarly sized particles observed. To remove the stirring from the solvent reservoir, an alternative reservoir configuration was designed. Instead of suspending the aqueous droplets

within a stirred vessel, the droplets were allowed to fall through a long column of solvent, precipitating out into particles before reaching the bottom of the reservoir. Using this technique, a highly monodisperse distribution of particles was prepared with particle size significantly larger than seen using the stirred reservoir. However, further experimentation is required to confirm if this reservoir design allows for the production of size tuneable protein microparticles.

Whilst this study demonstrated a continuous flow system for the production of size-tuneable aqueous droplets, the dehydration process was still completed as a batch driven process and so work could be undertaken to design a continuous dehydration process. Initial thoughts on this include a reservoir built into a channel through which the drying solvent flows and exits to pass through a filtration system, catching the dehydrated protein particles to be dried and collected.

Chapter 6 is the final research chapter of this thesis and describes two screening studies carried out to assess the applicability of the CCP technology to a wider selection of materials. First a range of solvents were selected and used as the drying solvent for the CCP process. Solvents were selected based upon their water absorption with pentanol and decanol as baseline solvents. Solvents selected for the study were: 2-methyl-1-propanol, pentanol, benzyl alcohol, methyl acetate, heptanol, 4-methyl-2-pentanol, octanol, decanol, ethyl acetate, and 2-ethyl-1-hexanol. This selection provided 8 alcohols and 2 esters with water absorption values clustered around those of pentanol and decanol. The small-scale vortex mixer method was used to run the screening study with the 1 mL pentanol reservoir replaced with 1 mL of the solvent to be screened. However, as each solvent had a different water absorption, it followed that the volume of aqueous BSA solution added to the reservoir should be varied for each solvent. To decide the volume of aqueous phase to add to each solvent, the maximum theoretical volume of water that could be dissolved in 1 mL of the solvent was calculated from the water absorption value. This was rounded down to the nearest 5 µL and used as the initial

volume of BSA solution to add to the 1 mL reservoir. After the first screening running using the initial volume of aqueous phase, the second screening run was completed with the volume of aqueous phase reduced by 25%. A third screening run was also completed with the volume of aqueous reduced by a further 25%. This process was designed to ensure that the drying solvent was not being overloaded with aqueous phase and stopping the reservoir from acting as an infinite well.

The results of this study demonstrated that nearly every solvent tested had the capacity to act as a drying solvent and produce some form of solid formulation. SEM analysis showed that the 6 of the 10 solvents tested produced spherical microparticle distributions similar in appearance to those seen throughout this thesis. 2-methyl-1-propanol, pentanol, heptanol, 4-methyl-2-pantanol, octanol and decanol all produced all produced microparticle distributions with similar mean particle diameter. Spherical microparticle were also found in the ethyl acetate and 2-ethyl-1-hexanol samples but only a small number of particles were found, potentially due to the very low volume of aqueous phase added to these solvents. The methyl acetate samples did solidify, but not into microparticles. Instead, these samples solidified into large flakes of material, not dissimilar in size and appearance to the crystals found in lyophilised BSA powder. Furthermore, the solidification of aqueous protein began almost immediately, with white flakes forming even before the mixture had been vortex mixed. This behaviour requires further study but potentially shows that aqueous proteins could be solidified simply by being dropped into methyl acetate. The benzyl alcohol samples were the only samples that did not produce discrete masses of material, instead forming a residue pock marked by particles and is likely explained by the chemistry of benzyl alcohol which results in a chemical with a relatively high water solubility and a relatively low water absorption.

Selected solid formulations were later rehydrated and analysed spectroscopically to assess protein structure. Fluorescence spectroscopy and FT-IR spectroscopy were

employed to assess protein tertiary structure and secondary structure. Lyophilised powder formulations and purposefully denatured solutions were also measured as control samples. Analysis showed that none of the samples showed any significant deviation from the lyophilised control samples.

The second screening test aimed to investigate the dehydration of multiple proteins to assess CCP for use with proteins other than albumins. Six proteins were selected representing a variety of different molecular sizes and biological functions. The proteins selected for this study were: human serum albumin, lysozyme, catalase, horseradish peroxide, glucose oxidase and insulin. Human serum albumin, lysozyme and insulin were prepared in dH_2O (insulin adjusted to pH 2) whilst catalase, horseradish peroxidase and glucose oxidase were prepared in PBS solution. Four solvents were also selected for use, chosen from the results of the first screening study. 2-methyl-1-propanol, pentanol, methyl acetate and 4-methyl-2-pentanol were selected as drying solvents. As with the previous study, the CCP vortex mixer method was used to create microparticles from all combinations of protein and solvent and any resultant solid material was imaged via SEM. SEM imaging showed that all proteins prepared in dH_2O produced samples containing the smooth, spherical microparticles seen previously (unless methyl acetate was used as the drying solvent). However, the proteins prepared in PBS produced samples containing crystalline structures, likely due to the salts found in PBS which would precipitate into salt crystals as the water dissolved into the drying solvent. As with the methyl acetate results above, this is an interesting result requiring further study. As with the previous solvent screening study, particle size was measured and proteins were rehydrated and analysed. These analyses showed that all proteins produced microparticles of similar size and that spectroscopic analysis showed that none of the samples showed any significant deviation from the lyophilised control samples.

The formation of salt crystals within a CCP sample indicates that the salts within the aqueous phase solidified along with the proteins. Further study into the effect this has on the proteins could yield interesting results and new avenues of research. Furthermore, this raises the question as to whether materials can be dehydrated using CCP, investigation into the dehydration of other biologics such as mAbs, nucleic acids or even entire cells could open up many new uses for this technology.

Bibliography

[1] C. Tanford and J. Reynolds, *Nature's Robots - A History of Proteins*. Oxfoed University Press, 2001.

[2] D. E. Koshland and F. Haurowitz, "Conformation of proteins in interfaces," *Encyclopedia Britannica*, 2020. https://www.britannica.com/science/protein/Conformation-of-proteins-in-interfaces#ref593795 (accessed Nov. 03, 2021).

[3] J. B. Sumner, "The Isolation and Crystallization of the Enzyme Urease," *Journal of Biological Chemistry*, vol. 69, no. 2, pp. 435–441, 1926, doi: 10.1016/s0021-9258(18)84560-4.

[4] W. P. Blackstock and M. P. Weir, "Proteomics: Quantitative and physical mapping of cellular proteins," *Trends in Biotechnology*, vol. 17, no. 3. pp. 121–127, 1999. doi: 10.1016/S0167-7799(98)01245-1.

[5] N. L. Anderson and N. G. Anderson, "Proteome and proteomics: New technologies, new concepts, and new words," *Electrophoresis*, vol. 19, no. 11, pp. 1853–1861, 1998, doi: 10.1002/ELPS.1150191103.

[6] U. Angkawinitwong, G. Sharma, P. T. Khaw, S. Brocchini, and G. R. Williams, "Protein therapeutics in the solid state," *Ther Deliv*, vol. 6, no. 1, pp. 59–82, 2015, [Online]. Available: http://discovery.ucl.ac.uk/1460690/1/Khaw_AAM_1460690.pdf

[7] P. J. Carter, "Introduction to current and future protein therapeutics: A protein engineering perspective," *Experimental Cell Research*. 2011. doi: 10.1016/j.yexcr.2011.02.013.

[8] M. P. Ratnaparkhi, S. P. Chaudhari, and V. A. Pandya, "Peptides and Proteins in Pharmaceuticals," *Int J Curr Pharm Res*, vol. 3, no. 2, 2011.

[9] H. A. D. Lagassé *et al.*, "Recent advances in (therapeutic protein) drug development," *F1000Res*, vol. 6, 2017, doi: 10.12688/f1000research.9970.1.

[10] J. F. Carpenter, M. J. Pikal, B. S. Chang, and T. W. Randolph, "Rational Design of Stable Lyophilized Protein Formulations: Some Practical Advice," *Pharm. Res.*, vol. 14. pp. 969–976, 1997. doi: 10.1023/A:1012180707283.

[11] H. M. L. Larsen, H. Trnka, and H. Grohganz, "Formation of mannitol hemihydrate in freeze-dried protein formulations - A design of experiment approach," *Int J Pharm*, vol. 460, no. 1–2, pp. 45–52, 2014, doi: 10.1016/j.ijpharm.2013.11.009.

[12] S. D. Allison, T. W. Randolph, M. C. Manning, K. Middleton, A. Davis, and J. F. Carpenter, "Effects of drying methods and additives on structure and function of actin: Mechanisms of dehydration-induced damage and its inhibition," *Arch Biochem Biophys*, vol. 358, no. 1, pp. 171–181, 1998, doi: 10.1006/abbi.1998.0832.

[13] Aniket, D. A. Gaul, D. L. Rickard, and D. Needham, "MicroglassificationTM: A novel technique for protein dehydration," *J Pharm Sci*, vol. 103, pp. 810–820, 2014, doi: 10.1002/jps.23847.

[14] T. M. Squires and S. R. Quake, “Microfluidics: Fluid physics at the nanoliter scale,” *Rev Mod Phys*, 2005, doi: 10.1103/RevModPhys.77.977.

[15] Y. Song, J. Hormes, and C. S. S. R. Kumar, “Microfluidic synthesis of nanomaterials,” *Small*. 2008. doi: 10.1002/smll.200701029.

[16] A. Jahn, W. N. Vreeland, D. L. Devoe, L. E. Locascio, and M. Gaitan, “Microfluidic directed formation of liposomes of controlled size,” *Langmuir*, 2007, doi: 10.1021/la070051a.

[17] S. Sugiura *et al.*, “Novel method for obtaining homogeneous giant vesicles from a monodisperse water-in-oil emulsion prepared with a microfluidic device,” *Langmuir*, 2008, doi: 10.1021/la703509r.

[18] H. C. Shum, D. Lee, I. Yoon, T. Kodger, and D. A. Weitz, “Double emulsion templated monodisperse phospholipid vesicles,” *Langmuir*, 2008, doi: 10.1021/la801833a.

[19] S. Ota, S. Yoshizawa, and S. Takeuchi, “Microfluidic formation of monodisperse, cell-sized, and unilamellar vesicles,” *Angewandte Chemie - International Edition*, 2009, doi: 10.1002/anie.200902182.

[20] P. C. Hu, S. Li, and N. Malmstadt, “Microfluidic fabrication of asymmetric giant lipid vesicles,” *ACS Appl Mater Interfaces*, 2011, doi: 10.1021/am101191d.

[21] S. Sugaya, M. Yamada, A. Hori, and M. Seki, “Microfluidic production of single micrometer-sized hydrogel beads utilizing droplet dissolution in a polar solvent,” *Biomicrofluidics*, vol. 7, no. 5, 2013, doi: 10.1063/1.4826936.

[22] S. Chen *et al.*, “Preparation of Coenzyme Q10 nanostructured lipid carriers for epidermal targeting with high-pressure microfluidics technique,” *Drug Dev Ind Pharm*, 2013, doi: 10.3109/03639045.2011.650648.

[23] C. X. Zhao, “Multiphase flow microfluidics for the production of single or multiple emulsions for drug delivery,” *Advanced Drug Delivery Reviews*. 2013. doi: 10.1016/j.addr.2013.05.009.

[24] K. Takahashi, S. Sugaya, M. Yamada, and M. Seki, “Production of non-spherical protein microparticles by controlling droplet dissolution in microfluidic devices,” *18th International Conference on Miniaturized Systems for Chemistry and Life Sciences, MicroTAS 2014*, pp. 73–75, 2014.

[25] M. Yamada, K. Takahashi, A. Hori, S. Sugaya, and M. Seki, “Morphology control of protein microparticles produced using microfluidic droplets in a non-equilibrium state,” *2015 International Symposium on Micro-NanoMechatronics and Human Science, MHS 2015*, pp. 1–4, 2016, doi: 10.1109/MHS.2015.7438252.

[26] M. B. Mbanjwa, H. Chen, and K. Land, “Microfluidic Preparation of Biocatalytic Protein Microspheres Utilising On-Chip Cross-Linking Method,” in *17th International Conference on Miniaturized Systems for Chemistry and Life Sciences*, 2013, no. 27–31, pp. 1248–1250.

[27] M. B. Mbanjwa *et al.*, “Production of self-immobilised enzyme microspheres using microfluidics,” *Process Biochemistry*, 2018, doi: 10.1016/j.procbio.2018.03.002.

[28] S. J. Shire, Z. Shahrokh, and J. Liu, “Challenges in the development of high protein concentration formulations,” *J Pharm Sci*, vol. 93, no. 6, pp. 1390–1402, Jun. 2004, doi: 10.1002/JPS.20079.

[29] M. Bowen, N. Armstrong, and Y. F. Maa, “Investigating high-concentration monoclonal antibody powder suspension in nonaqueous suspension vehicles for subcutaneous injection,” *J Pharm Sci*, vol. 101, no. 12, pp. 4433–4443, 2012, doi: 10.1002/jps.23324.

[30] D. Foulder, *Practical Biology A (Salters-Nuffield)*. London, England: Hodder Education, 2020.

[31] G. Walsh, *Proteins: Biochemistry and Biotechnology*, 2nd ed. Hoboken, New Jersey: John Wiley & Sons Inc., 2015. doi: 10.1002/9781119117599.

[32] Y. Zhang, “What’s biggest and what’s smallest?,” *Science 2.0*, 2010. https://www.science20.com/princerain/blog/whats_biggest_and_whats_smallest (accessed Nov. 02, 2021).

[33] K. Steward, “Essential Amino Acids: Chart, Abbreviations and Structure,” *Technology Networks Applied Sciences*, 2022. Accessed: Feb. 06, 2022. [Online]. Available: https://www.technologynetworks.com/applied-sciences/articles/essential-amino-acids-chart-abbreviations-and-structure-324357

[34] “Protein Structure: Primary, Secondary.” https://www.ono-7.top/ProductDetail.aspx?iid=53511327&pr=28.88 (accessed Feb. 06, 2022).

[35] F. Cramer, “Biochemical correctness: Emil Fischer’s lock and key hypothesis, a hundred years after - an essay,” *Pharm Acta Helv*, vol. 69, pp. 193–203, 1995.

[36] D. E. Koshland, “The Key–Lock Theory and the Induced Fit Theory,” *Angewandte Chemie International Edition in English*, vol. 33, no. 23–24, pp. 2375–2378, Jan. 1995, doi: 10.1002/ANIE.199423751/FORMAT/PDF.

[37] P. Edman, “Method for Determination of the Amino Acid Sequence in Peptides,” *Acta Chem Scand*, vol. 4, pp. 283–293, 1950.

[38] “Home - Protein - NCBI.” https://www.ncbi.nlm.nih.gov/protein/ (accessed Nov. 13, 2021).

[39] M. Kulmanov, M. A. Khan, and R. Hoehndorf, “DeepGO: predicting protein functions from sequence and interactions using a deep ontology-aware classifier”, doi: 10.1093/bioinformatics/btx624.

[40] M. Kulmanov and R. Hoehndorf, “DeepGOPlus: improved protein function prediction from sequence”, doi: 10.1093/bioinformatics/btz595.

[41] Z. Lv, C. Ao, and Q. Zou, “Protein Function Prediction: From Traditional Classifier to Deep Learning,” *Proteomics*, vol. 19, no. 14, Jul. 2019, doi: 10.1002/PMIC.201900119/FORMAT/PDF.

[42] A. Sureyya Rifaioglu, T. Doğan, M. J. Martin, R. Cetin-Atalay, and V. Atalay, “Deepred: Automated protein Function prediction with Multi-task Feed-forward Deep Neural Networks”, doi: 10.1038/s41598-019-43708-3.

[43] W. Kabsch and C. Sander, “Dictionary of protein secondary structure: pattern recognition of hydrogen-bonded and geometrical features,” *Biopolymers*, vol. 22, no. 12, pp. 2577–2637, 1983, doi: 10.1002/BIP.360221211.

[44] W. G. Touw, J. Black, T. A. H. Te Beek, E. Krieger, R. P. Joosten, and G. Vriend, “A series of PDB-related databanks for everyday needs,” *Nucleic Acids Res*, vol. 43, 2015, doi: 10.1093/nar/gku1028.

[45] I. Moraes, G. Evans, J. Sanchez-Weatherby, S. Newstead, and P. D. S. Stewart, “Membrane protein structure determination — The next generation,” *Biochimica et Biophysica Acta (BBA) - Biomembranes*, vol. 1838, no. 1, pp. 78–87, Jan. 2014, doi: 10.1016/J.BBAMEM.2013.07.010.

[46] B. Zhang, J. Li, and Q. Lü, “Prediction of 8-state protein secondary structures by a novel deep learning architecture,” *BMC Bioinformatics*, vol. 19, no. 1, pp. 1–13, Aug. 2018, doi: 10.1186/S12859-018-2280-5/TABLES/13.

[47] S. R. Maddhuri Venkata Subramaniya, G. Terashi, and D. Kihara, “Protein secondary structure detection in intermediate-resolution cryo-EM maps using deep learning,” *Nature Methods 2019 16:9*, vol. 16, no. 9, pp. 911–917, Jul. 2019, doi: 10.1038/s41592-019-0500-1.

[48] Y. Guo, W. Li, B. Wang, H. Liu, and D. Zhou, “DeepACLSTM: Deep asymmetric convolutional long short-term memory neural models for protein secondary structure prediction,” *BMC Bioinformatics*, vol. 20, no. 1, pp. 1–12, Jun. 2019, doi: 10.1186/S12859-019-2940-0/FIGURES/6.

[49] Y. Wang, H. Mao, and Z. Yi, “Protein secondary structure prediction by using deep learning method,” *Knowl Based Syst*, vol. 118, pp. 115–123, Feb. 2017, doi: 10.1016/J.KNOSYS.2016.11.015.

[50] C. Fang, Y. Shang, and D. Xu, “MUFOLD-SS: New deep inception-inside-inception networks for protein secondary structure prediction,” *Proteins: Structure, Function, and Bioinformatics*, vol. 86, no. 5, pp. 592–598, May 2018, doi: 10.1002/PROT.25487.

[51] W. Wardah, M. G. M. Khan, A. Sharma, and M. A. Rashid, “Protein secondary structure prediction using neural networks and deep learning: A review,” *Comput Biol Chem*, vol. 81, pp. 1–8, Aug. 2019, doi: 10.1016/J.COMPBIOLCHEM.2019.107093.

[52] E. Callaway, “‘It will change everything’: DeepMind’s AI makes gigantic leap in solving protein structures,” *Nature*, vol. 588, no. 7837, pp. 203–204, Dec. 2020, doi: 10.1038/D41586-020-03348-4.

[53] S. Jones and J. M. Thornton, “Review Principles of protein-protein interactions,” vol. 93, pp. 13–20, 1996.

[54] E. M. Phizicky and S. Fields, “Protein-protein interactions: methods for detection and analysis,” *Microbiol Rev*, vol. 59, no. 1, pp. 94–123, Mar. 1995, doi: 10.1128/MR.59.1.94-123.1995/FORMAT/PDF.

[55] K. Fosgerau and T. Hoffmann, “Peptide therapeutics: Current status and future directions,” *Drug Discov Today*, vol. 20, no. 1, pp. 122–128, 2015, doi: 10.1016/j.drudis.2014.10.003.

[56] Z. Antosova, M. Mackova, V. Kral, and T. Macek, “Therapeutic application of peptides and proteins: parenteral forever?,” *Trends Biotechnol*, vol. 27, no. 11, pp. 628–635, Nov. 2009, doi: 10.1016/J.TIBTECH.2009.07.009.

[57] S. Singh *et al.*, “PEPstrMOD: structure prediction of peptides containing natural, non-natural and modified residues,” 2015, doi: 10.1186/s13062-015-0103-4.

[58] B. Leader, Q. J. Baca, and D. E. Golan, “Protein therapeutics: a summary and pharmacological classification,” *Nature Reviews Drug Discovery 2007 7:1*, vol. 7, no. 1, pp. 21–39, Jan. 2008, doi: 10.1038/nrd2399.

[59] J. T. Pinto *et al.*, “Progress in spray-drying of protein pharmaceuticals: Literature analysis of trends in formulation and process attributes,” *Drying Technology*, vol. 39, no. 11, pp. 1415–1446, 2021, doi: 10.1080/07373937.2021.1903032.

[60] V. Ragoonanan and A. Aksan, “Protein stabilization,” *Transfusion Medicine and Hemotherapy*, vol. 34, no. 4, pp. 246–252, 2007, doi: 10.1159/000104678.

[61] S. Jacob *et al.*, “Stability of Proteins in Aqueous Solution and Solid State,” *Indian J Pharm Sci*, pp. 154–163, 2006, [Online]. Available: www.ijpsonline.com

[62] M. C. Manning, D. K. Chou, B. M. Murphy, R. W. Payne, and D. S. Katayama, “Stability of protein pharmaceuticals: An update,” *Pharm Res*, vol. 27, no. 4, pp. 544–575, 2010, doi: 10.1007/s11095-009-0045-6.

[63] P. Stärtzel *et al.*, “Freeze Drying of l -Arginine/Sucrose-Based Protein Formulations, Part I: Influence of Formulation and Arginine Counter Ion on the Critical Formulation Temperature, Product Performance and Protein Stability,” *J Pharm Sci*, vol. 104, no. 7, pp. 2345–2358, Jul. 2015, doi: 10.1002/jps.24501.

[64] A. P. Golovanov, G. M. Hautbergue, S. A. Wilson, and L.-Y. Lian, “A simple method for improving protein solubility and long-term stability.,” *J Am Chem Soc*, vol. 126, no. 29, pp. 8933–9, 2004, doi: 10.1021/ja049297h.

[65] S. E. Bondos and A. Bicknell, “Detection and prevention of protein aggregation before, during, and after purification,” *Anal Biochem*, vol. 316, no. 2, pp. 223–231, 2003, doi: 10.1016/S0003-2697(03)00059-9.

[66] J. F. Carpenter, B. S. Chang, W. Garzon-Rodriguez, and T. W. Randolph, “Rational Design of Stable Protein Formulations,” *Pharm Biotechnol*, vol. 13, pp. 109–133, 2002, doi: 10.1007/978-1-4615-0557-0.

[67] L. L. Chang and M. J. Pikal, “Mechanisms of protein stabilization in the solid state,” *J Pharm Sci*, vol. 98, no. 9, pp. 2886–2908, 2009, doi: 10.1002/jps.21825.

[68] G. Lee, “Spray-Drying of Proteins,” in *Rational Design of Stable Protein Formulations: Theory and Practice*, J. F. Carpenter and M. C. Manning, Eds. Boston, MA: Springer US, 2002, pp. 135–158. doi: 10.1007/978-1-4615-0557-0_6.

[69] Y.-F. Maa, P.-A. Nguyen, T. Sweeney, S. J. Shire, and C. C. Hsu, “Protein Inhalation Powders: Spray Drying vs Spray Freeze Drying,” *Pharm Res*, vol. 16, no. 2, pp. 249–254, 1999.

[70] S. H. Lee, D. Heng, W. Kiong Ng, H.-K. Chan, and R. B. H. Tan, “Pharmaceutical Nanotechnology Nano spray drying: A novel method for preparing protein nanoparticles for protein therapy,” *Int J Pharm*, vol. 403, pp. 192–200, 2011, doi: 10.1016/j.ijpharm.2010.10.012.

[71] I. Roy and M. N. Gupta, “Freeze-drying of proteins: some emerging concerns,” *Biotechnol Appl Biochem*, vol. 39, no. 2, p. 165, 2004, doi: 10.1042/BA20030133.

[72] E. Cao, Y. Chen, Z. Cui, and P. R. Foster, “Effect of freezing and thawing rates on denaturation of proteins in aqueous solutions,” *Biotechnol Bioeng*, vol. 82, no. 6, pp. 684–690, 2003, doi: 10.1002/bit.10612.

[73] D. Q. M. Craig, P. G. Royall, V. L. Kett, and M. L. Hopton, “The relevance of the amorphous state to pharmaceutical dosage forms: Glassy drugs and freeze dried systems,” *Int J Pharm*, vol. 179, no. 2, pp. 179–207, 1999, doi: 10.1016/S0378-5173(98)00338-X.

[74] T. Arakawa, S. J. Prestrelski, W. C. Kenney, and J. F. Carpenter, “Factors affecting short-term and long-term stabilities of proteins.,” *Adv Drug Deliv Rev*, vol. 46, no. 1–3, pp. 307–326, 2001, [Online]. Available: http://www.ncbi.nlm.nih.gov/pubmed/11259845

[75] N. Wathion, “Public Statement on Exubera (Insulin human),” London, Nov. 2008.

[76] R. Vehring, H. Snyder, and D. Lechuga-Ballesteros, “Spray Drying,” in *Drying Technologies for Biotechnology and Pharmaceutical Applications*, 1st ed., S. Ohtake, K. Izutsu, and D. Lechuga-Ballesteros, Eds. Weinheim: John Wiley & Sons, Ltd, 2020, pp. 179–216. doi: 10.1002/9783527802104.CH7.

[77] D. Santos, A. C. Maurício, V. Sencadas, J. D. Santos, M. H. Fernandes, and P. S. Gomes, “Spray Drying: An Overview,” in *Biomaterials - Physics and Chemistry - New Edition*, IntechOpen, 2017. doi: 10.5772/INTECHOPEN.72247.

[78] F. Emami, A. Vatanara, E. J. Park, and D. H. Na, “Drying technologies for the stability and bioavailability of biopharmaceuticals,” *Pharmaceutics*, vol. 10, no. 3, pp. 1–22, 2018, doi: 10.3390/pharmaceutics10030131.

[79] Aniket *et al.*, “Enzyme dehydration using microglassification™ preserves the Protein’s structure and function,” *J Pharm Sci*, 2015, doi: 10.1002/jps.24279.

[80] J.-C. Baret, “Surfactants in droplet-based microfluidics,” *Lab Chip*, vol. 12, no. 3, pp. 422–433, 2012, doi: 10.1039/C1LC20582J.

[81] Q. Xu and M. Nakajima, “The generation of highly monodisperse droplets through the breakup of hydrodynamically focused microthread in a microfluidic device,” *Appl Phys Lett*, vol. 85, no. 17, pp. 3726–3728, 2004, doi: 10.1063/1.3081407.

[82] S.-Y. Teh, R. Lin, L.-H. Hung, and A. P. Lee, “Droplet microfluidics,” *Lab Chip*, 2008, doi: 10.1039/b715524g.

[83] A. Jahn, J. E. Reiner, W. N. Vreeland, D. L. DeVoe, L. E. Locascio, and M. Gaitan, “Preparation of nanoparticles by continuous-flow microfluidics,” *Journal of Nanoparticle Research*. 2008. doi: 10.1007/s11051-007-9340-5.

[84] T. Trantidou, M. S. Friddin, A. Salehi-Reyhani, O. Ces, and Y. Elani, “Droplet microfluidics for the construction of compartmentalised model membranes,” *Lab Chip*, vol. 18, no. 17, pp. 2488–2509, 2018, doi: 10.1039/c8lc00028j.

[85] L. Bai and D. J. McClements, “Development of microfluidization methods for efficient production of concentrated nanoemulsions: Comparison of single- and dual-channel microfluidizers,” *J Colloid Interface Sci*, vol. 466, pp. 206–212, 2016, doi: 10.1016/j.jcis.2015.12.039.

[86] B. J. Briscoe, C. J. Lawrence, and W. G. P. Mietus, “Review of immiscible fluid mixing,” *Adv Colloid Interface Sci*, vol. 81, no. 1, pp. 1–17, 1999, doi: 10.1016/S0001-8686(99)00002-0.

[87] S. Carrillo De Hert and T. L. Rodgers, “Continuous, recycle and batch emulsification kinetics using a high-shear mixer,” *Chem Eng Sci*, vol. 167, pp. 265–277, 2017, doi: 10.1016/j.ces.2017.04.020.

[88] L. Lee, R. Hancocks, I. Noble, and I. T. Norton, “Production of water-in-oil nanoemulsions using high pressure homogenisation: A study on droplet break-up,” *J Food Eng*, vol. 131, pp. 33–37, 2014, doi: 10.1016/j.jfoodeng.2014.01.024.

[89] M. Vert *et al.*, “Terminology for biorelated polymers and applications (IUPAC Recommendations 2012),” *Pure Applied Chemistry*, vol. 84, no. 2, pp. 377–410, 2012.

[90] K. Saralidze, L. H. Koole, and M. L. W. Knetsch, “Polymeric Microspheres for Medical Applications,” *Materials*, vol. 3, no. 6, p. 3537, 2010, doi: 10.3390/MA3063537.

[91] S. Efimov, L. Gilburd, A. Fedotov-Gefen, V. Tz Gurovich, J. Felsteiner, and Y. E. Krasik, “Aluminum micro-particles combustion ignited by underwater electrical wire explosion,” *Shock Waves*, vol. 22, pp. 207–214, 2012, doi: 10.1007/s00193-012-0361-3.

[92] E. V. Korolev and A. S. Inozemtcev, “Preparation and Research of the High-Strength Lightweight Concrete Based on Hollow Microspheres,” *Adv Mat Res*, vol. 746, pp. 285–288, 2013, doi: 10.4028/WWW.SCIENTIFIC.NET/AMR.746.285.

[93] I. Genuth, “The Future of Electronic Paper,” *The Future of Things*. https://thefutureofthings.com/3081-the-future-of-electronic-paper/ (accessed Nov. 15, 2021).

[94] M. J. VanWijk, E. VanBavel, A. Sturk, and R. Nieuwland, “Microparticles in cardiovascular diseases,” *Cardiovasc Res*, vol. 59, no. 2, pp. 277–287, Aug. 2003, doi: 10.1016/S0008-6363(03)00367-5/2/59-2-277-FIG3.GIF.

[95] J. M. Herring, M. A. Mcmichael, and S. A. Smith, “Microparticles in Health and Disease,” *J Vet Intern Med*, vol. 27, no. 5, pp. 1020–1033, Sep. 2013, doi: 10.1111/JVIM.12128.

[96] W. Lohcharoenkal, L. Wang, Y. C. Chen, and Y. Rojanasakul, “Protein nanoparticles as drug delivery carriers for cancer therapy,” *BioMed Research International*. 2014. doi: 10.1155/2014/180549.

[97] M. Swierczewska, H. S. Han, K. Kim, J. H. Park, and S. Lee, “Polysaccharide-based nanoparticles for theranostic nanomedicine,” *Advanced Drug Delivery Reviews*. 2016. doi: 10.1016/j.addr.2015.11.015.

[98] N. Dimov, E. Kastner, M. Hussain, Y. Perrie, and N. Szita, “Formation and purification of tailored liposomes for drug delivery using a module-based micro continuous-flow system,” *Sci Rep*, 2017, doi: 10.1038/s41598-017-11533-1.

[99] M. Muhaimin, A. Yohana Chaerunisaa, and R. Bodmeier, “Real-time particle size analysis using focused beam reflectance measurement as a process analytical technology tool for continuous microencapsulation process,” *Scientific Reports* |, vol. 11, p. 19390, 123AD, doi: 10.1038/s41598-021-98984-9.

[100] G. Orive, E. Anitua, J. L. Pedraz, and D. F. Emerich, “Biomaterials for promoting brain protection, repair and regeneration,” *Nature Reviews Neuroscience*. 2009. doi: 10.1038/nrn2685.

[101] Microtrac, “Particle Analysis Techniques Compared.” https://www.microtrac.com/applications/knowledge-base/different-particle-analysis-techniques-compared/ (accessed Nov. 17, 2021).

[102] C. O. R. Abbireddy and C. R. I. Clayton, “A review of modern particle sizing methods,” *Proceedings of the Institution of Civil Engineers: Geotechnical Engineering*, vol. 162, no. 4, pp. 193–201, 2009, doi: 10.1680/geng.2009.162.4.193.

[103] B. Lorber, F. Fischer, M. Bailly, H. Roy, and D. Kern, “Protein analysis by dynamic light scattering: Methods and techniques for students,” *Biochemistry and Molecular Biology Education*, 2012, doi: 10.1002/bmb.20644.

[104] “Micro-Flow Image-based Particle Analysis for Biopharmaceuticals :: ProteinSimple.” https://www.proteinsimple.com/mfi_5000.html (accessed Nov. 18, 2021).

[105] B. K. Lee, Y. Yun, and K. Park, “PLA micro- and nano-particles,” *Advanced Drug Delivery Reviews*. 2016. doi: 10.1016/j.addr.2016.05.020.

[106] D. Liu, H. Zhang, F. Fontana, J. T. Hirvonen, and H. A. Santos, “Microfluidic-assisted fabrication of carriers for controlled drug delivery,” *Lab Chip*, 2017, doi: 10.1039/C7LC00242D.

[107] C. J. Martínez Rivas *et al.*, “Nanoprecipitation process: From encapsulation to drug delivery,” *International Journal of Pharmaceutics*. 2017. doi: 10.1016/j.ijpharm.2017.08.064.

[108] R. Donno *et al.*, “Nanomanufacturing through microfluidic-assisted nanoprecipitation: Advanced analytics and structure-activity relationships,” *Int J Pharm*, 2017, doi: 10.1016/j.ijpharm.2017.10.006.

[109] T. Govender, S. Stolnik, M. C. Garnett, L. Illum, and S. S. Davis, “PLGA nanoparticles prepared by nanoprecipitation: Drug loading and release studies of a water soluble drug,” *Journal of Controlled Release*, 1999, doi: 10.1016/S0168-3659(98)00116-3.

[110] G. M. Whitesides, “The origins and the future of microfluidics,” *Nature*. 2006. doi: 10.1038/nature05058.

[111] R. Paliwal, R. J. Babu, and S. Palakurthi, “Nanomedicine Scale-up Technologies: Feasibilities and Challenges,” *AAPS PharmSciTech*, 2014, doi: 10.1208/s12249-014-0177-9.

[112] R. Riahi, A. Tamayol, S. A. M. Shaegh, A. M. Ghaemmaghami, M. R. Dokmeci, and A. Khademshosseini, “Microfluidics for advanced drug delivery systems,” *Curr Opin Chem Eng*, 2015, doi: 10.1016/j.coche.2014.12.001.

[113] S. Freiberg and X. X. Zhu, “Polymer microspheres for controlled drug release,” *International Journal of Pharmaceutics*. 2004. doi: 10.1016/j.ijpharm.2004.04.013.

[114] J. H. Xu, S. W. Li, J. Tán, Y. J. Wang, and G. S. Luo, “Preparation of highly monodisperse droplet in a T-junction microfluidic device,” *AIChE Journal*, 2006, doi: 10.1002/aic.10924.

[115] J. Tan, S. W. Li, K. Wang, and G. S. Luo, “Gas-liquid flow in T-junction microfluidic devices with a new perpendicular rupturing flow route,” *Chemical Engineering Journal*, 2009, doi: 10.1016/j.cej.2008.10.024.

[116] C. Cramer, P. Fischer, and E. J. Windhab, “Drop formation in a co-flowing ambient fluid,” *Chem Eng Sci*, 2004, doi: 10.1016/j.ces.2004.04.006.

[117] L. Yobas, S. Martens, W.-L. Ong, and N. Ranganathan, “High-performance flow-focusing geometry for spontaneous generation of monodispersed droplets{”, doi: 10.1039/b602240e.

[118] T. Nisisako, “Microstructured devices for preparing controlled multiple emulsions,” *Chemical Engineering and Technology*. 2008. doi: 10.1002/ceat.200800119.

[119] S. S. Davis and I. M. Walker, “Multiple Emulsions as Targetable Delivery Systems,” *Methods Enzymol*, vol. 149, pp. 51–64, 1987, doi: 10.1016/0076-6879(87)49043-5.

[120] N. Garti, A. Romano-Pariente, and A. Aserin, “The effect of additives on release from w/o/w emulsions,” *Colloids and Surfaces*, 1987, doi: 10.1016/0166-6622(87)80264-0.

[121] D. Saeki, S. Sugiura, T. Kanamori, S. Sato, and S. Ichikawa, “Microfluidic preparation of water-in-oil-in-water emulsions with an ultra-thin oil phase layer,” *Lab Chip*, 2010, doi: 10.1039/B916318B.

[122] Y. H. Lin, C. H. Lee, and G. bin Lee, “A new droplet formation chip utilizing controllable moving-wall structures for double emulsion applications,” in *Proceedings of the IEEE International Conference on Micro Electro Mechanical Systems (MEMS)*, 2008. doi: 10.1109/MEMSYS.2008.4443583.

[123] Y. H. Lin, C. H. Lee, and G. bin Lee, “Droplet formation utilizing controllable moving-wall structures for double-emulsion applications,” *Journal of Microelectromechanical Systems*, 2008, doi: 10.1109/JMEMS.2008.924273.

[124] A. S. Utada, E. Lorenceau, D. R. Link, P. D. Kaplan, H. A. Stone, and D. A. Weitz, “Monodisperse Double Emulsions Generated from a Microcapillary Device,” *Science (1979)*, vol. 308, no. 5721, pp. 537–541, 2005, doi: 10.1126/science.1109164.

[125] S.-H. Kim and D. A. Weitz, “One-Step Emulsification of Multiple Concentric Shells with Capillary Microfluidic Devices**,” *Angew. Chem.*, vol. 123, pp. 8890–8893, 2011, doi: 10.1002/ange.201102946.

[126] W. J. Duncanson, A. Abbaspourrad, H. C. Shum, S. H. Kim, L. L. A. Adams, and D. A. Weitz, “Monodisperse gas-filled microparticles from reactions in double emulsions,” *Langmuir*, 2012, doi: 10.1021/la300915p.

[127] S.-H. Kim, J. W. Kim, J.-C. Cho, and D. A. Weitz, “Double-emulsion drops with ultra-thin shells for capsule templates,” *Lab Chip*, vol. 11, pp. 3162–3166, 2011, doi: 10.1039/c1lc20434c.

[128] R. Karnik *et al.*, “Microfluidic platform for controlled synthesis of polymeric nanoparticles,” *Nano Lett*, 2008, doi: 10.1021/nl801736q.

[129] N. Kolishetti *et al.*, “Engineering of self-assembled nanoparticle platform for precisely controlled combination drug therapy,” *Proceedings of the National Academy of Sciences*, 2010, doi: 10.1073/pnas.1011368107.

[130] L. Capretto, W. Cheng, D. Carugo, O. L. Katsamenis, M. Hill, and X. Zhang, “Mechanism of co-nanoprecipitation of organic actives and block copolymers in a microfluidic environment,” *Nanotechnology*, 2012, doi: 10.1088/0957-4484/23/37/375602.

[131] G. Gregoriadis and B. E. Ryman, “Liposomes as Carriers of Enzymes or Drugs: a New Approach to the Treatment of Storage Diseases,” *Proceedings of the Biochemical Society*, vol. 124, no. 5, 1971, doi: 10.1002/jctb.5000560808.

[132] E. Kastner, V. Verma, D. Lowry, and Y. Perrie, “Microfluidic-controlled manufacture of liposomes for the solubilisation of a poorly water soluble drug,” *Int J Pharm*, 2015, doi: 10.1016/j.ijpharm.2015.02.063.

[133] M. Guimarães Sá Correia, M. L. Briuglia, F. Niosi, and D. A. Lamprou, “Microfluidic manufacturing of phospholipid nanoparticles: Stability, encapsulation efficacy, and drug release,” *Int J Pharm*, 2017, doi: 10.1016/j.ijpharm.2016.11.025.

[134] K. T. Savjani, A. K. Gajjar, and J. K. Savjani, “Drug Solubility: Importance and Enhancement Techniques,” *ISRN Pharm*, vol. 2012, no. 100 mL, pp. 1–10, 2012, doi: 10.5402/2012/195727.

[135] E. Kastner, “Nanotechnology and Microfluidics: Formulation Design and on-chip Manufacture of Nanoparticles,” 2015.

[136] O. Rossier *et al.*, “Giant vesicles under flows: Extrusion and retraction of tubes,” *Langmuir*, 2003, doi: 10.1021/la026236t.

[137] T. Wang, Y. Deng, Y. Geng, Z. Gao, J. Zou, and Z. Wang, “Preparation of submicron unilamellar liposomes by freeze-drying double emulsions,” *Biochim Biophys Acta Biomembr*, 2006, doi: 10.1016/j.bbamem.2006.01.023.

[138] S. Pautot, B. J. Frisken, and D. A. Weitz, “Production of unilamellar vesicles using an inverted emulsion,” *Langmuir*, 2003, doi: 10.1021/la026100v.

[139] M. S. Long, A. S. Cans, and C. D. Keating, “Budding and asymmetric protein microcompartmentation in giant vesicles containing two aqueous phases,” *J Am Chem Soc*, 2008, doi: 10.1021/ja077439c.

[140] A. Jahn, W. N. Vreeland, M. Gaitan, and L. E. Locascio, “Controlled Vesicle Self-Assembly in Microfluidic Channels with Hydrodynamic Focusing,” *J Am Chem Soc*, 2004, doi: 10.1021/ja0318030.

[141] D. van Swaay and A. deMello, “Microfluidic methods for forming liposomes,” *Lab Chip*, 2013, doi: 10.1039/c2lc41121k.

[142] M. I. Angelova and D. S. Dimitrov, “Liposome Electro formation,” *Faraday Discuss. Chem. SOC*, vol. 81, pp. 303–311, 1986.

[143] Y.-C. Lin, M. Li, Y.-T. Wang, T.-H. Lai, J.-T. Chiang, and K.-S. Huang, “A NEW METHOD FOR THE PREPARATION OF SELF-ASSEMBLED PHOSPHOLIPID MICROTUBES USING MICROFLUIDIC TECHNOLOGY,” in *The 13th International Conference on Solid-Stare Sensors, Actuators and Microsystems*, 2005, pp. 1592–1595.

[144] P. S. Dittrich, M. Heule, P. Renaud, and A. Manz, “On-chip extrusion of lipid vesicles and tubes through microsized apertures,” *Lab Chip*, 2006, doi: 10.1039/b517670k.

[145] K. Funakoshi, H. Suzuki, and S. Takeuchi, “Formation of giant lipid vesiclelike compartments from a planar lipid membrane by a pulsed jet flow,” *J Am Chem Soc*, 2007, doi: 10.1021/ja074029f.

[146] A. Jahn, S. M. Stavis, J. S. Hong, W. N. Vreeland, D. L. Devoe, and M. Gaitan, “Microfluidic mixing and the formation of nanoscale lipid vesicles,” *ACS Nano*, 2010, doi: 10.1021/nn901676x.

[147] A. D. Stroock, S. K. W. Dertinger, A. Ajdari, I. Mezi, H. A. Stone, and G. M. Whitesides, “Chaotic Mixer for Microchannels,” *Science (1979)*, vol. 295, no. 5555, pp. 647–651, 2002.

[148] N. M. Belliveau *et al.*, “Microfluidic synthesis of highly potent limit-size lipid nanoparticles for in vivo delivery of siRNA,” *Mol Ther Nucleic Acids*, 2012, doi: 10.1038/mtna.2012.28.

[149] S. Moelbert, B. Normand, P. De, and L. Rios, “Kosmotropes and chaotropes: modelling preferential exclusion, binding and aggregate stability,” *Biophys Chem*, vol. 112, no. 1, pp. 45–57, 2004.

[150] A. Utoft, “Micropipette manipulation studies: Material Characterization of multiphase, multicomponent systems,” University of Southern Denmark, Odense, 2017.

[151] D. L. Rickard, P. B. Duncan, and D. Needham, “Hydration potential of lysozyme: Protein dehydration using a single microparticle technique,” *Biophys J*, vol. 98, no. 6, pp. 1075–1084, 2010, doi: 10.1016/j.bpj.2009.11.043.

[152] E. et al. Schindelin, J.; Arganda-Carreras, I. & Frise, “Fiji: an open-source platform for biological-image analysis,” *Nat Methods*, vol. 9, no. 7, pp. 676–682, 2012.

[153] B. Smith, “Hough Circle Transform.” UCB Vision Sciences, 2018.

[154] “F. Menges ‘Spectragryph - optical spectroscopy software’, Version 1.2.14, 2020, http://www.effemm2.de/spectragryph/.”

[155] S. Verheyden, A. Sillen, A. Gils, P. J. Declerck, and Y. Engelborghs, “Tryptophan Properties in Fluorescence and Functional Stability of Plasminogen Activator Inhibitor 1,” *Biophys J*, vol. 85, pp. 501–510, 2003.

[156] J. T. Vivian and P. R. Callis, “Mechanisms of Tryptophan Fluorescence Shifts in Proteins,” *Biophys J*, vol. 80, no. 5, pp. 2093–2109, May 2001, doi: 10.1016/S0006-3495(01)76183-8.

[157] A. Belatik, S. Hotchandani, R. Carpentier, and H. A. Tajmir-Riahi, “Locating the binding sites of pb(II) ion with human and bovine serum albumins,” *PLoS One*, vol. 7, no. 5, 2012, doi: 10.1371/journal.pone.0036723.

[158] R. F. Borkman and S. R. Phillips, “Tyrosine-to-tryptophan energy transfer and the structure of calt gamma-II crystallin,” *Exp Eye Res*, vol. 40, no. 6, pp. 819–826, 1985, doi: 10.1016/0014-4835(85)90127-7.

[159] O. K. Abou-Zied and O. I. K. Al-Shihi, “Characterization of Subdomain IIA Binding Site of Human Serum Albumin in its Native, Unfolded, and Refolded States Using Small Molecular Probes”, doi: 10.1021/ja8031289.

[160] M. Moinpour, N. K. Barker, L. E. Guzman, J. C. Jewett, P. R. Langlais, and J. C. Schwartz, “Determining protein structure by tyrosine bioconjugation,” *bioRxiv*, 2020, doi: 10.1101/2020.02.04.934406.

[161] M. Moinpour, N. K. Barker, L. E. Guzman, J. C. Jewett, P. R. Langlais, and J. C. Schwartz, “Determining protein structure by tyrosine bioconjugation”, doi: 10.1101/2020.02.04.934406.

[162] M. Eisenhawer, S. Cattarinussi, A. Kuhn, and H. Vogel, “Fluorescence Resonance Energy Transfer Shows a Close Helix-Helix Distance in the Transmembrane M13 Procoat Protein †,” *Biochemistry*, vol. 40, pp. 12321–12328, 2001, doi: 10.1021/bi0107694.

[163] J. Steinhardt, J. Krijn, and J. G. Leidy, “Differences between Bovine and Human Serum Albumins: Binding Isotherms, Optical Rotatory Dispersion, Viscosity, Hydrogen Ion Titration, and Fluorescence Effects*,” *Octobcv*, vol. 26, 1971, Accessed: Oct. 26, 2021. [Online]. Available: https://pubs.acs.org/sharingguidelines

[164] D. Li, D. Hong, H. Guo, J. Chen, and B. Ji, “Probing the influences of urea on the interaction of sinomenine with human serum albumin by steady-state fluorescence,” *J Photochem Photobiol B*, vol. 117, pp. 126–131, 2012, doi: 10.1016/j.jphotobiol.2012.09.007.

[165] S. Gorinstein *et al.*, “Intrinsic tryptophan fluorescence of human serum proteins and related conformational changes,” *J Protein Chem*, vol. 19, no. 8, pp. 637–642, 2000, doi: 10.1023/A:1007192017291.

[166] S. Corporation, “A585 Protein Analysis Using FTIR - Secondary Structure Analysis of Bovine Serum Albumin Using Curve Fitting,” 2000.

[167] A. Dong, S. J. Prestrelski, D. Allison, and J. F. Carpenter, “Infrared Spectroscopic Studies of Lyophi I izat ion-and Temperat u re4 nd uced Protein Aggregation.”

[168] A. Dong, J. M. Malecki, L. Lee, J. F. Carpenter, and J. C. Lee, “Ligand-induced conformational and structural dynamics changes in Escherichia coli cyclic AMP receptor protein,” *Biochemistry*, vol. 41, no. 21, pp. 6660–6667, 2002, doi: 10.1021/bi020036z.

[169] D. M. Byler and H. Susi, “Examination of the secondary structure of proteins by deconvolved FTIR spectra,” *Biopolymers*, vol. 25, no. 3, pp. 469–487, 1986, doi: 10.1002/bip.360250307.

[170] J. Coates, “Interpretation of Infrared Spectra, A Practical Approach,” *Encyclopedia of Analytical Chemistry*, pp. 10815–10837, 2006, doi: 10.1002/9780470027318.a5606.

[171] A. Elliot and E. J. Ambrose, “Structure of Sythetic Polypetides,” *Nature*, no. 4206, pp. 921–922, 1950.

[172] A. Dong, P. Huang, and W. S. Caughey, “Protein Secondary Structures in Water from Second-Derivative Amide I Infrared Spectra,” *Biochemistry*, vol. 29, no. 13, pp. 3303–3308, 1990, doi: 10.1021/bi00465a022.

[173] T. Miyazawa and E. R. Blout, “The Infrared Spectra of Polypeptides in Various Conformations: Amide I and II Bands,” *J Am Chem Soc*, vol. 83, no. 3, pp. 712–719, 1961, doi: 10.1021/ja01464a042.

[174] J. Bandekar and S. Krimm, “Normal mode spectrum of the parallel-chain β-sheet,” *Biopolymers*, vol. 27, no. 6, pp. 909–921, 1988, doi: 10.1002/bip.360270603.

[175] J. de Meutter and E. Goormaghtigh, “Searching for a better match between protein secondary structure definitions and protein FTIR spectra,” *Anal Chem*, vol. 93, no. 3, pp. 1561–1568, 2021, doi: 10.1021/acs.analchem.0c03943.

[176] A. Padmanaban and S. Menon, “Characterization of mAb aggregation”.

[177] “The principles of dynamic light scattering :: Anton Paar Wiki.” https://wiki.anton-paar.com/uk-en/the-principles-of-dynamic-light-scattering/ (accessed Mar. 29, 2022).

[178] “The principles of dynamic light scattering :: Anton Paar Wiki.” https://wiki.anton-paar.com/uk-en/the-principles-of-dynamic-light-scattering/ (accessed Mar. 29, 2022).

[179] T. van Nguyen *et al.*, “Protein-based microsphere biolasers fabricated by dehydration,” *Soft Matter*, vol. 15, no. 47, pp. 9721–9726, Dec. 2019, doi: 10.1039/C9SM01610D.

[180] European Medicines Agency, “ICH guideline Q3C (R6) on impurities: guideline for residual solvents,” Amsterdam, Aug. 2019. [Online]. Available: www.ema.europa.eu/contactsTelephone+31

[181] European Medicine Agency, “ICH Topic Q 1 A (R2) Stability Testing of new Drug Substances and Products Step 5 NOTE FOR GUIDANCE ON STABILITY TESTING: STABILITY TESTING OF NEW DRUG SUBSTANCES AND PRODUCTS,” London, Aug. 2003. Accessed: Mar. 28, 2022. [Online]. Available: http://www.emea.eu.int

[182] S. L. Lee *et al.*, "Modernizing Pharmaceutical Manufacturing: from Batch to Continuous Production," *Journal of Pharmaceutical Innovation*, vol. 10, no. 3. Springer New York LLC, pp. 191–199, Sep. 07, 2015. doi: 10.1007/s12247-015-9215-8.

[183] K. P. Cole and M. D. Johnson, "Continuous flow technology vs. the batch-by-batch approach to produce pharmaceutical compounds," *Expert Rev Clin Pharmacol*, vol. 11, no. 1, pp. 5–13, Jan. 2018, doi: 10.1080/17512433.2018.1413936.

[184] K. Plumb, "Continuous processing in the pharmaceutical industry: Changing the mind set," *Chemical Engineering Research and Design*, vol. 83, no. 6 A, pp. 730–738, 2005, doi: 10.1205/cherd.04359.

[185] T. D. C. Ltd, "3D flow focusing chips." pp. 1–16. [Online]. Available: http://www.dolomite-microfluidics.com/images/stories/PDFs/datasheets/3d-flow-focusing-chips-datasheet.pdf

[186] T. Fu, Y. Wu, Y. Ma, and H. Z. Li, "Droplet formation and breakup dynamics in microfluidic flow-focusing devices: From dripping to jetting," *Chem Eng Sci*, vol. 84, pp. 207–217, Dec. 2012, doi: 10.1016/J.CES.2012.08.039.

[187] N. M. Kovalchuk, M. Sagisaka, K. Steponavicius, D. Vigolo, and M. J. H. Simmons, "Drop formation in microfluidic cross-junction: jetting to dripping to jetting transition," *Microfluid Nanofluidics*, vol. 23, no. 8, Aug. 2019, doi: 10.1007/s10404-019-2269-z.

[188] K. Kinoshita *et al.*, "From Single Microparticles to Microfluidic Emulsification: Fundamental Properties (Solubility, Density, Phase Separation) from Micropipette Manipulation of Solvent, Drug and Polymer Microspheres," *Processes*, vol. 4, no. 4, p. 49, 2016, doi: 10.3390/pr4040049.

[189] P. S. Epstein and P. M. S, "On the Stability of Gas Bubbles in Liquid-Gas Solutions," *The Journal of Chemical Physics1*, vol. 18, no. 11, pp. 1505–1509, 1950.

[190] R. Stephenson, J. Stuart, and M. Tabak, "Mutual Solubility of Water and Aliphatic Alcohols," *J Chem Eng Data*, vol. 29, no. 3, pp. 287–290, 1984, [Online]. Available: https://pubs.acs.org/sharingguidelines

[191] Celanese Chemicals Europe, "Product Description and Handling Guide Methyl Acetate," 2011. [Online]. Available: www.celanese.com

[192] B. M. Chassy and A. Giuffrida, "Method for the lysis of gram-positive, asporogenous bacteria with lysozyme," *Appl Environ Microbiol*, vol. 39, no. 1, pp. 153–158, 1980, doi: 10.1128/aem.39.1.153-158.1980.

[193] P. A. Levashov *et al.*, "The bacteriolytic activity of native and covalently immobilized lysozyme against Gram-positive and Gram-negative bacteria is differentially affected by charged amino acids and glycine," *FEBS Open Bio*, vol. 9, no. 3, pp. 510–518, 2019, doi: 10.1002/2211-5463.12591.

[194] W. I. Taylor and D. Achanzar, "Catalase test as an aid to the identification of Enterobacteriaceae.," *Appl Microbiol*, vol. 24, no. 1, pp. 58–61, 1972, doi: 10.1128/aem.24.1.58-61.1972.

[195] K. Reiner, "Catalase-Test-Protocol.pdf," no. November 2010, pp. 1–9, 2010.

[196] J. Kaushal, S. Mehandia, G. Singh, A. Raina, and S. K. Arya, “Catalase enzyme: Application in bioremediation and food industry,” *Biocatal Agric Biotechnol*, vol. 16, no. July, pp. 192–199, 2018, doi: 10.1016/j.bcab.2018.07.035.

[197] E. Akyilmaz and E. Dinçkaya, “Development of a catalase based biosensor for alcohol determination in beer samples,” *Talanta*, vol. 61, no. 2, pp. 113–118, 2003, doi: 10.1016/S0039-9140(03)00245-5.

[198] Promega, “Protein Detection Tools for Western Blotting & ELISA.”

[199] F. Wen, Y. Dong, L. Feng, S. Wang, S. Zhang, and X. Zhang, “Horseradish peroxidase functionalized fluorescent gold nanoclusters for hydrogen peroxide sensing,” *Anal Chem*, vol. 83, no. 4, pp. 1193–1196, 2011, doi: 10.1021/ac1031447.

[200] H. Wu *et al.*, “Size-dependent tuning of horseradish peroxidase bioreactivity by gold nanoparticles,” *Nanoscale*, vol. 7, no. 10, pp. 4505–4513, Mar. 2015, doi: 10.1039/c4nr07056a.

[201] S. T. Morthensen, A. S. Meyer, H. Jørgensen, and M. Pinelo, “Significance of membrane bioreactor design on the biocatalytic performance of glucose oxidase and catalase: Free vs. immobilized enzyme systems,” *Biochem Eng J*, vol. 117, pp. 41–47, 2017, doi: 10.1016/j.bej.2016.09.015.

[202] G. Orosz, R. S. Givens, and R. L. Schowen, “A model for mechanism of peroxyoxalate chemiluminescence as applied to detection in liquid chromatography,” *Crit Rev Anal Chem*, vol. 26, no. 1, pp. 1–27, 1996, doi: 10.1080/10408349608050566.

[203] D. L. Bitterfield, A. Utoft, and D. Needham, “An Activity-Based Dissolution Model for Solute-Containing Microdroplets,” *Langmuir*, vol. 32, no. 48, pp. 12749–12759, 2016, doi: 10.1021/acs.langmuir.6b03126.

[204] E. Nishimoto, S. Yamashita, N. Yamasaki, and T. Imoto, “Resolution and characterization of tryptophyl fluorescence of hen egg-white lysozyme by quenching- and time-resolved spectroscopy,” *Biosci Biotechnol Biochem*, vol. 63, no. 2, pp. 329–336, 1999, doi: 10.1271/bbb.63.329.

[205] M. Lasagna, E. Gratton, D. M. Jameson, and J. E. Brunet, “Apohorseradish peroxidase unfolding and refolding: Intrinsic tryptophan fluorescence studies,” *Biophys J*, vol. 76, no. 1 I, pp. 443–450, 1999, doi: 10.1016/S0006-3495(99)77211-5.

[206] S. D’Auria, P. Herman, M. Rossi, and J. R. Lakowicz, “The fluorescence emission of the apo-glucose oxidase from Aspergillus niger as probe to estimate glucose concentrations,” *Biochemical and Biophysical Research Communications*, vol. 263, no. 2. pp. 550–553, 1999. doi: 10.1006/bbrc.1999.1330.

[207] M. Jiao, Y. L. Zhou, H. T. Li, D. L. Zhang, J. Chen, and Y. Liang, “Structural and functional alterations of two multidomain oxidoreductases induced by guanidine hydrochloride,” *Acta Biochim Biophys Sin (Shanghai)*, vol. 42, no. 1, pp. 30–38, 2010, doi: 10.1093/abbs/gmp107.

[208] I. B. Bekard and D. E. Dunstan, “Tyrosine autofluorescence as a measure of bovine insulin fibrillation,” *Biophys J*, vol. 97, no. 9, pp. 2521–2531, 2009, doi: 10.1016/j.bpj.2009.07.064.

[209] A. A. Salem, M. Lotfy, A. Amin, and M. A. Ghattas, “Characterization of human serum albumin’s interactions with safranal and crocin using multi-spectroscopic and molecular docking techniques,” *Biochem Biophys Rep*, vol. 20, p. 100670, Dec. 2019, doi: 10.1016/J.BBREP.2019.100670.

[210] M. Deiana *et al.*, “Two-photon macromolecular probe based on a quadrupolar anthracenyl scaffold for sensitive recognition of serum proteins under simulated physiological conditions,” *ACS Omega*, vol. 2, no. 9, pp. 5715–5725, Sep. 2017, doi: 10.1021/ACSOMEGA.7B00665.

[211] M. Chudzik, M. Maciązek-Jurczyk, B. Pawełczak, and A. Sułkowska, “Spectroscopic studies on the molecular ageing of serum albumin,” *Molecules*, vol. 22, no. 1, Jan. 2017, doi: 10.3390/molecules22010034.

[212] M. A. Miller, J. D. Engstrom, B. S. Ludher, and K. P. Johnston, “Low Viscosity Highly Concentrated Injectable Nonaqueous Suspensions of Lysozyme Microparticles,” *Langmuir*, vol. 26, no. 2, p. 1067, Jan. 2010, doi: 10.1021/LA9023426.

[213] M. X. Yang *et al.*, “Crystalline monoclonal antibodies for subcutaneous delivery,” *Proc Natl Acad Sci U S A*, vol. 100, no. 12, pp. 6934–6939, Jun. 2003, doi: 10.1073/PNAS.1131899100.

[214] S. J. Shire, Z. Shahrokh, and J. Liu, “Challenges in the development of high protein concentration formulations,” *J Pharm Sci*, vol. 93, no. 6, pp. 1390–1402, 2004, doi: 10.1002/JPS.20079.

[215] J. Liu, M. D. H. Nguyen, J. D. Andya, and S. J. Shire, “Reversible self-association increases the viscosity of a concentrated monoclonal antibody in aqueous solution,” *J Pharm Sci*, vol. 94, no. 9, pp. 1928–1940, 2005, doi: 10.1002/JPS.20347.

[216] N. Harn, C. Allan, C. Oliver, and C. R. Middaugh, “Highly concentrated monoclonal antibody solutions: direct analysis of physical structure and thermal stability,” *J Pharm Sci*, vol. 96, no. 3, pp. 532–546, 2007, doi: 10.1002/JPS.20753.

[217] M. A. Miller, J. D. Engstrom, B. S. Ludher, and K. P. Johnston, “Low Viscosity Highly Concentrated Injectable Nonaqueous Suspensions of Lysozyme Microparticles”, doi: 10.1021/la9023426.

[218] J. L. Fast, A. A. Cordes, J. F. Carpenter, and T. W. Randolph, “Physical Instability of a Therapeutic Fc Fusion Protein: Domain Contributions to Conformational and Colloidal Stability †,” *Biochemistry*, vol. 48, pp. 11724–11736, 2009, doi: 10.1021/bi900853v.

[219] A. Saluja, A. V. Badkar, D. L. Zeng, S. Nema, and D. S. Kalonia, “Application of high-frequency rheology measurements for analyzing protein-protein interactions in high protein concentration solutions using a model monoclonal antibody (IgG2),” *J Pharm Sci*, vol. 95, no. 9, pp. 1967–1983, 2006, doi: 10.1002/JPS.20663.

[220] S. K. Basu, C. P. Govardhan, C. W. Jung, and A. L. Margolin, “Protein crystals for the delivery of biopharmaceuticals,” *http://dx.doi.org/10.1517/14712598.4.3.301*, vol. 4, no. 3, pp. 301–317, Mar. 2005, doi: 10.1517/14712598.4.3.301.

[221] T. Ahamed *et al.*, “Phase behavior of an intact monoclonal antibody.,” *Biophys J*, vol. 93, no. 2, pp. 610–619, Apr. 2007, doi: 10.1529/BIOPHYSJ.106.098293.

[222] C. Marschall, M. Witt, B. Hauptmeier, and W. Friess, “Powder suspensions in non-aqueous vehicles for delivery of therapeutic proteins,” *European Journal of Pharmaceutics and Biopharmaceutics*, vol. 161, pp. 37–49, 2021, doi: 10.1016/j.ejpb.2021.01.014.

[223] S. Charudharshini, A. K. Weight, T. Bussemer, and A. M. Klibanov, “Non-Aqueous Suspensions of Antibodies are Much Less Viscous Than Equally Concentrated Aqueous Solutions,” *Pharm Res*, vol. 30, no. 7, pp. 1749–1757, 2013, doi: 10.1007/s11095-013-1017-4.

[224] L. X. Yu, T. P. Foster, R. W. Sarver, and W. M. Moseley, “Preparation, Characterization, and in Vivo Evaluation of an Oil Suspension of a Bovine Growth Hormone Releasing factor Analog,” *J Pharm Sci*, vol. 85, no. 4, pp. 396–401, Apr. 1996, doi: 10.1021/JS9503901.

[225] G. CHEN, P. HOUSTON, and A. SHEUNG-KING LUK, “INJECTABLE NON-AQUEOUS SUSPENSION,” Jul. 06, 2006

[226] T. Loftsson and M. E. Brewster, “Pharmaceutical applications of cyclodextrins: Basic science and product development,” *Journal of Pharmacy and Pharmacology*, vol. 62, no. 11, pp. 1607–1621, 2010, doi: 10.1111/j.2042-7158.2010.01030.x.

[227] R. A. Bellantone, “Fundamentals of Amorphous Systems: Thermodynamic Aspects,” in *Amorphous Solid Dispersions: Theory and Practice*, N. Shah, H. Sandhu, D. S. Choi, H. Chokshi, and A. W. Malick, Eds. New York, NY: Springer New York, 2014, pp. 3–34. doi: 10.1007/978-1-4939-1598-9_1.

[228] C. Cavallari, B. Albertini, L. Rodriguez, A. M. Rabasco, and A. Fini, “Release of indomethacin from ultrasound dry granules containing lactose-based excipients,” *Journal of Controlled Release*, vol. 102, no. 1, pp. 39–47, 2005, doi: 10.1016/j.jconrel.2004.09.017.

[229] H. Chen, C. Khemtong, X. Yang, X. Chang, and J. Gao, “Nanonization strategies for poorly water-soluble drugs,” *Drug Discov Today*, vol. 16, no. 7–8, pp. 354–360, 2011, doi: 10.1016/j.drudis.2010.02.009.

[230] E. M. M. del Valle, “Cyclodextrins and their uses: A review,” *Process Biochemistry*, vol. 39, no. 9, pp. 1033–1046, 2004, doi: 10.1016/S0032-9592(03)00258-9.

[231] J. U. A. H. Junghanns and R. H. Müller, “Nanocrystal technology, drug delivery and clinical applications,” *Int J Nanomedicine*, vol. 3, no. 3, pp. 295–309, 2008.

[232] R. G. Strickley, “Solubilizing excipients used in commercially available oral and injectable formulations,” *Pharm Res*, vol. 21, no. 2, pp. 201–230, 2004.

[233] S. Tommasini, M. L. Calabrò, D. Raneri, P. Ficarra, and R. Ficarra, “Combined effect of pH and polysorbates with cyclodextrins on solubilization of naringenin,” *J Pharm Biomed Anal*, vol. 36, no. 2, pp. 327–333, 2004, doi: 10.1016/j.jpba.2004.06.013.

[234] D. Sleep, “Albumin and its application in drug delivery,” *Expert Opin Drug Deliv*, vol. 12, no. 5, pp. 793–812, doi: 10.1517/17425247.2015.993313.

[235] F. Kratz, “Albumin as a drug carrier: Design of prodrugs, drug conjugates and nanoparticles,” *Journal of Controlled Release*, vol. 132, no. 3, pp. 171–183, 2008, doi: 10.1016/j.jconrel.2008.05.010.

[236] Y. Okamoto, K. Taguchi, M. Sakuragi, S. Imoto, K. Yamasaki, and M. Otagiri, “Preparation, Characterization, and in Vitro/in Vivo Evaluation of Paclitaxel-Bound Albumin-Encapsulated Liposomes for the Treatment of Pancreatic Cancer,” *ACS Omega*, vol. 4, no. 5, pp. 8693–8700, 2019, doi: 10.1021/acsomega.9b00537.

[237] T. W. Evans, “Biological effects of albumin unrelated to oncotic pressure.,” *Aliment Pharmacol Ther*, vol. 16, no. Supplement 5, pp. 6–11, 2002, doi: 10.1046/j.1365-2036.2002.00190.x.

[238] J. H. Shi, Y. Y. Zhu, J. Wang, J. Chen, and Y. J. Shen, “Intermolecular interaction of prednisolone with bovine serum albumin: Spectroscopic and molecular docking methods,” *Spectrochim Acta A Mol Biomol Spectrosc*, vol. 103, pp. 287–294, 2013, doi: 10.1016/j.saa.2012.11.034.

[239] A. T. M. Serajuddin, “Salt formation to improve drug solubility,” *Adv Drug Deliv Rev*, vol. 59, no. 7, pp. 603–616, 2007, doi: 10.1016/j.addr.2007.05.010.

[240] M. Khoder, H. Abdelkader, A. ElShaer, A. Karam, M. Najlah, and R. G. Alany, “Efficient approach to enhance drug solubility by particle engineering of bovine serum albumin,” *Int J Pharm*, vol. 515, no. 1–2, pp. 740–748, 2016, doi: 10.1016/j.ijpharm.2016.11.019.

[241] M. Bogdan, A. Pirnau, C. Floare, and C. Bugeac, “Binding interaction of indomethacin with human serum albumin,” *J Pharm Biomed Anal*, vol. 47, no. 4–5, pp. 981–984, 2008, doi: 10.1016/j.jpba.2008.04.003.

[242] V. D. TRIVEDI, H. VORUM, B. HONORÉ, and M. A. QASIM, “Molecular Basis of Indomethacin-Human Serum Albumin Interaction,” *Journal of Pharmacy and Pharmacology*, vol. 51, no. 5, pp. 591–600, 1999, doi: 10.1211/0022357991772691.

[243] C. O. Knowles, “22.4.2 Benzyl Benzoate,” in *Handbook of Pesticide Toxicology, Volume 3: Classes of Pesticides*, vol. 3, W. J. Hayes and E. R. Laws, Eds. Academic Press, 1991, pp. 1505–1508.

[244] “Isopropyl myristate: Uses, Interactions, Mechanism of Action | DrugBank Online.” https://go.drugbank.com/drugs/DB13966 (accessed Nov. 29, 2021).

[245] “Inactive Ingredient Search for Approved Drug Products.” https://www.accessdata.fda.gov/scripts/cder/iig/index.cfm (accessed Jan. 11, 2022).

[246] T. Hong, K. Iwashita, and K. Shiraki, “Viscosity Control of Protein Solution by Small Solutes: A Review,” *Curr Protein Pept Sci*, vol. 19, no. 8, pp. 746–758, 2017, doi: 10.2174/1389203719666171213114919.

[247] V. M. KNEPP, S. J. PRESTRELSKI, J. G. SMITH, and M. T. , F. HUANG, “STABLE PROTEIN AND NUCLEIC ACID FORMULATIONS USING NON-AQUEOUS, ANHYDROUS, APROTIC, HYDROPHOBIC, NON-POLAR VEHICLES WITH LOW REACTIVITY,” WO/1998/016250, Apr. 23, 1998

[248] “Injectability & Viscosity | Drug Development | Small Sample Viscosity.” https://www.rheosense.com/applications/viscosity/drug-injectability (accessed Jan. 11, 2022).

[249] G. C. Birk, “Formulation development of a highly concentrated suspension of Cilengitide,” Villingen-Schwenningen, 2015.

[250] R. M. Patel, “PARENTERAL SUSPENSION: AN OVERVIEW.”

[251] Y. Z. Yordanova, “Oil-Based Parenteral Depot Formulation for Veterinary Peptide Delivery,” Shumen, 2018.

[252] V. M. Knepp, A. Muchnik, S. Oldmark, and L. Kalashnikova, “Stability of nonaqueous suspension formulations of plasma derived factor IX and recombinant human alpha interferon at elevated temperatures,” *Pharm Res*, vol. 15, no. 7, pp. 1090–1095, 1998, doi: 10.1023/A:1011994514358.

[253] M. El-Badry, G. Fetih, and M. Fathy, “Improvement of solubility and dissolution rate of indomethacin by solid dispersions in Gelucire 50/13 and PEG4000,” *Saudi Pharmaceutical Journal : SPJ*, vol. 17, no. 3, p. 217, Jul. 2009, doi: 10.1016/J.JSPS.2009.08.006.

[254] Lindy Biosciences, “Microglassification,” 2021. https://www.lindybio.com/technology (accessed Oct. 29, 2022).

[255] Lindy Biosciences, “Who we are,” 2021. https://www.lindybio.com/about (accessed Oct. 29, 2022).